Inauguraldissertation

zur Erlangung der Doktorwürde der

Naturwissenschaftlich-Mathematischen Gesamtfakultät

der Ruprecht-Karls-Universität Heidelberg

Vorgelegt von

Dipl.-Chem. Stefanie Kannengießer

aus

Mannheim

Tag der mündlichen Prüfung: 28.06.2013

Optimization of the Synthesis of Ac-225-labelled DOTA-Radioimmunoconjugates for Targeted Alpha Therapy based on Investigations on the Complexation of Trivalent Actinides by DOTA

Erster Gutachter: Prof. Dr. Thomas Fanghänel

Zweiter Gutachter: Prof. Dr. Petra Panak

"We must not forget that, when radium was discovered, no one knew that it would prove useful in hospitals. The work was one of pure science. And this is a proof that scientific work must be considered from the point of view of the direct usefullness of it. It must be done for itself, for the beauty of science, and then there is always the chance that a scientific discovery may become, like the radium, a benefit for humanity."

(M. S.-Curie, 1921)

Acknowledgements

I would like to thank all those who have helped me in carrying out the research:

- Prof. Thomas Fanghänel (ITU) for the opportunity to conduct my PhD studies at his institute under his supervision and for the helpful discussions during that time
- Prof. Petra J. Panak (INE) for the opportunity to carry out the research on my TRLFS project in her group under her supervision and for always listening to my problems
- Prof. Horst Geckeis (INE) for facilitating the collaboration with his institute
- Dr. Frank Bruchertseifer (ITU) and Dr. Alfred Morgenstern (ITU) for their scientific supervision and guidance
- Dr. Christos Apostolidis (ITU) and Dr. Jean-Paul Glatz (ITU) for their storries and interest in my research
- the AIT group at ITU and especially Alexander Romanow for daily support inside and outside of the laboratory
- Dr. Johannes Lützenkirchen and Dr. Andrej Skerencak-Frech for their support with thermodynamic calculations
- Dr. Peter Kaden for the NMR measurements and related discussions
- those who read parts of my Dissertation and were "forced" to discuss it with me also during their free time (Christian Ruff, Dr. Peter Kaden, Dr. Sascha Trumm, Dr. Andrej Skerencak-Frech)
- Sascha Hofmann who read through all of my Dissertation and even had the heart to correct my English (even though I did not accept all of the "suggestions for improvement")
- all my familiy and friends, not only at ITU and INE, for everything they did for me during these last years.

Contents

0.1 Abstract

The successful application of α-emitters in targeted alpha therapy (TAT) goes together with developments in radionuclide production and labelling chemistry. Especially profound understanding of the coordination chemistry of the respective metal ion-ligand system is of major importance to develop protocols for the synthesis of radioimmunoconjugates and to predict the fate of radionuclides *in vivo*.

Radioconjugates of the therapeutic α-emitter Ac-225 with polyamino-polycarboxyl ligands as chelating agents are being actively studied [1, 2, 3, 4]. In particular the macrocyclic ligand 1,4,7,10-tetraazacyclododecane- 1,4,7,10-tetraacetic acid (DOTA) has shown promise due to the high kinetic- and thermodynamic stability ($\log K > 20$) of its complexes with trivalent metal cations [5]. The scope of the presented work was the experimental characterisation and evaluation of DOTA as a suitable chelator for trivalent actinides (An(III)), particularly in terms of stable binding of the long-lived alpha emitting radionuclide Ac-225 to biomolecules for safe application in radioimmunotherapy (RIT). The project included not only basic studies to contribute to a better understanding of the complexation mechanisms and kinetics, but, based on these findings, was aimed at the development of a robust labelling protocol for facile and effective synthesis of an Ac-225-DOTA-MabThera® conjugate. In the course of the investigations, focus was set on *in vitro* testing of the obtained radioimmunoconjugate, in particular the evaluation of the kinetic stability in presence of competing agents as well as in human blood serum. Assessment of the antigen binding affinity of the antibody conjugate completed the work.

The protocol for the design and synthesis of Ac-225 radiopharmaceuticals of McDevitt *et al* provided the starting point for this study [6]. This research group developed a synthetic scheme to radiolabel DOTA-proteins with Ac-225. Later, the protocol was applied to antibodies in form of a two-step synthesis, with the first step being the Ac-225 DOTA-Bn-NCS complexation, followed by the coupling of the Ac-225-DOTA-Bn-NCS to the mAb. The idea behind this two-step approach was that, when the complexation of Ac(III) with DOTA is conducted at elevated temperatures and basic pH (first step), presumably a more stable complex is formed. However, since higher temperature / pH are known to have a negative effect on the antibody efficiency, the conjugation to the biomolecule can hence only be conducted at lower temperatures in a second step. This two-step synthesis though suffers from yields below 10 %, which is assumed to be due to the competing hydrolysis reaction of the isothiocyanate moiety occurring at the pH used during the complexation step. This makes the labelling protocol an interesting subject for further studies on how this synthesis can be improved.

From the findings of McDevitt *et al* it was apparent that a number of variables needed to be investigated in order to improve on the low efficiency of the protocol. These studies were conducted previously and are summarised in the Diploma Thesis, S. Kannengießer, 2009 [7]. A one-step synthesis protocol was tested and the labelling yields for Ac-225 were found to be dependent on temperature and especially on the pH of the reaction mixture. Eventually, an optimised protocol for radiolabelling of DOTA-peptides and MabThera® with Ac-225 activities up to 2 µCi (= 74 kBq) per 100 µg mAb was established, offering labelling yields > 95 %. The present work now aimed on translation of the developed synthesis protocol to higher specific activities of clinical relevance (≥ 10 µCi (≥ 370 kBq) per 100 µg mAb).

To gain profound knowledge about the complexation reaction mechanism and the thermodynamic and kinetic properties of the An(III)-DOTA system, the coordination chemistry was initially studied by means of time resolved laser fluorescence spectroscopy (TRLFS). Since Ac(III) has no suitable spectroscopic properties, the metal ion complexation by DOTA was investigated with Cm(III) as substitute for the trivalent actinides. A comparable study on [Eu(III)DOTA]$^-$ has been reported before [8, 9, 10]. Besides determination of the kinetic rate constants and thermodynamic parameters (log K, $\Delta_R G$, $\Delta_R H$, $\Delta_R S$) at labelling-relevant temperatures up to 90 °C, attention was also paid to the detection of possible intermediate species which are frequently discussed in the literature [11].

TRLFS is a powerful speciation method which makes use of the excellent fluorescence properties of Eu(III) and Cm(III), both regarded as good representatives for trivalent lanthanides and actinides. With TRLFS it is possible to detect and characterise complex species in sub-micromolar concentrations without influencing the chemical equilibrium of the system. An experimental setup was chosen which allows for adjusting the concentration of the reactive DOTA species by variation of the pH of the reaction. Due to the slow kinetics of the complexation reaction at room temperature, experiments at 45 to 90 °C were conducted to identify the complex species and quantify their relative ratios by means of peak deconvolution. Based on the potentiometrically determined p$K_{a,n}$ values of $H_xDOTA^{(4-x)-}$ for the respective conditions, from these ratios the conditional complex stability constants log K of [Cm(III)DOTA]- were calculated (I = 0.1, 45 to 90 °C). Application of the van't Hoff law allowed for extrapolation of the log K at 25 °C to be 22.0±0.4. The parameters $\Delta_R G$, $\Delta_R H$ and $\Delta_R S$ obtained from the Gibbs Helmholtz relation indicate that the reaction is exergonic, endothermic and driven by the change of entropy.

Identification and further characterisation of the involved complex species was done by comparison of the fluorescence lifetimes, which give information about the first coordination sphere of the metal cation. Furthermore, additional investigations with NMR were executed to identify and understand the mechanism related to the complex formation with DOTA-Bn-NCS. Based on the results of the NMR study, the complexation kinetics of DOTA and DOTA-Bn-NCS were further investigated and compared to gain insight into the involved reaction mechanisms.

Proper understanding and interpretation of the thermodynamic behaviour of the Cm(III)-DOTA complex formation allowed for facile translation of the experimental settings to the Ac(III)-DOTA system. Since no spectroscopic methods are available for this system, Chelex cation exchange resin as well as Instant Thin Layer Chromatography (ITLC) were chosen as radiochemical speciation methods and were evaluated for their feasability. Determination and refinement of the stability constant log K of [Ac(III)DOTA]$^-$ for the temperature range of 25 to 90 °C was done in analogy to the Cm(III)-DOTA system, resulting in a log $K_{25\,°C}$= 19.5±0.4. To obtain reliable results, the protocol for the radiochemical separation of Ac-225 from Ra-225 required optimisation to ensure highest purity and quality of the radionuclide.

Based on these findings, the studies on the Ac-225-labelling of DOTA-Bn-NCS-MabThera® for targeted alpha therapy of Non-Hodgkins-Lymphoma were subsequently continued. The previously established protocol was modified and further optimised in order to be applicable for facile clinical synthesis of radioimmunocon-

jugates with higher specific activities (SA) within ∼20 min. In this regard, the antibody labelling kinetics were reviewed respective reaction temperature and ideal pH of the high-yield radiolabelling, which permitted further improvement of the labelling effectiveness (pH 9, 37 - 42 °C, 5 - 15 min; ave. yields 94 - 96 %, > 98 % RCP after purification). The protocol was successfully evaluated for reliability with SA up to 50 µCi (= 1.85 MBq) per 100 µg mAb.

The obtained radioconjugates were assessed for their kinetic stability in different buffers as well as under physiolocigal conditions in human blood serum and proved to be satisfyingly stable over up to 30 days (∼85 % Ac-225 still bound). Finally, a preliminary radiobiological study with cancer cells (K422 cell line, B-cell lymphoma) was conducted to determine the antigen binding affinity of the radiolabelled CD20-antibody (SA = 1 µCi (= 37 kBq)/100 µg mAb, B_{max}= 8.88 nM, K_d = 52.55 nM). The results give rise to further preclinical *in vitro* studies.

In summary, it was demonstrated that rapid, high-yield radiolabelling of DOTA-chelated mAbs is possible under alkaline conditions at rather low temperatures. Under these conditions a thermodynamically and kinetically stable radioimmunoconjugates with specific activities suitable for application in clinical TAT studies is formed while the integrity of the antibody is preserved.

0.2 Zusammenfassung

Die erfolgreiche Anwendung von Alpha-Strahlern in der zielgerichteten Krebstherapie ("targeted alpha therapy, TAT) geht einher mit den Entwicklungen in der Radionuklid-Produktion und Radiomarkierungschemie. Um Protokolle zur Herstellung von Radioimmunokonjugaten zu entwickeln und das Verhalten bzw. den Verbleib der Radionuklide im lebenden Organismus ("*in vivo*") vorherzusagen, ist ein fundiertes Verständnis der Koordinationschemie des betreffenden Metallion-Ligand-Systems außerordentlich wichtig.

Konjugate basierend auf Komplexen des therapeutischen Alpha-Strahlers Ac-225 mit Polyaminopolycarboxyl-Liganden ("Komplexone") sind aktuell Gegenstand verschiedener Studien [1, 2, 3, 4]. Besonders vielversprechend erscheint hier der Makrozyklus 1,4,7,10-Tetraazacyclododecan-1,4,7,10-tetraessigsäure (DOTA) aufgrund der hohen kinetischen- sowie thermodynamischen Stabilität (log K $>$ 20) seiner Komplexe mit dreiwertigen Metallkationen [5]. Ziel der vorgelegten Doktorarbeit war daher die experimentelle Charakterisierung und Bewertung von DOTA hinsichtlich seiner Eignung zur Chelatisierung dreiwertiger Actiniden (An(III)), besonders in Hinblick auf zuverlässige Bindung des langlebigen Radionuklids Ac-225 an Biomoleküle zur Verwendung in der Radioimmunotherapie (RIT). Neben grundlegenden Untersuchungen zum besseren Verständnis des Komplexierungsmechanismus und der Komplexierungskinetik, lag - darauf aufbauend - der Fokus des Projekts auf der Entwicklung eines robusten Markierungsprotokolls zur einfachen und effektiven Herstellung von Ac-225-DOTA-MabThera®. Im weiteren Verlauf der Untersuchungen lag das Augenmerk zudem auf der *in vitro*-Evaluierung der erhaltenen Radioimmunokonjugate, insbesondere auf deren kinetischer Komplexstabilität in Anwesenheit konkurrierender Liganden sowie im menschlichen Blutserum. Die Beurteilung der Antigen-Bindungsaffinität des markierten Antikörpers bildete den Abschluss dieser Arbeit.

Als Ausgangspunkt für die Untersuchungen diente das von McDevitt *et al* beschriebene Protokoll zur Synthese von Ac-225-Radiopharmazeutika [6]. Die Arbeitsgruppe entwickelte zunächst ein Syntheseschema für Ac-225 markierte, DOTA-basierte Proteine, welches später in Form einer Zwei-Stufen-Synthese auf Antikörper angewendet wurde. Hierbei findet im ersten Schritt die Komplexierung von Ac-225 durch DOTA-Bn-NCS statt, gefolgt von der Ankoppelung des Chelats an das Biomolekül. Dieses Vorgehen beruht auf der Annahme dass ein besonders stabiler Komplex gebildet wird wenn die Ac(III)-DOTA Komplexierung bei erhöhter Temperatur und unter alkalischen Bedingungen erfolgt. Da solche Reaktionsbedingungen aber bekanntermaßen einen negativen Einfluss auf die Funktionsfähigkeit des Antikörpers haben, kann die Anknüpfung an die Biomoleküle folglich nur bei milderen Bedingungen in einem zweiten Syntheseschritt realisiert werden. Ein Schwachpunkt dieser vorgeschlagenen Syntheseroute ist die schlechte Produktausbeute ($<$ 10 %), was vermutlich auf Hydrolyse der NCS-Funktionalität unter den gewählten pH-Bedingungen im ersten Syntheseschritt zurückzuführen ist. Diese Problematik mach das Markierungsprotokoll zu einem interessanten Studiengegenstand.

Aus den Schilderungen von McDevitt *et al* geht hervor, dass mehrere Reaktionsparameter genauerer Untersuchung bedürfen, um die Effizienz der Synthese drastisch zu erhöhen. Dies geschah bereits in vorherigen Studien und wurde in der Diplomarbeit vorgelegt (S. Kannengießer, 2009 [7]). Im Rahmen der Arbeit wurde

ein Ein-Stufen-Syntheseprotokoll entwickelt und erprobt, wobei eine Temperatur- sowie eine starke pH-Abhängikeit der Markierungsausbeuten nachgewiesen werden konnten. Es konnte schließlich ein verbessertes Protokoll zur Radiomarkierung von DOTA-Peptiden sowie explizit von DOTA-Mabthera® mit Aktivitäten von bis zu 2 µCi (= 74 kBq) pro 100 µg Antikörper implementiert werden, welches Produktausbeuten von $>95\,\%$ ermöglicht. Darauf aufbauend zielte die vorgelegte Doktorarbeit auf die Weiterentwicklung des Syntheseprotokolls zur zuverlässigen Anwendung mit höheren spezifischen Aktivitäten von klinischer Relevanz ($\geq$ 10 µCi ($\geq$ 370 kBq) per 100 µg mAb) ab.

Um ein grundlegendes Verständnis der Komplexierung sowie der thermodynamischen als auch kinetischen Eigenschaften des An(III)-DOTA Systems zu erlangen, wurde zunächst die Koordinationschemie mittels zeitaufgelöster Laser-Fluoreszenz-Spektroskopie (TRLFS) untersucht. Da Ac(III) keine geeigneten spektroskopischen Eigenschaften besitzt, wurden die Studien mit Cm(III) als Modellsystem durchgeführt; über eine vergleichbare Untersuchung am Eu(III)-DOTA System wurde vor einigen Jahren berichtet [8, 9, 10]. Von Interesse war in der vorliegenden Arbeit, neben der Bestimmung der Reaktionsraten und der thermodynamischen Parameter der Komplexierung von Cm(III) durch DOTA im markierungsrelevanten Temperaturbereich bis 90 °C (log K, $\Delta_R G$, $\Delta_R H$, $\Delta_R S$), auch der Nachweis möglicher auftretender Komplex-Zwischenspezies, welche oft in der Literatur diskutiert werden [11].

TRLFS ist eine leistungsfähige Speziationsmethode und basiert auf den spezifischen Fluoreszenzeigenschaften von Eu(III) und Cm(III), welche beide geeigente Repräsentanten für dreiwertige Lanthaniden und Actiniden darstellen. Als nichtinvasive Methode ermöglicht sie Nachweis und Bestimmung von Komplex-Spezies im sub-mikromolaren Konzentrationsbereich, ohne das chemische Gleichgewicht des Systems zu beeinflussen. Ein Experimentansatz wurde gewählt, der die Einstellung der Konzentration der reaktivsten DOTA-Spezies über Variation des pH-Wertes der Reaktion ermöglicht. Aufgrund der langsamen Kinetik der DOTA-Komplexierungen bei Raumtemperatur wurden die Experimente im Bereich von 45 - 90 °C ausgeführt. Die Zuordnung der auftretenden Komplexspezies und die darauf folgende Peakentfaltung ermöglichte die Quantifizierung ihrer relativen Anteile. Die Berechnung der konditionellen Komplexstabilitätskonstanten log K von $[Cm(III)DOTA]^-$ aus diesen Daten erfolgte auf Grundlage der in diesem Zusammenhang potentiometrisch bestimmten $pK_{s,n}$ Werte von $H_xDOTA^{(4-x)-}$ bei den entsprechenden Reaktionsbedingungen (I = 0.1 M; T = 45 - 90 °C). Mit Hilfe der van't Hoff Beziehung konnte der log K bei 25 °C zu 22.0±0.4 extrapoliert werden. Die Parameter $\Delta_R G$, $\Delta_R H$ und $\Delta_R S$ aus der Gibbs Helmholtz Relation beschreiben die Komplexierung als exergonisch, endotherm und entropiegetrieben.

Die Identifizierung und nähere Bestimmung der an der Reaktion beteiligten Komplexspezies gelang über den Vergleich der Fluoreszenz-Lebensdauern, welche Informationen über die erste Koordinationsphäre des Metallkations liefern. Darüber hinaus wurden zusätzliche Untersuchungen mittels NMR an DOTA-Bn-NCS durchgeführt um den Mechanismus der Komplexbildung aufzuklären und zu verstehen. Aufbauend auf diesen Ergebnissen wurde auch die Reaktionskinetik der An(III)-Komplexierung durch DOTA und DOTA-Bn-NCS nochmals genauer studiert und verglichen.

Durch das Verständnis und die Interpretation der Thermodynamik der Cm(III)DOTA Komplexbildung wurde ein einfaches Übertragen der experimentellen Bedingungen auf das Ac(III)DOTA System ermöglicht. Da hierauf keine nicht-invativen, spektroskopischen Methoden anwendbar sind, wurde Kationenaustausch (mit Chelex) bzw. Dünnschichtchromatographie (ITLC) als radiochemische Speziationsmethode ausgewählt und auf ihre Anwendbarkeit überprüft. Die Bestimmung der Stabilitätskonstante log K von [Ac(III)DOTA]$^-$ im Temperaturbereich von 25 - 90 °C erfolgte analog zum Cm(III)-DOTA System und ergab einen log $K_{25°C}$ von 19.5±0.4. Um verlässliche und reproduzierbare Ergebnisse zu erhalten, wurde im Rahmen dieser Experimente auch das Protokoll für die radiochemische Abtrennung von Ac-225 von Ra-225 hinsichtlich größtmöglicher Reinheit und Qualität der verwendeten Radionuklidlösung verbessert.

Basierend auf den gewonnenen Erkenntnissen wurden die Untersuchungen zur Synthese von Ac-225-DOTA-Bn-NCS-MabThera® zur Therapie von Non-Hodgkins-Lymphomen fortgesetzt. Das zuvor entwickelte Markierungsprotokoll wurde modifiziert und insoweit optimiert, dass es die zuverlässige und einfache Herstellung klinischer Radioimmunokonjugate mit höheren spefizischen Aktivitäten (SA) innerhalb ∼20 min garantiert. In diesem Zusammenhang wurde die Antikörper-Markierungskinetik bezüglich der Reaktionstemperatur und des idealen pH-Wertes für höchste Markierungsausbeuten neu überprüft, was eine weitere Verbesserung der Markierungseffizienz mit sich brachte (pH 9; 37 - 42 °C; 5 - 15 min; Ausbeuten 94 - 96 %, > 98 % RCP). Das neue Protokoll wurde erfolgreich auf Zuverlässigkeit für SA von bis zu 50 µCi Ac-225 (= 1.85 MBq) pro 100 µg mAb evaluiert.

Im weiteren Verlauf der Arbeit wurde die kinetische Stabilität der synthetisierten Radiokonjugate sowohl in verschiedenen Puffermedien als auch unter physiologischen Bedingungen im Blutserum über bis zu 30 Tage bestätigt (∼85 % Ac-225 noch gebunden). Abschließend wurde eine erste vorläufige radiobiologische Studie mit K422 Krebszellen (B-Zell Lymphome) durchgeführt, um die Antigen-Bindungsaffinität des markierten Antikörpers zu bewerten (SA = 1 µCi (= 37 kBq)/100µg mAb; B_{max} = 8.88 nM; K_d = 52.55 nM). Die Ergebnisse geben Anlass zu weiterführenden prä-klinischen *in vitro* Studien.

Zusammenfassend konnte im Rahmen der vorliegenden Doktorarbeit gezeigt werden, dass die Radiomarkierung DOTA-chelatierter Antikörper schnell und mit höchsten Produktausbeuten bei vergleichsweise niedrigen Temperaturen bei alkalischem pH möglich ist. Hierbei bildet sich ein thermodynamisch und kinetisch stabiles Radioimmunokonjugat, beladen mit spezifischen Aktivitäten wie sie für klinische TAT benötigt werden, während der Antikörper unter diesen Bedingungen weitgehend funktionsfähig zu bleiben scheint.

1 Introduction

1.1 Cancer Therapy

Modern medicine makes use of a variety of treatment modalities for cancer patients. Unfortunately, still many patients with metastasised diseases cannot be cured. If the tumour is clearly localized, surgery or external beam radiotherapy is the method of choice, while with disseminated and metastasising tumours systemic treatment such as chemo-, immuno- or radionuclide therapy is inevitable. In many cases prolonged survival can be achieved with traditional cytotoxic chemotherapy. However, due to its unselective nature, it causes significant toxicity also to healthy cells which leads to unpleasant side-effects like hair loss and hampers the treatment efficacy as it limits the total therapeutic dose that can be administered [12]. During the last decade, the concept of more selective radionuclide therapy with only minimal side-effects therefore became more and more accepted as alternative systemic treatment modality. By targeting a cell-killing agent like a radionuclide to tumour-associated structures, it is possible to combine the therapeutic efficacy of radiation with the opportunity of systemic treatment, as the targeting would increase the concentration of the cytotoxic agent in the tumours while reducing normal tissues toxicity [13].

Radionuclide therapy is based on the same effect mechanism as external beam radiation therapy (EBRT) employing high-enery electrons or gamma radiation, with both therapies achieving cell destruction by induction of severe DNA damage. The radiobiological mechanisms of cancer cell kill are more complex and different from those during EBRT, which results in radionuclide therapy requiring less radiation dose to achieve effects similar to EBRT [14]. While being a powerful method to eradicate disseminated single tumour cells and small metastases that are undetected by conventional scanning and would remain untreated in EBRT, bulky tumours and large metastases still often require treatment with surgery or chemotherapy before the remaining tumour cells can be reasonably treated with radionuclide therapy.

Systemic radioimmunotherapy as well as peptide - receptor therapy are growing branches in the field of nuclear medicine, proving to be successful for treatment of several cancer types. Also the development of monoclonal antibody-based therapeutics has been highly successful over the last two decades [15]. Nevertheless, to date only two medical radioimmunoconjugates are approved for routine application in cancer therapy. The best clinical results so far have been achieved for the treatment of chemotherapy-resistant hematological malignancies (lymphomas) with radiolabelled anti-CD20 antibodies (for details see paragraph 3.6.4.2) [16]. Recently, successful clinical studies with neuroendocrine tumours (gliomas) using radiolabelled, somatostatin-analogue peptides were reported [17]. However, treatment of many other tumours so far has been unsuccessful.

1.1.1 Historical Development of Radiation Therapy

Soon after W.C. Röntgen discovered the X-rays in 1895, first attempts have been made to use this energetic radiation for therapy of breast cancer with remarkable success (Emil Grubbe, 1896 [18]). Since then, X-rays were considered to be the magic weapon to heal several kinds of diseases. In 1896 H. Bequerel first observed radioactivity. With the discovery of polonium and radium by the Curies in 1898, the idea of radiation therapy with radioactive sources was born. Starting in 1901, radium was used for therapy of dermatological diseases ("Curie-therapy") and intratumoural cancer therapy ("Brachytherapy" , 1903) [19].

Pioneer work on the use of radiotracers was done by G.C. de Hevesy in 1923, who employed a radiolabelling method to investigate the uptake of radio-lead by plants and, to study metabolistic effects, the distribution of radio-phosphorus in animals (1935) [20]. At the same time, the German chemist and medical doctor P. Ehrlich developed the concept of targeted (chemo-)therapy, involving the synthesis of a toxin-labelled compound which selectively adresses pathogenic agents. This idea of using vector molecules as "magic bullets" ("Zauberkugeln") to deliver drugs, toxins, enzymes or nuclides to the diseased site, leaving unaffected organs untouched, increased the selectivity in therapeutic interventions dramatically and forms the basic principle of targeted radioimmunotherapy as it is applied today.

In the early thirties of the last century, the treatment of leukemia with P-32 was the first therapy applying radionuclides [21]. Historically, in RIT $\beta-$emitters have received the greatest focus. Since already more than 60 years, radioiodine therapy with I-131 is applied for therapy of thyroid cancer (in germany 60.000-70.000 treatments per year). In 2002, the first radiolabelled monoclonal antibody for β-therapy of non-Hodgkins lymphoma (Y-90-mur-anti-CD20, Zevalin®) has been approved by the Food and Drug Administration (FDA), followed by the I-131-labelled anti-CD20 murine antibody Bexxar® in 2003 [22]. Both drugs provide significantly better response rates for B-cell lymphomas compared to the corresponding non-radiolabelled antibody Rituxan® [23]. Excellent clinical outcome with 20-40 % complete remissions and an overall response rate of 60-80 % can be obtained [24, 25, 26].

In 1996, first human trails on the alpha emitting antibody construct Bi-213-CHX-A-DTPA-Hum195 began [27]. However, until today no radiopharmaceutical compounds labelled with α-particle- or Auger-electron emitters are approved yet.

1.2 Interaction of Radiation with Matter

There are mainly four different types of radiation, such being charged particles (α,β, Auger electrons), neutrons, γ-rays and fast electrons (for description of the various decay modes see 7.2 Glossary). While interaction with neutrons is of particular importance for radionuclide production (neutron-capture reactions), only γ-radiation and charged particles are of interest for nuclear medicine, with the latter irradiating tissue volumes with cellular (α), multicellular (β) and subcellular dimensions (Auger e^-), respectively [28].

Charged particles interact with valence electrons of irradiated matter either through excitation or ionisation processes, resulting in radiation induced reactions in the matter and a loss of kinetic energy with respect to the particle. Bremsstrahlung, the interaction with the nucleus, is an additional pathway for energy loss of charged

particles. In general, excitation of electrons is induced when the energy of the incoming particle is smaller then the binding energy, while ionisation is only induced when the energy of the charged particle is higher than the binding energy. The atom is then left with a positive charge.

Especially the high energy α-particles ($\sim$5 MeV) cause several thousands of ionisations per mm in air. In matter, the heavy α-particles only show minimal diversion from their linear ionistaion path (see LET, linear energy transfer, 7.2 Glossary [29]), while the lighter electrons are strongly deflected. When the maximum of ionisation processes is reached at the end of the ionistaion path (Bragg Peak, Fig. 1.1), all kinetic energy is lost and the charge of the α-particle is neutralized [30].

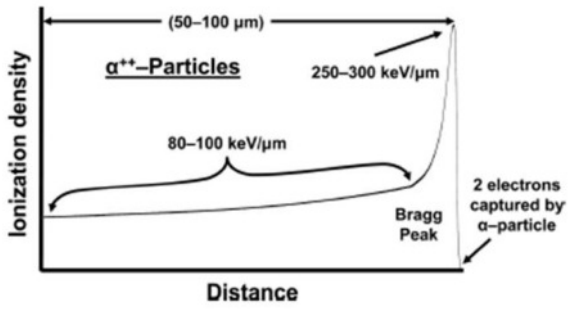

Figure 1.1: A typical Bragg curve for an alpha particle of several MeV of initial energy, showing the ionization density along the path as function of the traversed distance [30].

When γ-radiation interacts with matter it is either scattered or absorbed. For medical application, particularly the Compton scattering of γ-photons in tissue is of interest for imaging purposes.

1.2.1 Biological Effects of Ionising Radiation

Ionising radiation at cancer therapy is being used as external beam radiotherapy, brachytherapy, and targeted therapy with antibodies or other constructs delivering radionuclides to the tumour site. Ionising irradiation deposits energy in the nucleus, which produces single- (SSB) and double-strand breaks (DSB) in DNA. When repaired incorrectly, these DSBs lead to chromosomal aberrations which are eventually lethal for the cell. In addition, radiation induces damage in the cell membrane, which can also activate cell death pathways [31].

Depending on the time of exposure, ionising radiation initiates different biological effects, which can be categorised as radiochemical, biochemical and biological effects. Within approximately 1 µs the formation of (bio)radicals begins (radiochemical effect), followed by alteration of biological structures and cell membranes within the next seconds and minutes (biochemical effect). The fatal biological effects like apoptosis, cell death and genetic mutations become noticable after hours up to years.

The majority of radiation-induced alterations are modifications of the DNA bases. Most of the damage can be repaired by the cells. However, radiation with high LET (α, Auger-e^-) induces a high number of ionisation events within a short distance and therefore causes serious clustered DNA-strand breaks [32]. If two single strand breaks are spaced less than 14 bases apart, a DNA-double strand break is formed which cannot be effectively repaired [33]. Like this, the passage of one high

LET $\alpha-$particle can lead to cell death, while 1,000-10,000 times more of low LET $\beta-$particles are required to produce similar effects [34].

1.3 Targeted Radiotherapy

Any kind of radiation used to kill cancerous cells is difficult to aim and can thus have an adverse effect on surrounding healthy tissue. By utilisation of biomolecules, which are bond onto or internalised into the tumour cells, it is possible to deliver the attached radioactivity directly and solely to cancerous cells [34, 35]. The principle of targeted radiotherapy is thus the selective targeting of malignant cells, using tumour specific monoclonal antibodies (mAbs) or peptides with high tumour affinity which are labelled with a particle-emitting radionuclide [36]. These very selective and efficient carrier molecules are able to deliver a highly cytotoxic radiation dose to the targeted cells. Generally, a typical radioconjugate consists of three main components, being the tumour selective vector (e.g. mAb), the therapeutic radionuclide with the desired physical properties (e.g. Ac-225) and a chelator linking the two (e.g. DOTA, Fig. 1.2). The optimal linker should provide a stable linkage in circulation but degrade under specific conditions to facilitate excretion. Over all, the resulting radioimmunoconjugate (RIC) and especially the attached radiometal complex should display high stability and kinetic inertness in order to avoid release of the radionuclide as free metal cation under the challenge of human catabolism [37].

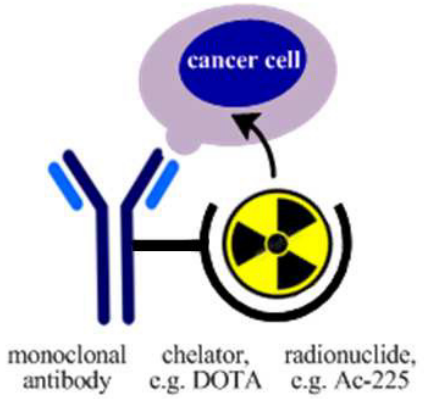

Figure 1.2: Principle of a radioimmunoconjugate (RIC) for targeted radiotherapy.

1.3.1 Radionuclides for Radiotherapy

For successful radiotherapy, the delivery of a high radiation dose to the tumour cells and a low dose to healthy tissue is crucial. The choice of radionuclide should therefore ideally be influenced by clinical parameters such as tumour location and uptake, size, morphology, physiology and radiosensitivity, as well as rapid blood clearance of the radionuclide. Also the receptor sites in tumours are typically limited in number, which requires that the chosen radionuclide has a high specific activity (for definition of the specific activity SA see 7.2 Glossary). In general, the choice of appropriate therapeutic nuclides is usually based on weighing of biological effectiveness, chemical properties and economical factors [38, 39]. For being applicable, the radionuclides hence need to meet certain requirements (modified from [40]) :

1. The radionuclide should emit particulate radiation such as α- or β-particles or Auger electrons which are excepted to cause high cytotoxicity. At the same time the decay energy should be deposited only locally at the tumour site. Additionally, undesirable high-energy γ- radiation, which would cause whole-body irradiation, needs to be kept as small as possible. However, to a certain extent,

low-energy γ-emission (100 - 200 keV) accompanying alpha or beta emissions can be advantageous for medical imaging and dosimetry purposes after administration of the drug.

2. The physical half-life of the radionuclide should match the biological half-life of the pharmaceutical radioconjugate for which it is intended to be used. An overly long physical half-life increases the amount of radionuclides that need to be delivered to the tumour to achieve therapeutic levels of decays before the drug is excreted. At the same time, increased toxicity will result from the persistent decay of the long-lived nuclide if it is lost from the conjugate or if the conjugate is not cleared from the body soon after the treatment. On the other hand, a short half-life is only advantageous when the cancer cells are immediately accessible, while an extremely short half-life would not even allow enough time for labelling and targeting. This would result in the majority of the decays occurring either before administration of the drug or outside of the tumour in healthy, sensitive tissues, e.g the bone marrow. The most suitable physical half-lifes for targeting of disseminated cells range from hours to days and from days to weeks for achieving significant uptake in solid tumours [41]. As a rule of thumb, the physical half-life of a radionuclide should be 1.5 - 3 times longer than the time that it takes its radioimmunoconjugate to reach the peak target uptake. Usually a half-life of 1 to 14 days is regarded as optimal for both achieving high specific activities during labeling and good therapeutic efficiency as well as for facilitating of a centralised radionuclide production and worldwide distribution strategy [42].

3. The chemical properties of the radionuclides should allow for rapid high-yield labelling with high specific activities. Ideally the labelling should work under mild conditions, leading to a thermodynamically and kinetically stable radioconjugate which is expected to be catabolised rapidly without accumulating in healthy organs or tissue.

4. When selecting appropriate nuclides, the daughter nuclides must also been taken into account since they have different chemical properties than the mother and therefore may be metabolised differently from the parent isotope. This is particularly important if the daughters are long-lived and/or bone seeking.

5. For routine clinical use, the radionuclides should be readily available in high quality and allow for cost efficient production in large scales [43]. Especially radionuclides close to the line of stability in the nuclide chart are easy to produce by direct nuclear reactions. Several reactor-, accelerator- and generator-based production methods are applied today to meet the increasing demand for therapeutic radionuclides. Their radiochemical purity always needs to be sufficient and reproducible, as trace amounts of other radionuclides can affect the radiolabelling and radiochemical purity of the radiopharmaceutical. Other impurities such as trace metal contaminants must also be minimised as they often compete with the radionuclide for complex formation [44].

An overview of the most commonly studied radionuclides for medical application is given in Table 1.1.

It has been shown that each of the classes of particle emitting radionuclides can only be used in an optimal way for tumours of a certain size, which is due to the

Table 1.1: Overview of radionuclides which are commonly applied in radiotherapy and nuclear imaging (data derived from [45]).

Nuclide	***Emission energy [MeV]***	$t_{\frac{1}{2}}$	***Nuclide***	***Emission energy [MeV]***	$t_{\frac{1}{2}}$
Imaging (γ)			***Therapy (α)***		
Tc-99m	0.142	6.01 h	At-211	5.980	7.21 h
In-111	0.173, 0.247	2.805 d	Bi-212	6.051	1.009 h
Imaging (β^+)			Bi-213	8.537	0.8 h
Cu-64	1.675	12.701 h	Ac-225	5.3-5.8	10.0 d
As-72	1.17	1.1 d	***Therapy (β)***		
Y-86	1.479	14.7 h	Cu-67	0.58	2.58 d
Zr-89	0.9	3.27 d	As-77	0.226	1.6 d
I-124	1.53	4.18 d	Y-90	2.282	2.67 d
Therapy (Auger)			I-131	0.606	8.04 d
In-111	0.86	2.805 d	Lu-177	0.497	6.75 d
I-123	1.234	13.2 h	Re-186	0.973	3.78 d
I-125	0.179	60.1 d	Re-188	2.118	16.94 h

characteristic behaviour of the respective particles in tissue. The type of particle emitted is directly related to the tissue penetration and cell killing ability of the radionuclide [46]. Radionuclides which emit high-energy beta particles are especially suitable for treatment of large and bulky tumours.

The β-particles have a longe range in tissue (0.5 - 12 mm, corresponding to several 100 cell diameters) which allows for better penetration and irradiation of the tumour. Also the emitted particles do not travel along linear tracks but show a so-called crossfire effect, which creates a field effect and, within the emission path length, also affects cells in the vicinity of the targeted cells (Fig. 1.3). This is particularly favourable for the treatment of solid tumours [47, 48]. Like this, beta particles are able to overcome possible tumour heterogeneity and increase the therapeutic effectiveness [49]. Inside the cell nucleus of tumour cells mostly only DNA single strand breaks (SSBs) are induced. Since the range of high-energy β-particles is several mm, β-emitters are not applicable to e.g. micrometastases or leukemia. The major part of their energy is not deposited immediately along the emission track but at some distance from the actual decay event; therefore it is likely that most of the decay energy is deposited outside of the tumour cells. At the same time, cellular internalisation is unnecessary and targeting close to or at the cell membrane is sufficient; also not every cell needs to be targeted. However, this also means, that damage to healthy tissue is always an issue associated with the use of beta emitters [37], which is especially critical when resulting in life-threatening bone marrow suppression from bystander cell kill of bone seeking radionuclides as in the case of Y-90 therapy [50, 51].

Radionuclides emitting low energy β-particles such as Cu-67 and I-131 are considered to be options for treatment of small tumour deposits or even single disseminated tumour cells [52]. However, since a comparatively large amount of radionuclides per cell is needed when low-energy β-particles are used, preference is given to α-emitters where fewer radionulides per cell are sufficient [53].

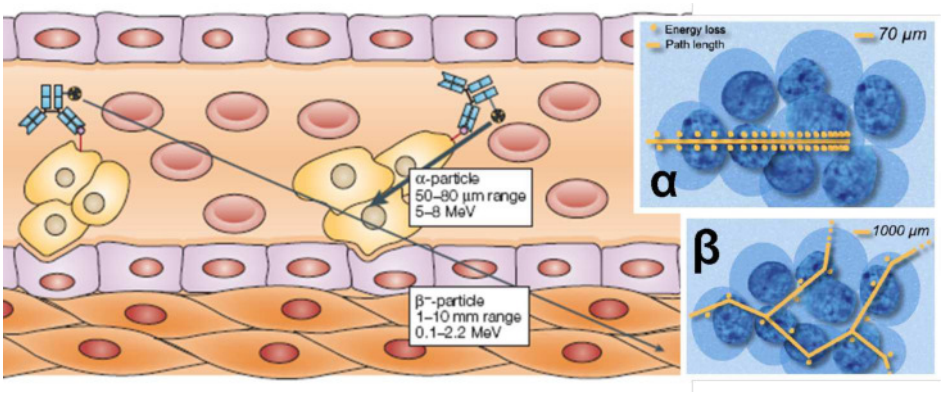

Figure 1.3: The short path length of $\alpha-$particles compared to the longer path length of $\beta-$particles [54]. Due to their greater mass and charge, the energy deposited per unit path length in tissue is far higher for $\alpha-$particles (high LET,$\sim$100 keV/µm up to $\sim$300 keV/µm at the end of the track, *top*) than for $\beta-$particles (low LET, 0.2 keV/µm, *bottom*) [47].

Alpha-emitting nuclides are useful for therapy of small and disseminated, single tumour cells since they have a high linear energy transfer and short range in tissue (2 - 4 cell diameters, Fig. 1.3) [55, 27, 56, 57, 58]. The decay energy is hence deposited locally and on a short distance, which causes dense ionisation along the tracks of the α-particles. Since the distance between two ionisations is almost the same as the distance between two strands of DNA, alpha radiation results in predominantly non-repairable, clustered DNA double strand breaks (DSBs) inside the tumour cell nucleus which in the following induce cell death pathways, mostly apoptosis [31, 42]. Like that, even at low dose rates individual tumour cells can be effectively sterilized with possibly only a single α-partcile [34]. Radionuclides emitting $\alpha-$particles display cytotoxicity which is $>$100 times higher than of $\beta-$particles [59] and are able to break β /γ- radiation- as well as chemoresistence [13]. However, most α-emitters have short half-lifes which complicates their production and use for labelling. The concept of applying longer lived "*in vivo* nanogenerator" nuclides such as Ac-225 or Th-227, which produce cascades of several α-particles emitted almost simultaneously at the decay site (see paragraph 3.7.2.), seems to be a promising way to facilitate the production and logistics of this therapeutically very attractive radionuclides [60, 61, 47].

Also the low-energy Auger electrons are considered to be suitable for treatment of single and spread tumour cells [62, 63]. Auger electrons are extremely radiotoxic and cause severe damage if their track hits the DNA. However, the major challenge remains the short range of energy deposition, which is usually in the submicrometre range ($<$0.6 µm), corresponding to less than one cell diametre. Since Auger electrons are not able to traverse a cell nucleus, Auger-emitters have only local effect and are merely therapeutically usefull if they can be internalised into the cell DNA, permitting the decay to occur in close proximity to the double strands [45, 64]. DNA-intercalators like cis-diamminedichlororplatinum(II) ("cisplatin") were suggested for delivery of Auger-electron emitting platinum nuclides [65, 66]. When labelled with radioisotopes of platinum (Pt-191, Pt-193m and Pt-195m), the large number of Auger-electrons in their decay (up to 35 electrons) will result in high probability for DSBs.

The main characteristics of the discussed charged particles are listed in Table 1.2.

Table 1.2: Summary of the characteristic properties of charged particles applicable for radiotherapy.

Property	α	β	***Auger - e^-***
engery	$4-9\,MeV$	$0.1-2.5\,MeV$	$1-15\,keV$
range in tissue [µm]	$30-110$	$150-13500$	$0.04-0.6$
corresp. cell diameters	$1-10$	$10-1000$	$\ll 1$
typical diameters	*cell nucleus* : $5-20\,\mu m$	*tumour cell* : $10-30\,\mu m$	DNA : $2\,nm$
LET [keV/µm]	$80-130$	$0.2-0.7$	$4-26$
effect	$DNA-DSBs$	$DNA-SSBs$, $crossfire$	$severe\ DNA-DSBs$

To achieve high therapeutic effectiveness of a radioconjugate, each of the three types of radionuclide emitters needs to be coupled to a particular carrier matching their special characteristics. The most commonly used vector molecules are antibodies and peptides, with the latter showing significantly better tumour penetration and blood clearance. To construct radioconjugates with ideal therapeutic effectiveness, a peptide should rather be labelled with short-lived β- or Auger electron-emitters to treat solid tumours in which the peptide can be internalised. For longer-lived α-emitters, antibodies are suitable carriers since they remain in circulation for a long time before being excreted, which makes them attractive for systemic administration. If a full-length antibody which has slow tumour penetration, is labelled with a short-lived radionuclide, it is likely that most of it has decayed before the antibody conjugate sufficiently accumulates in the tumour. The following Table 1.3 summarises the suitable particle - carrier combinations for the respective treatment modalities; selection on the basis of size and presentation of the disease is crucial [54].

Table 1.3: Guideline for the buildup of radioconjugates matching the specific therapeutic needs.

Systemic administration				
particle	***properties***	***carrier***	***properties***	***tumour***
α	high LET, short range, long $t_{\frac{1}{2}}$	antibody	remains in circulation	small, metastases
Locoregional administration				
particle	***properties***	***carrier***	***properties***	***tumour***
α	high LET, short range, short/long $t_{\frac{1}{2}}$	peptide	tumour penetration	small
β	cross-fire, long range, short/long $t_{\frac{1}{2}}$	peptide	tumour penetration	solid, heterogeneous
Auger electron	short range	peptide / fragment	tumour penetration, internalization	small

In conclusion, alpha particle emitting radionuclides remain the most promising approach for treatment of disseminated, metastasised tumours and can readily offer potent, single cell kill without severe cytotoxicity to healthy tissue. Linked to targeting biomolecules, the *in vivo* nanogenerator Ac-225 which emits 4 α-particles is

considered as suitable nuclide with excellent properties for therapy of these types of diseases and is hence subject of this work.

1.3.2 Targeted Alpha Therapy with Ac-225

Targeted Alpha Therapy (TAT) provides specifically localized, internal radiotherapy using alpha particle emitting radionuclides linked to vectors with specific tumour cell binding properties. At present, radioimmunoconjugates labelled with the $\alpha-$emitters Bi-212, Bi-213 and At-211 are being actively studied [67] but also Ac-225 has shown promise as therapeutic nuclide [3, 55, 68, 1].

For TAT applications with Ac-225, the metal cation must be linked to a monoclonal antibody (mAb) or immunoprotein through a suitable bifunctional chelating agent. Limiting factor, however, for the application of Ac-225 is the availability of a chelating agent which is able to stably bind this radionuclide as well as its daughters [69, 70]. Furthermore, the chelator must be able to withstand the immense recoil energy of α-particles, which, with 100 - 200 keV, is higher than the binding energy of macrocyclic metal ion complexes (for an estimation of the recoil energy of the Ac-225 decay see 7.2 Glossary) [34, 71].

At physiological pH, the therapeutic Ac-225 complex must show high thermodynamic stability ($\log K > 19$) and high kinetic stability over days and weeks in order to minimise any release of the cytotoxic isotope. One method to achieve increased stability of a metal complex is to "trap" the radiometal in a rigid ligand cage, which slows down the complex dissociation kinetics drastically. Because of this, rigid polyamino-carboxyl ligands such as EDTA, DTPA and DOTA, also known as complexones, were suggested as suitable ligands for medical application. Comparison of the thermodynamic stability constants of these ligands allows a first assessment of the most suitable radionuclide complexes for TAT [2].

1.4 Radiopharmaceutical Aspects

1.4.1 Radiopharmaceuticals

Radiopharmaceuticals are drugs, mostly based on small organic compounds (peptides) or macromolecules (antibodies), which are not stoichiometrically labelled with a defined amount of radionuclides. They specifically accumulate in the targeted tissue and enable, with respect to the properties of the nuclide, radioimaging ($\gamma-$and β^+-emitters for SPECT and PET) or localised radiotherapy ($\alpha-$, $\beta-$, Auger-e^--emitters). Diagnostic radiopharmaceuticals are not intended to have pharmacological effects and, since only trace amounts of the drug are administered ($10^{-6}-10^{-8}$M [44]), they also induce no side effects. The effects of therapeutical radiopharmaceuticals depend on the radiation properties of the radionuclide. Especially for therapeutic applications the specific activity of the administred radioconjugate is important and should be high. This is because in radioconjugate preparations there is always a certain amount of unlabelled compound present, which does not contribute to the radiation-induced cytotoxicity but is likely to successfully compete with the more effective labelled compound for the receptors on tumour cells [38].

The cyctotoxic efficiency of radiopharmaceuticals depends on the kinetics of target localisation and retention of the radionuclide. Another factor is the radiation sensitivity of the target cell compared to sensitive healthy cells. Most cytotoxic agents

used for chemo- or radiation therapy have a low so-called therapeutic index (benefit vs. risk), which means that the maximum tumour cell killing dose can also damage healthy cells [44, 72]. It is expected that the use of antibodies as "magic bullets" enhances the therapeutic index due to their selective localisation. For example, with Zevalin® it was demonstrated that the delivery of radiation to radiosensitive lymphoma cells was nearly 1000-fold increased over the delivery to normal tissue [73]. Incited by the good clinical results of these antibody-based drugs, the research conducted in the ITU's alpha immunothearpy action focusses not only on developement and further implementation of radiopharmaceuticals based on the peptides DOTATOC and DOTA-Substance P, but also on the design and optimisation of radiopharmaceuticals bases on antibodies, e.g. DOTA-rituximab, as investigated in the present work.

1.4.2 Administration of the Radiopharmaceuticals

To avoid non-specific irradiation of healthy tissues, it is necessary for the carrier biomolecule to identify accessible tumour targets easily and rapidly [47]. Unfortunately, access to the tumour is one of the big challenges in RIT since tumours produce a quite chaotic vascular system in which blood flow is slow, can be interrupted or even reversed. Not all tissue cells are connected to blood vessels, which was however found to be crucial for successful RIT treatment since antibodies mostly localise along the blood vessels. Hence, there are areas of the tumour which are relatively resistant to radiation therapy and therefore reduce the efficacy of RIT [74, 75, 76].

In general, the distribution of a radiopharmaceutical in a targeted solid tumour is inhomogeneous. This is mainly due to the inability of the radiolabelled molecules to evenly penetrate the tumour mass or due to differences in specific binding-site density of individual tumour cells. Here, the use of fragmented antibodies might open up a faster way for infiltration of solid tumours.

Generally there are different ways to deliver therapeutic radiation doses, such being external beam irradiation, implantable "seeds" and locoregional - or systemic administration via intravenous injection, respectively (Fig. 1.4). Until today, the last two became the most commonly used approaches for clinical radiotherapy [77, 78, 79, 44].

Local TAT requires lower activity than systemic TAT to achieve comparable efficacy, which is because the antibody- or peptide-conjugate can easily diffuse between cancer cells after local administration. According to the time required for tumour targeting, long-lived alpha emitters are better suited for systemic application than short-lived, which are more effective in a locoregional approach [80]. Systemic therapy efficacy depends on vascular supply to the disease site, the half-life of the alpha emitting radioisotope, the diffusion rate of the targeting vector and the dilution of the dose by the blood volume. However, systemic administration is ideal for targeting blood-borne cancers, which are disseminated and highly accessible [45]. An example for the more effective locoregional approach is the treatment of brain tumours. The drug is applied through an implanted reservoir system or catheter, since especially in the case of brain tumours the blood-brain-barrier greatly restricts access of large molecules such as antibodies through systemic administration (Fig. 1.4) [81, 82].

A major limitation to a more general application of RIT is the irradiation of healthy tissue by the radio-mAb-conjugate. Therefore, RIT is especially limited by

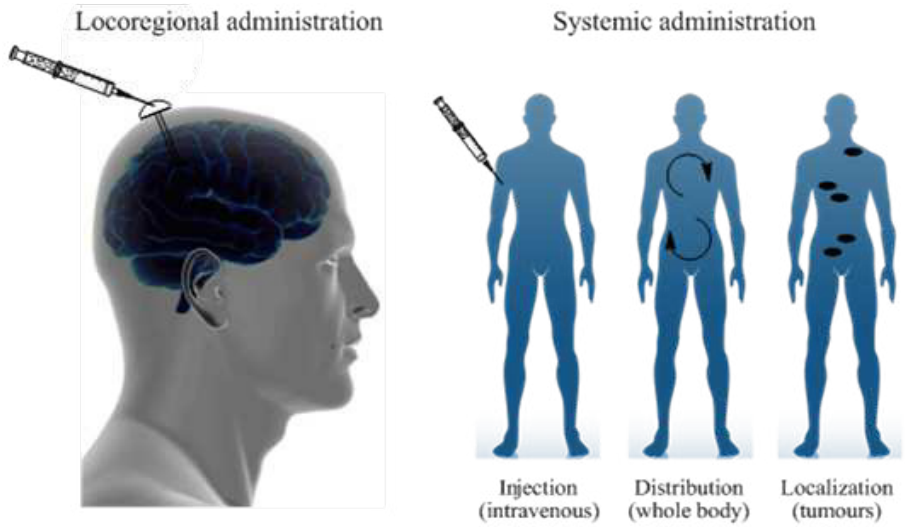

Figure 1.4: *left*: Locoregional drug administration for the treatment of brain tumours; *right*: Systemic administration of target-specific radiopharmaceuticals allows treatment of disseminated, metastatic tumours.

the absorbed dose to the radiosensitive bone marrow [83, 21]. Due to physiological barriers, targeting, uptake and blood clearance of antibodies is often too slow. For instance, tumour uptake with systemically administered IgG molecules often reaches a maximum only after one or two days. With exception of antibodies targeting leukaemia, most (> 99 %) of the injected antibody therefore remains circulating in the blood or is not associated with the target tumour. This prolonged circulation time of untargeted antibodies is usually in the range of days or weeks and results in increased radiation exposure of catabolising organs (liver and kidneys)[14]. For such a systemic approach long-lived nuclides are more suitable, because a larger fraction will be excreted before most of them have decayed [70].

1.4.3 Development of Radiophamaceuticals

After conducting the first prosperous radiochemical labelling experiments it usually takes several years until a new radiopharmaceutical drug is approved for routine application in clinical therapy. A number of preclincal *in vitro* (stability of radioconjugates under physiological conditions; immunoreactivity, binding affinity, internalisation, cytotoxicity), *in vivo* (animals: stability of radioconjugates in a living organism; biodistribution, tumour/healthy organ uptake, identification of dose-limiting organs, maximum tolerated dose; extrapolation to the human organism) and clinical patient studies (phase I-IV) need to be conducted and finalised successfully. The most advanced radiopharmaceutical drug is Alpharadin® (radium-223 chloride, $t_{\frac{1}{2}} = 11.4$ d, cascade of 4 $\alpha-$particles), which is used for therapy of prostate cancer and bone metastases and is currently tested in phase III studies [84, 85, 86].

Most therapeutical α-labelled radioconjugates used in targeted radiotherapy are currently in phase II studies. The work presented in this PhD thesis aims on the optimisation of the radiochemical synthesis of Ac-225-labelled rituximab, followed by *in vitro* evaluation of the radioimmunoconjugate. This project contributes to the preclinical *in vitro* studies required to take the research on Ac-225-labelled antibodies for therapy of Non-Hodgkins-Lymphoma to the next level.

2 Scope and Motivation

The successful application of α-emitters in radioimmunotherapy goes together with developments in radionuclide production and labelling chemistry. Especially profound understanding of the coordination chemistry of the respective metal ion-ligand system is of major importance to develop protocols for the synthesis of radioimmunoconjugates and to predict the fate of radionuclides *in vivo*.

The scope of the presented work is the experimental characterisation and evaluation of 1,4,7,10-tetraazacyclododecane-1,4,7,10-tetraacetic acid (DOTA) as a suitable chelator for trivalent actinides (An(III)), particularly in terms of stable binding of the long-lived alpha emitting radionuclide Ac-225 to biomolecules for safe application in RIT. The project includes not only basic studies to contribute to a better understanding of the complexation mechanisms and kinetics, but, based on these findings, is aimed at the development of a robust labelling protocol for facile and effective synthesis of an Ac-225-DOTA-CD20-antibody conjugate. In the course of the investigations, focus is set on *in vitro* testing of the obtained radioimmunoconjugate, in particular the evaluation of the kinetic stability in presence of competing agents as well as in human blood serum. Assessment of the antigen binding affinity of the antibody conjugate completes the work.

The protocol for the design and synthesis of Ac-225 radiopharmaceuticals of McDevitt *et al* provided the starting point for this study [6]. This research group developed a synthetic scheme to radiolabel DOTA-proteins with Ac-225. Later, the protocol was applied to antibodies in form of a two-step synthesis, with the first step being the Ac-225 DOTA-Bn-NCS complexation, followed by the coupling of the Ac-225-DOTA-Bn-NCS to the mAb. The idea behind this two-step approach was that, when the complexation of Ac(III) with DOTA is conducted at elevated temperatures and basic pH (first step), presumably a more stable complex is formed. However, since higher temperature/pH are known to have a negative effect on the antibody efficiency, the conjugation to the biomolecule can hence only be conducted at lower temperatures in a second step. This two-step synthesis though suffers from yields below 10 %, which is assumed to be due to the competing hydrolysis reaction of the isothiocyanate moiety occurring at the pH used during the complexation step [87]. This makes the labelling protocol an interesting subject for further studies on how this synthesis can be improved.

From the findings of McDevitt *et al* it was apparent that a number of variables needed to be investigated in order to improve on the low efficiency of the protocol. These studies were conducted previously and are summarised in the Diploma Thesis, S. Kannengießer, 2009 [7]. A one-step synthesis protocol was tested and the labelling yields for Ac-225 were found to be dependent on temperature and especially on the pH of the reaction mixture. Eventually, an optimised protocol for radiolabelling of DOTA-peptides and MabThera® with Ac-225 activities up to 2 µCi (= 74 kBq) per 100 µg mAb was established, offering labelling yields > 95 %. The present work now aims on translation of the developed synthesis protocol to higher specific activities of clinical relevance ($\geq$ 10 µCi ($\geq$ 370 kBq) per 100 µg mAb).

To gain profound knowledge about the complexation reaction mechanism and the thermodynamic and kinetic properties of the An(III)-DOTA system, the coordination chemistry was initially studied by means of time resolved laser fluorescence spectroscopy (TRLFS). Since Ac(III) has no suitable spectroscopic properties, the metal ion complexation by DOTA was investigated with Cm(III) as substitute for the trivalent actinides. Besides determination of the kinetic rate constants and thermodynamic parameters (log K, $\Delta_R G$) at labelling-relevant temperatures up to 90 °C, attention was also paid to the detection of possible intermediate species which are frequently discussed in the literature [11].

TRLFS is a powerful speciation method which makes use of the excellent fluorescence properties of Eu(III) and Cm(III), both regarded as good representatives for trivalent lanthanides and actinides. With TRLFS it is possible to detect and characterise complex species in sub-micromolar concentrations without influencing the chemical equilibrium of the system. For temperatures of 45 to 90 °C, measurements with fixed metal-to-ligand ratios at different pH were conducted to identify the complex species and quantify their relative ratios by means of peak deconvolution. Based on the potentiometrically determined $pK_{a,n}$ values for DOTA in the respective temperature range, from these ratios the conditional thermodynamic complex stability constants log K of [Cm(III)DOTA]$^-$ were calculated. Application of the van't Hoff law allowed for extrapolation of the log K at 25 °C. Identification and further characterisation of the involved complex species was done by comparison of the fluorescence lifetimes, which give information about the first coordination sphere of the metal cation. A comparable study on [Eu(III)DOTA]$^-$ has been reported before [8, 9, 10].

Furthermore, additional investigations with NMR were executed to identify and understand the mechanism related to the complex formation with DOTA-Bn-NCS. Based on the results of the NMR study, the complexation kinetics of DOTA and DOTA-Bn-NCS were further investigated and compared to gain insight into the involved reaction mechanisms.

Proper understanding and interpretation of the thermodynamic behaviour of the Cm(III)-DOTA complex formation allowed for facile translation of the experimental settings to the Ac(III)-DOTA system. Since no spectroscopic methods are available for this system, Chelex cation exchange resin as well as Instant Thin Layer Chromatography (ITLC) were chosen as radiochemical speciation methods and were evaluated for their feasability. Determination and refinement of the stability constant log K of [Ac(III)DOTA]$^-$ for the temperature range of 25 to 90 °C was done in analogy to the Cm(III)-DOTA system. To obtain reliable results, the protocol for the radiochemical separation of Ac-225 from Ra-225 required optimisation to ensure highest purity and quality of the radionuclide.

Subsequently, the studies on the Ac-225-labelling of DOTA-Bn-NCS-MabThera® were continued. The previously established protocol was modified and further optimised in order to be applicable for facile clinical synthesis of radioimmunoconjugates with higher specific activities (SA) within $\leq$20 min. In this regard, the antibody labelling kinetics were reviewed respective reaction temperature and ideal pH of the high-yield radiolabelling, which permitted further improvement of the labelling effectiveness (pH 9; 37 - 42 °C; 5 - 15 min; ave. yields 94 - 96 %, $>$ 98 % RCP after purification). The protocol was successfully evaluated for reliability with SA up to 50 µCi (= 1.85 MBq) per 100 µg mAb. The obtained radioconjugates were assessed

for their kinetic stability in different buffers as well as under physiologicgal conditions in human blood serum and proved to be satisfyingly stable over up to 30 days.

Finally, a preliminary radiobiological study with cancer cells (K422 cell line, B-cell lymphoma) was conducted to determine the antigen binding affinity of the radiolabelled CD20-antibody (SA = 1µCi (= 37 kBq)/100µg mAb; B_{max} = 8.88 nM; K_d = 52.55 nM). The results give rise to further preclinical *in vitro* studies.

For recapitulation, in the following flowchart the successive experimental steps undertaken in the present PhD study are outlined:

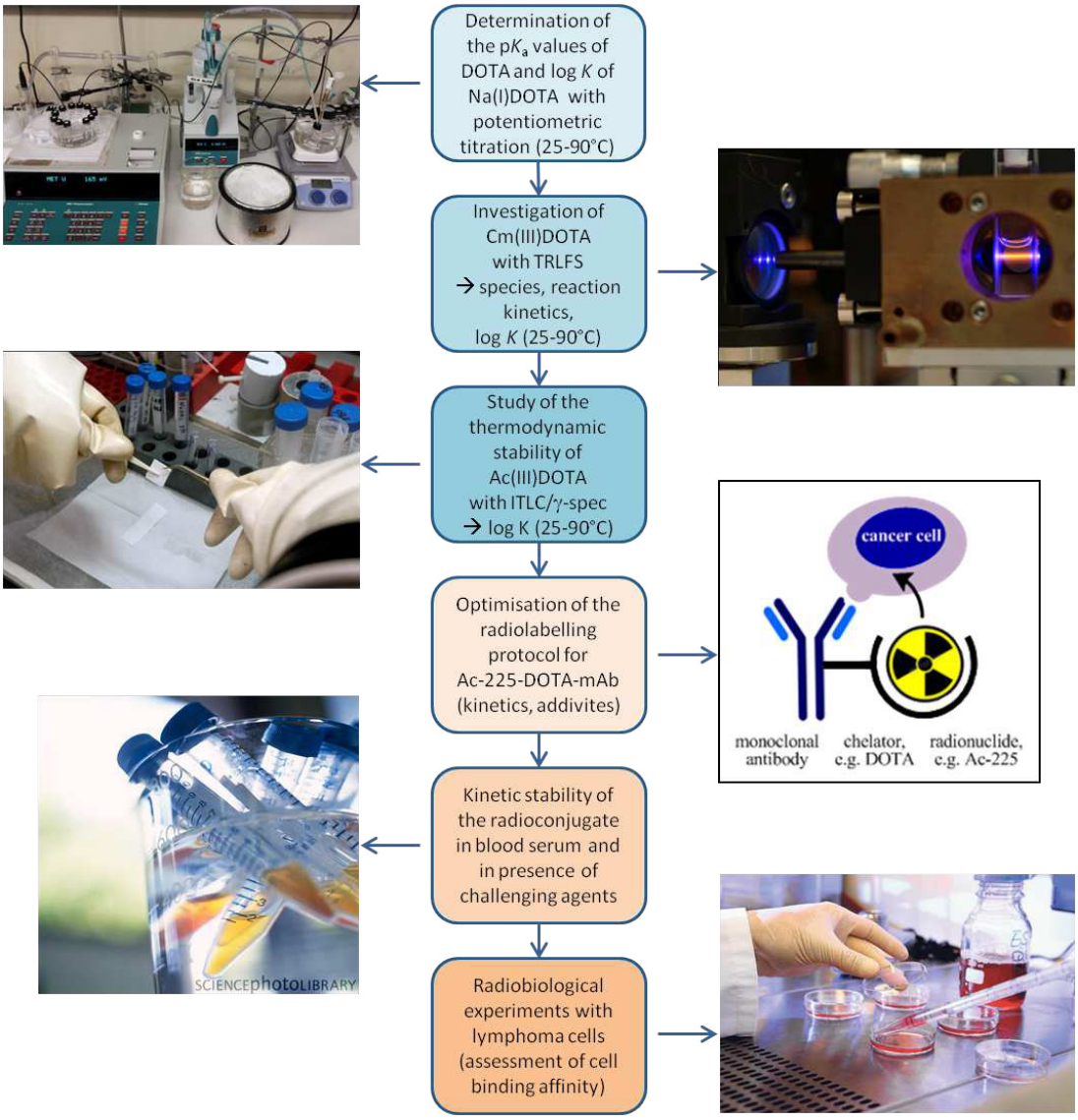

In summary, it is demonstrated in this work that high-yield radiolabelling of DOTA-chelated mAbs is possible by chosing appropriate reaction conditions which seem to preserve the integrity of the antibody and still result in thermodynamically and kinetically stable radioimmunoconjugates with high specific activities suitable for TAT.

3 Knowledge

3.1 Chemistry of the f-Elements

The series of the f-elements comprise the lanthanide (4f) and actinide (5f) elements. The two eponymous elements lanthanum and actinium are actual members of the third side group of the PSE and are, strictly speaking, no lanthanide or actinide elements. However, according to the definition that the two series encompass all elements that have chemical properties attributable to the presence of low-lying 6/7p, 5/6d and 4/5f orbitals, with the tripositive cations having the electronic configuration $6/7p^0$ $5/6d^0$ and $4/5f^n$ (n = 0, 1,...14), Ac and La are commonly included [88]. While the majority of lanthanides has stable nuclides, all actinide elements are radioactive. The elements thorium, protactinium and uranium occur naturally, while the transuranium elements are synthesised in reactors, e.g. neptunium to curium by neutron capture reactions (n, γ).

3.1.1 Oxidation States

Contrary to the lanthanide elements, which mostly appear as Ln^{3+}, there are many possible oxidation states known for actinide elements in solution, with the lighter actinides showing a great variety of stable oxidation states (Fig. 3.1). However, the oxidation state 3+ (electron configuration $f^n d^0 s^0$) is generally the most favoured, especially with actinium and the heavier actinide elements starting from curium, which will only occur as trivalent aquo ions $An(H_2O)_9^{3+}$in aqueous solution [89]. An exception from this behaviour is Nobelium, for which the 2+ state is energetically stabilised due to the closed 5f shell.

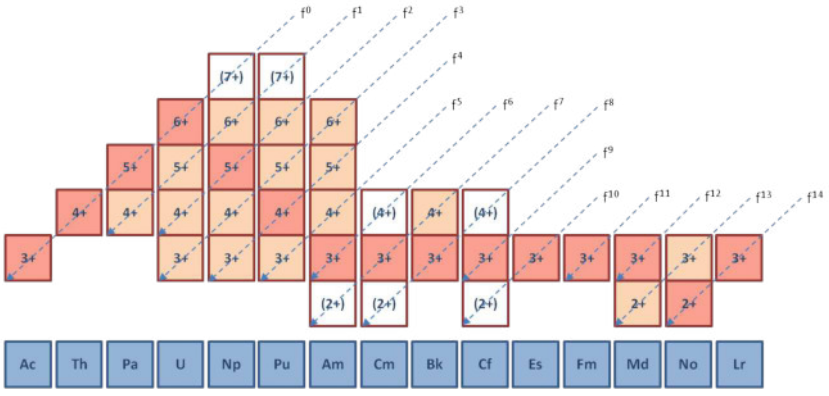

Figure 3.1: Known oxidation states of the actinide elements. Red squares: most stable oxidation states. Modified from [90].

In general, the f-electrons are inner electrons, which are effectively shielded by the outer s- and p-electrons of the next higher full shell. This effect is more pronounced for the lanthanides (4f) than for the actinides (5f). For f^n configurations with $n \leq 6$, a lower energy is required for the promotion of a 5f electron to a 6d orbital (actinides)

than it is needed to promote a 4f electron to a 5d orbital (lanthanides). This is the reason for the high electrochemical stability of the higher oxidation states of many lighter actinides, while the lanthanides favour the oxidation state 3+. The reverse is the case for f^n systems with $n \geq 7$. Here the energy needed for the promotion of a 5f electron to a 6d orbital is higher than for the 4f $\rightarrow$ 5d transition. This results in relatively low electrochemical stability of the heavier actinides in high oxidation states. The heavier actinides therefore prefer the oxidation state 3+, as it is found for the lanthanide elements in solution [91].

The reason for this trend is what is referred to as the lanthanide and actinide contraction [94]. The f-electrons are located near the nucleus and therefore they reduce both the energy and the spatial extent of the wave function. Due to this contraction of the f-orbitals, there is a systematic decrease of the ion radii with increasing atomic number (Fig. 3.2). At the same time, the energy difference between the f-orbital and the higher d- and s-orbitals increases. Therefore, the electron transition for reaching higher oxidation states becomes more difficult.

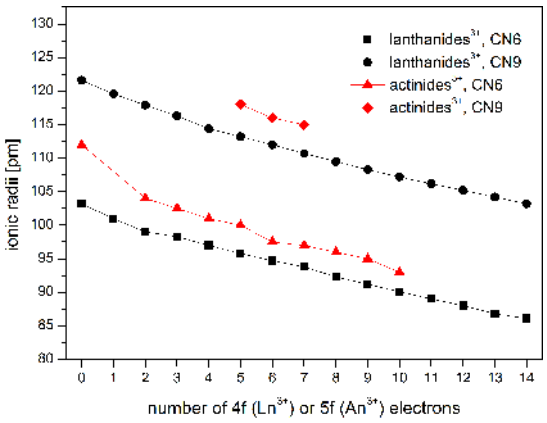

Figure 3.2: Systematic decrease of the ionic radii of trivalent actinide and lanthanide ions for coordination numbers 6 and 9 ("lanthanide/actinide contraction") [92, 93].

For the actinides it follows that with increasing atomic number the spatial extent of the 5f orbitals decreases: Hence the chemistry of actinides from $Z \geq 95$ (Am) is comparable to the chemistry of the lanthanides.

3.1.2 Coordination Chemistry of f-Elements

Trivalent actinides and lanthanides are small ions with high ionic charge and are hence difficult to polarise. They are categorised as hard acids (Pearson HSAB concept) and therefore form strong complexes with naturally occuring inorganic ligands, with the strength of complexation decreasing in the row:

$$CO_3^{2-} > OH^- > F^- > PO_4^{3-},\ SO_4^{2-} > NO_3^-,\ Cl^-,\ (ClO_4^-)\ .$$

Since ClO_4^- is classified as non-coordinating ligand and hence does not influence the spectroscopical behaviour of Cm(III), in the present work the TRLFS studies were conducted in perchloric acid media, employing $NaClO_4^-$ as background electrolyte.

The inner f-electrons of the lanthanides and actinides are normally not involved in chemical bonding, although the weaker shielding of the actinide 5f electrons in contrast to the lanthanide 4f electrons would allow their participation in covalent bonds. Therefore, the interactions between Ln(III) and An(III) cations with organic ligands, preferably with hard donors such as amine-N and carboxylate-O, are predominantly ionic with small covalent contribution in case of the actinides [94, 95]. As long as there are no stronger ligands present, the aqueous coordination chemistry of An(III)/Ln(III) is dominated by hydrolysis, as OH^- is one of the strongest ligand

for these metal cations [96]. Hydrolysis becomes relevant at pH $\geq$ 6 , which e.g. largely constrains the spectroscopic application of Cm^{3+} to the acid pH region.

In complexes of transition metals, covalency and ligand field effects are important factors contributing to the thermodynamic stability of the complexes. Opposed to that, actinide and lanthanide complexes are in general kinetically labile since their bonds have only low covalency. In ionic bonds, the bond strength and thus the strength of the complexes is directly related to the effective charge density of the metal cation. For actinides, if steric effects are of no influence, with a given ligand the complex stability usually increases in the following order (the ions Na^+ and Ca^{2+} are included for comparison) [97, 94]:

	$Na^+ <<$	$Ca^{2+} <$	$AnO_2^+ <$	$An^{3+} \leq$	$AnO_2^{2+} <$	An^{4+}
oxidation state :	+I	+II	+V	+III	+VI	+IV
effective ionic charge :	+1.0	+2.0	+2.2±0.1	+3.0	+3.3±0.1	+4.0
coordination number (CN) in solution :			4	8 - 9	6	7 - 8

There is no strict order concerning the oxidation states, which is explained by the fact that the oxidation states +V and +VI are represented by linear coordinated actinyl ions. Due to the two axial coordinated electronegative O^{2-} atoms the effective charge of the metal cation is decreased, which has direct influence on the complex stability.

The predominantly ionic nature of f-ion-ligand coordination is also reflected in the complex formation enthalpies and entropies. The formation of inner-sphere 1 : 1 complexes in aqueous media is usually characterised by positive entropy and weakly positive or weakly negative enthalpy. For simple ligands, the change of enthalpy, and thus the stability constant, is often dominated by the change of entropy. In aqueous media, the positive changes of the entropy are usually due to dehydration of the inner coordination sphere [98, 99]: since free An(III) and Ln(III) ions in aqueous acidic solution are coordinated by 9±0.5 water ligands, the complex formation involves substitution of these molecules by a polydentate chelator, for instance, resulting in an increase of entropy.

The electrostatic attraction between An(III)/Ln(III) cations and ligands is proportional to the product of the effective ionic charge of metal ion and ligand divided by the bond length. The bond length, and thus the thermodynamic strength of the metal-ligand interaction, can be reduced by steric effects between the ligands. The degree of steric hindrance depends on the ionic radius of the central ion as well as on the number and spatial distribution of the donor atoms. The flexibility of the conformation of open chain chelate ligands and the ring size of macrocyclic chelate ligands are important factors for the stability of complexes with polydentate ligands.

3.1.3 Actinium

Actinium was discovered by Debierne more than hundred years ago [100]. The isotope Ac-225, a daughter of U-233 and transiently present in the (extinct) Np-237 ($t_{\frac{1}{2}} = 2.1 \cdot 10^6$y) 4n+1 radioactive series, is one of the most popular alpha emitters for TAT [3, 1]. Already in 1984 Ac-225 was suggested by Gansow *et al* as promising radionuclide for RIT [68].

Actinium is the first actinide in the periodic table (electronic structure [Rn]6d7s2) and the electronic homologue of the first lanthanide lanthanum (electronic structure [Xe]5d6s2) [100]. Little is known about the chemistry of actinium. The chemical properties of actinium are similar to those of the rare earths and lanthanum, in particular, with both elements showing identical reduction potentials ($Ac^{3+} + 3e^- \rightarrow Ac$; E = -2.62 V). Due to their analogy, some thermodynamic properties of Ac(III) can be estimated from La(III) [101]. The stability constants of Ac-complexes are the same as, or slightly smaller than, those of the corresponding La-complexes. The difference is attributable to the difference in the ionic radii of the metal cations. Since the ionic radius for Ac^{3+} is reported to be 1.12 Å for CN = 6, Ac(III) is the largest and most basic (= less subject to hydrolysis) tripositive metal ion known. For comparison, La(III) with the ionic radius for La^{3+} being 1.03 Å (CN = 6) is more sensitive to hydrolysis [88].

There is only a limited number of actinium compounds known. As expected for an f^0 ion, its compounds are colourless, with no absorption in the UV–Vis region. Some characteristics of the chemical behaviour of Ac-225 in aqueous solution include, that in absence of any chelating agent, Ac-225 undergoes hydrolysis forming $[Ac(OH)_{3-x}]^{x-}$(x = 0, 1, 2) species. These hydroxides form radiocolloids and bind to the surface of reaction vessels and impurities present in solution. In a living organism, however, Ac-225 will not be present as "free", uncomplexed species but will be bound to metal-transport serum proteins.

The hydrolysis of Ac^{3+} is the weakest of all 3+ ions. The determination of its first hydrolysis constant has been subject of several studies. Kulikov et al., who studied the hydrolytic behaviour of Ac-225 via electromigration, predicted that in aqueous solution (I = 0.1 M, 298 K) no hydrolytic process occurs until pH 10.4 [102]. Several years later the first hydrolysis constant for Ac^{3+} for the equilibrium

$$K_{1H} = \frac{[AcOH^{2+}]\,[H^+]}{[Ac^{3+}]} \tag{3.1}$$

was calculated to be pK_{1H}= 9.4±0.1, which is slightly higher than the constant determined for La^{3+} (pK_{1H}= 9.0±0.1) [103].

$Ac(OH)_3$ is the most soluble of all f-element trihydroxides, which is consistent with the large Ac^{3+} being the most basic trivalent cation [88].

3.1.3.1 Properties of the Radionuclides in the U-233 Decay Chain

Actinium-225 is an intensively studied, very potent therapeutic alpha emitter [104]. It has a half-life of 10 days, which is not only convenient in terms of centralised production, quality control and shipment of the Ac-225-radioconjugates, but also helps to deliver more dose to tumour tissue since it is compatible with the time it takes for antibodies to localise at the tumour in sufficient concentrations [105]. During the decay of one Ac-225 atom, four α- particles are emitted with a total energy of more than 33 MeV, of which ∼90 % is carried by short-range high-LET $\alpha-$particles capable of killing a cell with one or two hits in close proximity (50 - 80 µm) to the target [106]. In this cascade no disturbing emission of (high-energy) gamma rays occurs, except for 2 useful gamma emissions (Fr-221, Bi-213), which are used to quantify e.g. radiolabelling yields by gamma-spectrometry.

Ac-225 is a daughter nuclide of Th-229 ($t_{\frac{1}{2}}$ = 7880 a), which is a decay product of U-233:

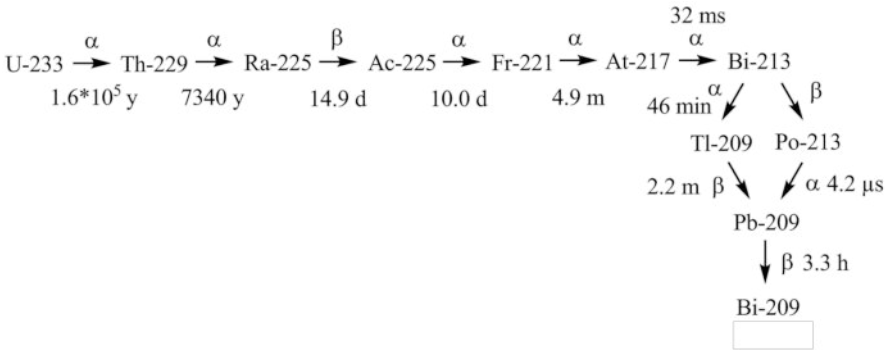

Figure 3.3: The U-233 / Th-229 decay chain. Data derived from [107].

Thorium is classified as an actinide although its chemical properties differ from that of actinium and the other actinides. In aqueous solution Th-229 exists as Th^{4+}, while Ac-225 is present as Ac^{3+}, which froms the basis for separation of these two nuclides by e.g. extraction and cation exchange chromatography. Generally, the occurrence of different cation valencies in a decay cascade suggests some differences in the coordination properties, reactivity and stability of the respective nuclides with various complexing agents.

Th-229 decays by alpha emission to the β^--emitting Ra-225 ($t_{\frac{1}{2}}$ = 14.9 d), which is the direct mother of Ac-225. With an ionic radius of 1.4 Å, Ra^{2+} cations are larger than the most abundant metal cations in blood serum. Due to its similarity to other alkali metals like Ca^{2+}, Ra^{2+} naturally accumulates in bones (see Alpharadin®, paragraph 1.5.3) [108, 69].

Through emission of one alpha particle, Ac-225 decays into its first daughter Fr-221. Not much is known about the biological behaviour of Fr-211, but it is expected to behave like other alkali metals having a 1+ charge. Therefore Fr-221 is probably trafficking and mimicking K^+ and will be pumped out of the cells, thereby causing toxicity throughout the body. This could virtually eliminate any therapeutic application of its mother Ac-225 due to a lack of viable chelation chemistry [109].

With a half-life of 46 min, Bi-213 is the next Ac-225 decay product worth mentioning. It is the longest-lived daugther of Ac-225 and usually appears in the oxidation state 3+ with an ionic radius of 1.03 Å (CN 6). According to Pearson's HSAB theory, Bi(III) is a borderline metal, but has a high affinity for multidentate ligands containing O- and N-donor atoms [110]. It also forms very stable complexes with halides, especially iodide, a property which is used to selectively elute it as BiI_5 from the Ac-225/Bi-213 generator [111]. The coordination number in Bi(III) complexes varies from 3 to 9. Bi(III) is known to bind to Zn(II)- and Fe(III)-sites of proteins *in vivo* (e.g. transferrin).

Bismuth-213 is a mixed alpha- and beta-emitter which, with a branching ratio of 98% (β^-), mainly decays to the pure α-emitter Po-213. However, due to the very short half-life of Po-213 ($t_{\frac{1}{2}} = 4.2$ µs), Bi-213 itself can be regarded as α-emitter [112]. In unchelated form it is known to accumulate in the kidneys within minutes after systemic Ac-225 injection, and therefore nephrotoxicity was hypothesised to be the dose-limiting toxicity in Ac-225 RIT [113][109].

Together with the extremely long-lived Bi-209 ($t_{\frac{1}{2}} = 1.9 \cdot 10^{19}$a), the β-particle emitting daughter Pb-209 ($t_{\frac{1}{2}} = 3.25$ h) marks the end of the 4n+1 decay chain, which eventually terminates with stable Tl-205. Pb-209 is probably able to relocate from the tumour and will localise in the liver, blood cells, and in the bone structure,

eventually causing toxicity[114]. However, the amount of Pb-209 in the liver can be decreased by intravenous injections of EDTA solution [68].

Overall, the decay of Ac-225 produces six principal radionuclide daughters, each individually lethal to cells, in a rapid and highly cytotoxic chain reaction. The radiotoxicity of four alpha particles in total probably necessitates only one decay per tumour cell. Radiotherapy with Ac-225 is therefore expected to work at low doses, reducing side effects.

3.2 Complex Stability

The most important property a radioimmunoconjugate needs to have is being thermodynamically and kinetically stabile *in vivo*. The stability of a complex is influenced by factors such as metal ion electronegativity, effective ionic radii, and steric factors resulting from differences in ligand size. Therefore the coordination chemistry of metals and ligands needs to be understood.

3.2.1 Thermodynamic and Kinetic Stability

Thermodynamic equilibrium constants provide useful information about the stability of complexes in solution under defined conditions. Equilibrium constants indicate the spontaneous direction of a reaction (e.g. whether a metal chelate will be thermodynamically stable in serum, or whether it will tend to dissociate) but can not reveal the rate of a reaction [115].

For use in nuclear medicine, a chelating agent must form a metal complex with high thermodynamic stability to retain the chemical integrity of the RIC in competition with metal cations and natural chelators contained in blood, e.g. albumin and transferrin [115]. However, once the radiopharmaceutical is injected into the blood stream, it is diluted and its concentration may become so low that dissociation of the radiometal from the chelate will eventually be thermodynamically favoured. For example, injection of 10 mg of labelled mAb into 3 litres of blood results in a concentration of $2 \cdot 10^{-8}$ M antibody [116].

Hence, high thermodynamic stability constants are not the sole requirement. Under *in vivo* conditions, which are not considered in these thermodynamic constants, the solution stability of a radiopharmaceutical in blood is predominantly determined by the kinetic inertness of the complex, with the term "kinetic inertness" referring to the rate of dissociation of the radionuclide from the chelate [117]. Especially chelators with highly basic groups (e.g. the polyaminocarboxylate's N-atoms with $pK_a > 7.4$) will bind H^+ avidly at physiological pH which favours complex dissociation. This can reduce the effective *in vivo* stability of radioconjugates by a large factor.

In addition, the loss of metal ions from the complex is also controlled by kinetic factors that depend on the structure of the chelate. Metal ion complexes of acyclic chelating agents such as EDTA and DTPA show fast dissociation kinetics while metal complexes of macrocyclic chelators are much more kinetically inert. By reason of the macrocyclic effect, DOTA is superior over open-chained ligands in terms of kinetic stability: for dissociation of rigid macrocyclic chelate complexes, more than one bond to the metal cation needs to be broken at once which is hampered by the very

limited flexibility of the ligand cage (for more information on the chelate/macrocyclic effect see 7.2 Glossary).

3.2.2 Stability Constants of Complexes

The complex formation constant, also referred to as stability constant of a complex, is a thermodynamic equilibrium constant. It is usually given for a complex formation in solution and acts as an indicator for the strength of the coordination of a metal ion to a ligand. Stability constants are important in chemistry, medicine and biology for estimation of the thermodynamic stability of complexes *in vitro* and *in vivo*. A large number of complex stability constants for various ligand systems accumulate in databases, however often showing large variations for the same metal ion-ligand system. This is often explained with problems to thoroughly attain thermodynamic equilibrium and is especially delicate for reaction systems underlying slow reaction kinetics.

The complex formation reaction of a metal cation M^{m+} and a ligand L is a substitution reaction. Metal ions in solution will never be present as "free" metal ions but always as hydroxo- and aquo ions, meaning that the water needs to be substituted by the ligand to form the ML complex. The equation for the complex formation is therefore written as

$$[M(H_2O)_n] + L \rightleftharpoons [M(H_2O)_{n-1}L] + H_2O \ . \tag{3.2}$$

Since in solution the number of water molecules attached to each metal ion is constant and since in dilute solutions the concentration of water is effectively constant, H_2O is omitted in the equation. Hence the equilibrium constant for the reaction is given by

$$\beta = \frac{[ML]}{[M][L]} \ . \tag{3.3}$$

This overall stability constant β is the constant for the formation of a complex from reagents.

The stepwise stability constants K need to be applied if the whole complexation reaction consists of a row of several separate complexation steps. K_1 , K_2 , ... K_n refer to one step of the complex formation each.

$$ML_{n-1} + L \rightleftharpoons [ML] \ ; \qquad K_n = \frac{[ML]}{[ML_{n-1}]\,[L]} \ , \tag{3.4}$$

$$logK = log\frac{[Ml]}{[ML_{n-1}]} - log[L] \ . \tag{3.5}$$

An overall constant can always be expressed as the product of stepwise constants. It follows that

$$\beta = K_1 \cdot K_2 \cdot ...K_n \ . \tag{3.6}$$

The stability constants log K_n defined above are association constants and should not be confused with $pK_{a,n}$ values which are acid dissociation constants, where K_{diss} is the stepwise acid dissociation constant

$$pK_a = -logK_{diss} = log\left(\frac{1}{K_{diss}}\right) \ . \tag{3.7}$$

For example, DOTA is denoted by H_4L and thus has four stepwise dissociation constants (see Table 3.1 25°C, I = 0.1 M)[11]. With these $pK_{a,n}$ values the species distribution of the ligand can be calculated in relation to the pH of the reaction system (Fig. 3.4).

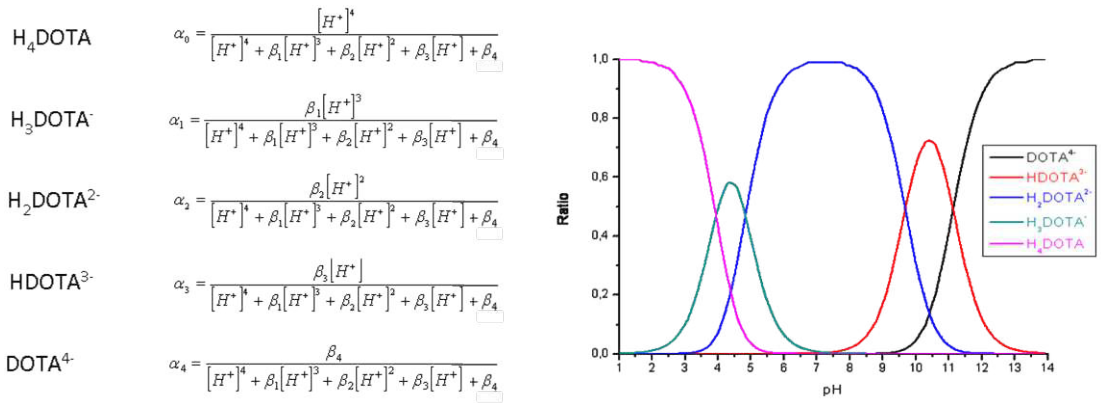

Figure 3.4: DOTA species distribution over the entire pH range, calculated from the respective alpha values.

3.2.2.1 Ionic Strength, Temperature Dependence of *K*

The thermodynamic equilibrium constant K^0 for the equilibrium $M + L = ML$ is defined as

$$K^0 = \frac{\{ML\}}{\{M\}\{L\}} , \tag{3.8}$$

where $\{ML\}$, $\{M\}$ and $\{L\}$ are the activities of the chemical species. With the activity being the product of concentration and activity coefficient γ_i, the expression is written as

$$K^0 = \frac{[ML]}{[M][L]} \cdot \frac{\gamma_{ML}}{\gamma_M \cdot \gamma_L} = \frac{[ML]}{[M][L]} \cdot \Gamma , \tag{3.9}$$

where $[ML]$, $[M]$ and $[L]$ represent the concentration of the species.

The factor Γ is a quotient of activity coefficients. To avoid the use of activities in the equation, stability constants are usually determined in a medium consisting of a solution of background electrolyte at constant, high ionic strengt (e.g. 0.1 mol/l $NaClO_4$). Like this, Γ can be assumed to be always constant and further calculations are hence simplified. As a result, all stability constants published refer to the specific electrolyte medium and specific ionic strength for which they were determined.

Since all equilibrium constants vary not only with ionic strength but also with temperature, the respective temperature at which the constant was determined also needs to be indicated. For example, in exothermic reactions with negative enthalpy $\Delta_R H$, K decreases with temperature, while for endothermic reactions (positive $\Delta_R H$) K increases with the temperature:

$$\frac{dlnK}{dT} = \frac{\Delta H^0}{RT^2} . \tag{3.10}$$

3.3 Time Resolved Laser Fluorescence Spectroscopy

One powerful method to determine complex stability constants and other thermodynamic parameters is the Time Resolved Laser induced Fluorescence Spectroscopy. TRLFS is well-established and widely used for ultratrace analysis and speciation studies of actinides and lanthanides [118]. TRLFS is able to provide information about the direct chemical environment of a metal cation, including type and number of innersphere - coordinated ligands. This metal cation, however, needs to have suitable fluorescence properties, like it is observed for the actinide Cm(III) and lanthanide Eu(III), which can be detected even in concentrations as low as $10^{-9} - 10^{-12}$ M and 10^{-7} M, respectively [119, 96].

Subject of the fluorescence spectroscopic investigations are transitions between electronic states of the metal ion, which is surrounded by coordinating ligands. Interpretation of fluorescence spectra therefore requires knowledge about the electronic structure, the quantum mechanic selection rules applying for transitions between electronic states, as well as of the influence of the ligand field on the electronic structure. Resulting from the effective shielding of the nf- shells by the closed (n+2)s- and p-shells, the interaction of f-elements with the ligand field is only weak. Nevertheless, this interaction gives rise for splitting and shifting of the energy levels, which allow for predications about the coordination sphere of the actinide or lanthanide [96].

There are three main spectroscopic techniques to gather information about the metal-ligand system, such being the recording of excitation- and emission spectra as well as fluorescence lifetime measurements (see paragraph 3.3.3). In this work, only the latter two techniques were applied.

Emission spectra of the investigated metal ions display the spectral intensity distribution of the fluorescene emission at constant excitation wavelength. In general, the observed emission bands will change their intensity and shape and shift to different wavelengths depending on the progress of complex formation. From the experimental data the species distribution and thereby the stability constants of the investigated complex can be calculated. Both the complex formation- and dissociation rates can also be determined by TRLFS.

3.3.1 Luminescence

After absorption of electromagnetic radiation of a certain wavelength, for some molecules an emission of light with longer wavelength can be observed. This behaviour is referred to as luminescence, which includes two possible processes called fluorescence and phosphorescence (Fig. 3.5).

When light is absorbed by electrons of a molecule, the electrons are promoted from the ground state S_0 to a less stable singlet excited state S_1 (*blue*, $\triangle_R S$). The energy of the absorbed photon equals the energy difference of the two states, $E = h \cdot \nu$. Hereupon the electrons relax spontaneously into a ground state S_1 by losing energy through collision of the metal cation with solvent molecules (vibronic relaxation, VR, *orange*, τ =10 fs - 10 ps).

Relaxation into the ground state S_0 is realised either through non-radiative internal conversion (IC, *purple*) or through emission of the absorbed energy in form of fluorescence light (*green*). Since due to VR not all of the energy is emitted as light, the fluorescence light is of lower energy (longer wavelength, "Stokes shift") than the

absorbed light:

$$\lambda_{fluorescence} > \lambda_{absorbance} \tag{3.11}$$

The fluorescence lifetime refers to the average time the molecule stays in its excited state before emitting a photon (τ =1 ns - 1 µs).

However, if the excited molecule undergoes inter system crossing (*black*), the electrons cross over from the excited singlet state S_1 to the corresponding excited triplet state T_1 ($\triangle S \neq 0$). Since the relaxation process $T_1 \rightarrow S_0$ is spin forbidden and hence slow, triplet states have a longer lifetime than singlet excited states. Thus the molecule will emit the energy over a certain time period while coming back to the ground state (τ =1 ms - 100 s); this process is called phosphorescence (*red*).

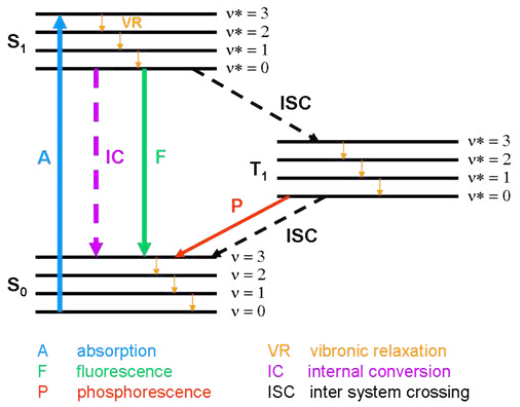

Figure 3.5: Jablonski diagram for luminescence processes.

Some f-elements have suitable fluorescence properties, with e.g. the lanthanides Gd^{3+}, Tb^{3+} and Eu^{3+} and the actinides U(VI), Am^{3+} and Cm^{3+}, which exhibit strong fluorescence emission in aqueous solution. During this PhD study, mainly experiments with Cm^{3+} and few measurements with Eu^{3+} were conducted. Strictly speaking, the investigated process have lifetimes in the range of 65 - 1200 µs and should actually be classified as phosphorescence processes. Nevertheless, the luminescence of Eu^{3+} and Cm^{3+}, which is described in detail in the following paragraph, is commonly referred to as fluorescence, to which is adapted in this work [96].

3.3.2 Fluorescence Properties of Cm(III) and Eu(III)

TRLFS measurements are based on the luminescence effects resulting from Laporte-forbidden f-f-transitions of electrons after excitation by laser light of a certain wavelength. The basis of the (long-lived) fluorescence of Cm(III) is a high energy difference between the electronic ground state and the excited state. For Eu(III) even longer-lived fluorescence is observed, which is due to the better shielding of the f-electrons of the lanthanides.

From the change of position, intensity and shape of the emission band and the lifetime of the fluorescence, it is possible to characterise the chemical environment of the Cm(III) / Eu(III) ion. Contrary to Cm^{3+}, the position of the emission band, influenced by changes in the ligand field, will only change marginally in the case of Eu(III), which again results from better f-electron shielding. However, the symmetry of the ligand field significantly influences the splitting of its emission bands. In general, the higher the symmetry is, the less the bands are split.

For spectroscopy with Cm(III) and Eu(III) an excitation wavelength of 396.6 nm (corresponding to the energy of the F-transition) and 394.0 nm, respectively, is applied. In the case of the Cm(III) aquo ion (electron configuration $Cm^{3+} = [Rn]5f^7$) an excitation from the degenerated Z-ground state ${}^8S'_{\frac{7}{2}}$ to the F-state takes place, followed by non-radiative relaxation into the A-state ${}^6D'_{\frac{7}{2}}$ (Fig. 3.6). The large

energy difference of ~16,800 cm^{-1} between the degenerated A- and the Z-states forms the basis for the fluorescence process: Fluorescence mainly results from subsequent relaxation by ${}^6D'_{\frac{7}{2}} \rightarrow {}^8S'_{\frac{7}{2}}$ transition, which gives a characteristic emission band for the Cm(III) aquo ion at 25 °C (593.8 nm, FWHM = 7.7 nm) [119].

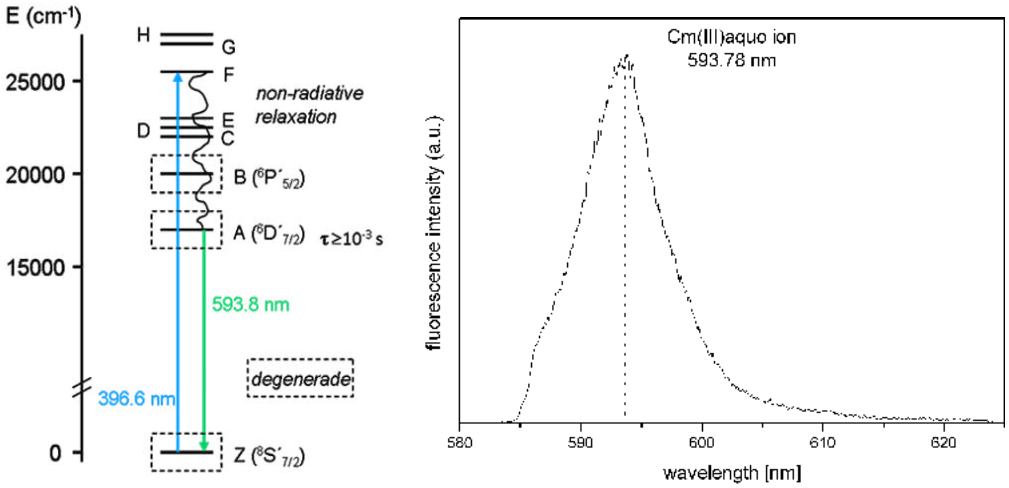

Figure 3.6: *left*: Term-diagram of Cm(III); *right*: The emission band of the Cm(III) aquoion (593.8 nm [119]).

Changes in the coordination sphere of Cm(III), which result from substitution of water molecules by complexing ligands, will have a significant effect on the degenerated ${}^6D'_{\frac{7}{2}}$ states leading to a splitting and lowering of the center of the A-states (Fig. 3.7). This decreases the energy difference between the A_1- and the Z- state and results in a bathochrome shift of the emission band ("red-shift" to higher wavelength) which is characteristic for each complex species and hence facilitates speciation studies [120]. In some cases, also transitions from the A_2 or A_3 states become visible as "hot bands" .

As general approximation, the stronger the complexation is, the more the bands are red-shifted [96].

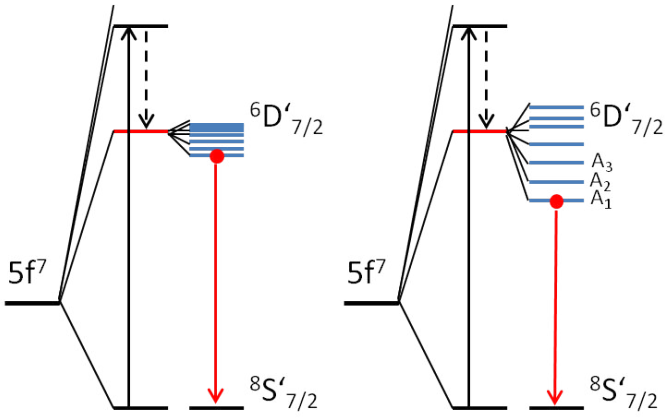

Figure 3.7: Splitting of the A-states (${}^6D'_{\frac{7}{2}}$) of Cm(III) under the influence of a coordinating ligand (*right*).

3.3.3 Fluorescence Lifetimes

By measuring the fluorescence lifetime τ of the distinct An(III)/Ln(III) species, which is the lifetime of the respective excited state, information about the number of inner-sphere water molecules n and hence about the respective coordination state of the metal cation can be gathered [121, 122]. This is possible since, by coupling with the high-energy OH oscillators of the water molecules (~3500 cm^{-1}), an efficient non-radiative decay path is provided to overcome the large energy gap between the Z-ground state and the first excited A- state, which consequently results in decreased flourescence lifetimes ("quenching" , Fig. 3.8) [96].

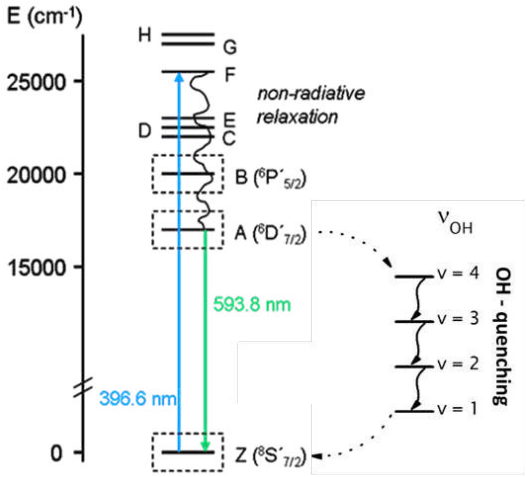

Figure 3.8: Principle of the non-radiative relaxation of the excited Cm^{3+} $^6D'_{\frac{7}{2}}$ state via OH-oscillation overtones ν.

Ligands like D_2O, which do not contain OH oscillators, have a significantly reduced quenching effectivity since the frequence for OD-oscillations is lower (~2520 cm^{-1}) and thus the respective energy transfer is less likely. This is reflected by the fluorecence lifetimes in D_2O systems (ms) being a lot longer than in H_2O sytems (µs) [96].

Cm(III) can accomodate a maximum number of nine water molecules in its first hydration shell. In this case the quenching of the flourescence lifetime is maximised, which reflects in a short lifetime of 65 µs for the Cm(III) aquoion [119]. Therefore the fluorescence lifetime of Cm(III) species coordinated with less than nine water molecules is increased compared to the fully hydrated Cm(III). Essentially this means, the higher the number of H_2O ligands in the first coordination sphere, the shorter is the fluorescence lifetime. The influence of quenching ligands in the second coordination sphere is negligible [96].

The relation of n with the flourescence decay rate $k_{obs} = \frac{1}{\tau[ms]}$ is given by the equation

$$k_{obs} = k_{rad} + k_{non-rad} + n \cdot k_{H_2O} \ , \tag{3.12}$$

with k_{rad} and $k_{non-rad}$ being the rate constants for the radiative and non-radiative deexcitation process, respectively [123]. k_{H_2O} is an additional rate constant which accounts for vibronic quenching by the coordinated water molecules [124].

The rate constant k_{obs} usually follows first order kinetics for one species, which complies with monoexponential decrease of the fluorescence intensity [96]. Since

determination of the rate constants is not trivial, a facile empirical equation was established by Kimura *et al* which allows for calculation of the number of quenching aquo ligands in the first coordination sphere of Cm(III) [125]:

$$n(H_2O) = 0.65 \cdot k_{obs}[ms^{-1}] - 0.88 \,, \tag{3.13}$$

with $n(H_2O)$ being the number of water molecules in the inner sphere and k_{obs} being the measured flourescence decay constant. The equation generally has an uncertainty of n±0.5. However, the Kimura equation is only valid for 25 °C [126]. In a recently published paper, Tian and Rao reported on the change of the flourescence lifetime of the Cm(III)aquo ion in the range of 10 to 85 °C, which they ascribe to the thermal population of higher levels of the first excited state ($^6D'_{\frac{7}{2}}$) of Cm(III). An adaption of the Kimura equation for the respective temperature range is presented by the authors and will be discussed later in this work (paragraph 5.2.1.4) [127].

To experimentally determine the flourescence lifetime of the $^6D'_{\frac{7}{2}}$ state of Cm(III), the emission intensity of the $^6D'_{\frac{7}{2}} \rightarrow^8 S'_{\frac{7}{2}}$ transition is measured at increasing delay times. Therefore, by applying a delay-generator, the time between laser pulse and opening of the camera shutter is gradually increased. The lifetime τ is then obtained by fitting of the integrated, declining fluorescence intensity I at the time t after the laser pulse according to the exponential equation

$$I(t) = I_0 \cdot exp\left(-\frac{t}{\tau}\right) \,, \tag{3.14}$$

with I_0 being the initial intensity at $t = 0$ [120]. By plotting of the natural logarithm $ln(I)$ against t, the flourescence decay rate $k_{obs} = \frac{1}{\tau[ms]}$ is derived from the slope of the graph. The rate constant k_{obs} is applied to the Kimura equation 3.13 to calculate $n(H_2O)$.

3.4 Ligands for Coordination of Multivalent Metal Cations

The use of trivalent actinides like Ac-225 in TAT holds potential, but since suitable conjugates with sufficient *in vivo* stability are still under evaluation, the widespread use of Ac-225 as radiotherapeutic agent is limited by the toxicity of this radionuclide. One approach to reduce the toxicity is to "trap" the radiometal in a rigid ligand cage, which can be achieved with chelating ligands like EDTA, DTPA, and DOTA. The successfull chelator should retain at least 90% of the Ac-225 over the 10 d half-life of the radionuclide. However, it is difficult to estimate *in vitro* how stable a radionuclide complex must be to not release the metal ion *in vivo*. Normal tissue toxicity is a major reason why many compounds that are efficient *in vitro* fail in clinical studies [128].

3.4.1 General Considerations for Ligand Choice

The wide variety of radionuclides utilised for imaging and radiotherapy requires the design of ligands suitable for stable coordination of the particular nuclide. Unfortunately, no single chelator is compatible with the full spectrum of available metal ions of different valency, and fundamental differences in properties and coordination chemistry define that different cations vary in their preference of specific ligands

[129, 37]. Therefore, the characteristics of the metal ion, such as electronegativity, preferred coordination number, effective ionic radius, metal-binding character (hard vs. soft) and reactivity (hydrolysis vs. complexation) must be considered when searching for a suitable chelate [130].

Especially radiometal complexations must meet certain requirements: the radiolabelling procedure must be quick, simple, efficient, reproducible and affordable, resulting in complexes which are thermodynamically and kinetically stable *in vivo*. The stability of the resulting complexes strongly depends on the nature of donor atoms and steric factors such as ligand structure. Most M(III) cations are classified as hard acids, which preferentially coordinate to hard donors (O, N, F). For example, the negatively charged carboxylate oxygens are strong electron donors for hard (= highly charged) metals. Contrary to an amine group, the carboxylate group is sterically very efficient and coordinates to metal ions without bringing a large number of atoms to lie close to the metal ion.

Generally, amines are typical N-donor functions (lone pair in sp^3 orbital), with the basicity toward metal ions increasing in the order

$$NH_3 < RNH_2 < R_2NH < R_3N.$$

Nitrogen can also share its lone-pair with hydrogen ions and form an ammonium species. After protonation this N-atom can no longer coordinate to a metal ion. Therefore the competition of protons for nitrogen atoms significantly affects the complexation properties of the amines [129]. In the case of azamacrocycles, e.g., protonation significantly modifies the ligand rigidity and hence determines the complexation rates [8].

Guidelines for selection of the metal ion and ligand [130]:

- The metal ion should be of suitable size to fit in the cavity of the ligand to achieve in-plane coordination, which is more stable than out-of-plane coordination.
- Oxygen atoms (e.g. carboxylate) as "hard" donors bind metal cations in high oxidation states (hard acids) stronger than "softer" donors (e.g. nitrogen donor atoms). Contrary to covalent "soft-soft" interactions, "hard-hard" interactions are usually of electrostatic nature, which is particularly suitable for coordination of f-elements that form predominantly ionic bonds.
- Since the length of the metal–oxygen bonds is very short, a large metal ion may on average coordinate to more O-donors than a smaller metal ion.
- Rigid, cyclic chelating agents with a fixed cavity size provide higher selectivity on the basis of size compared to open chain analogues.
- Preorganisation of ligands usually is of great advantage for rapid complexation; especially macrocycles provide a preformed metal binding site.

A rigid, preorganised macrocyclic chelator such as DOTA, capable of providing a large number of O-donor groups, will therefore have very favourable properties [69].

The main issue when testing a ligand for Ac-225 is, that a chelator is required which stably binds Ac-225 as well as its daughters. Therefore the chelate must withstand the immense α- particle recoil energy of 100 - 200 keV, which however is greater than the chemical binding energy of actinide complexes (for exemplary energy calculation see glossary "*recoil energy*"). Currently no conventional chelate that would withstand this energy release is known. In addition, the monovalent first daugther Fr-221 requires significantly different chelation chemistry than its trivalent mother. Thus, maintaining an intact Ac-225 conjugate after its first alpha decays seems unlikely. It is believed, however, that the half-life of Fr-221 ($t_{\frac{1}{2}} = 4.9$ min) is too short to allow for significant dislocation from the tumour site. Only the longest-lived daugther Bi-213 can leave the tumour site before it decays, but may get sufficiently diluted in the patient's body to not cause serious radiotoxicity.

3.4.2 Complexones

Polyamino-polycarboxylate chelators, so-called complexones, are known to be suitable chelators for Ln(III)/An(III) and other metal cations with various valencies [5]. There are two classes of complexones with either acyclic or macrocyclic structures. The open-chain polydentate chelators EDTA (EthyleneDiamineTetraacetic Acid, Fig. 3.10, *left*) and DTPA (DiethyleneTriaminePentaacetic Acid, Fig. 3.10, *right*) are commonly used for chelation therapy after heavy metal intoxication. EDTA forms especially strong complexes with di- and trivalent metal cations, e.g. Fe(III). Complexes of EDTA with Ac-225 (log K ~14) have also been investigated, but insufficient *in vivo* stability was found [2, 128].

Today, DTPA-derived ligands represent the most commonly used acyclic chelators applied in RIT. DTPA is an expanded version of EDTA with five carboxymethyl groups. Like EDTA, it has a high affinity for especially large metal ions, e.g. Ln/An. Therefore DTPA has been approved by the US FDA for chelation therapy of Pu poisoning. The pentaanion $DTPA^{5-}$ is potentially an octadentate ligand, while $EDTA^{4-}$ is hexadentate. Since an increase in the number of donor atoms of the ligand results in higher complex stability, the complex formation constants for DTPA complexes in general are considerably larger than those for EDTA [2, 5].

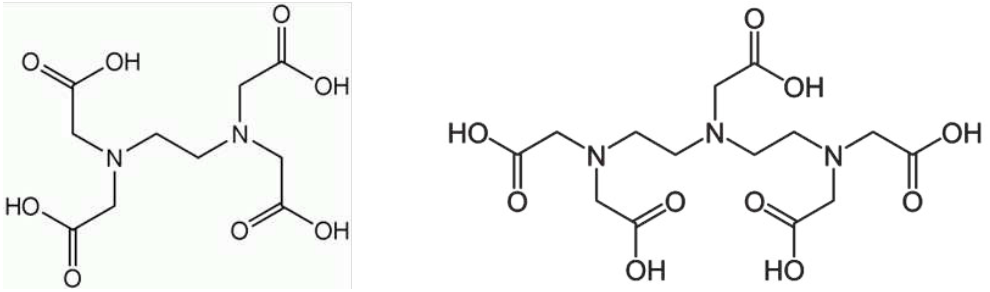

Figure 3.9: Molecule structures of ethylenediamine tetraacetic acid (EDTA, *left*) and diethylenetriamine pentaacetic acid (DTPA, *right*).

Derivates of DTPA are applied in nuclear medicine for therapy and imaging. The chelator tiuxetan in the antibody-conjugate ibritumomab tiuxetan (Zevalin®) is a modified version of DTPA [54, 38]. DTPA is also used as a complexing agent for Gd(III) in MRI (Magnevist) [131].

In general, the dynamic acyclic ligands are effective chelators which possess rapid complex formation kinetics even at ambient temperatures, but often present limited kinetic complex stability *in vitro* and *in vivo*. This instability restricts the use of DTPA-radioimmunoconjugates to local, endocavitary treatments [47]. To retain the rapid complexation kinetics but drastically slow down the opening of the chelate ring, the sterically reinforced, semi-rigid cyclohexyl-DTPA (CHX-DTPA) was synthesised and evaluated for systemic application as Bi-213-CHX-DTPA-antibody conjugate [132, 67]. CHX-DTPA-mAb complexes were also tested for use with Ac-225, however poor *in vivo* stability was indicated [2, 128]. Since DTPA-derivates allow for rapid radiolabelling at ambient temperature, they may still be preferred for labelling of heat-sensitive mAbs with short-lived radionuclides.

3.4.3 Macrocyles

An important difference between macrocyclic ligands and their open-chain analogues is that the former, based on the size of the ring cavity, generally show selectivity for metal ions. At the moment, rigid macrocylic cyclen- or cyclam-derived ligands are the most promising class of chelating agents for radiotherapy since they have key properties which match well with biomedical applications [133]. They form extremely stable and inert complexes with a wide variety of metal cations [134, 135]. The slow complex dissociation rates, however, go together with slower complex association rates compared to the acyclic analogues; hence, labelling at higher temperatures is often required.

It is known that azamacrocyclic ligands like TETA (1,4,8,11- tetraazacyclododecan- 1,4,8,11- tetraacetic acid, Fig. 3.10, *middle*) provide excellent binding environments for e.g. Cu(II) ions, combining rapid metalation and solubility in water with resistance to bioreduction and transchelation of Cu(II) in vivo [136, 137]. The most commonly used macrocyclic chelators for actinides and lanthanides are different derivatives of DOTA (1,4,7,10- tetraazacyclododecane- 1,4,7,10- tetraacetic acid, Fig. 3.10, *left*). As alternative to DOTA, HEHA (1,4,7,10,13,16- hexaazacyclohexadecane- 1,4,7,10,13,16- hexaacetic acid, Fig. 3.10, *right*) was also proposed being a suitable ligand for Ac-225, offering 12 coordination sites and a large binding cavity [2, 138].

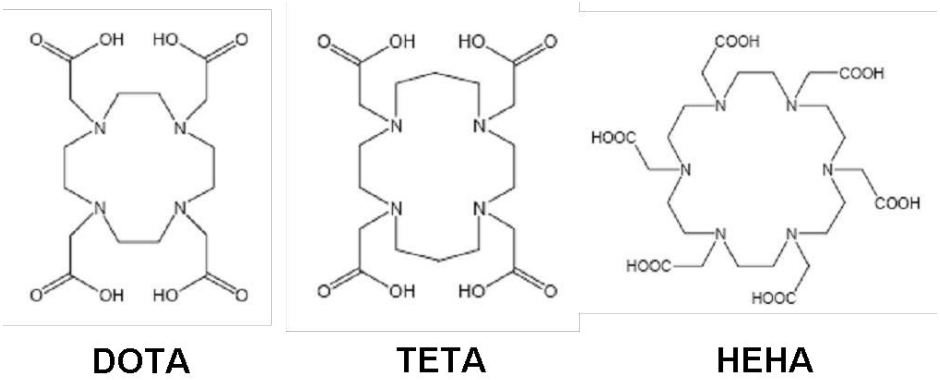

Figure 3.10: Molecule structures of 1,4,7,10-tetraazacyclododecane-1,4,7,10-tetraacetic acid (DOTA, *left*), 1,4,8,11-tetraazacyclododecane-1,4,8,11-tetraacetic acid (TETA, *middle*) and 1,4,7,10,13,16- hexaazacyclohexadecane-1,4,7,10,13,16-hexaacetic acid (HEHA, *right*).

It was reported that complexation rates with HEHA are only 10 times slower than with DTPA and about 100 times faster than with DOTA. Exceptional in vivo stability of Ac-225-HEHA was announced, but stability evaluations by other authors produced inconsistent results and also instability of the Ac-225-HEHA-conjugates was reported [45, 4, 1]. The same applies for TETA [137], and due to this uncertainty DOTA is still being investigated as superior ligand for RIT.

The macrocyclic complexones have the form of H_xL ligands and hence contain x dissociable protons. Therefore, coordination of metal ions as well as their dissociation from these aza-acid- chelators is strongly dependent on the pH.

3.4.3.1 DOTA

DOTA is a twelve-membered macrocyclic tetraaza ligand. It consists of a cyclene ring skeleton, which is modified to form a polyaminocarboxylic acid with four acetate side arms by alkylation of the parent tetramine ring with bromoacetic acid at pH 11.2 [135]. DOTA is a potential octadentate ligand and has excellent complex forming properties for di- and trivalent cations [139, 140].

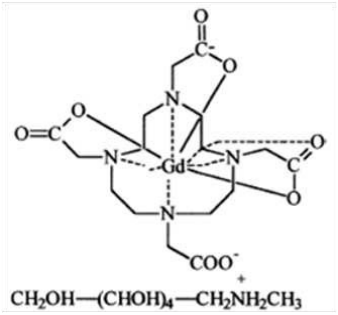

Figure 3.11: The Gd(III)DOTA complex Dotarem®, commonly used for MRI applications [131].

Several DOTA complexes are applied in nuclear medicine for imaging and therapeutical purposes. In form of its Gd(III) complex, for example, DOTA is commonly used as MRI contrast agent (Dotarem®, Fig. 3.11) [141, 142]. Driven by the medical imaging field, needing a ligand which form complexes that possess high thermodynamic stability and kinetic inertness at physiological conditions, the properties of DOTA were investigated in more detail.

In fact, DOTA forms the most stable complexes known with the Ln^{3+} ions (log K >24). These Ln(III)DOTA complexes are much more rigid than the lanthanide chelates of acyclic ligands have enhanced thermodynamic and kinetic stability relative to the analogue complexes with EDTA or DTPA. Unfortunately, the extremely slow complex formation rates of the rigid macrocycle under mild conditions were found to be problematic in many RIT applications:

- DOTA-based chelating agents require elevated temperatures and/or long reaction times. The higher temperature is problematic since it can lead to a significant loss of immunoreactivity of the applied antibodies [143].

- The slow kinetics of the labelling reaction are particularly problematic when short-lived radionuclides are involved. Hence, lengthy labelling protocols are not realisable [22, 139]. For example, the synthesis of the Bi(III)DOTA-conjugates requires 15-20 min for complex formation, purification and characterisation of the radioconjugate, while the half-life of Bi-213 is only 46 min. Like this, a large quantity of the patient's dose is already lost during preparation time. DOTA is therefore not perfectly suitable for short-lived radionuclides, but is nevertheless successfully applied in TAT [144, 145].

Comparative studies with open-chain and macrocyclic structures demonstrated that the macrocyclic structure is essential to prevent *in vitro* and *in vivo* dissociation of the radionuclides from the conjugates [146]. This phenomenon is referred to as "macrocyclic effect" and is a result of enthalpic and entropic contributions from the preorganization of the macrocycle [147, 38].

3.5 Complexes of DOTA

3.5.1 The Structure of DOTA Complexes

3.5.1.1 The General Structure of [M(III)DOTA]-Complexes

In total, DOTA has eight donor groups (four tertiary nitrogen atoms and four carboxylate oxygen atoms) which are potentially available to coordinate di- and trivalent metal ions. The tetraaza ring skeleton of DOTA acts as a frame to constrain its eight donor atoms into a nearly spherical arrangement of a square antiprism (Fig. 3.12). In this geometry, the tetraaza frame adopts the quadrangular [3333] conformation, which is the most stable conformation of cyclododecane [139, 140]. These DOTA complexes are remarkably rigid and nonlabile, a property that complexes of acyclic analogues (EDTA or DTPA) do not have.

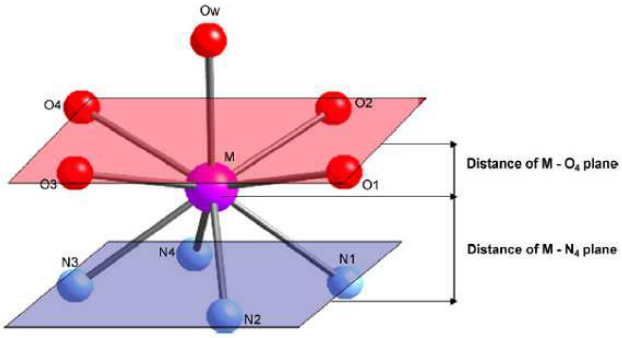

Figure 3.12: The two planes of the DOTA macrocycle in a Ln(III)DOTA complex [140].

Not necessarily all available donor atoms are used for coordination of a metal cation. For example, Fe(III) was found to be coordinated by the 4 nitrogens and 3 of the available carboxylate arms. In general, all structural and coordination differences between the complexes can be traced back to differences in the ionic radii of the metal ions [140, 38]. Due to its size the trivalent Ac-225 ion is expected to be eight-coordinated by DOTA, but probably not deep inside of the ligand cage (Ac^{3+}= 1.12 Å in CN6 [92]).

3.5.1.2 The Structure of Ln(III)/An(III) Complexes with DOTA

Due to their large size, the coordination numbers of An(III) and Ln(III) ions are usually between 8 and 10. In Ln(III)/An(III) complexes with DOTA, CN 8 and 9 are the most common. The complexes have either square antiprismatic (SAP) or twisted square antiprismatic (TSAP) geometry with approximate C_4 symmetry [140, 148, 149]. The difference in the two conformers is the orientation of the carboxylate arms of DOTA, which however affects the coordination of large metal ions (Fig. 3.13) [150]. The SAP geometry is favoured by the heavier Ln(III), while the lighter

Ln(III) prefer TSAP geometry [151]. In CN 9 complexes with DOTA, in solution an additional aquo ligand is bound to saturate the ninth coordination site.

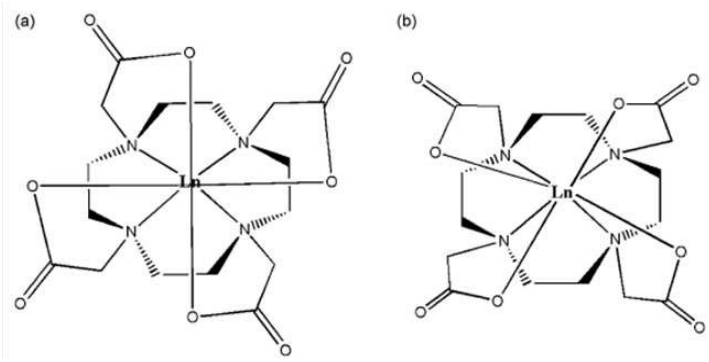

Figure 3.13: The LnDOTA isomers: (a) square antiprismatic (SAP) and (b) twisted square antiprismatic (TSAP) [140].

The X-ray crystal structure of Na[EuDOTA(H_2O)]·4 H_2O for example shows, that Eu(III) is ninefold coordinated, complexed by the octadentate DOTA and one water molecule (Fig. 3.14)[152]. Measurement indicate a strained chelate, which is probably because Eu^{3+} is too large to fit into the lowest energy [3333] square conformation of the dodecane ring; hence the complex is slightly distorted. Due to similar ion size and bonding behaviour, the coordination chemistry of Cm(III) is expected to be similar to Eu(III).

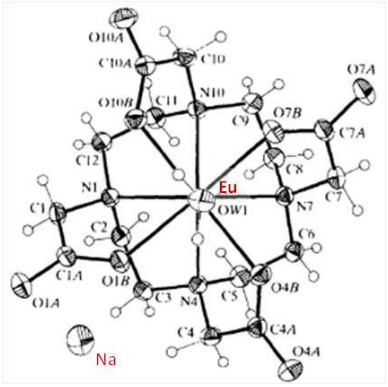

Figure 3.14: Crystral structure of Na [EuDOTA(H_2O)]· 4 H_2O; modified from [152].

In the case of the ninefold coordinated lanthanides, the exchange between octa- and nonacoordinated species by coordination – decoordination of one water molecule is superimposed over the conformational equilibrium [153]. This forms the basis for the water exchange ability of the Gd(III)DOTA complex applied in MRI [154].

3.5.2 Stability of Complexes with DOTA

3.5.2.1 Thermodynamic Stability of the [MDOTA]$^-$ Complexes

With respect to the coordination number, complexes of DOTA can be assigned to two groups with CN = 6, 7 such as Fe(III)DOTA (log K = 29.4) and CN = 8, 9 such as Bi(III)DOTA (CN 8, log K =30.3, Fig. 3.15). The last group also includes the complexes of DOTA with trivalent actinides and lanthanides (CN 9) [140].

Bi(III) forms the most stable of all DOTA complexes. The bond length to all eight coordinating N- and O-donor atoms are almost the same (2.5 Å) with the Bi(III)–N average bond being a bit shorter since the softer Bi(III) is stronger attracted by the N-donor atoms of the ring. This makes the Bi(III)DOTA complex very compact and hence stable because shorter M–N bond distances in general result in the metal cation being better encapsulated by the macrocyclic chelate; thus decomplexation is limited [110].

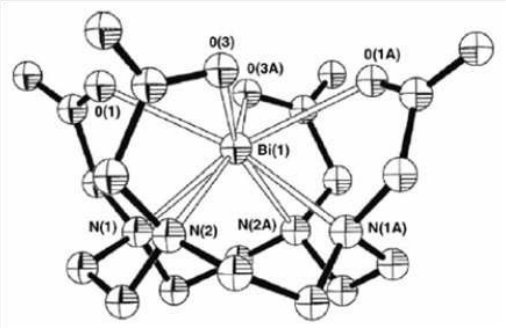

Figure 3.15: Representation of the C_4v-symmetric Bi(III) environment in Na[Bi(DOTA)]·H_20 (X-ray crystal structure)[110].

The coordination number and structure of the metal-DOTA-complexes are related to their stability. As a general rule, a higher coordination state results in increased complex stability since the electron density of the ligand can be better accommodated. As an exception from this rule, CN 9 complexes generally have lower stabilities than CN 8 complexes, because the coordination of water as capping ligand to the ninth coordination site pulls the metal out of the N-plane of the DOTA ring [155, 140]. This makes the N-atoms more accessible to protons and hence leaves the complex more labile towards acid-catalysed dissociation.

This effect is reflected in Bi(III)DOTA having a higher complex stability constant than the 9-coordinated Eu(III) and La(III) [140]:

	$Bi(III)DOTA >$	$Eu(III)DOTA >$	$La(III)DOTA$
$log\ K$:	∼30.3	∼24.2	∼22.0

In combination with the often high complex stability constants, the low selectivity of DOTA for di- and trivalent cations can be problematic, since, e.g. during labelling, DOTA-based immunoconjugates are highly sensitive to the presence of M(II)/M(III) ion contamination, principally Ca(II) and Fe(II)/Fe(III). For example, some inefficient labellings of DOTA derivates with Y-90 were found to result from Ca^{2+}, Zn^{2+}, Mg^{2+} and Fe^{3+} successfully competing for the ligand [156].

Since DOTA contains n = 4 dissociable protons (Table 3.1), the pH has strong influence on the formation of complexes as well as on their kinetic stability. The two stronger basic sites with pK_a= 11.45 and 9.64 are assigned to N-atoms of the ring, and the two weaker bases (pK_a= 4.60 and 4.11, respectively) to the carboxylate groups; the other two amines are almost nonbasic. This assignment was proven by NMR [157]. Acidic pH prompts protonation of the two strongly basic amino groups and hence catalyses dissociation of the metal complex. The carboxylate groups are less prone to acid-assisted dissociation.

Over the years a number of questionable stability constants of metal-DOTA complexes have accumulated in the literature. The discrepancies are often due to the long equilibration times which are required and insufficient experimental time frames. Also the use of different electrolytic salts influences the resulting constants (interaction of Na^+ or K^+ with DOTA); this will be discussed in paragraph 5.1.3. Some published and evaluated complex stability constants for the equilibrium M^{m+} + $DOTA^{4-}$

Table 3.1: Acid dissociation constants $pK_{a,n}$ for H_4DOTA (25°C, I = 0.1 TMACl). Data derived from [11].

Equilibrium	$pK_a = -\log K_{diss} = -\log\left(\frac{[H_{n-1}DOTA][H^+]}{[H_nDOTA]}\right)$
$H_4DOTA \rightleftharpoons H_3DOTA^- + H^+$	log K_{diss} = - 4.11 (COOH)
$H_3DOTA^- \rightleftharpoons H_2DOTA^{2-} + H^+$	log K_{diss} = - 4.60 (COOH)
$H_2DOTA^{2-} \rightleftharpoons HDOTA^{3-} + H^+$	log K_{diss} = - 9.64 (NR_3H^+)
$HDOTA^{3-} \rightleftharpoons DOTA^{4-} + H^+$	log K_{diss} = - 11.45 (NR_3H^+)

= $[M^{m+}DOTA]^{(4-m)-}$ are presented in the following Table 3.2. The similarity of the log K values within the row of Ln(III) and transition metal cations indicates that DOTA is quite unselective [158].

Table 3.2: Complex stability constants log K for complexes of DOTA with various metal cations at 25 °C, I = 0.1; taken from NIST database [159]; *blue*: evaluated by IUPAC [5].

metal	*log K*	*metal*	*log K*	*metal*	*log K*	*metal*	*log K*	*metal*	*log K*
Li^+	4.3	Y^{3+}	24.6	Tb^{3+}	24.1	Mn^{2+}	20.0	Al^{3+}	17.0
Na^+	4.2	La^{3+}	22	Dy^{3+}	24.2	Fe^{2+}	19.8	Ga^{3+}	21.3
K^+	1.6	Ce^{3+}	25	Ho^{3+}	24.1	Co^{2+}	20.2	In^{3+}	23.9
Be^{2+}	13.6	Pr^{3+}	23.5	Er^{3+}	24.1	Ni^{2+}	20.0	Pb^{2+}	24.3
Mg^{2+}	11.5	Nd^{3+}	23.7	Tm^{3+}	24.0	Cu^{2+}	22.3	Bi^{3+}	30.3
Ca^{2+}	17.2	Sm^{3+}	24.1	Yb^{3+}	26.1	Zn^{2+}	20.8	Fe^{3+}	29.4
Sr^{2+}	15.0	Eu^{3+}	26.2	Lu^{3+}	23.9	Cd^{2+}	21.3		
Ba^{2+}	12.9	Gd^{3+}	25.0			Hg^{2+}	26.4		

3.5.2.2 Stability constants of the Ln(III)DOTA Complexes

Ions of the f-elements are hard acids and coordinate ligands containing hard donors predominantly via ionic-polar interactions. Hence, the stability of An(III)/Ln(III) complexes is expected to correlate with the basicity of the ligand. $[Ln(DOTA)]^-$ complexes are the most inert complexes of the rare earths known so far [160]. This inertness, as well as the high thermodynamic stability and conformational rigidity are the result of a very good match between sizes of Ln(III) ions and the preformed cavity of the DOTA ligand.

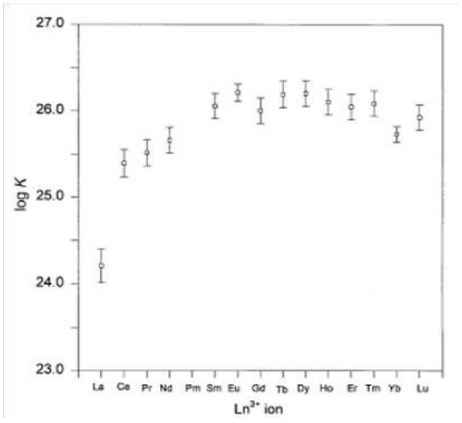

Figure 3.16: Formation constants log K for all [Ln(III)DOTA]$^-$ complexes determined versus Eu(III) determined by Wu and Horrocks [9].

In the series of the Ln(III)DOTA complexes, a drastic increase of the log $K_{25\,°C}$ values was found by Horrocks *et al*, going from the largest ion La(III)

to its slightly smaller neighbour Ce(III), followed by a moderate linear increase to Eu(III) (Fig. 3.16). The stability constants then remain roughly constant for the rest of the Ln(III) series. This trend is in accordance with findings by Toth *et al* for 37 °C [160] and was also reported for various DOTA derivatives [161]. The constrained DOTA ligand apparently accommodates the smaller lanthanides with ease, but discriminates against larger ions [9, 160], leaving the respective complexes considerably more flexible [134]. The structure of the respective DOTA complexes becomes more compact for the heavier elements, since their smaller ionic radii create greater ionic potential and thus stronger attraction for the charged ligand [162]. Also the metal bound water is pushed away when the cation sinks deeper into the ligand cavity, which results in increased water exchange rates and a trend to actual higher chelate stability, going from lighter to heavier Ln(III) [140].

3.5.3 Mechanism of [M(III)DOTA]$^-$Complexation/Dissociation

Many studies have been conducted and reviewed with regard to the mechanism of M(III)DOTA complex formation [11, 163, 164, 8, 165, 139, 166, 167, 168], with some authors disagreeing on details like the occurence of varying intermediate complex species. To elucidate this issue, the complexation mechanism is also investigated in the context of the TRLFS experiments presented in this work. The authors generally propose a two- or three-step mechanism of first electrostatic capture of the metal ion, followed by its encapsulation during which stepwise deprotonation of the amines occurs. This is associated with energy cost due to rearrangement of the carboxylate arms and the orbitals of the ternary amines involved in metal ion binding, as well as of the 12-membered ring into the proper geometry. To lower the total energy barrier, research on DOTA derivatives with pre-arranged rings is progressing with the intention to potentially increase the rate of complex formation ("CHX-DOTA" [43]).

- **Step I** describes the formation of the $[M(H_2DOTA)]^+$ complex ("intermediate I" , Fig. 3.17). Here, the M^{3+} ion is located outside of the ligand cage formed by all eight donor atoms. The two protons present in this intermediate species are bound to two opposed N-atoms of the tetraaza ring and are oriented towards the inside of the cage. Due to repulsion by these protons, the M^{3+} ion is only bound to the four O-atoms of the carboxylic groups and is located above the oxygen plane. The coordination number of nine for Ln^{3+}/An^{3+} cations is reached by additional coordination of five water molecules.

$$M^{3+} + [H_nDOTA]^{4-n} \rightarrow [M(H_2DOTA)]^+ + (n-2)H^+$$

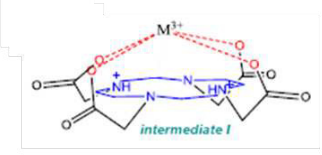

Figure 3.17: Formation and assumed structure of intermediate I. The exact geometrie as well as the water molecules coordinated to achieve CN = 9 are omitted for clarity.

- **Step II** refers to the fast formation of "intermediate II" , the [M(HDOTA)] complex by dissociation of one proton; the last proton is still attached to its ring

nitrogen atom and likely adopts an exo conformation to minimise electrostatic repulsion (Fig. 3.18). The M^{3+} is now coordinated by all four carboxylic groups and also probably by at least one N-atom of the ring, which leads to a distortion of the N4-plane. Like this, the cation is located in the plane spanned by the four O-atoms.

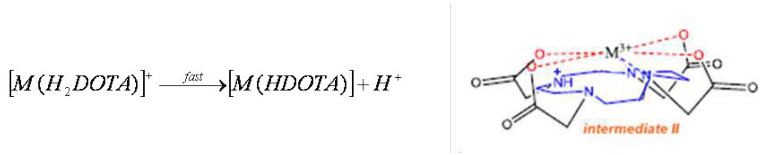

Figure 3.18: Formation and assumed structure of intermediate II. The exact geometrie as well as the water molecules coordinated to achieve CN = 9 are omitted for clarity.

- **Step III** is said to be the rate determining step and describes the formation of the final $[MDOTA]^-$ complex which occurs through a concerted rearrangement of the intermediate II: while the last proton dissociates, the M^{3+} slowly penetrates the N4O4 cage (Fig. 3.19). This proton dissociation was shown to be favoured by OH^- or H_2O. In the end, a complex results in which all eight donor atoms are bound to the M^{3+} ion. If required, in aqueous solution an existent ninth coordination site will be saturated by a H_2O molecule.

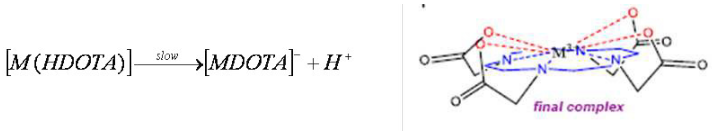

Figure 3.19: Formation and assumed structure of the final complex. The exact geometrie as well as the water molecules coordinated to achieve CN = 9 are omitted for clarity.

Different theories concerning the release of the protons from the intermediate complexes are reported. The respective protons are located inside the cage and are hence barely accessible to outside base [11]. Generally, three different pathways are discussed:

1. The first pathway (Toth *et al*) involves an insertion of OH^- or H_2O into the coordination cage [164]. This OH^- catalyzed deprotonation is a well known pathway in proton exchange reactions of α-amino carboxylic acids. The plausibility of this way however depends on the conformational flexibility of the intermediate complexes. The $[M(H_2DOTA)]^+$ complex seems to be flexible enough to allow this mechanism; [M(HDOTA)] however appears to be too rigid due to the additional M-N bond.

2. In the second pathway, Kumar *et al* propose a prior nitrogen inversion, in which the proton is brought from the inside to the outside of the ligand cage [167]. This pathway, however, does not seem to be very likely since quaternary amines have large nitrogen inversion barriers. Hence, the energy needed for this process is too high.

3. Jang *et al* proposed a third pathway for the removal of the last proton, based on molecular modelling [139]. It was found that in an optimised structure of

[Y(HDOTA)], one of the carboxylate oxygens is located very close to the NH^+ group of the ring. In this structure the distance and bond angles are extremely favourable for proton transfer from the ring NH^+ group to a carboxylate oxygen, which thus makes the proton easily accessible to the outside base (OH^-, H_2O). The energy barrier for this proton migration is not very high, which is in favour of this hypothesis. As the proton is transferred, the M^{3+} moves spontaneously (since there is little conformational change) and concerted to the inside of the ligand cage to form the final complex.

The last path represents the reverse of the proposed path for the acid-catalysed dissociation of $[MDOTA]^-$. First, protonation of a carboxylate function takes place and a transfer of the proton to the attached N-atom in the ring follows. This results in electrostatic repulsion of M^{3+} and the proton, which eases dissociation of the complex. However, this proton transfer is very slow due to the rigid complex structure. As a consequence, the dissociation of these $[MDOTA]^-$ complexes is expected to be extremely slow, in particular at physiological conditions with non-acidic pH 7.4 [164].

3.5.3.1 pH- and Temperature- Dependence of the M(III) Complexation with DOTA

In several studies a general pH-dependency of the M(III)DOTA complex formation rate k was observed. It was found that k increases with higher pH, which is due to the base assisted proton loss in the last step of the complexation being rate determining. By contrast, at acidic pH the competition between M^{3+} and H^+ for the coordination sites of DOTA constricts the complexation since it prompts protonation of the carboxyl groups.

With regard to the different protonated species occurring at different pH, Wang *et al* as well as Pasha *et al* investigated the reactivity of the DOTA ligand [168, 161]. Besides L^{4-} being the most reactive species by far, they reported that the monoprotonated species HL^{3-} is a lot more reactive than the double-protonated H_2L^{2-} species. The lower reactivity was assigned to the larger electrostatic repulsion of the incoming metal cation caused by the two protonated N-atoms in the ring. In addition, the presumed formation of strong pH-dependent H-bonds with the carboxylate arms attachted to them probably hinders the rearrangement into the final complex [157]. The species H_3L^- is assumed to be highly unreactive. In general, the higher protonated the species, the more hindered is the fluxionality of the ligand and the slower is the complex formation. Based on these findings, it is suggested that the complex formation occurs by direct encounter between the e.g. Ln^{3+}/An^{3+} ions and the fully deprotonated ligand.

Early NMR studies by Desreux *et al* showed that the rigidity of the DOTA macrocycle is lost when the temperature is increased [169]. It was proposed that the slow kinetics of metal-DOTA complex formation depend on the dynamics of the conversion between the major two complex isomers (square antiprismatic and twisted square antiprismatic, see Figure 3.13). They both have identical ring conformation and differ only in the orientation of the acetate arms. Thus, with elevated temperatures, the isomer-conversion rate which allows flexibility of the acetate arms is increased, resulting in the rate of M(III)DOTA complexation being much higher.

3.5.4 Bifunctionalised DOTA Chelators for Radioimmunotherapy

Not only the stable complexation of the radiometal, but also the stable conjugation of the radionuclide complex to a protein or mAb must meet one critical requirement: the chelate should be stably linked to the carrier without impairing its affinity for its target receptor or antigen. This can be achieved by strong covalent linkage through thiourea, thioether, (sulfon-)amide, ester or disulfide bonds [170].

A "bifunctional chelating agent" (BFCA) is a molecule which possesses both a linker for conjugation to biomolecules as well as a chelate functionality for stable complexation of radionuclides [44]. Suitable for RIT is a bifunctional ligand that stably coordinates the nuclide with clinically acceptable complexation kinetics while staying attached to the tumour-specific carrier under *in vivo* conditions [50]. The choice of BFCA is largely determined by the nature and oxidation state of the radionuclide, since different metal ions require different donor atoms and chelator frameworks. Therefore, it is important to understand the coordination chemistry of BFCAs with any given nuclide they are to be labelled with. Aromatic isothiocyanates like p-SCN-Bn are often used to link DTPA and DOTA to biomolecules.

For conjugation of DOTA to carrier molecules two approaches are used [44]:

- ***Attaching the biomolecule to the chelating arms***: Here, one carboxylic acid moiety of DOTA is activated to permit formation of a stable CONH amide bond with the biomolecule. Conjugation like this leaves only three carboxylate groups available for stable complexation of the metal. However, the *in vivo* stability of these complexes with trivalent radionuclides remains sufficiently high, as it was demonstrated in the case of DOTA-Substance P (Fig. 3.21) [7, 144]. Nevertheless, the availability of the fourth carboxylic acid function is useful to reduce the overall charge of the chelate to 1-, which offers a potential way for modifying the *in vivo* pharmacokinetics of the bioconjugates.

- ***Linking to the carbon atoms of the chelate backbone***: In this approach, DOTA is linked to mAbs through connection of the linker to the ring while maintaining all four carboxylate groups for coordination of the trivalent metal ions. One example for this type of BFCA is *p*-SCN-Bn-DOTA (2-(*p*-isothiocyanatobenzyl)-DOTA, "DOTA-NCS" , Mw = 697.45 g/mol, Fig. 3.20) [171].

Since for stable coordination of Ac-225 probably all four carboxylic groups of DOTA are needed, *p*-SCN-Bn-DOTA is used as ligand for Ac-225 in TAT. This isothiocyanate-functionalised DOTA is conjugated to mAbs by formation of thiourea linkages with amino functions of their lysine groups according to the following reaction:

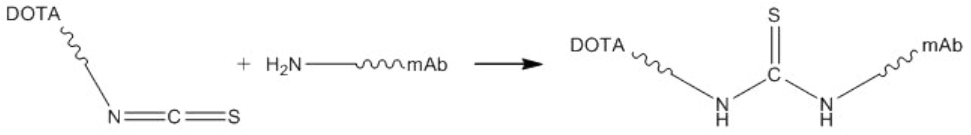

The reaction with amines in aqueous solution takes place at pH ∼8.5 - 9.0 [6, 173]. Once conjugated, the thiourea bond is extremely stable. The ideal mAb-chelator conjugate is not "overmodified" but has a suitable degree of chelates present while still showing the same chemical and biological behaviour as the naked biomolecule (such as selective binding to a receptor or the ability to incorporate into a biological

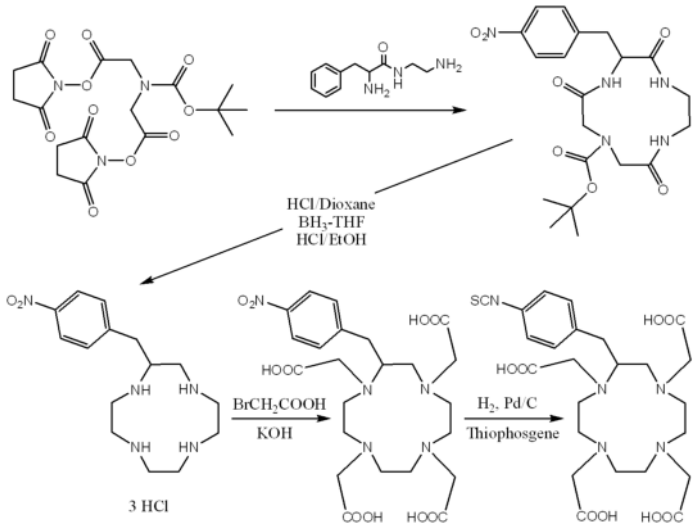

Figure 3.20: Synthesis of the bifunctional chelator *p*-NCS-Bn-DOTA (*bottom right*) [172].

membrane)[174, 175]. To the CD20-antibody used in the present study, an average number of ∼3 - 6 DOTA-NCS chelators per antibody molecule is attached.

3.6 Common Carrier Molecules and Targeted Antigens/Receptors in Radionuclide Therapy

3.6.1 Selection of a Suitable Therapeutic Carrier Molecule

For application in systemic nuclear medicine, suitable carrier biomolecules have to be identified which allow for selective delivery of the attached radionuclide to the respective targeted tissue. These so-called molecular recognitioning tools need to have certain properties:

1. To be really selective, the carrier biomolecule usually needs to exhibit a 3D-shape that will fit exclusively onto a patch on the target receptor molecule. This is also known as the "key-lock-principle" .

2. The carrier should have high affinity to the corresponding receptor in order to recognise its structure and strongly bind to it, even if the receptor is less abundant *in vivo*. The carrier molecule should not bind to any other proteins or structures in order to deliver high concentrations of the cytotoxic agent only to the tumour while avoiding normal tissue [176]. Furthermore, the biomolecule should show satisfying resistance to the applied chemical/labelling conditions. An ideal targeting carrier should also allow for stable radiolabelling without losing tumour affinity or specificity.

3. The selected carrier should quickly find its target in the patient's body. At the same time, unbound molecules which did not succeed in targeting should be rapidly excreted through the kidneys. This feature is typically found with rather small water-soluble molecules such as proteins and antibody fragments; e.g. minibodies with molecular weigths below 50 kDa are cleared from the body within hours, while antibody derivates of 70 kDa and larger can not easily pass the renal filtration barrier [177, 178]. However, if a therapeutic conjugate is

excreted too rapidly, this may hamper the residence time in the tumour and prevent achieving cytotoxic dose levels necessary for therapeutic efficacy.

4. In targeted therapy, the total dose delivered to the tumour should be very high compared to normal tissue. Especially with disseminated tumour cells, longer blood circulation times are required in order to allow for the vector to localise and accumulate in the targeted tissue. Longer circulation times are typically found with large, intact antibodies (150 kDa), which may reduce the total dose needed to be administered. These big immunoglobulins (IgGs) can remain in circulation up to 3 - 4 weeks while being metabolised slowly by the reticuloendothelial system. Too long circulation times, however, can increase the dose received by normal organs and tissues, especially the bone marrow, up to lethal doses. Thus, consideration of the plasma half-life of the carrier biomolecule is of high importance [179].

5. The size of the carrier molecule for RIT also needs to be matched with the properties of the targeted tumour. Since solid tumours present a limited vascular supply with anoxic regions distant from the blood vessels, a heterogeneous uptake of the biomolecule is only guaranteed with smaller, rapidly penetrating molecules. Large IgG molecules only penetrate slowly (>1 mm in two days [180]) since they hardly overcome the increased interstitial pressure and long transportation routes inside the tumour [181]. This hampers their accumulation in bulky tumours compared to haematological diseases, which is why intact antibodies are more effective in delivering radionuclides to diffuse, liquid malignancies.

Besides peptides and full antibodies, various other carrier molecules with different molecular weight (antibody fragments e.g. scFvs, 27 kDa; minibodies, 80 kDa), shape and lipophilicity have been suggested and evaluated for radionuclide therapy [182, 183, 184]. As a rule of thumb, tissue penetration, fast tumour targeting and uptake as well as body clearance will increase with decreasing size of the delivering biomolecule, while target residence time and thus delivered dose will decrease.

3.6.2 Peptides for Peptide-Receptor-Radionuclide Therapy

Peptide receptor radionuclide therapy (PRRT) with radiolabelled peptide analogues is a promising treatment modality especially for patients with tumours that cannot be resected easily, e.g. glioma [185, 17]. Peptides in general have some advantages as they are small and show rapid kinetics as well as very good tissue penetration. Furthermore they can be synthesised chemically and generally withstand harsh labelling conditions like temperatures up to 95 °C, while antibodies only allow for labelling temperatures up to 45 °C. Some peptides are currently investigated for cancer therapy, e.g. the proteins DOTATOC (e.g. OctreoTher® [186]; Bi-213-DOTATOC [187, 3]) and DOTA-Substance P.

DOTA-Substance P is a DOTA-peptide conjugate consisting of 11 amino acids which selectively binds to NK-1-receptors expressed on brain tumour blood vessels. Since the native Substance P is subject to metabolic degradation in the body, for use in TAT the more robust derivate DOTA-[Thi8, Met(O2)11]-Substance P was developed displaying higher binding affinity than the unmodified conjugate (Fig. 3.21) [144]. Its Bi-213 complex is currently successfully applied in clinical studies with glioma patients using the locoregional approach [188]. The molecular weight

of only 1.8 kDa enables DOTA-Substance P to rapidly and sufficiently distribute in the tumour tissue. So far, the studies indicate that radiotherapy with Substance P shows no relevant toxicity.

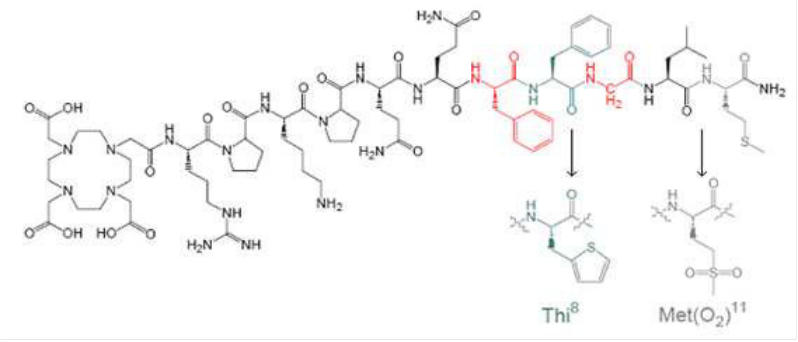

Figure 3.21: Molecule structure of native DOTA-Substance P and the amino acid substitutes for improved DOTA-[Thi8, Met(O2)11]-Substance P [189].

In previous studies, a protocol for labelling of DOTA-Substance P with Ac-225 was established and the *in vitro* stability of the radioconjugate was confirmed [7]. Together with the protocol for the synthesis of an Ac-225-labelled antibody, this protocoll was finally optimised in the frame of the present work. At ITU studies are ongoing to evaluate the *in vitro* behaviour of the Ac-225 radioconjugate.

3.6.3 Antibodies

Antibodies or immunoglobulines are proteins, which are produced by the immune systeme as a response to a certain antigen. Antibodies specifically bind to one matching antigen, a principle which is exploited to target radiolabelled antibodies to tumour cells expressing the respective antigens ("key-lock-principle" , Fig. 3.22). Defined, clonal populations of antibodies, so-called monoclonal antibodies (mAbs) of the IgG type (molecular weight ∼150 kDa) [190], are commonly applied for immunotherapy (e.g. anti-CD20 for therapy of non-Hodgkins lymphoma). However, these heavy molecules only slowly accumulate in the targeted tissue (penetration is less than one millimetre in two days [180]). Antibodies consist of two identical heavy chains and two identical light chains, which are connected by disulfide bridges to form a Y-shaped structure. The light polypeptide chains both contain one constant and one variable domain, while the heavy polypeptide chains contain one variable and three to four constant domains each. The variable domains of one light chain and one heavy chain form the antigen binding site [191, 182].

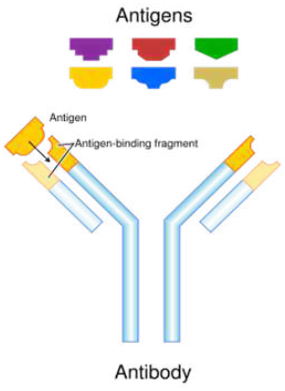

Figure 3.22: Key-lock principle of an antibody binding to an antigen.

The reversible binding of an antibody to its antigen is non-covalent and based on van-der-Waals -, Coulomb - and hydrophobic interactions as well as hydrogen bonds, resulting in a high binding affinity.

Precondition for the high specifity of the binding is the sterical conformance of the threedimensional antibody and antigen structures, allowing them to come as close as 1 Å or less.

The first antibodies proposed for cancer therapy have been of murine origin, which were soon found to cause an immunoreaction known as Human Anti-Mouse Antibody (HAMA) response [192]. As a result, chimeric antibodies were developed through fusion of the variable region of the mouse antibody with the constant region of a human antibody [37]. In 1997, rituximab (Rituxan, MabThera®, Mw 144544 g/mol, Fig. 3.23), an anti-CD20 antibody for the treatment of non-Hodgkins lymphoma (NHL) was the first chimeric antibody to be approved by the FDA for therapy of cancer [56, 193]. Since 2002, two murine IgG antibodies indicated for systemic therapy of B-cell Lymphoma have been approved by the FDA, namely Y-90-Ibritumomab-tiuxetan (Zevalin®, 2002) and I-131-tositumomab (Bexxar®, 2003) [54, 194, 195, 37]. Both are administered intravenously and are comparatively rapidly cleared from blood. Excellent clinical results were obtained for refractory or relapsed low-grade NHL, and toxicity is usually mild. To date, antibodies labelled with $\alpha-$emitters like Ac-225 are among the most potent cytotoxic agents known and appear to be safe in preclinical *in vivo* studies [67].

Some undesirable side effects can be observed especially with unconjugated antibodies, including severe pain. With radiolabelled diagnostic and therapeutic antibodies, physiological side effects are typically of less concern since the amounts of administered drug are significantly lower than for nonradioactive immunotherapy. Serious side effects however can arise from insufficient *in vivo* stability of the radioimmuno- conjugate as it was reported for Zevalin®, of which severe bone-marrow toxicity was found to be a major side effect [50].

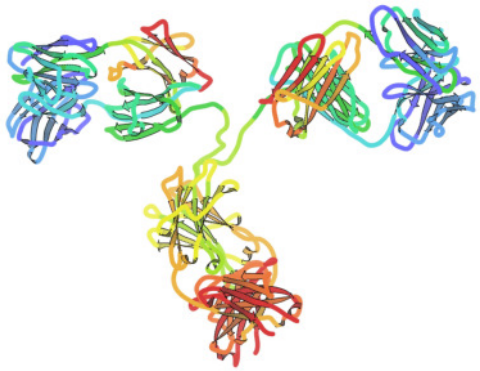

Figure 3.23: Structure of rituximab [196].

3.6.3.1 Affinity, Internalisation and Retention

The affinity of an antibody characterises the binding to the target antigen [182]. The binding is mainly realised through non-covalent bonds formed between amino acids on the complementarity determining regions (CDR) of the antibody and those on the surface of the antigen. When conjugating the antibody with the BFCA, it is hence extremely important to not manipulate these binding regions [44]. High affinity is a necessity for good tumour localisation, in particular with single disseminated cells. However, antibodies with high affinity often bind only to the rim of the tumour and do not penetrate into deeper regions of the tumour mass. Thus the centre of the tumour remains unaffected by radiation unless the radionuclide attached to the mAb emits particles with very long tissue range. In scenarios with solid tumours it can therefore be beneficial to use agents with lower affinity that allow for better penetration.

Besides the targeting properties also the internalisation properties of antibodies are crucial for effective RIT. Especially the intratumoural residence time of the emitted radionuclides is critical for therapeutic success: the longer the radionuclide is retained inside or near the tumour cell, the higher is the delivered dose. High retention can be achieved by employing vector molecules with either high affinity and stable binding or good internalisation properties. In case of internalisation, the delivered radionuclides come in close proximity to the DNA, while emissions from surface-bound radioconjugates may also pass harmlessly away from the cell. This is an advantage when nuclides like Ac-225 or Bi-213 are used since internalisation minimises dislocation of the daugther nuclides, which will decay within the tumour instead, contributing to the sterilisation of the cells [185]. In 2000, for instance, the first TAT-patients in Europe (Basel) were treated with a Bi-213-labelled DOTA-peptide targeted against glioblastoma [197]. Considering the short half-life of Bi-213, internalisation of the peptide was necessary to achieve therapeutic effects.

Today it is known that most antibodies which bind to the cell surface are internalised, followed by proteolytic degradation of the IgG in the lysosome. While lipophilic catabolites diffuse through phospholipide membranes and leak from the cell, the hydrophilic and charged metal chelate catabolites are trapped inside the cell. They can only leave by externalisation, a process that is slower than diffusion. Therefore radionuclides accumulate in tumours.

3.6.4 Antibody Mediated Radioimmunotherapy

Antibodies recognise specific cell surface macromolecules (antigens) and usually bind to them with affinities in the range of $10^{-7} - 10^{-11} \frac{1}{M}$. For targeting with monoclonal antibodies, selection of suitable antigens expressed by cancer cells as well as of the cellular function related to these antigens are critical for successful radioimmunotherapy. One of the most important antigens in tumour therapy is CD20, an antigen which is expressed on more than 90 % of B-cell non-Hodgkins lymphoma ($>10^5$ antigens per cell) [198, 199].

3.6.4.1 Targeted Antigens

The ideal antigen for targeting should be readily accessible, present in substantial amounts and (over-)expressed mainly on the targeted cancer cells, which means that the antigen should be tumour specific to avoid unwanted toxicity. It should also be stable on the cell surface and not being shed or secreted into circulation, since this would consequently release the antigen-bound labelled mAb and therewith cause inadvertent distribution of the radioconjugate [198].

3.6.4.2 Radioimmunotherapy of Haematologic Malignancies

The FDA-approval of the two antibodies Bexxar® and Zevalin® was the highlight of successful application of radiolabelled antibodies in cancer therapy. Together with rituximab, they are used for treatment of non-Hodgkins lymphoma patients [200]. Lymphomas are in general sensitive to chemotherapy and some are remarkably sensitive to radiation [68]. Radiotherapy of lymphomas is based on immunotargeting of the hematopoietic cluster differentiation antigen CD20 expressed on B-cells, while RIT of leukemias has focused on antigens on malignant B and T cells [201, 21].

CD20, initially discovered already in 1981 by Nadler *et al* [202], is an excellent target because it is neither shed nor internalised. It is a 33 - 36 kDa transmembrane phosphoprotein involved in the activation, proliferation and differentiation of B-lymphocytes. CD20 is not tumour specific, but it is characterised by its high frequency of expression on most of B-cell NHLs (∼90 %). With a high antigen density of >105 antigens per B-cell and a fairly homogeneous expression on the cell surface, very efficient tumour targeting can be achieved [199]. The CD20 surface antigens are successfully used as targets for cancer therapy with unlabelled and radiolabelled antibodies. A standard treatment for diffuse large B-cell lymphomas is a combination of chemotherapy and the unlabelled anti-CD20 antibody rituximab [21]. However, most patients with disseminated B-cell lymphoma cannot be cured this way. Therefore research focus was set on the development of a synthesis route for radiolabelled rituximab [7].

3.7 Therapeutic Radionuclides: Advantages, Production

Production of highliy pure artificial radionuclides is inevitable to meet the increasing demand for radiopharmaceuticals. Radionuclides, especially neutron rich $\beta-$ emitters, can be produced in nuclear reactors by neutron capture reactions (e.g. (n,γ), (n,p), (n,α), (n,fission)...). Alternatively, since the products are often not carrier-free, particle accelerators ("cyclotrons") are used, e.g. for production of Ac-225 via [107, 203]:

$$^{226}Ra\,(p,2n)^{225}Ac\,. \tag{3.15}$$

An advantage of the use of charged particle irradiation in cyclotrons is, that the produced radionuclide is a different chemical element than the target material. This facilitates effective chemical separation so that radionuclides with high specific activities can be obtained.

More convenient on the small scale, e.g. in hospitals, is the production with radionuclide generators, allowing chemical separation of the therapeutical attractive decay product from the long-lived mother nuclide which is sorbed to the generator resin [204]. Radionuclide generators are commonly used for production of carrier-free $\alpha-$ and $\beta-$ emitting nuclides with short half-lives, where centralised production and shipment is not realisable. The generator is milked by selective elution of the short-lived daugther nuclide. The process can be repeated as soon as enough of the long-lived mother nuclide has decayed to allow the decay equilibrium to be established again.

3.7.1 Production of Ac-225

Ac-225 is currently obtained from the decay of Th-229 ($t\frac{1}{2}$ = 7880 a) through one intermediate radionuclide, the beta-emitting Ra-225 ($t\frac{1}{2}$ = 14.9 d). Th-229 was received by liquid-liquid extraction from aged U-233, which has been produced as part of the US molten salt breeder reactor research program in the 1960s/'70s. Meanwhile the Th-228 component of this waste (resulting from the decay of U-232, which is invariably produced as impurity during production of U-233 through neutron irradiation of Th-232) has largely decayed and purified Th-229 is used for radionuclide production [109].

There are only three Th-229 sources worldwide which permit production of relevant amounts of clinical-grade Ac-225. One Th-229 "cow" is located at the Institute for Transuranium Elements (ITU) in Karlsruhe, Germany (215 mg (~46 mCi (= 1.7 GBq)) of Th-229, providing a total of ~350 mCi (= 13 GBq) Ac-225 per year), a second one at the Oak Ridge National Laboratory (ORNL), USA, (~150 mCi (= 5.6 GBq) and a third source at the Russian Institute of Physics and Power Engineering (IPPE) [205]. The ITU's Th-229 cow can provide 43 mCi (= 1.6 GBq) of Ra-225 and 39 mCi (= 1.4 GBq) of Ac-225 every 9 weeks plus an additional amount of Ac-225 which is occasionally separated from decaying Ra-225 [206].

At ITU, Ac-225 is separated from Th-229 in a two-step chromatographic process in nitric acid media (Fig. 3.24; for further details see paragraph 4.1.1.1) [207]. Th-229 is adsorbed on anion exchange resin and stored in 8 M HNO_3. Every 9 weeks, Ra-225 and Ac-225 are separated from Th-229 through anion exchange chromatography (DOWEX 1x8), followed by extraction chromatography to separate Ac-225 from its mother.

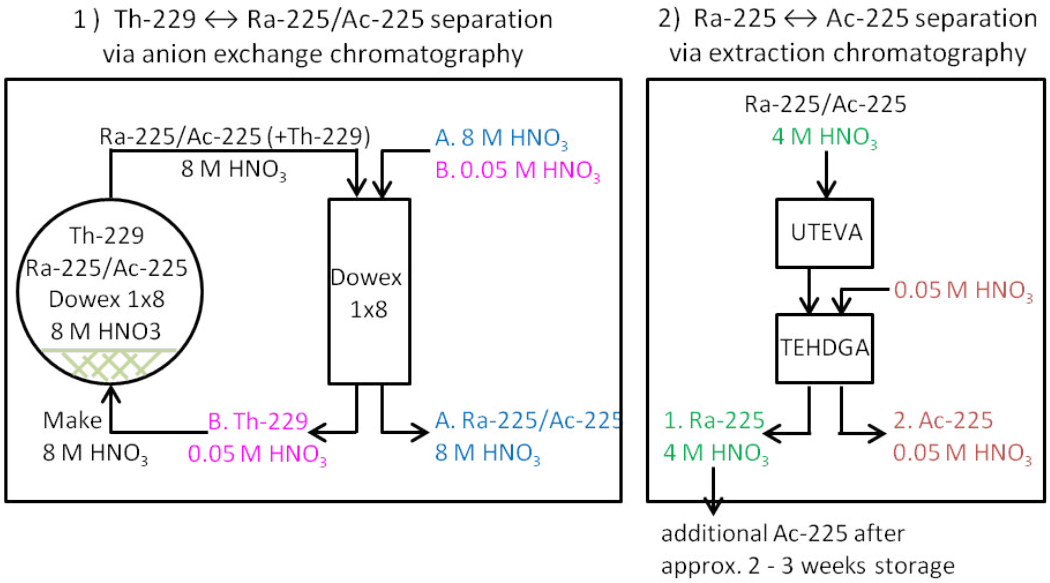

Figure 3.24: Procedure for separation of Ra-225 / Ac-225 from Th-229; *left*: Anion exchange chromatography for separation of Ra-225/Ac-225 from Th-229; *right*: Extraction chromatography to separate Ac-225 from Ra-225 (adopted from [207]).

The production process yields > 95 % carrier-free Ac-225 with a radiochemical purity of > 99 %. Quality is ensured by frequent controls with alpha - and gamma spectrometry as well as ICP-MS (Fig. 3.25) [205]. The obtained Ac-225 is either loaded on a radionuclide generator for production of Bi-213 or is directly applied for radiolabelling of peptides and antibodies [112]. The purified Ra-225 is stored for separation of additinoal amounts of actinium after 2-3 weeks [207].

The four-step production process of Ac-225 from Th-229 used at ORNL was described by Boll et al [208]. This production scheme combines cation and anion exchange chromatography. After separation of Ra-225 and Ac-225 from thorium by repeated anion exchange in 8 M HNO_3, the Ac-225 / Ra-225 fraction is passed through an anion exchange column to remove Fe ions, which entered into the process as impurity present in nitric acid solutions (analytical grade HNO_3 typically contains 0.2–0.5 ppm of Fe or ~0.5 mg per 1.5 L). Fe^{3+} is of particular concern, as

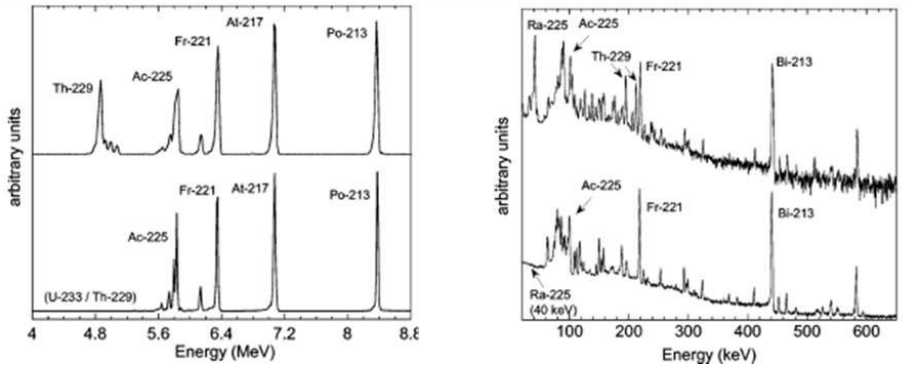

Figure 3.25: Alpha-spectra (*left*) and gamma- spectra (*right*) of the ITU's Th-229 source (*top*) and the purified product Ac-225 (*bottom*) [112].

its complex formation constant with commonly applied chelating ligands like DTPA and DOTA exceeds that of Ac(III) (see Table 3.2). When eluted with 10 M HCl, Fe^{3+} forms negatively charged chloro-complexes which are strongly retained by anion exchange resins while Ac^{3+} and Ra^{3+} show little or no retention. The separation of Ac-225 from Ra-225 is achieved by cation exchange chromatography and leads to > 99 % radiochemical pure Ac-225.

As reported by ORNL, ICP-MS analysis for metal impurities in decayed Ac-225 samples showed that Ca(II) at a level of $\sim$0.1 mg per mCi of Ac-225 is the major metal ion impurity in the samples. Besides Fe (5 µg per mCi of Ac-225), other detected metal ion impurities include Mg, Cr and Mn [208].

Th-229 can act as an almost eternal source of Ac-225 by virtue of its 7880-year half-life, however providing only limited amounts of Ac-225 per year. Since the demand for Ac-225 and Bi-213 is constantly increasing, other methods need to be considered to artificially produce sufficient activities of Ac-225. Ten years ago it was estimated by Geerlings et al. that on average a total dose of 1.25 mCi (= 46.3 MBq, $2{\cdot}10^{-8}$g) Ac-225 is needed per patient [36]. Currently, the most promising process for large-scale, cost-efficient production of curies of Ac-225 is through proton bombardment of Ra-226 following the reaction:

$$^{226}Ra\,(p,2n)^{225}Ac\,. \tag{3.16}$$

For this process, a medium-sized cyclotron with proton energies below 30 MeV is required as it was experimentally demonstrated by Apostolidis et al. The radiochemical separation of Ac-225 from the radiated Ra-226 target yielded a final product which was suitable for TAT [107, 203].

An alternative way of production of Ac-225 is the photo nuclear reaction at linac energies via the production of Ra-225 trough photon-induced transmutation of Ra-226:

$$^{226}Ra\,(\gamma,n)^{225}Ra\,. \tag{3.17}$$

Ra-225 will then eventually undergo β^-−decay to form Ac-225 [209, 203, 210].

3.7.2 Radionuclide (Nano-)Generators

A convenient way of production of medical radionuclides are generators [204, 211, 212]. Generators, often referred to as "cows" , are chromatographic columns loaded

with a longer-lived mother nuclide, which is used to continuously generate a shorter-lived daugther nuclide by radioactive decay. This daughter nuclide can be selectively eluted.

Principle of a radionuclide generator: A mother nuclide A decays to a daughter nuclide B, which then decays to C:

$$A \longrightarrow B \longrightarrow C \; . \tag{3.18}$$

The net formation rate of the daughter B is:

$$dN_B/dt = \lambda_A N_A - \lambda_B N_B \; . \tag{3.19}$$

Practically, there are two different scenarios:

1. **Secular equilibrium**: $T\frac{1}{2}(A) \gg T\frac{1}{2}(B)$, which means that $\lambda_A \ll \lambda_B$. It follows that
$$N_B = (\lambda_A/\lambda_B) \cdot N_A \cdot (1 - e^{-\lambda_B t}) \; . \tag{3.20}$$
Since $N_A \approx$ *constant* this means that the establishment of the radioactive equilibrium is only dictated by the half-life of the daugther nuclide. *Example*: Separation of Ra-225 ($T\frac{1}{2} = 14.9\,d$) from Th-229 ($T\frac{1}{2} = 7340\,y$).

2. **Transient equilibrium**: $T\frac{1}{2}(A) > T\frac{1}{2}(B)$, which means that $\lambda_A < \lambda_B$. It follows that the decay of the mother nuclide also needs to be considered:
$$N_B = [\lambda_A/(\lambda_B - \lambda_A)] \cdot N_{0,A} \cdot e^{-\lambda_A t} \cdot (1 - e^{-(\lambda_B - \lambda_A)t}) \; . \tag{3.21}$$
Example: Separation of Ac-225 ($T\frac{1}{2} = 10.0\,d$) from Ra-225 ($T\frac{1}{2} = 14.9\,d$).

Several requirements need to be met when using a nuclide generator. The elution yields need to be constantly high while the highest possible radiochemical purity of the eluted daughter nuclide needs to be guaranteed. However, especially high LET alpha particle emitter generators are sensitive to radiation damage which eventually leads to generator failure (e.g. radiolytic degradation of the resin, accompanied by parent nuclide breakthrough; column cracking; sintering of the resin and hence hindered flow-through [111]). Furthermore, the continuous generation of radical species on the resin, which results in impure eluate, can lead to poor radiochemical labelling yields. In general, inorganic resins are less subject to radiolytic damage than resins based on organic compounds[27]. Effects of radiation damage from high LET systems to ion exchange resins are well documented [213, 71].

A radionuclide generator should always allow for easy and rapid separation of the mother and often very short-lived daughter, with the daugther being obtained in a chemical form which is suitable for direct application in subsequent radioconjugate synthesis. Two of the most important generator systems used in nuclear medicine are the Mo-99/Tc-99m generator for SPECT and the Ac-225/Bi-213 generator for α-therapy (see paragraph 3.7.2.1). With approx. 30 million applications per year, Tc-99m is the most commonly utilised radionuclide in nuclear medicine. This is partly owed to its manifold coordination chemistry which facilitates the development of new radiopharmaceuticals (8 different possible oxidation states from -I to +VII) [214]. The mother nuclide Mo-99 is commercially reactor-produced by intense neutron-bombardment of highly purified U-235 targets (n,fission).

3.7.2.1 Production of Bi-213: The Ac-225/Bi-213 Generator

ITU's Ac-225/Bi-213 generator system is commonly applied in clinical and preclinical studies throughout the world (Fig. 3.26). The developed generator provides up to 25 mCi of pure chemically reactive Bi-213, which can be readily used for radiolabelling [112, 111]. Ac-225 is adsorbed on the inorganic resin AGMP-50 from which Bi-213 can be selctively eluted with NaI. Due to its short physical half-life, the duration of generator elution, radiolabelling and of compound purification must be short to obtain reasonable amounts of Bi-213-radioconjugates of high quality and radiochemical purity. Overall, the optimised protocol allows for Bi-213-RIC production within only 20 minutes. The ITU's Bi-213 generator is currently sucessfully applied in locoregional therapy of glioma [145].

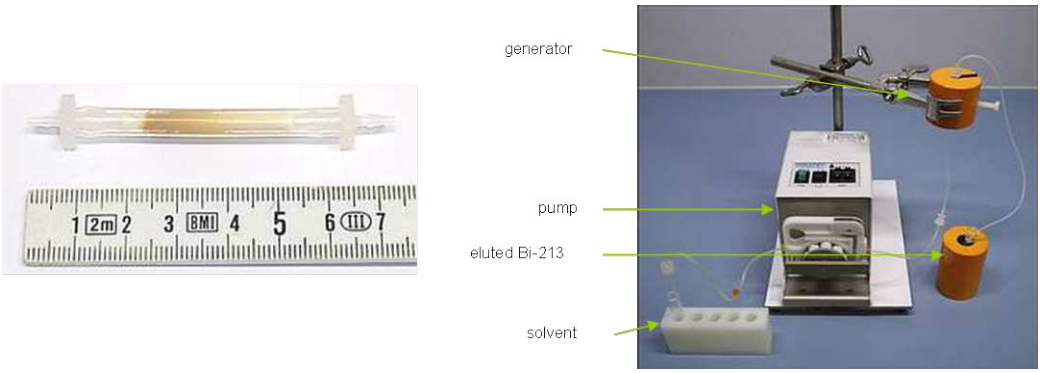

Figure 3.26: ITU's Ac-225/Bi-213 generator. Setup for semi-automated elution using a peristaltic pump connected with a silicone tube [7].

However, the half-life of 46 min complicates the clinical preparation of radioconjugates for untrained personnel. Also the use of Bi-213 as therapeutic radionuclide is limited to situations in which fast targeting of cancer cells can be achieved, such as in case of leukemia or in locoregional treatment approaches (e.g. glioma).

One solution to this constraint is to deliver an Ac-225 / Bi-213 generator device of molecular dimensions to the target tumour cell. The idea of applying such an "*in vivo* nanogenerator" dates back to the 1920's.

3.7.2.2 The Ac-225 *in vivo* Generator

The concept of using Ac-225 as *in vivo* generator, with each Ac-225 atom producing a cascade of 4 alpha particle at the targeted site, was proposed by McDevitt [60, 61, 3]. The generator consists of a single Ac-225 generator atom attached to the delivery vehicle via a bifunctionalised DOTA derivate (Fig. 3.27). In addition to being much more potent than a single Bi-213 atom, the half-life of the Ac-225 *in vivo* generator (10.0 d) also facilitates targeting of slowly accessible tumours. Critical for the success of this generator approach, however, is the retention of the 4 daughter alpha emitters at or in the target cells. Hence, selection of tumour antigen systems that internalise the Ac-225 generator conjugate helps to retain the daughters and therefore lead to enhanced potency; however, internalisation is not compulsary [1].

When applying *in vivo* generators, it has to be considered that daughter nuclides may be metabolised in a different way to the parent, which is particularly important if the daughter nuclides have a long physical half-life. Since the first alpha emission in the decay chain invariably generates sufficient recoil energy to release the immediate

daughter nucleus from the chelating moiety (see Glossary "recoil energy"), it is likely that subsequent $\alpha-$emitting daughters with changed periodicity will circulate and distribute elsewhere, causing toxicity to healthy organs and tissue. However, it is

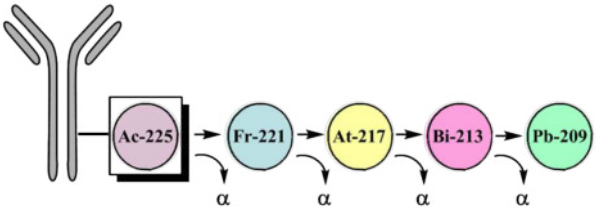

Figure 3.27: The Ac-225 in vivo generator, releasing 4 alpha particles.

possible that the long half-life of Ac-225 facilitates effectual biological clearance of chelated Ac-225 before perceptible decay occurs [4].

Recently, a novel study on the *in vivo* generator Th-227-p-SCN-Bn-DOTA-MabThera® has been published [215, 216, 217].

3.7.3 Ac-225 vs. Bi-213

The use of Ac-225 in TAT has advantages over the use of its short-lived daugther nuclide Bi-213. Ac-225 shows extreme cytotoxicity in comparison to Bi-213 which produces no α-particle cascade. From the ∼27 MeV energy which is released during the decay of one single Ac-225 atom and its subsequent decay daughters, over 90 % is carried by short-range, high LET α particles. According to the literature, it was found that 1 µCi (= 37 kBq) of Ac-225 delivers a dose of 7.5 Gy of energy to the tumour tissue, inducing a tumour cell killing rate of 99.99 % [138]. The better efficacy of Ac-225 over Bi-213 can be attributed to the 4 times higher absorbed radiation dose due to the 4 alpha emissions. In clinical trails with leukemia patients it was found that 1 mCi Bi-213 (= 37 MBq) per kg body weight is needed for efficient treatment, while with administration of only 2 µCi Ac-225 (= 74 kBq) per kg body weight comparable results are achieved [201]. It was also reported that tumour-specific Ac-225 radioimmunoconjugates kill tumour cell lines *in vitro* at doses up to 1000 times lower than that of the comparable Bi-213-containing constructs [48]. However, in other studies the Ac-225 conjugates displayed ∼35 % lower immunoreactivity compared to Bi-213 [197].

Bi-213 is mainly applicable in locoregional approaches [144] or in combination with fast diffusing carriers which facilitate fast tumour targeting. One advantage of Bi-213 is the half-life of 46 min, which is very suitable for *in vitro* evaluation because after 8 h more than 99.9 % of Bi-213 has decayed [199]. This is also convenient for patient treatments since it reduces the residence time in hospital. Nevertheless, the short half-life of Bi-213 complicates the preparation of radioimmunoconjugates for clinical use. In summary, the higher efficiency (4α) and longer half-life of Ac-225 overcomes its lower immunoreactivity compared to Bi-213 and could therefore be the nuclide of choice in the future.

3.8 The Fate of Ac-225 Radioconjugates in the Organism

3.8.1 Radioconjugate Stability in Serum

The rigid structure of the macrocyclic chelators greatly hinders dissociation of the radionuclide from the RIC. However, once injected into the blood circulation, the RICs are extremely diluted, which favours the loss of the metal ion. In addition, blood serum contains substantial concentrations of challenging molecules such as metal-binding proteins, carbonate and chelatable metal ions (e.g. Ca^{2+}, Mg^{2+}) that compete for chelators on the RIC [218]. An overview of the most importent blood serum components is given in Table 3.3. Also protonation of the chelating groups at physiological pH 7.4 is an issue. Thus, if a radionuclide dissociates from its chelator, it will most probably not return [219].

Table 3.3: Concentration of human blood serum components of particular interest with respect to radioimmunoconjugate stability under physiological conditions [142].

Species	*concentration [mol/L]*
Na^+	$1.5 \cdot 10^{-1}$
Ca^{2+}	$2.5 \cdot 10^{-5}$
Cu^{2+}	$1.8 \cdot 10^{-5}$
Zn^{2+}	$1.5 \cdot 10^{-5}$
phosphate	$3.8 \cdot 10^{-4}$
carbonate	$2.5 \cdot 10^{-5}$
HSA	$6 \cdot 10^{-4}$
HSTF	$3.7 \cdot 10^{-5}$

The proteins in serum which are most likely to compete for the nuclide are transferrin (TF), human serum albumin (HSA) and human serum transferrin (HSTF), a combination of TF and HSA [218, 118, 220]. Though transferrin has strong preference for metal cations with high positive charge, HSTF is the primary serum transport molecule of various tri- and tetravalent metal ions. Metal binding to both types of transferrin generally requires simultaneous binding of carbonate as a synergistic anion.

Human Serum Albumin comprises approximately 50 % of blood serum protein and is the most abundant protein in human blood plasma [221]. HSA is the major Zn^{2+} transport protein in blood and is known to bind many metals non-specifically. Both protein types are strong competitors for radionuclides under *in vivo* conditions. Considering that the concentration of natural chelators in blood is much higher than the concentration of injected labelled conjugate, the stability of the complex should ideally be several orders of magnitude higher than the stability of the corresponding complex with blood proteins. In a study by Montavon *et al* it was determined that a chelate requires a stability constant of at least $\log K = 19$ at physiological conditions in order to withstand the competition from HSA, HSTF as well as carbonate, in particular [221].

Evaluation of the stability of radioimmunoconjugates *in vivo* is complicated by the variety of metabolic pathways available to the antibody and its radionuclide [115]. Therefore *in vitro* serum stability studies under simulated physiological conditions (i.e. incubating the samples at 37 °C / 5 % CO_2 atmosphere, since carbonate

complexation is predominant in serum at physiological pH 7.4) are conducted over an appropriate time period. However, stability *in vitro* does not necessarily warrant *in vivo* stability [83].

Radionuclides which are lost or released from their conjugates, particularly the decay-generated and uncomplexed daughter nuclides, will be coordinated by the metal-binding proteins blood. However, if the driving force for the chelate dissociation is the formation of a new, thermodynamically stronger complex with another ligand, than a so-called "transchelation" occurs. This effect was reported by Kaspersen *et al* for an Ac-225-Bn-DTPA conjugate in serum containing cell culture medium (pH 7.2) [71]. Due to transchelation, Ac-225 was found to be released from the RIC within 15 - 30 min. This study indicates the importance of the kinetic inertness for medicinal RICs .

3.8.2 Biodistribution

It is important to know or estimate the potential problems and damage a radionuclide can cause after its conjugate is injected into the patient. Generally, radioconjugates in the body are likely to lose the complexed nuclide over time, which results in free nuclide circulating through the body, following the pharmacokinetics and biodistribution of simple salts [115].

Radiotoxicity occurs predominantly in organs which metabolise radiolabelled biomolecules, such as the liver and kidneys [128, 113]. The long-term renal toxicity caused by rapidly redistributed Bi-213 is still the main concern of radioimmunotherapy with Ac-225 [67, 222, 223]. Due to the short half-life of Fr-221 and At-217 it is not possible to get significant data for their in vivo distribution, but because of their short half-life they are probably not able to dislodge far from the decay site. Internalisation into the targeted cells helps to prevent extreme radiotoxicity since Fr-221 and Bi-213 then retained in or near the cell [113, 60].

Also radiosensitive organs with prolonged exposure to nuclides from the blood are subject to radiotoxicity, which is why the use of bone-seeking radionuclides is critical. Thus, RIT is especially limited by the absorbed dose to the bone marrow.

3.9 Strategies for Radionuclide Labellings

For successful design of therapeutic radioimmunoconjugates, the choice of the labelling method is as important as the choice of the radionuclide, chelator and vector. While considering a variety of biological and pharmacological factors, the best method for stable attachment of a given nuclide to a given carrier has to be selected and optimised [224].

3.9.1 General Considerations for the Development of Labelling Protocols

There are a number of general radiochemical requirements which need to be met in order to develop an efficient labelling strategy:

- The selected radionuclide should be relatively cheap, available in sufficient amounts and, idealy, readily applicable for radiolabelling without further processing.

- The overall-yield of the labelling procedure should be maximised and loss of expensive radionuclides should be avoided. For radionuclide therapy, this includes that the specific activity of the radioconjugate should be as high as possible. However, high labelling yields often require lengthy reaction times and, at the same time, high concentrations of all reagents. Since long reaction times with a high concentration of radionuclide increases the risk of radiolysis, labelling procedures should be kept as short as possible.

- The labelling method should lead to no chemical modification or distortion of the biomolecule's ternary structure, which often relies on disulfide bridges. A cleavage of a crucial disulfide bond may cause loss or significant decrease of binding affinity and target specificity. Also modification of amino acids at the binding site as well as radiolysis can turn a radioconjugate more or less non-functional. The risk of severe radiolytic damage is particulary high for biomolecules labelled with therapeutic high LET nuclides, where the major part of decay energy is deposited in a small volume [225]. Strategies for prevention of radiolysis during labelling, storage and transportation have to be developed. It has been demonstrated that e.g. the addition of the scavengers ascorbic - or gentisic acid efficiently protects antibodies even during labelling with α-emitters [226, 227]. Sufficient dilution of the product can also prevent radiolysis during transport and storage [70, 228].

- The labelling method should produce a thermodynamically stable radioconjugate with adequate kinetic stability during storage, transportation and in blood circulation. Since rapid formation of thermodynamic stable complexes with e.g. macrocycles like DOTA often require elevated temperatures, a labelling temperature needs to be selected which allows for quick and complete conversion without damaging the temperature sensitive antibodies (max. T = 45 °C). Peptides are more resistant to higher temperatures (e.g. T = 95 °C) [229].

- The labelling and purification methods should be reliable, robust and facile in order to eliminate the probability of human errors when conducted by less trained personnel. This can be achieved by mimising the process steps, e.g. the number of solution transfers. Also heating and purification steps should be avoided if possible. The purification method should guarantee for high radiochemical purity,

typically higher than the purity that is acceptable for diagnostic radioconjugates. When high radioactivities need to be handled, the implementation of an automated device for labelling and purification should be possible [230].

- The labelling protocol should match the distribution strategy. Facile protocols are crucial for the development of labelling kits for routine use in hospital or when centralised production with subsequent distribution of the conjugates is not possible. A labelling kit generally provides more flexibility and minimises the influence of radiolysis.

3.9.2 Labelling Approaches

Generally, besides direct radiolabelling, there are two main approaches to synthesise a radioimmunoconjugate (Fig. 3.28) [44, 193]:

1. **The pre-labelling approach** or "preformed chelate" approach is a two step synthesis, involving the formation of the functionalised metal chelate in the first step and conjugation of this chelate to a biomolecule in a separate second step. An example for this pre-labelling is the protocol for the synthesis of Ac-225-DOTA-radiopharmaceuticals applied by McDevitt *et al* [6]. In this approach the targeting biomolecule is not exposed to the sometimes required harsh conditions (e.g. elevated temperature, extreme pH) of the coordination step. However, a major disadvantage of this synthesis route is the low radioconjugate yield. Additionally, multiple step radiosyntheses are often complex and too time consuming for routine clinical use. Also it is very difficult to develop a kit formulation.

2. **In the post-labelling approach**, a bifunctionalised chelating agent is first attached to the biomolecule to form the immunoconjugate. Once the conjugate is prepared it can be stored under appropriate conditions (buffer pH 7.4, fridge/freezer). The radiolabelling can then be conducted by direct reaction of the conjugate with the radionuclide. The reaction conditions need to permit effective complexation without damaging the biomolecule. In the majority of cases, a well-optimised post-labelling provides a labelling efficiency of about >95%, which often excludes the necessity of an additional purification step. This approach combines the ease of direct labelling with the well-defined chemistry of the preformed chelate approach and is the most practical approach for kit formulation and development of commercial products.

An example for the supremacy of this one-step over the two-step approach is the radiolabelling of monoclonal antibodies with At-211 ($t_{\frac{1}{2}} = 7.1$ h) [214]. The standard pre-labelling approach includes two radiochemical steps, namely the chelation (at pH 5.5) and the conjugation to the mAb (at pH 8.5), achieving yields of 30 - 60 % within 60 min reaction time. Here, the activity loss through decay during labelling causes the low yields, which indicates that more rapid one-step protocols are especially advantageous for labelling with short-lived radionuclides. The protocol was optimised by Lindegren *et al* who developed a synthesis scheme involving only one radiochemical step, the chelation at pH 5.5, with the conjugation to the antibody (pH 8.5) being conducted in a previous, independent step [231]. With this protocol, yields of 60 - 80 % were achieved within 15 min, which minimised the activity loss by decay. With this approach, however, 10 % unspecific binding of At-221 to the

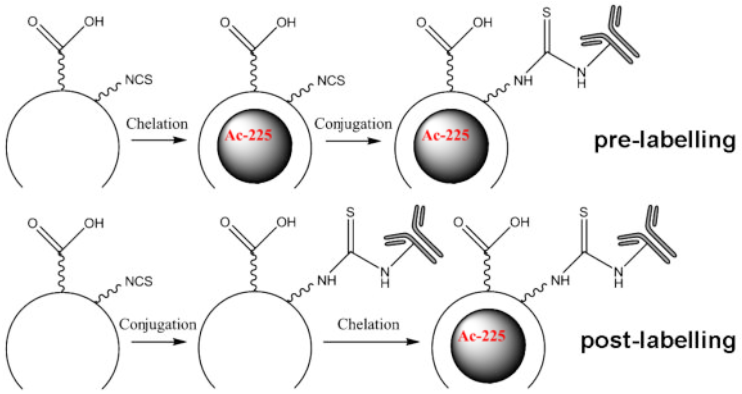

Figure 3.28: Scheme of the two main approaches for the synthesis of radioimmunoconjugates: pre-labelling approach (2 steps, *top*); post-labelling approach (1 step, *bottom*). Modified from [44].

mAb was observed. The radioconjugates synthesised via both routes show poor *in vivo* stability; therefore, they are only applied in locoregional therapy schemes.

3.9.3 Protocols for Radiolabelling of Antibodies and Peptides with Ac-225

As mentioned above, a two-step synthesis protocol for the radiolabelling of DOTA-mAb-conjugates with Ac-225 was developed by McDevitt *et al* [6]. The protocol however suffers from low overall-yields of labelled antibody. It was postulated that heating to 60 °C, which allows a certain degree of ring flexibility, is necessary to achieve complete and stable Ac-225 coordination by DOTA. This temperature is however unsuitable for the retention of the mAb function. Therefore, a pre-labelling procedure was proposed to spare the antibody the harsh conditions.

This procotol was already pre-optimised in previous studies [7]. A post-labelling protocol for peptides and antibodies was introduced and evaluated at ITU, leading to significant improvements in terms of reaction time and labelling yields. Both protocols are discussed in the following paragraph.

3.9.3.1 Labelling protocol of McDevitt *et al*:

1) Ac-225-DOTA-complexation: Ac-225, dissolved in 0.2 M HCl (0.86±0.40 mCi (= 31.8 MBq)), is mixed with 10 mg/ml DOTA-NCS in MFW (0.229±0.098 mg), 0.015 - 0.020 ml of 150 g/l L-ascorbic acid (radioprotectant) and 0.025 - 0.150 ml of 2 M TMAA. The pH of the resulting solution is 5.4±0.3. The mixture is heated to 56±3 °C for 42±14 min. Heating to 50 - 60°C for 30 - 60 min allows for the reaction to rapidly complete and form the most stable species.

At the end of the reaction the solution is separated via column chromatography. The column and washes are counted after 30 min using a gamma detector to determine the Fr-221 activity, and from this, the respective percentage of Ac-225 chelated by the DOTA-NCS. The efficiency of this first step is, on average, 93±7 % (and has been improved recently to give 99 %, [87]). This means, that 1 in about 5000 DOTA molecules is coordinating an Ac-225 ion [6].

However, HPLC studies showed that this first step largely degrades the isothiocyanate moiety which is required for conjugation to the antibody in the second step.

It is suspected that this degredation resulting from hydrolysis of the isothiocyanate moiety under the acidic conditions [232].

2) Reaction of Ac-225-DOTA-NCS with the IgG: The solution containing the product of the first reaction step is mixed with IgG (0.9±0.4 mg), 0.015 - 0.020 ml of 150g/l L-aa and 0.025 - 0.150 ml of 1 M sodium carbonate buffer. The pH of the resulting solution is 8.7±0.3. The reaction mixture is then warmed up to 36±2 °C for 52±14 min. At the end of this time period, 0.020 ml of 10 mM DTPA is added in order to complex any free metals during the subsequently conducted size exclusion purification (10 DG column, 1 % HSA as mobile phase). To determine the radiochemical purity, ITLC-SG is used. The strips are counted in the gamma detector after equilibrium between Ac-225 and Bi-213 is established. The average radiochemical yield is 9.8±4.5 % of ∼98 % radiochemical pure product. The results of both steps translate into a final drug with about 1 in 775 IgG molecules radiolabelled with Ac-225.

The yields are low but sufficient for preclinical and clinical trials, as the extreme potency of these RIC reagents allows studies to commence with 50200 nCi (= 1.9-7.4 kBq) activity. Another issue of this labelling method is the low specific activity, which may constrain the use of the conjugates for diseases with relatively low antigen expression.

3.9.3.2 Labelling Protocol established at ITU (Diploma Thesis)

From the findings of McDevitt et al., it was apparent that a number of variables needed to be investigated in order to improve on the poor effciency of the labelling. These studies were conducted at ITU and are summarised in the Diploma Thesis, S. Kannengießer, 2009 [7]. Revision of reaction parameters such as reaction time, temperature, metal-to-ligand-ratio and reaction pH facilitated the establishment of an optimised one-step-protocol for radiolabelling of DOTA-Substance P, DOTA-F3 and DOTA-MabThera®. The labelling yields were found to be notably dependent upon the pH of the reaction mixture.

Initially, in an independent, previous step, the employed peptides and antibodies are chelated with DOTA, characterised and stored in NaOAc-buffer at 4 °C. They can be readily used for radiolabellings.

One advantage of the following protocol is that radioactivity is only involved during one step of the protocol. The ideal labelling was proven to take place at pH 9 (100 µl 2 M TRIS, 50 µl 20 % AA) and requires heating to 37 - 45 °C for 15 min to come to full conversion (> 95 %). Since this protocol has been only evaluated for specific activities of up to 2 µCi (= 74 kBq) per 100 µg mAb, the aim of the present PhD project is to translate the established protocol to higher specific activities of ≥ 10-20 µCi (= 370-740 kBq) per 100 µg mAb (required for clinical studies).

4 Materials and Methods

In this work, several methods were applied to prepare the reactants and separate, purify and analyse the obtained complexes and radioconjugates. These methods were chosen based on common practice and have been refined following previous work within the field. All chemicals were purchased from Merck or Sigma Aldrich and were of highest purity available. Purified water (MilliQ, $\rho = 18.2$ MΩ) was used to prepare all solutions

4.1 Preparation and Characterisation of the Reactants

4.1.1 Actinium-225

4.1.1.1 Production of Ac-225

ITU's Th-229 source (46 mCi (= 1.7 GBq)) can provide 43 mCi (= 1.6 GBq) Ra-225 and 39 mCi (= 1.4 GBq) Ac-225 every 9 weeks (∼63 d). The milking of Ra-225/Ac-225 from the Th-229 cow is based on ion exchange chromatography in nitric acid medium [112, 207].

Ac-225 is obtained through radionuclide separation from provided Ra-225 following the protocol for a combined UTEVA-DGA extraction chromatography. Since Ra-225 has a half-life of $t_{\frac{1}{2}} = 14.9$ d, fresh actinium can be efficiently separated from the Ra-225 stock every two weeks. However, due to the half-life of Ac-225 ($t_{\frac{1}{2}} = 10.0$ d) there will be a long term net loss of Ac-225 (Fig. 4.1). As long as Ra-225 and Ac-225 are stored together, the daily net loss of Ac-225 is 2 %, resulting from 5 % in-growth from decay of Ra-225 and a 7 % loss through Ac-225 decay [208].

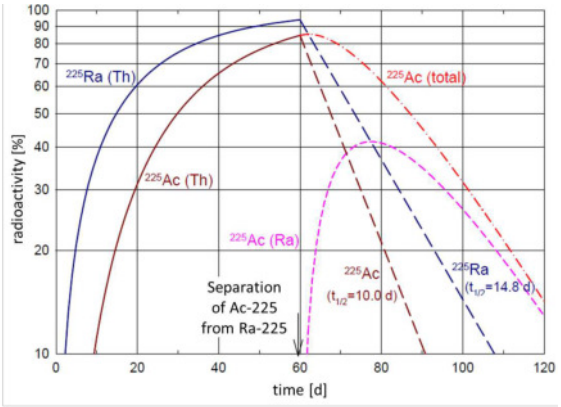

Figure 4.1: Growth of Ra-225 (a) and Ac-225 (b) and decay of Ra-225 (c) / Ac-225 (e); Ac-225 growing in freshly purified Ra-225 (d); (f) total Ac-225 activity, sum of (d) and (e). Modified from [208].

Ra-225/Ac-225 Separation Procedure A BioRad column is packed with 0.9 ml of UTEVA resin (Uranium and TEtraValent Actinides, based on dipentyl-pentyl phosphonate) and plugged with glass wool. A second column is packed with 0.6 ml of pre-conditioned DGA-branched resin (*N,N,N',N'*-Tetrakis-2-EthylHexyl-DiGlycolAmide, "TEHDGA") and closed with a 8.0 mm frit. The UTEVA column is then placed on top of the DGA column and both are conditioned with few milliliters of 4 M HNO_3 prior to use [207].

The load solution (Ra-225 stock in 4 M HNO_3) is applied to the UTEVA column followed by washing with 4 M HNO_3. Under these conditions, Ac-225 will be adsorbed onto the DGA resin while Ra-225 will flow through. When the remaining activity on the UTEVA is negligible the column is removed. The DGA column is then washed with few millilitres of 4 M HNO_3 until the eluted fraction is colourless. All washing fractions need to be monitored for Ac-225 breakthrough (γ-spec). After washing, the DGA column is incubated with 300 µl (= half bed volume) of 0.05 M HNO_3 for 8 - 10 min. Ac-225 is then eluted from the column with 0.05 M HNO_3. The first fraction (400 µl) is discarded; the majority of Ac-225 is eluted in fraction 2 and 3 (150 µl each). In general, the washing/elution steps should be kept to a minimum to avoid bleeding of the organic extracting agents from the resins, which were demonstrated to readily complex metal cations in solution and hence potentially disturb further reactions (see paragraph 5.4.1.3).

4.1.1.2 Purification of Ac-225

To ensure highest chemical purity of the obtained Ac-225, additional purification was found to be necessary. Residual organic impurities from the extraction process are removed by passing the Ac-225 solution through a BioRad column filled with 1 ml of Eichrom pre-filter resin. The eluate is then evaporated to dryness and redissolved with concentrated nitric acid. The solution is again evaporated at $\geq$140 °C in order to oxidize remaining organic impurities. This process is repeated once with concentrated HNO_3 and once with 0.05 M HNO_3. The residing Ac-225 is finally redissolved with approx. 200 µl of 0.05 M HNO_3, resulting in a concentrated $Ac(NO_3)_3$ stock solution ready for further use.

4.1.1.3 Quality Control of Ac-225

ICP-MS analyses were performed on various Ac-225 stock solutions to detect metallic impurities [233]. The impurities are brought into the system through chemicals (HNO_3, water) and materials used (plastic ware, vials). Especially bi- and trivalent cations are of concern, e.g. Fe(II)/(III), Ca(II), Mg(II), Cr(II), Mn(II), since these cations form highly stable complexes with DOTA (Table 3.16) and will compete with Ac(III) during complexation [208, 156]. The concentrations of most metals were very low or below detection limit. However, iron and calcium were found to be present in large excess over actinium. It is hence recommended to always wash all vials prior to use and generally avoid iron contamination.

An UTEVA-based cleanup of Ac(III) stock solutions from cumulative Bi(III) daugther nuclides (Bi-213, Bi-209), which are also expected to disturb the labelling reaction (log $K_{\mathrm{Bi(III)DOTA}}$~30.3), was not successful. It is recommended to always use freshly prepared Ac-225 ($<$ 5 days, preferably only 1 or 2 days after separation) to avoid competition from exponentially ingrowing Bi-209 (Fig. 5.40, *green*).

To ensure high radiochemical purity and quality of the obtained Ac-225, a sample of the Ac-225 fraction is measured using gamma spectrometry. No activity of the mother nuclides Th-229 and Ra-225 is detected in the γ-spectrum if the separation process was successful.

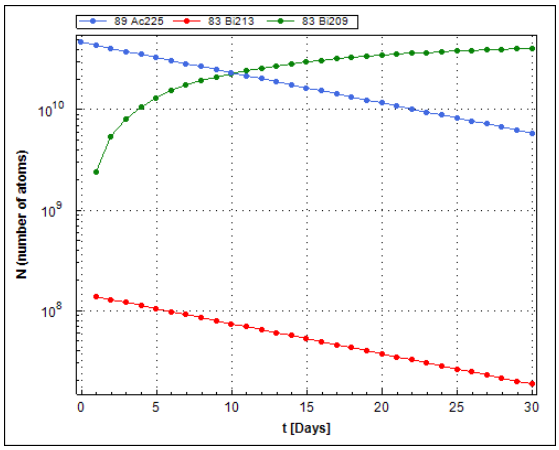

Figure 4.2: Decay of 1 µCi Ac-255 (*blue*) during 30 days. Calculated and drawn with Nucleonica decay engine [234].

4.1.1.4 Gamma Spectrometry

A gamma spectrometer determines the energy of gamma rays emitted upon radioactive decay. The gamma rays produced by different radionuclides vary in energy and intensity, so they are specific for each radionuclide. The area of the peak is proportional to the amount of radionuclide in the sample. The detectors used were high-purity germanium semiconductor detectors (high resolution HpGe detector (Canberra), connected to a DSPEC jr 2.0 signal amplifier (Ortec)).

Since the γ-emission probability of Ac-225 is too low to give reliable results (Table 4.1), the two γ-lines of the Ac-225 daughter nuclides Fr-221 and Bi-213 are used for quantification (Fig. 4.3). The measurements are performed after the decay equilibrium of Ac-225 is attained. The activity of the mother is then extrapolated from the counts of the daughters.

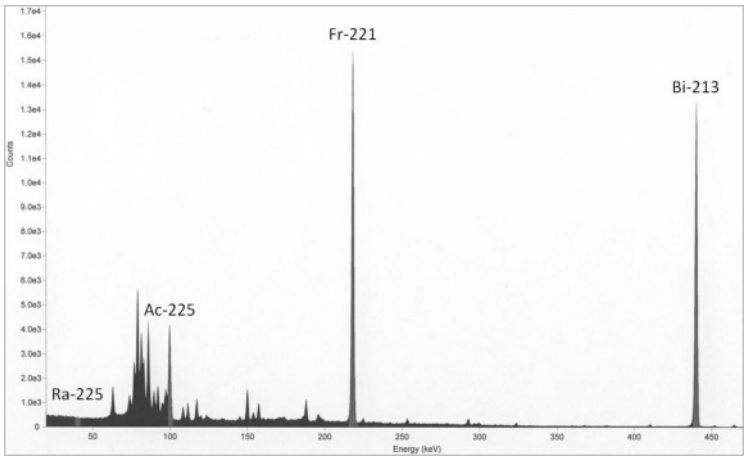

Figure 4.3: A typical gamma spectrum of Ac-225, in secular decay equilibrium with its daughters Fr-221 and Bi-213.

Table 4.1: Main γ-energies of Bi-213, Fr-221, Ac-225 and Ra-225 with associated emission probabilities [235].

Nuclide	***γ- energy*** $[keV]$	***γ- emission probability*** [%]
Bi-213	440.46	26.1
Fr-221	218.1	11.6
Ac-225	99.8	1.7
Ra-225	40	30

4.1.2 Curium-248

Cm-248 is commonly obtained by alpha decay of Cf-252 ($^{252}_{98}Cf \rightarrow ^{248}_{96}Cm$) [88, 236]. The Cm(III) in the present work was received as $Cm(ClO_4)_3$ stock solution in 0.1 M $HClO_4$. The isotopic mass distribution of the Cm(III) stock solution is 97.1 % Cm-248, 2.8 % Cm-245, $<$ 1 % Cm-243, Cm-244, and Cm-246.

4.1.3 DOTA, DOTA-NCS

DOTA and the bifunctionalised derivative DOTA-NCS (*p*-SCN-Bn-DOTA) were purchased from Fluka/Sigma-Aldrich Co. LLC and Macrocyclics, Inc., respectively, and were used as received. All solutions of DOTA, DOTA-NCS and its mAb-conjugates were prepared and stored in a 0.15 M NaCl/0.05 M NaOAc buffer. To monitor the chemical purity, samples of DOTA were analysed with NMR and mass spectrometry.

4.1.4 Rituximab, anti-CD20 antibody

The chimeric antibody MabThera® (CD20 rituximab, Mw_{ave} 143,859.70 g/mol, $C_{6416}H_{9874}N_{1688}O_{1987}S_{44}$[196]) is commercially available (Roche Deutschland Holding GmbH). For being applicable in TAT, a suitable number of chelating moieties needs to be attached without diminishing its antigen-binding ability.

4.1.4.1 Conjugation with DOTA-NCS

The preparation of mAb-ligand conjugates is based on the chemical attachment of the bifunctionalised chelator to the antibody. In the case of DOTA, *p*-SCN-benzyl-DOTA (DOTA-Bn-NCS, Mw 697.45 g/mol) is used (see paragraph 3.5.4). The conjugates are formed by formation of very stable thiourea bonds between the isothiocyanate group and the amino group of the ε-lysine chain.

For preconcentration and trans-buffering of MabThera®, Millipore filtration devices are used which permit retention and nearly quantitative recovery of the mAb (Amicon® Ultra-4 Centrifugal Filter Units, 4 ml volume, with membrane of NMWL of 30 kDa). To 1 ml of the MabThera® solution (c = 10 mg/ml, Mw $\sim$ 150.000 g/mol) 3 ml 0.15 M NaCl/0.05 M $NaHCO_3$ buffer (pH 9) is added. The solution is centrifuged until 1 ml remains in the filter. This washing step is repeated 3 times.

DOTA-NCS is then added to the MabThera® solution after is was dissolved in 1 ml 0.15 M NaCl/0.05 M $NaHCO_3$ buffer. The required amount of chelator was

calculated according to the following equation:

$$\frac{10\,mg\,MabThera®}{150.000\,g/mol} \cdot 697.45\,g/mol \cdot 15 = 0.697\,mg\,DOTA - NCS\,. \qquad (4.1)$$

To obtain the desired ratio of chelator/mAb, the chelator is usually introduced in 15-fold excess. The mixture (2 ml, pH 7.5 - 8) is stirred over night (18 h). Afterwards the mAb-conjugate requires 3 times washing with 0.15 M NaCl/0.05 M $NaHCO_3$ buffer (pH 9) and is then trans-buffered by washing with 0.15 M NaCl/0.05 M NaOAc buffer (pH 7.4, 4 times). Finally the conjugate is recovered into a total volume of 1000 µl of 0.15 M NaCl/0.05 M NaOAc buffer and stored at +4°C [237]. With this protocol, an average number of 3 - 6 chelators per antibody molecule was deducted from previous studies.

4.1.4.2 Concentration of Chelated Antibody

To evaluate the concentration of the antibody conjugate, various methods are available with most of them relying on colorimetric assays [238, 239] or UV-Vis spectroscopy [240].

Colorimetric Hartre-Lowry Protein Assay: Various dilutions of protein standard and of the chelated antibody solution are prepared in a micro plate. 25 µl of reactant A (containing copper ions) and 200 µl of reactant B are added to each of the samples. The plate is slightly shaken to mix the solutions and is then incubated for 15 min at room temperature. The colour intensity of the solutions is related to the protein concentration. Afterwards the plate is read in a micro plate reader set to 620 nm. From the protein standard dilutions a calibration curve is fitted (Fig. 4.4). By comparison with the results for the mAb-conjugate samples, the concentration of the antibody can be intrapolated [239].

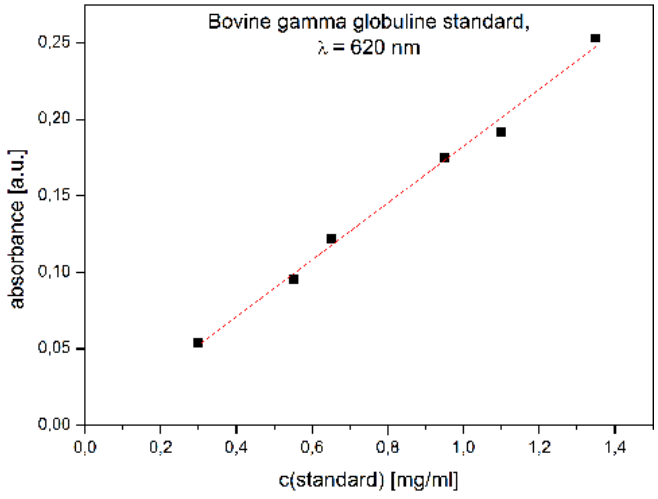

Figure 4.4: Calibration curve for the BioRad protein assay; absorbance (A) as function of the concentration of the standard solutions.

UV-Vis-Spectroscopy (Wavescan): For accurate determination of concentrations, UV absorbance spectroscopy is the preferred method because it is not dependent on additives causing additional errors [240]. UV absorbance spectra of the *p*-SCN-Bn-DOTA-mAb-conjugate in acetate buffer are measured at 280 nm since the absorption band at 230 nm is not specific (Fig. 4.5) [193]. In preliminary experiments, the extinction coefficient was determined experimentally using IgG standard ($\varepsilon = 1.388\ \frac{ml}{mg \cdot cm}$; for a typical mAb (IgG) solution $\varepsilon = 1.4\ \frac{ml}{mg \cdot cm}$) [241]. The DOTA ligand itself shows no UV absorbance. The concentration of the antibody is calculated according to the Beer-Lambert Law [240]:

$$\frac{A_{280}}{\varepsilon} = c \cdot l\ ,\ l = 1\,cm\ . \tag{4.2}$$

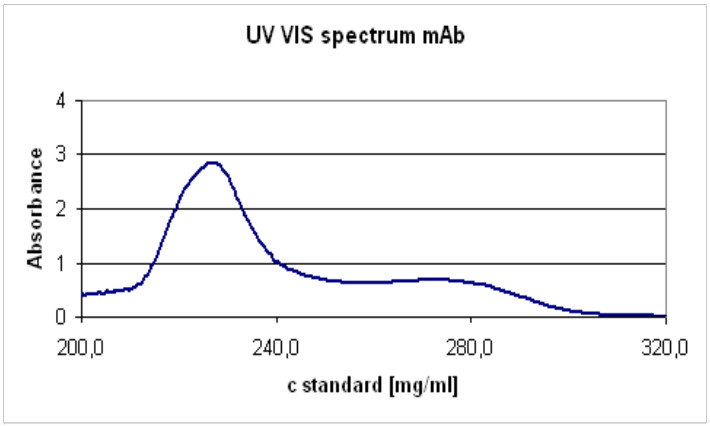

Figure 4.5: UV-absorbance spectrum for determination of the concentration of the DOTA-chelated antibody. *Here*: c = 9.1 mg/ml

4.1.4.3 High Performance Liquid Chromatography (HPLC)

Since some biomolecules are known to form dimers or polymers as a consequence of cross-linking due to bifunctional chelator substitution, the chelated antibody should be analysed with respect to this property. In the case of MabThera®, which in the present work is chelated with DOTA-NCS containing only one reactive group, dimerisation is not expected.

To check on this assumption, one exemplary DOTA-NCS-mAb sample was analysed in our group by HPLC. The potentially contained dimeric and monomeric fractions can be seperated and quantified with a size exclusion chromatographic column [242]. The analysis was performed using a Waters chromatography system (20 µl sample loop injector, Waters 2487 Dual -λ−absorbance detector, a Waters 600 controller and Millennium software). A size exclusion column TSK-GEL-G3000SWXL (TOSCH Bioscience, 7.8 mm x 30 cm L, particle size 5 µm) as a stationary phase and PBS pH 7.4 as mobile phase were used at a pump velocity of 1 ml/min.

For the DOTA-NCS-chelated MabThera® dimerisation was not observed. The recorded, representative spectrum shows only one peak at 8 min, which is typical for monomeric IgG type antibodies [241].

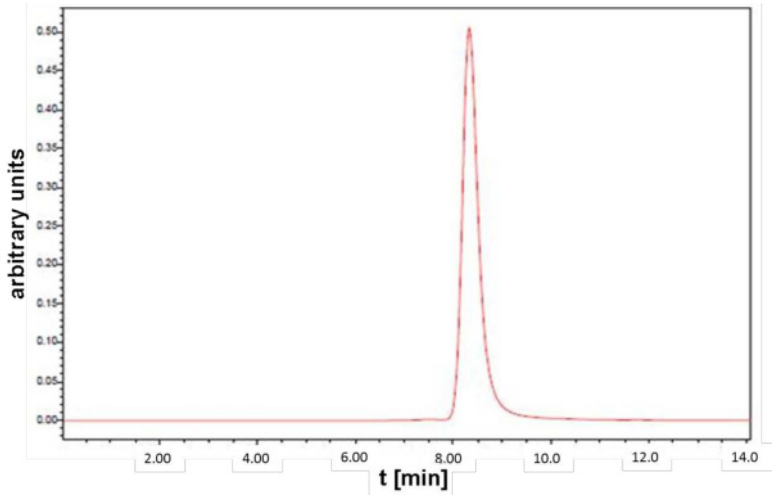

Figure 4.6: SE-HPLC chromatogram of DOTA-NCS-chelated MabThera®.

4.1.4.4 Number of Chelators

In order to achieve optimal and reproducible performance of chelated antibodies, it is necessary to know the number of chelators per mAb-molecule (Ch/mAb) [238]. The average level of substitution is a fundamental characteristic that has influence on the labelling behaviour of the antibody conjugate and its antigen binding efficiency. The ideal conjugate has a suitable degree of chelators attached and still shows the same chemical and biological behaviour as the unlabelled biomolecule (e.g. selective binding to a receptor; ability to incorporate into biological membranes) [243, 244]. The quantification of usually only few low molecular weight ligands attatched to a monoclonal antibody requires a simple but accurate and reproducible method, e.g. spectrophotometry or radiochemical assays [242].

Radiotitration/Radioisotope binding assay: The procedure is based on titration of the mAb-conjugate with carrier-added radiotracer [244, 245]. In this study, a La(III) standard is used as carrier for Ac-225. The molar excesses of metal ions for labelling over chelators on the conjugate increases in each titration step. Eventually, the excess of metal ions is so high that Ac-225 is not able to bind to the DOTA mAb-conjugate anymore.

Due to the poor kinetics of Ac-225-DOTA-complex formation, the assay is conducted as a batch. The labelling follows the usual protocol. To the Ac-225 solution (5 µCi (= 185 kBq), in 0.05 M HNO_3), La(III)-Spex-standard or $La(NO_3)_3$ is added to obtain a Ac-225/La(III) stock solution with c(M(III))= $7.2 \cdot 10^{-5}$ M. To the reaction batch (150 µl 2 M TRIS, 20 µg DOTA-mAb), increasing volumes of Ac-225/La(III) solution are added in 2 µl steps (2 - 20 µl) to achieve 1, 2, 3... excess moles of lanthanum compared to moles of mAb. After the reaction (15 min at 45 °C), 5 µl of each solution is withdrawn and ITLC is performed to determine the percentage of free Ac-225. A titration curve for a representative binding assay is presented in Figure 4.7. The number of chelators equals the x-value at the inflexion point of the curve, indicating that all chelator sites are filled with M(III).

For all three chelated and characterised antibody preperations used during this project, the Ch/mAb ratios were found to be between 4 and 6. With this method, in-

formation about the average Ch/mAb range can be gained but not a precise Ch/mAb value.

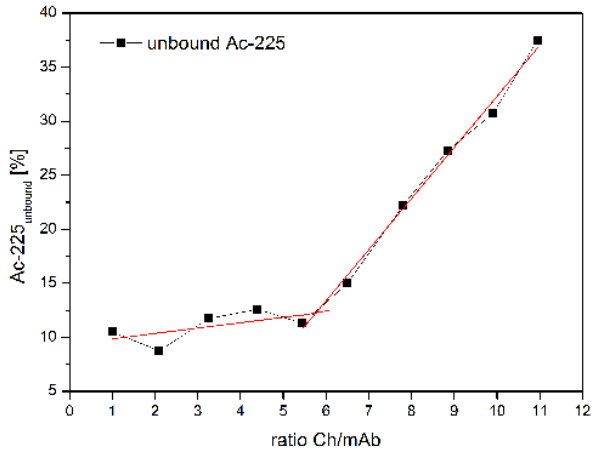

Figure 4.7: Radioisotope binding assay, titration curve: plot of Ch/mAb ratio against free Ac-225 fraction. From the inflexion point of the curve a Ch/mAb ratio of 5.5 to 6 is deduced.

4.1.5 K422-cell line, B-cell Lymphoma Cells

The K422 cells are cultured in suspension at a rate of approx. 10^6 cells/ml (37 °C, 5 % CO_2 atmosphere). Every second day, half of the volume of the cell suspension is withdrawn and replaced by an equal volume of new medium (RPMI-1640, containing 10 % FBS, 1 % Penicillin/Streptomycine, 1 % L-Glutamine). Prior to use in experiments, an aliquot of approx. 600 µl is analysed with the Vi-Cell cell counter (Beckman Coulter, Inc.) for total cell count/ml and viability.

4.2 Experiments

4.2.1 pH-Measurement

The pH measurements of the samples and solutions prepared for the various experiments were performed using a glass-combination-electrode pH meter (Ross, Orion, Thermo Scientic, Waltham, MA, USA) which was by default calibrated with buffer solutions of pH 1, 3, 5, 7 and 9. With active samples inside the glovebox, additional pH checks with pH indicator strips (Merck) were conducted prior to and after each reaction.

4.2.2 Potentiometry

4.2.2.1 Determination of p$K_{a,n}$ Values of DOTA by Potentiometric Titration (25 - 90 °C)

To accurately determine the acid dissociation constants of DOTA at temperatures up to 90 °C, automated potentiometric titration with CO_2-free NaOH was chosen. The experiments were conducted with a Titroprocessor 686 connected to a Multi-Dosimat 665 (Methrohm) and a Ross pH electrode (Thermo Scientific), which, prior to every titration, was calibrated on the millivolt scale for each temperature using Merck's standard buffer solutions of pH 2 to 12. Nernstian response of the electrode was confirmed. The experimental setup is illustrated in Figure 4.8. Special care

was taken to avoid loss of liquid through evaporation and to exclude atmospheric CO_2 from the experiment (connection to argon line).

The titration cell consists of a 20 ml glass vial which is tigthly closed with a lid. The lid contains access holes for placement of the pH-electrode (Orion 8220Bn, Thermo Scientic, Waltham, MA, USA) as well as for the connector tube of the titroprocessor, through which the titration solution is injected into the sample cell in defined portions of 10 - 50 µl. To avoid an increase of pressure inside the cell during heating, a glass pipe with very small diameter is mounted onto the lid and cooled from outside to simultaneously function as a condensation trap. The titration cell is placed in an oil bath on a hot plate with integrated magnetic stirrer to allow for constant thorough mixing of the sample solution.

The sample solutions are prepared with an initial concentration of 5 mM DOTA and 0.1 M $NaClO_4$ in 10 ml MilliQ water (MFW). By addition of 20 µl of 1 M $HClO_4$, the solution is first acidified to the point where the ligand is fully protonated ($\leq$3), resulting in a total start volume of 10.02 ml. Before the experiment is started, the closed vial containing the sample solution and the magnetic stir bar is weighed; the weighing procedure is repeated at the end of the experiment. From the difference of the theoretical sample-cell weight (starting-weight plus added volume of 0.1 M NaOH in mg) to the actual weight, the extent of sample loss by evaporation is quantified. In preliminary experiments, the setup was optimised to keep the evaporation error smaller than 1 % of the total sample end volume.

At the beginning of the titration, the argon-flooded titration cell is equilibrated on the hot plate at the respective temperature. After the temperature has stabilised, dropwise addition of CO_2-free 0.1 M NaOH in portions of 10 - 50 µl is started, allowing the system to equilibrate for 15 seconds before the millivolt reading of the electrode is recorded and the next portion of base is added. The titration is aborted when by addition of a portion of 100 - 150 µl of 0.1 M NaOH no significant change of pH is achieved any more (above pH ~11). The results are processed and analysed using the software Fiteql 4.0 [246].

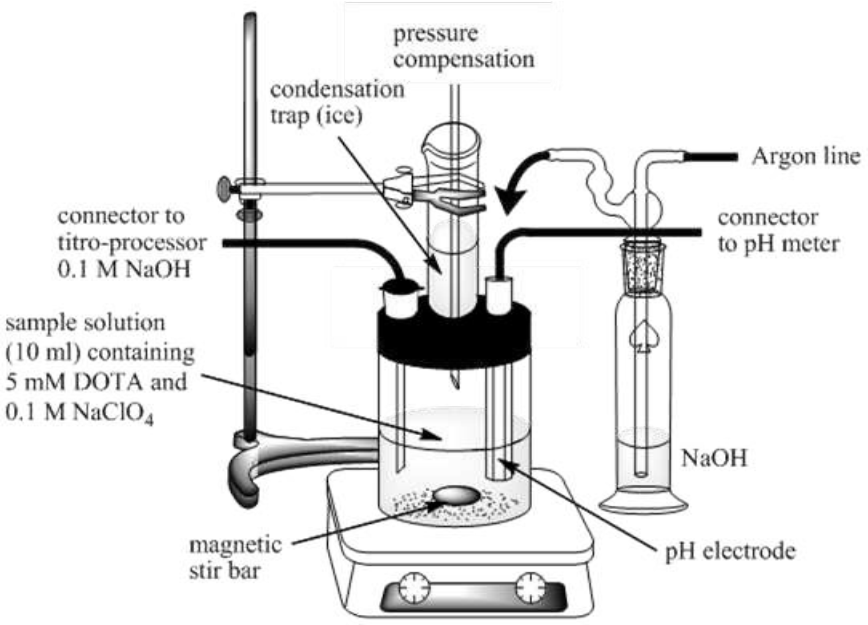

Figure 4.8: Schematic drawing of the constructed titration cell and experimental setup.

4.2.2.2 Determination of the Stability Constants of $[NaDOTA]^{3-}$ by Potentiometric Titration (45 - 90 °C)

For determination of the stability constants log K for the complexation of Na^+ by DOTA, the same experimental setup was chosen as described in 4.2.1. The samples were prepared likewise, containing $TMAClO_4$ as background electrolyte. According to common practice [135], both corresponding sets of titration data in $NaClO_4/TMAClO_4$ are analysed and fitted simultaneously using the software Fiteql 4.0.

4.2.3 Time Resolved Laser Fluorescence Spectroscopy

4.2.3.1 The Laser system

The measurements are performed using an excimer-pumped dye laser system (Lambda Physics EMG 201 MSC and FL 3002). The excimer laser is emitting at a wavelength of 308 nm with a frequence of 10 Hz. The dye laser allows excitation experiments in the range of 368 - 402 nm; a wavelength of 396.6 nm is used for Cm(III) excitation. Figure 4.9 shows a typical TRLFS setup. The fluorescence emission signal is detected in an angle of 90 ° to the laser beam by a quartz fibre, which is connected to an optical multichannel analyser. The multichannel analyser consists of a polychromator (Jobin Yvon, HR 320) with a 1200 lines/mm grating and an intensified photodiode array camera (Spectroscopic Instruments, ST 180, IRY 700G).

Emission spectra are recorded from 580 - 620 nm after a delay time of 1.2 µs to discriminate short-lived fluorescence of the organic ligand as well as any Rayleigh or Raman scattering effects. The delay time is controlled by a PG 200 pulse generator. The TRLFS set-up is operated with a computer by using the software POSMA. The cuvette containing the sample is placed in a temperature-controlled copper holder. All measurements are performed at T = 25 °C if not stated otherwise.

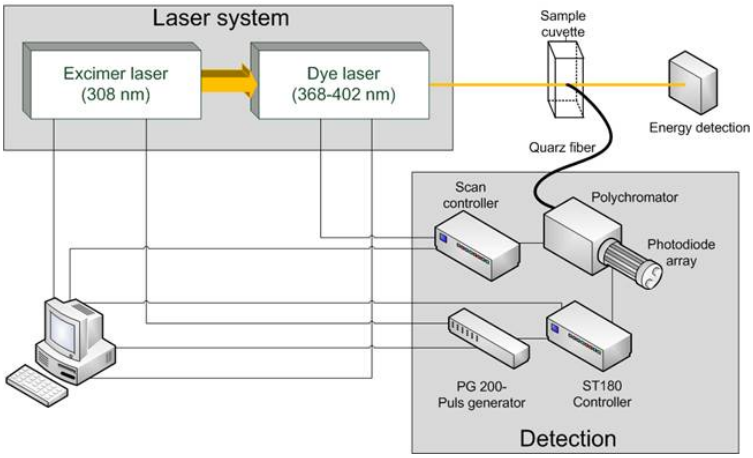

Figure 4.9: A typical TRLFS setup.

4.2.3.2 Sample Preparation

The samples are adjusted to constant ionic strength I = 0.1 by using 0.1 M $NaClO_4$ solution. Each sample contains a Cm(III) concentration of $1 \cdot 10^{-7}$ M. The concentrations of DOTA in the samples as well as the pH of the solution is varied (see respective experiments for further details); however, the ligand is always used in excess over the metal ion. The total sample volume is 1 ml. By deconvolution of the obtained fluorescence emission bands a species distribution is determined.

Characterisation of Cm(III) Species in H_2O and D_2O: In order to characterise the Cm(III)DOTA complex species, samples containing $1 \cdot 10^{-7}$ M Cm(III) and $1 \cdot 10^{-6}$ M DOTA are prepared in H_2O and D_2O in order to determine the respective fluorescence lifetimes. The pH of the solutions is 2.9; no hydrolysis of Cm(III) is expected in this pH region. For characterisation of the Cm(III) solvent species, samples containing only $1 \cdot 10^{-7}$ M Cm(III) are prepared in 1 ml of the respective solvent. Before measurement, the samples containing Cm(III) and DOTA or DOTA-NCS are cooled to 5 - 10 °C to quench the reaction or heated to 90 °C for 2 h to achieve full conversion, respectively. The samples containing only Cm(III) are measured immediately after preparation (solvens species). The emission intensity is measured at increasing delay times in the range of Δt = 5 to 10 µs, depending on the expected lifetime of the respective Cm(III) species.

Determination of the Kinetic Rate Constants of the Cm(III)-DOTA/Cm(III)-DOTA-NCS Complex Formation (25 - 93.5 °C): For investigating the reaction kinetics, samples are prepared containing $1 \cdot 10^{-7}$ M Cm(III) and an excess of DOTA or DOTA-NCS in 1 ml H_2O. The ratio of Cm(III):DOTA/DOTA-NCS for the respective reaction temperatures is chosen in a way to allow the reaction to come to full conversion within an observation period of 1 to 2 hours (see Table 5.9 in paragraph 5.2.2.1 for further details). The pH of all solutions is 2.9 if not stated otherwise. No hydrolysis of Cm(III) is expected in this pH region, while a sufficient amount of the reactive DOTA species is formed at this pH to allow full complexation of the present Cm(III).

The sample cuvettes are placed in the temperature controlled copper holder of the spectrometer and heated to the respective temperature. The samples are constantly mixed with a magnetic stir bar during the course of the measurements. A spectrum of the sample is recorded every minute until only the spectrum of the pure Cm(III)DOTA species is observed. The recorded spectra are subjected to peak deconvolution. From the obtained species distribution the kinetic rate constants are calculated.

Determination of the Thermodynamic Data for Cm(III)DOTA (45 - 90 °C): In order to get reliable values for complex stability constants, attention has to be drawn to proper equilibration of the samples. Since the complexation reaction is slow, the samples require incubation at elevated temperatures to approach the equilibrium in reasonable time. Samples containing $1 \cdot 10^{-7}$ M Cm(III) and $3 \cdot 10^{-7}$ M DOTA (experiments at 70 - 90 °C), $5 \cdot 10^{-7}$ M DOTA (experiment at 60 °C) or $5 \cdot 10^{-6}$ M DOTA (experiment at 45 °C) are prepared in aqueous solution. Individual samples are prepared for each investigated pH value between pH 2 and 4.

The pH of the samples is adjusted using solutions containing different molarities of $HClO_4$ in H_2O as solvent. Since the low-pH solutions in the range of 2 - 4 have some self-buffering effect and only small concentrations of H^+ will be released during the reaction, no additional buffer is necessary [9].

The samples are then incubated at elevated temperatures (45, 60, 80 and 90 °C, respectively) for 24 h. For the experiment carried out at 70 °C, a heating period of 3 days was found to be required to reach equilibrium [9]. The spectra are recorded while keeping the sample cuvettes at the respective temperatures in the temperature controlled copper holder. The obtained spectra are subjected to peak deconvolution. From the species distribution the stability constants are calculated.

4.2.4 NMR Measurements

For recording of the NMR spectra, 600 µl of DOTA-NCS dissolved in D_2O ($c = 1 \cdot 10^{-3}$M) and adjusted to pH 3, 5.5 or 9, are filled in NMR tubes and placed in the temperature controlled sample holder of the Bruker NMR spectrometer. After the first spectra is recorded, the temperature is gradually increased. After each heating step, the sample is equilibrated at the respective desired temperature for 5-10 min before the spectrum is recorded and the next heating step is initiated. At the end of the heating cycle, the sample is cooled to room temperature and remeasured for comparison with the initially recorded spectrum.

4.2.5 Investigation of the Complexation of Ac(III)-DOTA

4.2.5.1 Radiochemical Speciation by Chelex Chromatography

For separation of free Ac(III) from DOTA-complexed Ac(III), the sample can be passed through a Chelex 100/200 mesh cation exchange chromatography column (1 ml volume bed, 100 - 200 mesh, Na^+ form, BioRad, Richmond, CA, adjusted to pH 7.4). Chelex resin is a weakly acidic styrene divinylbenzene copolymer containing paired iminodiacetic acid as chelating groups for highly selective binding of polyvalent metal ions [247]. The actual selectivity for any specific system depends on factors like pH, ionic strength, and the presence of other complex-forming species. Chelex resin is stable over the entire pH range and functionally active from pH 2 - 12. Depending on the pH of the sample passed through the column, many metals (with exception of monovalent cations) can be adsorbed as chelate species. In these chelates, two 5-membered rings define the structure in which the iminodiacetic groups act as tridentate ligands. The bond strength within the complex is usually very high.

The polypropylene chromatographic columns (Bio-Spin from BioRad Laboratories, Inc., Fig. 4.10, *left*) are packed with approximately 0.5 ml of hydrated resin, fixed with a PE frit with 120 µm pore diameter. Due to the pH of the Chelex 100/200 mesh resin in sodium form (pH ∼11), the resin requires extensive washing with 0.9 % NaCl until the pH is neutral [248]. The sample solution (containing Ac(III) as free metal as well as complexed with DOTA) is then loaded onto the conditioned Chelex column. By elution with 5 consecutive portions of 1 ml of 0.9 % NaCl, the complexed actinium fraction is passed through the column and collected in fractions F1 - F5. The free Ac-225 fraction is retained quantitatively on the Chelex column and is then eluted with subsequent portions of 1 ml of 1 M HCl (F6) and 2 ml of

0.9 % NaCl (F7 - F8, Fig. 4.10, *right*). Each fraction is measured in the gamma spectrometer. The parent nuclide Ac-225 is measured via gamma detection when in secular equilibrium with its daughters. For quantification, the amounts of the Ac-225-DOTA fractions and the free Ac-225 fractions are calculated by expressing the corresponding activities as a percentage of the total activity of all fractions.

The Chelex resin efficiently distinguishes between free metal (aquo) ions and metal-ligand complexes in the load solution. Hence this method is able to provide a reliable speciation. However, no information about the form or stability of the formed complexes is available. It is also not possible to differentiate between complexes formed by different ligands present in solution, e.g. between Ac-225-DOTA and Ac-225 hydroxo species.

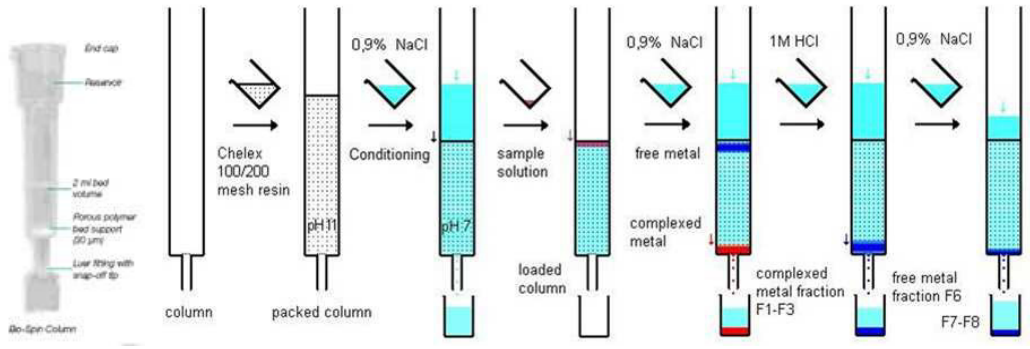

Figure 4.10: *left*: Bio-Spin column [248]; *right*: principle of Chelex separation.

4.2.5.2 Radiochemical Speciation by Instant Thin Layer Chromatography

ITLC is able to provide information about the amount of complexed and free radionuclides in the sample. Thin layer chromatography is a solid-liquid form of chromatography where the stationary phase is usually a polar absorbent and the mobile phase is a single solvent or a mixture of solvents. It is especially useful in cases of mAb-containing sample solutions when speciation with Chelex is not possible due to the chemical affinity of the mAb towards the organic resin. This so-called radio-ITLC serves as a method for quality control of radiopharmaceuticals [249, 250].

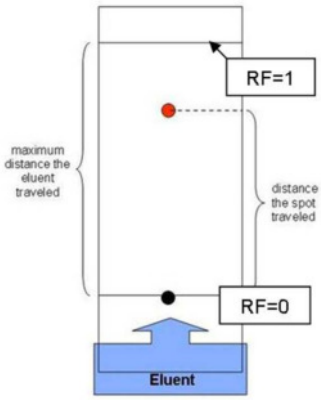

Figure 4.11: Principle of ITLC. The sample is applied to the strip at Rf = 0 (black dot) and travels with the eluent (red dot; *here:* Rf = 0.7).

ITLC-SG (Pall Corporation (PLL) or Varian Medical Systems, Inc.) is a porous and slightly acidic pure glass fibre sheet impregnated with a monosilicic acid gel that gives excellent resolution for non polar compounds. The ITLC-SG plates are cut into strips of 1-1.5 cm x 10 cm size. Na-citrate (0.05 M, pH 5.5) or 0.05 M EDTA is used as eluent (mobile phase).

For analysis, an aliquot (5 - 10 µl) of the sample is deposited on the ITLC-strip (approximately 1 cm from the bottom, Fig. 4.11). The strip is then placed in a

shallow pool of eluent within a developing chamber. The eluent then slowly rises up the ITLC strip due to capillary forces.

As soon as the mobile phase moves past the deposited sample spot, equilibrium between adsorbed molecules on the solid phase (ITLC-strip) and molecules in solution (mobile phase) is established for each component of the sample. In general, different components vary in solubility and strength of their adsorption onto the ITLC plate, so that some components of the sample will be carried further up the strip than others. Hydrophilic compounds will travel up with the solvent front if water-based eluents such as e.g. physiological sodium chloride solution or sodium citrate buffer are used, while lipophilic compounds will move with water-free solvents.

In the described system, the radioconjugate remains at the spot of application and will not move with the eluent front (Rf = 0) while free actinium moves with the solvent front (as citrate- or EDTA-complex, Rf = 0.9). When the mobile phase reaches the top of the strip, the strip is removed from the developing chamber and cut into two pieces (1/3 top, 2/3 bottom) after it was let to dry. The pieces are analysed via gamma-spectrometry and -at times- radiographic imaging when secular equilibrium is reached. For quantification, the amounts of the labelled radioconjugate and the non-bound nuclide are calculated by expressing the corresponding activities as a percentage of the total activity on the ITLC strip.

The ITLC-SG/0.05 M EDTA system can also be applied for studies in human blood serum. In general, the separation achieved with ITLC is not as good as with HPLC. Nevertheless, in the case of long-lived radionuclides, which require several hours until secular decay equilibrium is reached (e.g. ∼2 h for Ac-225 to equilibrate with Fr-221), ITLC has advantages over (radio-)HPLC. With ITLC, an representative aliquot can be quantitatively analysed with gamma spectrometry after appropiate equilibration. On contrary, with HPLC especially free radionuclides are difficult to elute quantitatively due to adsorption effects on the column. In addition, with on-line radio HPLC the time to reach decay equilibrium is not given and the single peaks for the mother and daughter nuclides can not be resolved quantitatively.

Radiographic Imaging: Autoradiography of developed ITLC strips is conducted by scanning of the exposed phorsphorous screen using the Bio-Rad Molecular Imager with Quantity One software, which facilitates quantification of the activity deposited on the respective regions of the ITLC strip (Fig. 4.12). Exposure time depends on the total activity on the strip.

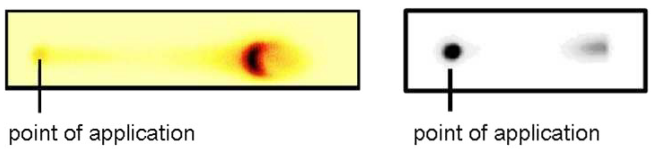

Figure 4.12: Radiographic images; *left*: Ac-225 blank sample on ITLC-SG, developed with 0.05 M Na-citrate. Free Ac-225 traveled with the eluent (Rf = 0.9). *right*: 3MM/0.9 % NaCl ITLC-system: free Ac-225 remains at the point of application, while Ac(III)DOTA travels with the solvent front.

ITLC Separation of the Ac-225-DOTA Complex: In this work an ITLC system was established which is applicable to separation of the Ac(III)DOTA complex from free Ac(III). This ITLC System (Whatman 3MM as solid phase, 0.9 % NaCl as mobile phase, Fig. 4.12, *right*) presents a substitute method for Chelex 100 and proved to be more reliable over the whole pH range. The properties of various ITLC papers which were assessed are summarised in the following Table 5.20. The ITLC systems implemented in the present work are highlighted in blue. For

Table 4.2: Results of the assessment of various ITLC systems to identify suitable systems for reliable separation of free Ac(III) from Ac(III)DOTA and Ac(III)DOTA-mAb. The most suitable ITLC systems are highlighted in blue.

ITLC paper	*eluent*	*blank (free Ac-225)*	*Ac(III)DOTA*	*Ac(III)DOTA-mAb conjugate*	*Ac(III)-serum proteins*	*suitable for HBS study*
ITLC-SG	0.05 M Na-citrate	Rf = 0.9		Rf = 0	Rf = 0.8	++
ITLC-SG	0.05 M EDTA	Rf = 0.9		Rf = 0.1	Rf = 0.8	++
Biodex	0.05 M Na-citrate	Rf = 1		Rf = 0	n.a.	o
3MM	acetone:H_2O 1:1	Rf = 0	Rf = 0			o
3MM	MeOH:0.9 % NaCl 1:1	Rf = 0	Rf = 0			o
3MM	0.9 % NaCl	Rf = 0	Rf = 0.9			o
3MM	0.05 M Na-citrate	Rf = 1	Rf = 0.9			o

routine DOTA-antibody radiolabelling (separation of mAb-bound and free Ac-225) and also for evaluation of the radioimmunoconjugate stability in HBS, the ITLC-SG/Na-citrate (or EDTA) combination is very suitable (++) since it was found to reliably separate the Ac-225-mAb-conjugate from the Ac-225 bound to serum components. The 3MM/sodium cloride system was the only combination involving polar solvents which was found reliable for separation of the polar Ac-DOTA complex from unbound radionuclide.

4.2.5.3 Sample Preparation

Speciation studies with Chelex (60 °C): 100 µl 0.2 M buffer (TRIS for samples with pH $>$ 7.5 or NaOAc for samples with pH $<$ 7) plus 50 µl 2 % ascorbic acid are adjusted to the required pH by adding defined volumes of 1 M HNO_3 or 1 M NaOH, respectively. The mixture is stirred very well and an aliquot corresponding to the volume of added acid/base is discarded. Hereupon the reactants, namely 0.2 µg DOTA in 10 µl 0.15 M NaCl/0.05 M NaOAc buffer and 0.6 µCi (∼22 kBq) Ac-225 in 2 µl 0.05 M HNO_3 are added, resulting in a total sample volume of V_{total} = 162 µl. After the reaction (15 min at 60 °C) the sample is separated via Chelex chromatography. The Ac(III)DOTA complex is eluted with 0.9 % NaCl and collected in fractions F1 - F5, while free Ac-225 is eluted with 1 M HCl in fractions F6 - F8. The fractions are measured in the gamma counter and the complexation yield is calculated relative to the total activity found in all fractions. From the ratio of bound and unbound Ac-225 species distributions are obtained, from which the stability constants are calculated.

Speciation studies with ITLC (45 - 90 °C): To the reaction mixture, consisting of 150 µl aqueous solution adjusted to the respective pH between 2.5 and 4.5 (I = 0.1 M $NaClO_4$), 0.2 µg of DOTA in 10 µl 0.15 M NaCl/0.05 M NaOAc-buffer and 0.6 µCi (∼22 kBq) of Ac-225 in 2 µl 0.05 M HNO_3 are added if not stated otherwise. The total concentration of DOTA in the sample is $3 \cdot 10^{-6}$ M, the total concentration of Ac-225 is $3 \cdot 10^{-10}$ M. The batches are heated to the respective temperature (45 - 90 °C) for 24 h (60 - 90 °C) or 48 h (45 °C). Afterwards the samples are separated with ITLC (3MM / 0.9 % NaCl) and analysed by gamma-spectrometry. The stability constant can be calculated from the species distribution, which is obtained from the ratio of bound and unbound Ac-225.

4.2.6 Radiolabelling, Radioconjugate Purification and *in vitro* Evaluation

4.2.6.1 Standard Labelling Protocol

The reaction mixture (100 µl 2 M TRIS, 50 µl 20 % ascorbic acid, 5 µl 4 M HNO_3, x µCi Ac-225 in 0.05 M HNO_3 and 100 µg DOTA-NCS-CD20 in 0.15 M NaCl / 0.05 M NaOAc-buffer; total pH = 8.5 - 9) is heated for 15 min at 45 °C in a clean eppendorf tube (1.5 ml). Subsequently, the batch is separated using ITLC (SG / 0.05 M trisodium citrate ("Na-citrate"), pH 5.5). The strips are let to dry and cut in two in order to measure their activity by gamma spectrometry after secular equilibrium is attained. With this protocol, usually labelling yields of 90 % and higher are achieved. The obtained radioimmunoconjugate is purified via PD10 size exclusion chromatography if yields are below 90 %, resulting in a more than 98 % radiochemically pure product.

The protocol is also applicable for radiolabelling of DOTA-Substance P at 90 °C, pH 8.5 - 9, leading to yields above 95 % within 15 min reaction time.

4.2.6.2 Optimised Labelling Protocol for the DOTA-Chelated Antibody

Various experiments gave rise to the assumption that the radioprotectant ascorbic acid interferes with the labelling reaction (see paragraph 5.4.2.1 ff). In the protocol the ascorbic acid is therefore replaced by an additional amount of buffer. Moreover, the omission of ascorbic acid allows the reaction to be carried out in only 0.2 M TRIS buffer. This modification also applies to the labelling of DOTA-Substance P at 90 °C (pH 9).

The reaction mixture (100 µl 0.2 M TRIS, ≤ 50 µCi (≤ 1.9 MBq) Ac-225 in 0.05 M HNO_3 and 100 µg DOTA-NCS-CD20 in 0.15 M NaCl/0.05 M NaOAc-buffer; total pH = 8.5 - 9) is heated for 5 to 15 min at 37, 42 or 45 °C in a clean and sterile eppendorf tube (1.5 ml). The reaction batch is subsequently separated by ITLC (SG/0.05 M Na-citrate, pH 5.5). The strips are let to dry, cut in two and analysed by gamma-spectrometry after secular equilibrium is reached. This optimised protocol allows for labelling yields of 94 % and higher (see Table 5.21 in paragraph 5.4.3.2) within 5 to 15 min. If yields are below 90 %, the Ac-225-radioimmunoconjugate is purified via PD10 size exclusion chromatography to obtain a product with more than 98 % RCP. If the labelled antibody is not diluted for immediate application in further experiments, ascorbic acid (20 %) needs to be added to the solution in order to prevent radiolysis which would lead to protein denaturation and instability of the Ac-225-radioconjugate.

4.2.6.3 Size Exclusion Chromatography

The obtained RIC needs to be purified from all low molecular weight impurities such as residual ligand, ascorbic acid (if applied in the protocol) and unbound radionuclides (if labelling yields are below 90 %) before it can be applied in serum studies or administrated to patients [251]. This purification can be done by SE-HLPC as well as more easily by passing the reaction solution through a PD10 desalting column. Both methods are based on size exclusion.

PD10 Desalting Column (Sephadex): Pre-packed PD10 desalting columns (Amersham Biosciences, particle size range: 85 - 260 µm, exclusion limit Mr 5000) are designed for rapid, convenient sample clean-up of proteins and other large biomolecules e.g. mAbs [252]. It is used for desalting, buffer exchange and removal of low-molecular weight impurities. The PD10 SE-chromatography is a gel filtration technique; the medium is Sephadex G-25 (based on cross-linked dextran), which enables effective and rapid separation of large molecules (Mr $>$ 5000) of interest from e.g. undesired salts or free radionuclides in the sample (Mr $<$ 1000, Fig. 4.13). The hydrophilic matrix minimises non-specific adsorption and gives high recoveries of up to 90 % during buffer exchange of mAbs.

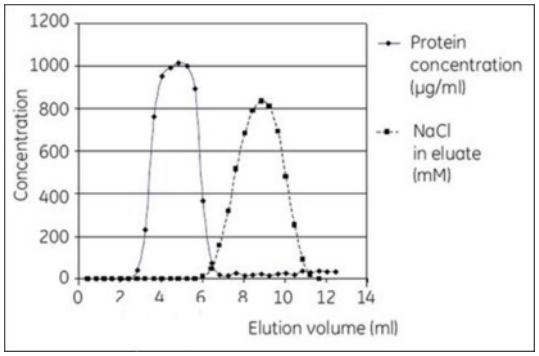

Figure 4.13: Typical elution profile for purification of a protein-containing sample with PD10: the protein is eluted in the first fraction (2 - 6 ml), followed by the low-weigth impurities [252].

After pre-conditioning of the column using phosphate buffered saline ("PBS" , 0.1 M NaCl/0.05 M Na_3PO_4, pH 7.4), the liquid sample (in TRIS buffer) is passed through the column by gravity. Molecules that are larger than the largest pores of Sephadex are excluded from the matrix and are hence eluted first, while molecules smaller than the largest pores penetrate the matrix and are therefore retained on the column. The 2.9 ml dead-volume fraction F0 of load solution is collected and measured. In order to achieve an elution profile with sharp and narrow peaks, it is recommended to first apply only the sample and let it soak in, followed by (2900 µl – x(sample)µl) µl of PBS. Subsequently, the column is eluted with 2 ml of PBS and gamma measurements of Ac-225 in the fraction F1 are performed. It was shown that the mAb-radioconjugate is eluted in F1 while free Ac-225 is striped from the column only after elution with approximately 6 ml.

The addition of 10 µl of 1.5 mg/ml DTPA to the sample prior to column loading is useful to remove unbound Ac(III) from the sample and quantitatively elute it from the column in form of its DTPA complex [245]. Since DTPA is a weaker chelator for Ac-225 than DOTA, no transchelation of Ac-225 from the radioconjugate to DTPA is expected. Figure 4.13 shows a typical elution profile for separation of serum albumin from NaCl.

To determine the final radiochemical purity of radiolabelled mAbs, quality control of the fractions containing only RIC is conducted in form of ITLC, followed by gamma measurement of the strips.

4.2.6.4 Conjugate Stability in Human Blood Serum

In vitro serum stability is a useful qualitative screening procedure to identify unstable metal complexes by assessment of their potential to maintain stable complexes without dissociation of the metal ion *in vitro*. However, serum stability of a complex *in vitro* does not necessarily warrant suitability of this complex for *in vivo* application since in the living organism, carbonate complexation is predominant at physiological pH (blood pH = 7.3 - 7.4) [218, 83]. Nevertheless, serum stability studies are still a viable preliminary *in vitro* screening method to estimate complex stability for RIT application [253].

Preparation of Human Blood Serum: Blood is collected from healthy volunteers and allowed to clot for 1 h at 37 °C in a humidified incubator at 5 % CO_2 atmosphere. The samples are then centrifuged and the supernatant (serum) is removed and sterilised using a 0.22 µm syringe filter [115]. Alternatively, before the samples are centrifuged, EDTA or Heparin can be added to fresh blood to prevent clotting. Then, after the blood cells accumulated at the bottom, the serum can be poured off. HBS prepared like this can be stored frozen (-20 °C) and is used for *in vitro* serum stability studies after warming to RT. It requires filtering before use [241].

Challenge Method: The general stability of radiopharmaceuticals is assessed by studying transchelation effects using different challenging agents (CA) for competition with the ligand or the radionuclide [245]. Examples for commonly used CAs are EDTA/DTPA, carbonate- and saline-buffers as well as serum proteins [254, 255]. When introduced to a solution containing the RIC, a chelator (in high excess) can compete with the chelated mAb for the metal cation. If the chelator is more capable of complexing the radionuclide than the chelated mAb, the nuclide will dissociate from the mAb-conjugate and form a complex with the chelator. Vice versa, the radioconjugate can also be challenged by a solution containing 100-fold molar excess of metal cations. In this work, the stability of the Ac-225-DOTA-NCS-mAb is hence evaluated in in PBS, EDTA and carbonate-containing solutions as well as in HBS (incubation at 37 °C in humid 5 % CO_2 atmosphere), with dilution factors of 1:10 and 1:20 for each sample.

Serum Stability Studies: The radiolabelled conjugates usually need to be purified (e.g. via size exclusion filtration) before being put in serum, in order to prevent contamination through uncoordinated nuclides or unlabelled mAb at the beginning of the stability study [50]. The stability of the Ac-225-radioconjugates under simulated physiological conditions is investigated by adding the RIC reaction solution to human blood serum at pH 7.4 at a ratio of 1 : 10 or 1 : 20 and lower, so that dilution is significant [256]. The sample is then incubated at 37 °C (humid, 5 % CO_2 atmosphere) in vials with filter-lid [251, 115].

To determine the quantity of Ac-225 still stably chelated by the DOTA-mAb, at various time points over 30 days (equals 3 $t_{\frac{1}{2}}$ of Ac-225) aliquots of 20 µl are removed and analysed with ITLC-SG/0.05 M EDTA or Na-citrate, pH 5.5. Before spotting on the ITLC strip, the sample aliqout is incubated with 4 µl 0.01 M DTPA at 37 °C for 15 min to achieve transchelation of potentially HSA/TF-bound Ac-225 to DTPA [60]. DTPA is supposed to coordinate the Ac-225 stronger than the serum proteins,

while at the same time no transchelation of Ac-225 from the radioconjugate to DTPA will occur [257]. Like this, the initially serum bound nuclide fraction will not be included in the mAb/protein fraction at the bottom of the ITLC strip but will travel up as DTPA complex with the solvent, as free Ac-225 does too. The stability of the Ac-225-radioconjugate in serum is determined vs. Ac-225 blank control.

4.2.6.5 Cell Binding Ability/Affinity (Scatchard Analysis)

The binding affinity of a radiolabelled antibody is tested by incubating of 9 samples containing $1 \cdot 10^6$ cells/ml in the corresponding cell medium with increasing amounts of the (purified) radioimmunoconjugate (SA = 1 µCi/100 µg mAb) , which results in total conjugate concentrations between 1 and 25 mg/ml. The volume of all solution is then adjusted to equal total volume by addition of PBS. After incubation for ∼60 min at 37 °C in humid 5 % CO_2 atmosphere, the samples are centrifuged and the supernatant is collected. All cell pellets are washed two times with 1 ml PBS. The pellets and all solutions are measured in the gamma counter.

The equilibrium dissociation constant K_d and the maximum binding capacity B_{max} is calculated from the percentage of RIC bound to the cells using the software GraphPad Prism [223, 258, 193]. Before the experiment, the stability of the RIC should be tested in cell culture media for several days to guarantee that the radionuclide remains stably attached to the mAb during the time of the binding study.

5 Results and Discussion

5.1 Potentiometry

5.1.1 Potentiometric Determination of the p$K_{a,n}$ Values of DOTA in the Temperature Range of 25 to 90 °C

It is known in the literature, that effective complexation reactions with DOTA at RT are very slow (∼4 - 5 weeks) and require elevated temperatures in order to accelerate the reaction by granting some flexibility to the otherwise rigid macrocycle. It is also known that the most reactive species of DOTA are the deprotonated species $DOTA^{4-}$ and $HDOTA^{3-}$, as well as H_2DOTA^{2-} (Fig. 5.1), which is suggested to form a first intermediate complex species before the complexation proceeds to the final, stable complex [168, 11]. Hence, accurate determination of the thermodynamic stability of a metal cation - DOTA complex at certain reaction conditions (temperature, background electrolyte) implies knowledge about the acid dissociation constants ($K_{a,n}$) under these conditions.

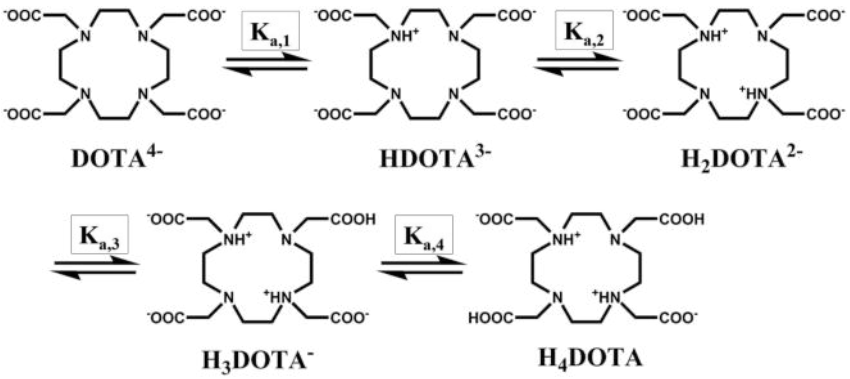

Figure 5.1: Stepwise association constants for the tetrabasic DOTA, modified from [259]. The fully protonated H_4DOTA exists as zwitterion, forming intramolecular H-bonds between the prontonated N's and the carboxylic groups attatched to them [157].

In the present study the determination of the p$K_{a,n}$ values at elevated temperatures is crucial, since the Ac-225 radiolabelling of the DOTA-chelated antibodies and peptides is intended to be accomplished at temperatures of 37 - 45 °C or 90 °C, respectively. Therefore the complex stability constants (K) of $[Ac(H_xDOTA)]^{(1-x)-}$ are to be determined in the temperature range of 45 - 90 °C, which then allows extrapolation of the log K at 25 °C. Since peptides and antibodies are commonly stored in solutions containing sodium salts, all experiments were performed in $NaClO_4$ as background electrolyte at constant ionic strength of 0.1 M. As sodium is known to form complexes with DOTA (log K = 4.02 - 4.2 at 25 °C, 0.1 M TMACl [142, 5]), it must be taken into account when analysing the experimental data.

The p$K_{a,n}$ values are determined in the temperature range between 25 and 90 °C by potentiometric titration with 0.1 M NaOH (paragraph 4.2.2.1). For this a custom-built experimental setup was established including a titration cell which facilitates heating of the sample solution without causing evaporation errors or pressure increase. In addition, it allows flooding of the cell with inert gas (argon) at the beginning of the experiment, in order to avoid contact with ambient CO_2 during titration and therewith the formation of carbonate species at alkaline pH. The applied setup is illustrated in Figure 4.8.

The sample solutions were prepared as described in paragraph 4.2.2.1 and contained a starting concentration of 5 mM DOTA and 0.1 M $NaClO_4$ in 10.02 ml H_2O. Following equilibration at the respective temperature, the titration curves were recorded for 25, 45, 60, 70, 80 and 90 °C by stepwise addition of 0.1 M NaOH. After each titration step the system was equilibrated for 15 seconds. The obtained titration curves are presented in Figure 5.2. The experimental data was fitted with the Software Fiteql 4.0 to obtain the accurate p$K_{a,n}$ values [246]. The results are summarised in Table 5.1.

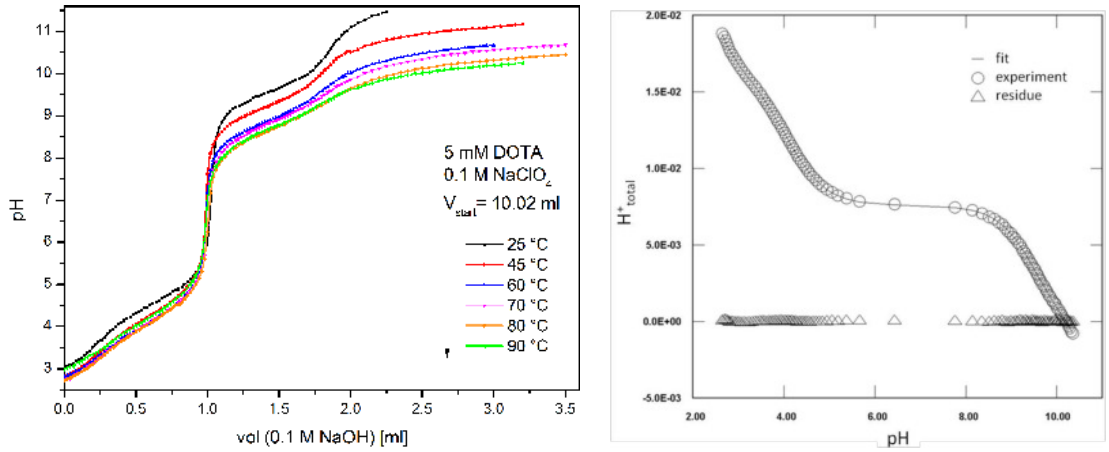

Figure 5.2: *left*: Potentiometric titration curves for the experiments conducted at 25 - 90 °C. [DOTA] = 5 mM; I = 0.1 M $NaClO_4$. *right*: exemplary fit for 45 °C. The solid line represents the model, the circles the experimental data points, and the triangles the deviation from the model.

The titration curve for DOTA at 25 °C (Fig. 5.2, *black*) shows two buffer regions from pH 3 - 6 and pH 8 - 11.5, each with two distinct saddle points correlating with the four p$K_{a,n}$ values. The curves recorded at higher temperatures mainly display the same curve shape, with the saddle points being not as clearly visible with increasing temperature. A temperature dependent trend is noticable especially in the alkaline pH region, reflecting the dissociation of the less acidic protons pKa_1 and pKa_2. The obtained p$K_{a,n}$ values (Table 5.1) decrease with increasing temperature. The indicated errors are derived from the standard deviation σ of the optimised parameters calculated by Fiteql according to standard experimental error estimations implemented in the software (ΔpH: 0.02 units; *relative* $\Delta c(total)$: 2 %; *absolute* $\Delta c(total)$: 1 µM, negligible; *total error* $= c(total) \cdot$ *relative* $\Delta c(total)$ + *absolute* $\Delta c(total)$). Since these errors are usually rather small, they are commonly indicated as 3σ [261], which is in good accordance with the experimental errors estimated based on multiple repeated titrations [262].

Table 5.1: Determined p$K_{a,n}$ values for DOTA in 0.1 M $NaClO_4$ in the temperature range of 25 - 90 °C (present work (p.w.)) in comparison with literature values for DOTA at 25 °C in various electrolyte media as well as available literature data for DTPA and TETA. The values without error range were calculated from the respective literature data.

Conditions	**log** β_{H1}	**log** β_{H2}	**log** β_{H3}	**log** β_{H4}	**log** β_{H5}	**p*Ka₁***	**p*Ka₂***	**p*Ka₃***	**p*Ka₄***	**p*Ka₅***
					DOTA					
25 °C, 0.1 M TMACl [162]	29.82	18.09	8.69	4.19±0.06	-	11.73±0.03	9.40±0.02	4.50±0.04	4.19±0.06	-
25 °C, 0.1 M KCl [162]	29.55	18.41	8.91	4.30±0.09	-	11.14±0.07	9.50±0.01	4.61±0.09	4.30±0.09	-
25 °C, 0.1 M NaCl [162]	27.05	17.68	8.54	3.91±0.07	-	9.37±0.05	9.14±0.08	4.63±0.12	3.91±0.07	-
25 °C, 0.1 M $NaClO_4$(p.w.)	27.04±0.04	17.73±0.03	8.59±0.03	4.18±0.02	-	9.31±0.04	9.14±0.03	4.41±0.03	4.18±0.02	-
45 °C, 0.1 M $NaClO_4$(p.w.)	26.72±0.04	17.63±0.03	8.69±0.03	4.14±0.02	-	9.09±0.04	8.94±0.03	4.55±0.03	4.14±0.02	-
60 °C, 0.1 M $NaClO_4$(p.w.)	25.74±0.04	16.90±0.03	8.19±0.03	3.95±0.03	-	8.84±0.04	8.71±0.03	4.24±0.03	3.95±0.03	-
70 °C, 0.1 M $NaClO_4$(p.w.)	25.60±0.06	16.90±0.05	8.46±0.04	4.00±0.03	-	8.70±0.06	8.44±0.05	4.46±0.04	4.00±0.03	-
80 °C, 0.1 M $NaClO_4$(p.w.)	25.14±0.06	16.67±0.04	8.40±0.05	3.99±0.04	-	8.47±0.06	8.27±0.04	4.41±0.05	3.99±0.04	-
90 °C, 0.1 M $NaClO_4$(p.w.)	25.17±0.07	16.65±0.08	8.22±0.06	3.83±0.05	-	8.52±0.07	8.43±0.08	4.39±0.06	3.83±0.05	-
					DTPA					
10 °C, 1.05 M $NaClO_4$[260]	27.65±0.05	25.14±0.06	22.61±0.03	18.23±0.03	9.73±0.02	9.73	8.50	4.38	2.53	2.51
25 °C, 1.05 M $NaClO_4$[260]	26.85±0.04	24.48±0.04	21.92±0.03	17.69±0.02	9.43±0.02	9.43	8.26	4.23	2.56	2.37
40 °C, 1.05 M $NaClO_4$[260]	26.46±0.07	24.14±0.06	21.54±0.04	17.34±0.03	9.29±0.03	9.29	8.05	4.20	2.60	2.32
70 °C, 1.05 M $NaClO_4$[260]	26.16±0.14	23.68±0.15	21.01±0.08	16.75±0.07	8.91±0.06	8.91	7.84	4.26	2.67	2.48
25 °C, 0.15 M $NaClO_4$[5]	26.95	24.95	22.27	18.09	9.76±0.02	9.76±0.02	8.33±0.03	4.18±0.03	2.68±0.03	2.0±0.1
					TETA					
15 °C, 0.2 M $NaNO_3$[259]	28.77	17.53	7.67	3.27±0.03	-	11.24±0.03	9.86±0.03	4.40±0.03	3.27±0.03	-
25 °C, 0.2 M $NaNO_3$[259]	28.19	17.15	7.47	3.17±0.03	-	11.04±0.03	9.68±0.03	4.30±0.03	3.17±0.03	-
35 °C, 0.2 M $NaNO_3$[259]	27.25	16.77	7.27	3.07±0.03	-	10.48±0.03	9.50±0.03	4.20±0.03	3.07±0.03	-

5.1.2 Discussion

A first titration at 25 °C was conducted to test the reliability of the method and to reproduce the literature p$K_{a,n}$ values for DOTA in presence of 0.1 M Na^+(Table 5.1). Especially pKa_1 and pKa_2, assigned to the dissociation of the amine protons, are known to be highly dependent on the selected background electrolyte (Na^+-, K^+-, $NMe_4{}^+$(TMA-) salts), which is due to complexation of the alkali metal cations by the $DOTA^{4-}$ species [135]. This results in lower apparent dissociation constants [263], differing from the values obtained in TMA systems where pKa_1 values of up to >11 are commonly found (Table 5.1) [11, 162]. This influence is illustrated by comparison of titration curves recordet in $NaClO_4$ and Me_4NClO_4(TMAClO_4) at 70 °C, showing significant deviation at alkaline pH (Fig. 5.3), from which the respective log K of the $[NaDOTA]^{3-}$ complex can be deduced. This will be discussed in paragraph 5.1.3. The literature values reported for 25 °C (0.1 M NaCl, Table 5.1) were reproduced with satisfying accordance, proving the quality of the established experimental setup.

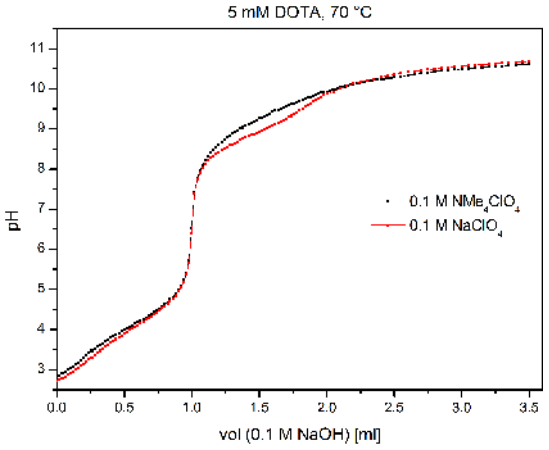

Figure 5.3: Comparison of the titration curves with $NaClO_4$ and TMAClO_4 as background electrolytes.

At elevated temperatures, a clear temperature dependent decrease of the p$K_{a,n}$ values of DOTA is observed (Figure 5.2), particularly for pKa_1 and pKa_2, which is in accordance with the study on the open-chain analogue DTPA by Tian *et al*, indicating that the ligand becomes a stronger acid at higher temperatures; here, a variation of up to 0.82 for pKa_1 in the temperature range between 10 and 70 °C was reported (Table 5.1)[260]. A similarly strong decrease of the p$K_{a,n}$ with increasing temperature is expected for DOTA and has been observed before by Desreux, who determinded smaller p$K_{a,n}$ values for DOTA at 80 °C than at 25 °C (in 1 M NaCl) [157]. The effect was also observed for the larger macrocycle TETA (Table 5.1[259]).

Accordingly, the obtained pKa_1 and pKa_2 values for deprotonation of the amino groups of DOTA significantly decrease with increasing temperature (Fig. 5.4, *pink and blue*). A variation of 0.84 for pKa_1 in the temperature range between 25 and 90 °C is observed, which is comparable with the result for pKa_1 of DTPA. Since it is hypothised that at least one of these amino-protons is oriented towards the inside of the ring, it is likely that temperature induced flexibility of the ring allows the surrounding OH^- to easier attack and detach the last proton. The dissociation of the two protons of the carboxylic functions at acid pH (pKa_3 and pKa_4, Fig. 5.4, *red and bl*ack) show no significant temperature dependence, complying with findings reported for the temperature dependence of carboxyl- pK_a up to 90 °C (variation of ∼0.2, [123]). In summary, the protonation of DOTA generally becomes weaker at higher temperatures.

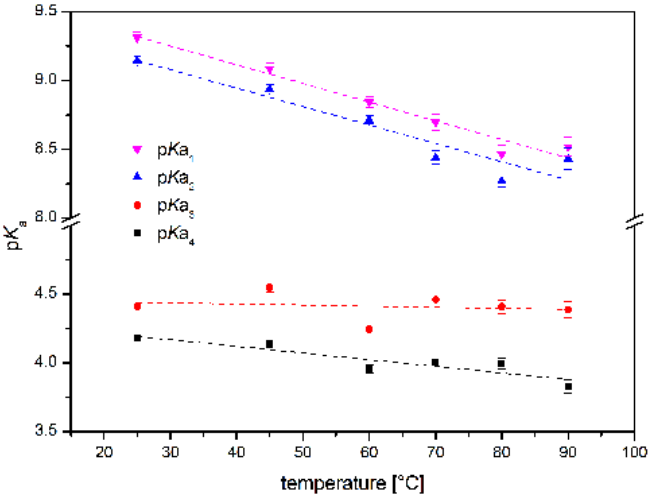

Figure 5.4: Trend of the pK_a values for DOTA in 0.1 M $NaClO_4$ in the temperature range of 25 - 90 °C.

In direct comparison, both ligands show very similar thermodynamic behaviour. From the slope and the intercept of the linear van't Hoff plots of log β_H vs. 1/T (Fig. 5.5) it is deduced that the protonation reactions of DOTA as well as of DTPA are all exothermic ($\Delta_R H < 0$). The values determined for $\Delta_R H$ and $\Delta_R S$, in comparison with the data for DTPA, are listed in Table 5.2.

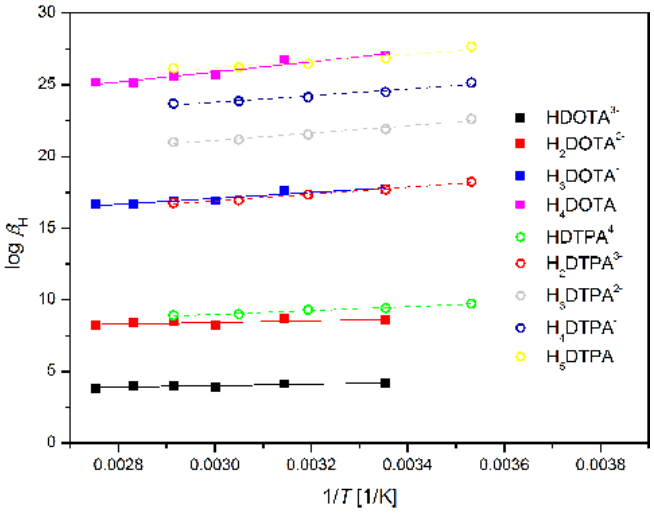

Figure 5.5: Van't Hoff plot of the protonation constants of DOTA (p.w., solid lines) and DTPA ([260], dashed lines) at I = 0.1 M $NaClO_4$(DOTA) or 1.05 M $NaClO_4$(DTPA). The solid symbols/lines are the experimental data/fits obtained in the present work. Open symbols/dashed lines: data/linear fits for DTPA.

The stepwise protonation enthalpies are all negative, which is consistent with the general trend that the protonation constants decrease as the temperature is increased. The protonation of DOTA and DTPA is promoted by both favourable enthalpic and entropic factors ($\Delta_R S > 0$).

Table 5.2: Thermodynamic parameters for the protonation of DOTA (I = 0.1 M $NaClO_4$) in comparison to DTPA (I = 1.05 M $NaClO_4$). The values for DTPA without error range were calculated from the respective literature data for the overall protonation enthalpies and entropies [260].

Equilibrium	$\Delta_R H$ *[kJ/mol]*	$\Delta_R S$ *[J·mol^{-1}K^{-1}]*
$H^+ + DOTA^{4-} \rightleftharpoons HDOTA^{3-}$	-28.1±1.4	85±4
$H^+ + HDOTA^{3-} \rightleftharpoons H_2DOTA^{2-}$	-27.8±2.3	82±7
$H^+ + H_2DOTA^{2-} \rightleftharpoons H_3DOTA^{-}$	-1.6±2.2	80±7
$H^+ + H_3DOTA^{-} \rightleftharpoons H_4DOTA$	-3.3±1.2	68±4
$H^+ + DTPA^{5-} \rightleftharpoons HDTPA^{4-}$	-26.2±1.4	93±5
$H^+ + HDTPA^{4-} \rightleftharpoons H_2DTPA^{3-}$	-26.4	69
$H^+ + H_2DTPA^{3-} \rightleftharpoons H_3DTPA^{2-}$	-11.6	42
$H^+ + H_3DTPA^{2-} \rightleftharpoons H_4DTPA^{-}$	-0.8	46
$H^+ + H_4DTPA^{-} \rightleftharpoons H_5DTPA$	1.4	51

It is apparent that two (DOTA) or three (DTPA) of the $\Delta_R H$ have more negative values than the other two. This is typical for amine protonation being a markedly exothermic reaction, while the protonation of carboxylic acids is an almost athermic reaction, since the energy required for dehydration of H^+ and the carboxylate group is probably compensated by the energy released by the combination of the two species with opposite charges (H^+, COO^-) [142, 260]. The larger negative enthalpies hence clearly suggest that the first two protonations forming $HDOTA^{4-}$ and H_2DOTA^{3-} occur at two transannular nitrogen atoms, as it is expected due to steric and electrostatic repulsion. The last two protonation steps occur at the acetate groups attached to the unprotonated N-atoms, since the other two acetate arms are involved in hydrogen bonding with the protonated, charged NR_3H^+.

Such a protonation sequence (Fig. 5.1) for DOTA has been evidenced by Desreux *et al* by means of NMR spectroscopy [157] and explains why the diprotonated form of the ligand (H_2DOTA^{2+}) is orders of magnitude less reactive than the monoprotonated and fully deprotonated ligand species [264].

The favourable entropic contributions for DTPA and DOTA mainly result from desolvation processes due to charge neutralisation after protonation. The increasing stiffening of the DOTA ligand with successive protonation results in a loss of entropy which is reflected by the lower $\Delta_R S$ in the last protonation steps [142].

5.1.3 Determination of the log *K* for Na(I)DOTA in the Temperature Range of 25 to 90 °C

As mentioned before, investigation of the thermodynamic and kinetic stability of the DOTA complexes in presence of Na^+ is crucial when studying Ac-225-DOTA-mAb conjugates for application in biological systems. Therefore 0.1 M $NaClO_4$ is consistently applied as background medium in all experiments. However, the formation of DOTA complexes with Na^+ is delicate for determination of acid dissociation- ($pK_{a,n}$, discussed in paragraph 5.1.1) or complex association constants (log K) in this medium, because it reduces the concentration of free $DOTA^{4-}$ required for calculation of the complex stability constants. It is known that both log K and $pK_{a,n}$ values

determined in media containing Na^+ or K^+ as background electrolytes are lower than those determined in media with non-coordinating cations like TMA^+; the effect is however not as pronounced with K^+ as it is with Na^+. To obtain correct results for the sought complexes it is hence important to quantify the interaction of Na^+ with DOTA at the relevant temperatures.

The log K of $[Na(DOTA)]^{3-}$ is determined by potentiometric titration of DOTA with NaOH in 0.1 M $NaClO_4$ and 0.1 M $TMAClO_4$ medium, respectively (Fig. 5.6, *left*), followed by simultaneous fitting of the two corresponding data sets at the respective temperature (Fig. 5.6, *right*). After indroduction of the $pK_{a,n}$ values for DOTA at 25 - 90 °C determined in 0.1 M $NaClO_4$ into the fit, this permits determination of the log $K_{Na(I)DOTA}$ from the deviations in the titration curves (Fig. 5.3, [135]). The results are summarised in Table 5.3, with the corresponding van't Hoff plot shown in Figure 5.6.

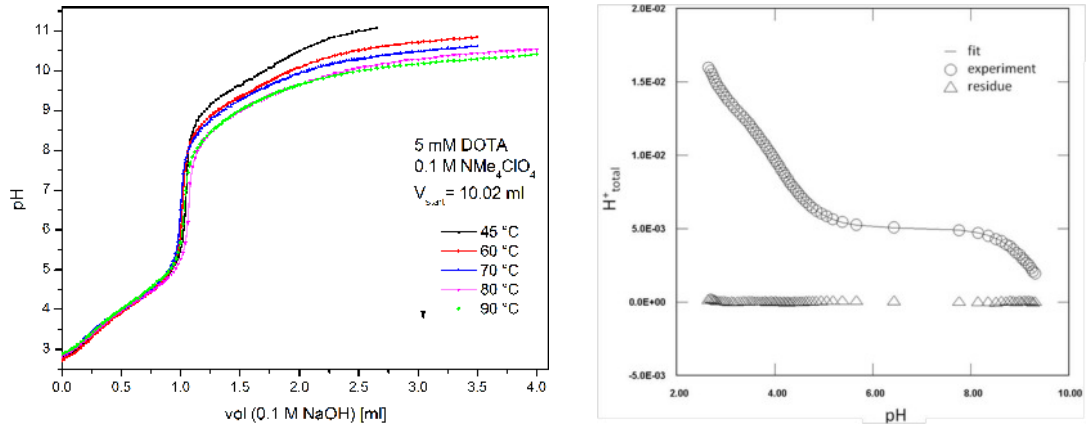

Figure 5.6: *left*: Potentiometric titration curves for the experiments conducted at 45 - 90 °C, [DOTA] = 5 mM; I = 0.1 M $TMAClO_4$. *right*: Exemplary fit for simultaneous fitting of the experimental data in $NaClO_4$ and $TMAClO_4$ medium (Fiteql 4.0, T = 45 °C). The solid line represents the model, the circles the experimental data points, and the triangles the deviation from the model.

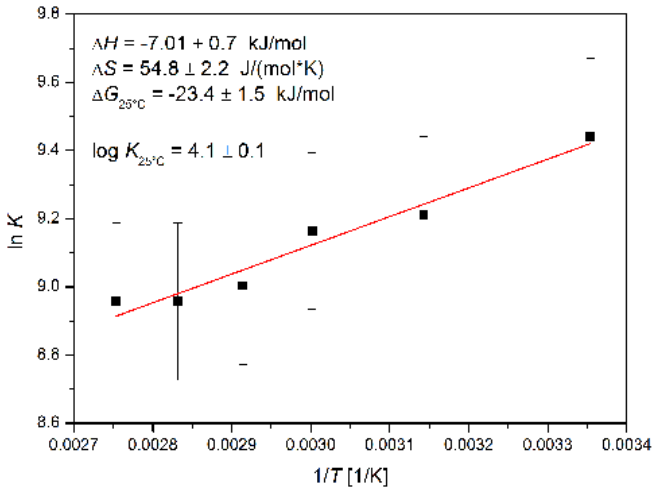

Figure 5.7: Van't Hoff plot for derivation of the thermodynamic parameters of the Na(I)DOTA complexation.

Table 5.3: Thermodynamic constants derived for the formation of $[Na(DOTA)]^{3-}$.

T [°C]	*log K Na(I)DOTA*	$\Delta_R H$ *[kJ/mol]*	$\Delta_R S$ *[J·mol^{-1}K^{-1}]*	$\Delta_R G$*[kJ/mol]*
25[141]	4.03, 4.2±0.03			
25	4.1±0.1	-7.0±0.7	54.8±2.2	-23.4±1.4
45	4.0±0.03			
60	3.98±0.04			
70	3.91±0.05			
80	3.89±0.04			
90	3.89±0.07			

As it is apparent from Table 5.3, the log K values for Na(I)DOTA decrease with temperature, indicating an exothermic reaction ($\Delta_R H < 0$). This trend is rated as reasonable, since for complexation of Na^+ with other complexones like $EDTA^{4-}$ similar $\Delta_R H$ between -5 and -10 kJ/mol were reported in various electrolyte media [265]. However, since open-chain ligands are not directly comparable with macrocyclic ligands, this is only an indication and should not be considered as proof.

5.1.4 Determination of the p$K_{a,n}$ Values of DOTA under Sodium-free Conditions in the Temperature Range of 25 to 90 °C

Knowing the log K values for the Na(I)DOTA complexation now permits calculation of the p$K_{a,n}$ values under sodium-free conditions (Table 5.4). The titration data obtained in $NaClO_4$ is re-fitted by inclusion of the log $K_{Na(I)DOTA}$ into the Fiteql input file. Like this, estimation of the p$K_{a,n}$ values, which were received if Na(I) would not disturb the deprotonation, is possible. The data obtained this way are expected to be in analogy with the literature data for the 0.1 M TMACl system, in which particularly the value for pKa_1 is significantly increased (up to ~12.60, [11]).

The sodium-free values derived in the present work, together with the data for $\Delta_R H$ and $\Delta_R S$ for the respective protonation equilibria are presented in Fig. 5.8 and Table 5.5. The p$K_{a,n}$ data for 25 °C comply with the literature values for the comparable metal-free TMACl system (25 °C, I = 0.1 M) [165, 162, 266].

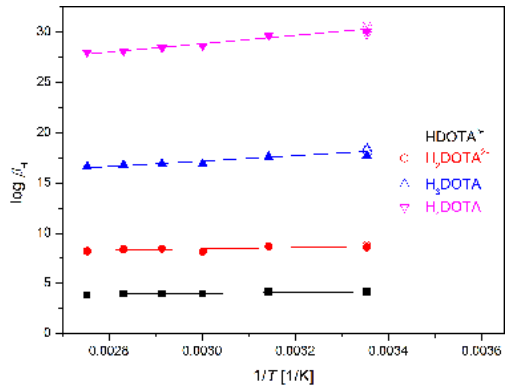

Figure 5.8: Van't Hoff plot of the sodium-independent protonation constants of DOTA at different temperatures (I = 0.1 M, solid symbols) compared to literature data for 0.1 M TMACl (open symbols) [165, 162, 266].

As expected, the data for $\Delta_R H$ and $\Delta_R S$ are conform with the data obtained for the DOTA protonation in presence of Na^+ (paragraph 5.1.1), except for the first protonation equilibrium, which is influenced by metal-cations and hence gives higher values under metal-free conditions. The obtained $\Delta_R H$ values are again assigned to two groups ascribed to the protonation of the amines ($\Delta_R H \sim$ -30 kJ/mol) and the carboxyl functions ($\Delta_R H \sim$ -2 to -3 kJ/mol) as discussed in paragraph 5.1.2.

Table 5.4: Determined $pK_{a,n}$ values for DOTA under sodium-free conditions in the temperature range of 25 - 90 °C (I = 0.1 M $TMAClO_4$, present work (p.w.)) in comparison with data derived for the protonation of DOTA in presence of sodium (I = 0.1 M $NaClO_4$, present work (p.w.)) as well as literature values for DOTA at 25 °C in 0.1 M TMACl medium.

Conditions	**p*Ka₁***	**p*Ka₂***	**p*Ka₃***	**p*Ka₄***
DOTA (in absence of Na(I))				
25 °C, 0.1 M TMACl [162]	11.73±0.03	9.40±0.02	4.50±0.04	4.19±0.06
25 °C, 0.1 M TMACl [266]	12.00±0.1	9.70±0.06	4.67±0.02	4.13±0.04
25 °C, 0.1 M TMACl [165]	12.60±0.01	9.70±0.01	4.50±0.01	4.14±0.01
25 °C, 0.1 M (p.w.)	12.35±0.04	9.15±0.03	4.41±0.03	4.18±0.02
45 °C, 0.1 M (p.w.)	12.05±0.04	8.93±0.03	4.55±0.03	4.14±0.02
60 °C, 0.1 M (p.w.)	11.75±0.04	8.72±0.03	4.24±0.03	3.95±0.03
70 °C, 0.1 M (p.w.)	11.55±0.06	8.44±0.05	4.46±0.04	4.00±0.03
80 °C, 0.1 M (p.w.)	11.32±0.06	8.40±0.04	4.41±0.05	3.99±0.04
90 °C, 0.1 M (p.w.)	11.36±0.07	8.43±0.08	4.37±0.06	3.83±0.05
DOTA (in presence of Na(I))				
25 °C, 0.1 M $NaClO_4$(p.w.)	9.31±0.04	9.14±0.03	4.41±0.03	4.18±0.02
45 °C, 0.1 M $NaClO_4$(p.w.)	9.09±0.04	8.94±0.03	4.55±0.03	4.14±0.02
60 °C, 0.1 M $NaClO_4$(p.w.)	8.84±0.04	8.71±0.03	4.24±0.03	3.95±0.03
70 °C, 0.1 M $NaClO_4$(p.w.)	8.70±0.06	8.44±0.05	4.46±0.04	4.00±0.03
80 °C, 0.1 M $NaClO_4$(p.w.)	8.47±0.06	8.27±0.04	4.41±0.05	3.99±0.04
90 °C, 0.1 M $NaClO_4$(p.w.)	8.52±0.07	8.43±0.08	4.39±0.06	3.83±0.05

Table 5.5: Thermodynamic parameters for the protonation of DOTA (I = 0.1 M) under Na(I)-free conditions in comparison to the values (I = 0.1 M $NaClO_4$) derived in presence of Na(I) in the present work (Table 5.2).

	Equilibrium	$\Delta_R H$ ***[kJ/mol]***	$\Delta_R S$ ***[J·mol⁻¹K⁻¹]***
Na(I)-media	$H^+ + DOTA^{4-} \rightleftharpoons HDOTA^{3-}$	-28.1±1.4	85±4
	$H^+ + HDOTA^{3-} \rightleftharpoons H_2DOTA^{2-}$	-27.8±2.3	82±7
	$H^+ + H_2DOTA^{2-} \rightleftharpoons H_3DOTA^-$	-1.6±2.2	80±7
	$H^+ + H_3DOTA^- \rightleftharpoons H_4DOTA$	-3.3±1.2	68±4
Na(I)-free media	$H^+ + DOTA^{4-} \rightleftharpoons HDOTA^{3-}$	-34.9±1.5	120±5
	$H^+ + HDOTA^{3-} \rightleftharpoons H_2DOTA^{2-}$	-26.2±1.7	88±5
	$H^+ + H_2DOTA^{2-} \rightleftharpoons H_3DOTA^-$	-2.0±2.2	78±7
	$H^+ + H_3DOTA^- \rightleftharpoons H_4DOTA$	-3.4±1.3	68±4

5.1.5 DOTA Species Distributions at Various Temperatures and Their Relevance for An(III) Complexation/Radiolabelling

Knowing the acid dissociation constants at various temperatures not only permits the calculation of thermodynamic stability constants of complexes but also of the ratio of the various protonated ligand species at the respective temperatures (Fig. 5.9). This again indicates pH conditions suitable for rapid metal ion complexation by the reactive ligand species. This is particularly interesting in terms of optimisation of the radiolabelling of the DOTA-chelated peptides and antibodies, with the latter needing to be spared from harsh reaction conditions.

The labelling protocols for Ac-225-DOTA-antibody conjugates established so far describe two significantly different reaction-pH as the most favourable. The group of McDevitt *et al* suggests to conduct the Ac-225-DOTA complexation at pH 5.5 (60 °C, TMAA buffer, [6]), while in previous studies a reaction pH of 9 was found to be more suitable for radiolabelling (45 °C, TRIS buffer, Diploma thesis [7]). The chemical integrity of the antibody is known to be preserved at this pH, as the coupling of DOTA to the antibody according to McDevitt *et al* is routinely accomplished at pH∼9 ($NaHCO_3$-buffer), .

In Figure 5.9 the discussed pH conditions (5.5 and 9, respectively) are marked by dashed lines. From comparison of the species present under these conditions it is obvious, that at pH 9 at 45 °C already a large fraction of the total DOTA is present in form of the reactive $HDOTA^{3-}$(40 %) as well as in form of the highly reactive $DOTA^{4-}$ species (30 %). The percentage of the latter increases until it is predominant at 90 °C (70 %), which corresponds to the conditions for peptide radiolabelling that were found to be suitable in previous studies (pH 9 / 90 °C, [7]).

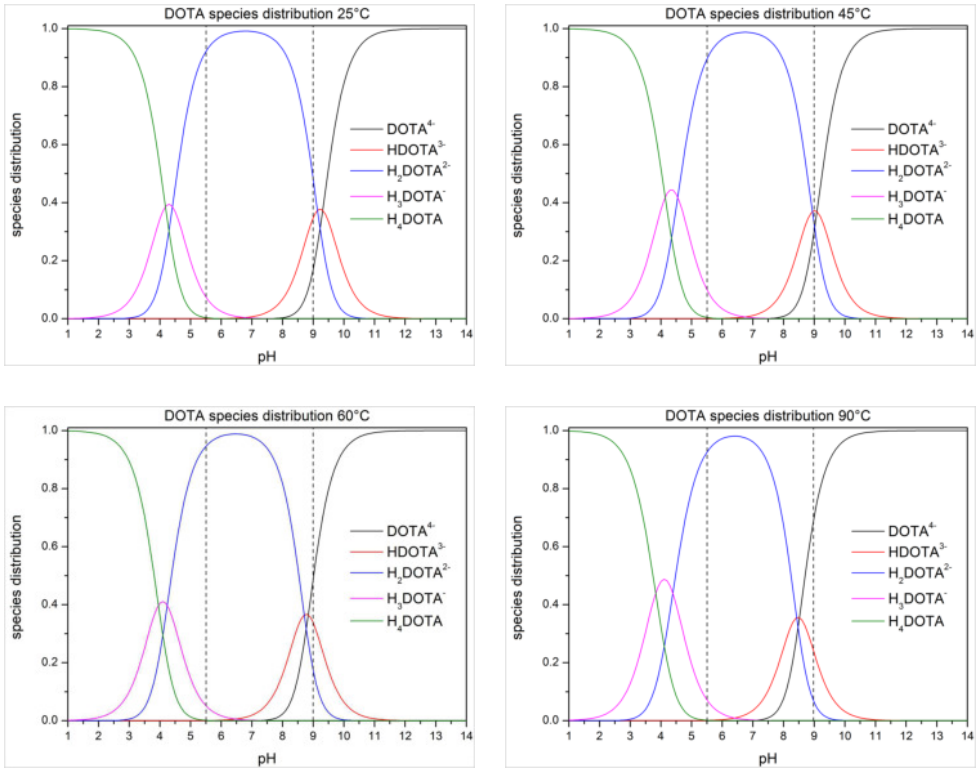

Figure 5.9: DOTA species distribution at 25 - 90 °C calculated with the respective experimentally determined pK_a values (0.1 M $NaClO_4$, PHREEQC). The dashed lines indicate the pH conditions suggested for radiolabelling of DOTA-chelated antibodies with Ac-225 (pH 5.5 [6] , pH 9 [7]).

At pH 5.5, however, at all temperatures 90 % of DOTA is invariantly present in form of H_2DOTA^{2-}, a species which is described to be not as reactive as the fully deprotonated species [168], which under these conditions is only present in extremely small amounts ($\sim 10^{-15}$M). The concentrations of the other protonated species have no significance for the equilibrium reaction.

Generally, at a given temperature, the complexation of metal cations by DOTA will proceed the more rapid the less protons need to be replaced. Hence the radiolabelling is expected to be more efficient the higher the ratio of the most reactive species ($DOTA^{4-}$) is; alkaline pH conditions are thus suggested to be favourable over acidic conditions. The base-assisted detatchment of the last proton is also fostered when working at alkaline conditions and thus potentially offers the possibility to use lower temperatures to achieve effective complexation. Therefore it is believed that the protocol of McDevitt *et al* (pH 5.5/60 °C), which suffers from low overall-yields of $\sim$10 % [6], can be substituted by the protocol suggested previously (pH 9/45 °C), giving yields of 90 % and higher [7]. Further refinement and evaluation of this protocol is subject of the present study.

5.2 Investigation of the Cm(III)-DOTA System with TRLFS

The major aim of the thermodynamic investigations with An(III)DOTA is to determine the complex stability of the Ac(III)DOTA complex, and hence evaluate the thermodynamic stability of the Ac-225-DOTA-mAb radioimmunoconjugates. It has been estimated by Monatvon *et al* that RICs require log $K > 19$ in order to be stable under physiological conditions [221]. Determination of the complex stability constants can be accomplished with well established spectroscopic methods such as UV-Vis spectroscopy or TRLFS, which allow for accurate determination of the species distribution at defined reaction conditions. Since DOTA shows no UV-Vis absorbance and Ac(III) has no suitable spectroscopic properties either, TRLFS investigations were conducted with Cm(III) as representative for Ac(III) and trivalent actinides in general.

The objective of this TRLFS study was to investigate the complexation chemistry of Cm(III)DOTA in order to gain profound knowledge about the reaction mechanism as well as the kinetic- and thermodynamic properties of the system. Besides determination of the complex stability constant of $[Cm(DOTA)]^-$, also the detection of possible intermediate species, which have been reported for the Eu(III)-DOTA-system, was of particular interest [8]. Initially, identification and structural characterisation of the respective Cm(III) species was done by comparison of the fluorescence lifetimes. In the second step, the kinetic reaction rates of the complexation with DOTA and the bifunctionalised derivative DOTA-NCS (*p*-SCN-Bn-DOTA) were reviewed at varying temperatures. Eventually, batch experiments at different pH were conducted in the temperature range of 45 - 90 °C to determine the thermodynamic parameters of the system. The relative ratios of the Cm(III) species were quantified by means of peak deconvolution. From these ratios the conditional stability constants log K for $[Cm(DOTA)]^-$ were calculated based on the $pK_{a,n}$ values determined for the respective reaction conditions (see chapter 5.1).

5.2.1 Characterisation of the Various Cm(III) Species

5.2.1.1 Cm(III) aquo ion

The emission spectrum of the solvated Cm(III) species in 0.1 M $HClO_4$ is presented in Figure 5.10. The emission band of the Cm(III) aquo ion has a maximum at 593.8 nm and a FWHM of 7.8 nm, which is in accordance with the literature values (593.8 nm, FWHM 7.7 nm [119]). The fluorescence lifetime of this species was determined to be 66.7 µs, which results from coordination of Cm(III) by a high number of quenching H_2O ligands, and also complies with the literature (65 - 68 µs [119, 96]). By using the Kimura equation (Eq. 3.13), the number of water ligands in the first coordination sphere was calculated to be n = 8.9±0.5 [125]. This is consistent with the Cm(III) being coordinated by 9 H_2O molecules, as it was reported before [119].

5.2.1.2 The Cm(III)DOTA/DOTA-NCS Species in H_2O

Various authors discuss the occurrence of partially protonated intermediate complex species which eventually become deprotonated to form the final DOTA complex (see paragraph 3.5.3). To potentially determine these intermediate species,

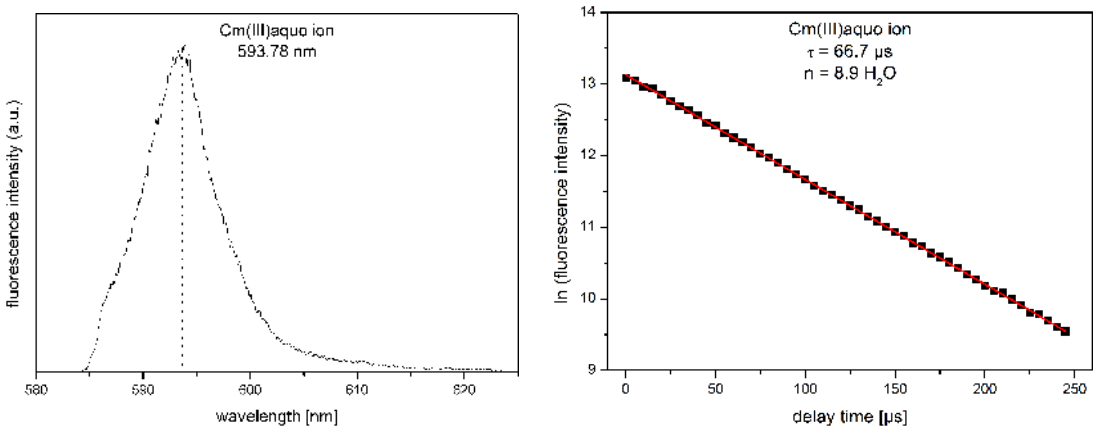

Figure 5.10: *left*: Emission band of the Cm(III) aquo ion; *right*: Decrease of fluorescence intensity of the Cm(III) aquo ion as function of the delay time.

a sample was prepared as described in paragraph 4.7.2.1 with a metal-to-ligand ratio of 1 : 10. This sample was incubated at 90 °C for 30 days and measured intermittently. During this period only one emission band with a maximum at 608.1 nm was detected (25 °C, FWHM = 6.1 nm, Fig. *5.12 top*). Such a large redshift is typically associated with strongly complexing ligands [267]. The fluorescence lifetime of the species was determined to be 278.8 µs, corresponding to a Cm(III) complex species with n = 1.45±0.5 H_2O ligands. Since Cm(III) has a maximum of 9 available coordination sites and DOTA is known to act as octadentate ligand for An(III)/Ln(III), this emission band is concluded to represent the complex species $[CmDOTA(H_2O)]^-$. The results are in accordance with the literature values for this complex (τ = 280 µs, 1.4 H_2O [126]). For simplification, this complex is referred to as Cm(III)DOTA in the course of this report.

The emission band for the equivalent $[CmDOTA\text{-}NCS(H_2O)]^-$ complex as well as for the antibody conjuagte $[CmDOTA\text{-}NCS(H_2O)]^-_x$-mAb is slightly shifted to higher wavelengths (608.4 nm (FWHM = 6.3 nm) and 608.5 nm (FWHM = 6.2 nm), respectively, Fig. *5.12 middle* and *bottom*). This indicates the influence of geometry on the crystal field and likely results from varying bond lengths induced by changes of the DOTA binding pocket due to increased steric demand of the side chain.

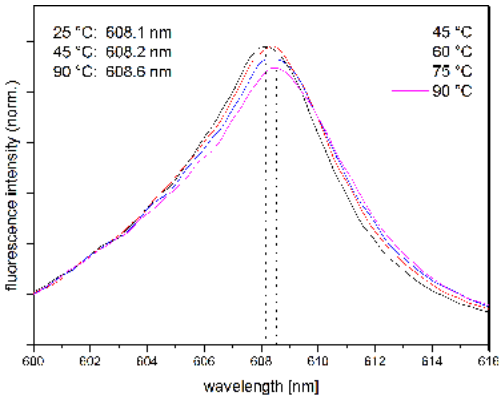

Figure 5.11: Spectra demonstrating the temperature induced shift of the Cm(III)DOTA emission band from 608.15 nm (45 °C) to 608.56 nm (90 °C). The value for 25 °C is included for comparison.

With increasing temperature also a slight shift of the $[Cm(DOTA)]^-$ emission band to higher wavelength was observed (Fig. 5.11), an effect which was also reported for the Cm(III) aquo ion changing between 8- and 9-fold coordination [268]. One possible explanation for this finding is that at higher temperatures the metal cation is better encapsulated by DOTA, resulting in small variations of the

Cm(III)-O and Cm(III)-M bond lengths and hence in slightly different coordination geometry, which is reflected by slightly different emission maxima. The measurements also indicate a slight increase of fluorescence lifetime going from DOTA to DOTA-NCS-mAb.

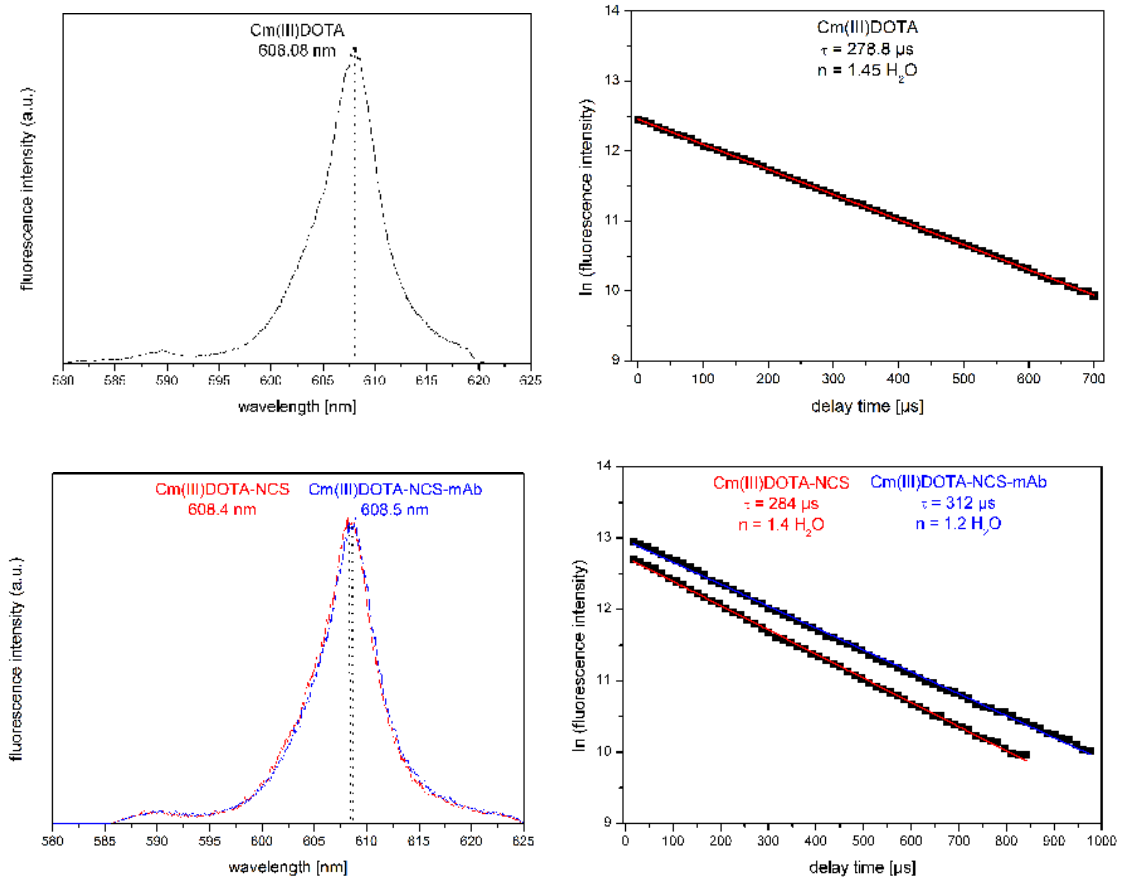

Figure 5.12: *top left*: Emission band of the $[CmDOTA(H_2O)]^-$ complex; *top right*: Decrease of fluorescence intensity of the $[CmDOTA(H_2O)]^-$ complex as a function of delay time; *bottom*: Emission band and decrease of fluorescence intensity of the $[CmDOTA\text{-}NCS(H_2O)]^-$ complex and the respective antibody conjuagte $[CmDOTA\text{-}NCS(H_2O)]^-$-mAb as a function of delay time. According to Kimura, the error for n is ±0.5 [125].

5.2.1.3 Cm(III)DOTA in D_2O

In accordance to the literature on Eu(III)DOTA, in the present study one residual water molecule was found to be coordinated to the metal cation to saturate the ninth coordination site of the Cm(III)DOTA complex [8]. However, the experimentally determined value of n = 1.45±0.5 is slightly higher than the expected value of n = 1. This deviation was also found in a simultaneously conducted study by Schmitt, who reported n = 1.65±0.5 instead of n = 1 for the similar Cm(III)-DTPA system [269]. In order to reveal the reason for this discrepancy, the fluorescence lifetime of Cm(III)DOTA was measured in D_2O. Since D_2O molecules do not induce fluorescence quenching, this experiment enables determination whether DOTA shows a quench effect itself. DOTA has no O-H bond, but also quenching resulting from C–H or N–H oscillators has been reported before (e.g. [270]).

The measurements in D_2O resulted in τ = 1158 µs for the Cm(III) aquo ion (*Lit*: 1130 - 1200±30 µs [119, 96]) and τ = 787 µs for the $[CmDOTA(D_2O)]^-$ complex (Fig. 5.13). The difference between these two values indicates the quenching properties of DOTA and hence explains the deviation of the experimental values discussed above. Thus, it can be safely assumed that a complex species $[CmDOTA(H_2O)]^-$ is formed, which complies with the DOTA complexes found for the Ln(III) series [9].

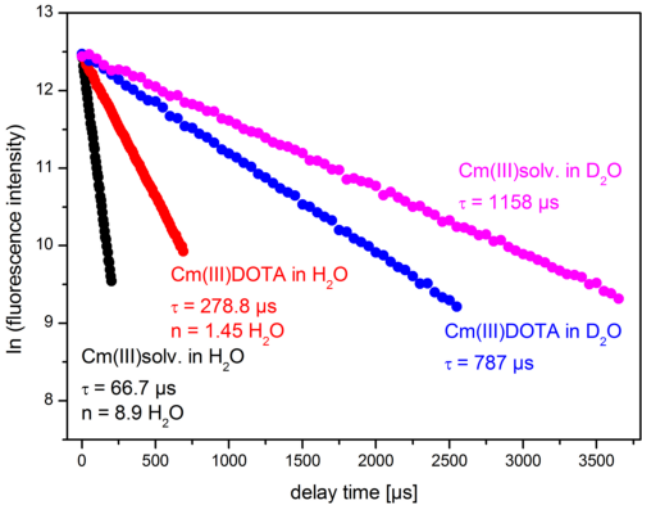

Figure 5.13: Decrease of fluorescence intensity of the Cm(III)solvens species and Cm(III)DOTA in H_2O / D_2O as a function of delay time. The species coordinated with the most quenching ligands has the shortest fluorescence lifetime. The error for n is ±0.5 [125].

5.2.1.4 Intermediate Species

In the context of the kinetic experiments (see paragraph 5.2.2.1.), for the first time a shoulder with an emission maximum at 598.8 nm was observed on the right flank of the Cm(III) aquo ion band (Fig. *5.14 left*). However, it was not possible to characterise this species by determination of its fluorescense lifetime, since transformation to the final complex occurred rapidly during the recording of the flourescence decay. Nevertheless, it is apparent that the detected species at 598.8 nm is coordinated by less H_2O than the Cm(III) aquo ion since the emission band is shifted to higher wavelengths. This is characteristic for coordination of Cm(III) by ligands (*here*: DOTA) with concomitant extrusion of H_2O. However, the only moderate red-shift of the band gives rise to the assumption that the metal cation in this state is only coordinated by some of the carboxylic groups of DOTA.

During further experiments another emission band at 602.3 nm was observed (Fig. 5.14 *right*). It was not possible to obtain a pure spectrum of this intermediate species and thus a triexponential fit had to be applied to analyse the respective fluorescence lifetime measurement. With τ for the Cm(III) aquo ion being set to 67 µs and τ for $[CmDOTA(H_2O)]^-$ being fixed to 278 µs (paragraph 5.2.1.1 and 5.2.1.2), the fit revealed an estimated lifetime of τ ~122 µs for the intermediate complex, which, according to the Kimura equation, translates into n = 5.4±0.5 H_2O molecules in the first coordination sphere (Fig. 5.14 right).

Considering the quenching influence of DOTA (paragraph 5.2.1.3), this likely correlates to n = 5±0.5 H_2O, which complies with the intermediate species

$[M(III)(H_2DOTA)(H_2O)_5]^+$ postulated in the literature on Eu(III)DOTA [8, 11]. In this species the metal ion is located on top of the DOTA cage and is coordinated by the four acetate arms and five water molecules. However, as it was not possible to measure this Cm(III)-DOTA intermediate species more accurately, and because tri-exponential fits naturally have large uncertainties, no clear statement can be made if the observed emission really arose from the sought species.

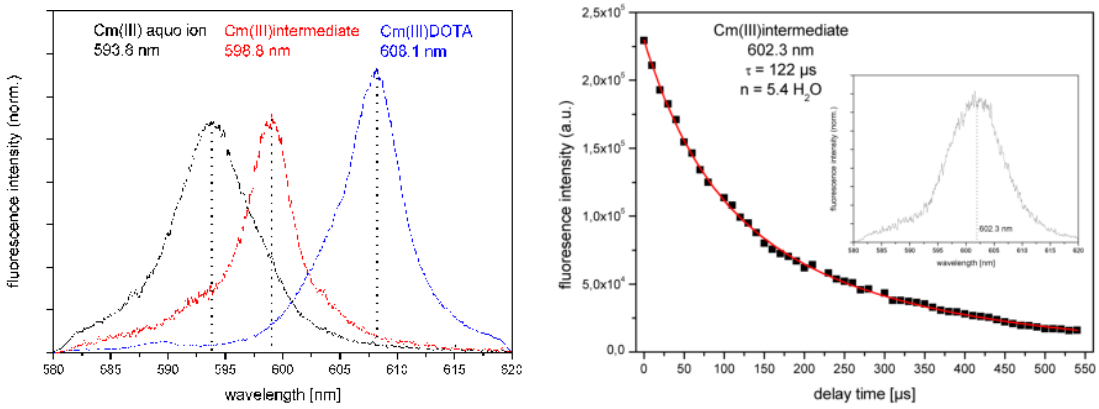

Figure 5.14: *left*: Emission bands of the different Cm(III) species (pure spectra). *right*: Observed emission band (*inset*) and triexponential fit of the decrease of fluorescence intensity of the postulated intermediate species at 602.3 nm ($[Cm(H_2DOTA)(H_2O)_5]^+$) as a function of the delay time. The error for n is ±0.5 [125].

The emission band at 598.8 nm was reproduced in several experiments; hence further investigations concentrated on revealing the structure of this intermediate species. To eventually measure the lifetime of the pure species, attempts were made to slow down the reaction kinetics by working at low temperatures (0 - 5 °C). The reaction batch containing $1 \cdot 10^{-7}$ M $Cm(ClO_4)_3$ and a 1000-fold excess of DOTA was deep frozen immediately after mixing (liquid N_2/isopropanol) and placed in the cooled sample holder. Spectra were recorded by passing the laser beam through the liquid phase forming below the sample ice cube.

Like this, the reaction was halted in a state where mainly the Cm(III) aquo ion, the intermediate species of interest and only a marginal fraction of the final Cm(III)DOTA complex were observable (Fig. 5.15). The recorded lifetime was again fitted triexponentially and revealed an average fluorescence lifetime of 86.3 µs for the intermediate complex, translating into n = 6.7±0.5 H_2O molecules in the first coordination sphere. This likely corresponds to a species $[Cm(H_2DOTA)(H_2O)_7]^+$ with Cm(III) being bound by only two acetate arms of DOTA.

Not only the short fluorescence lifetime, but also the only minor shift of the emission band are aspects in favour of twofold coordination over fourfold coordination. The shift to 598.8 nm is comparable to the shift induced by two carboxylate groups as found for the Cm(propionate) 1:2-complex $[Cm(Prop)_2]^+$ with an emission maximum at 598.9 nm [123], while for coordination of 4 carboxylic groups a more red-shifted band at ~603-604 nm would be expected (compare Cm(III)EDTA at 603.8 nm [119], see Table 5.6).

Preliminary DFT-calculations also suggest an energetically favourable chair conformation of DOTA with each two arms up/down oriented in the ground state as

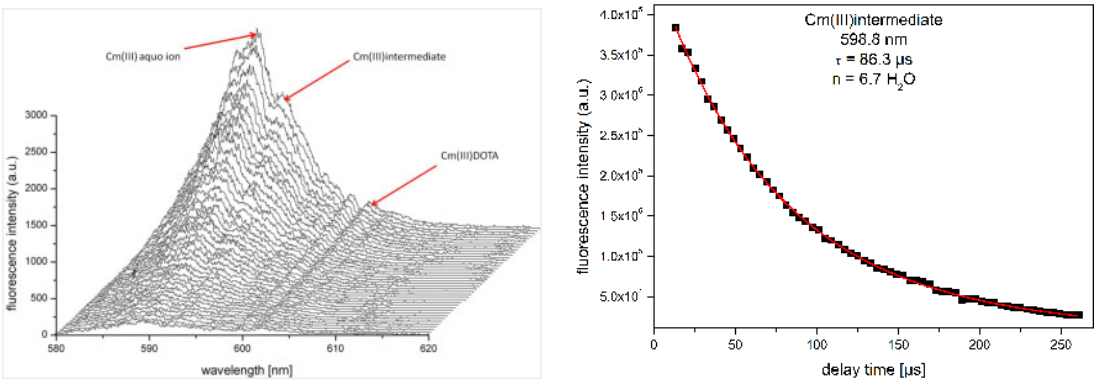

Figure 5.15: Decay of the fluorescence intensity of the intermediate species at 598.8 nm (*left*) and triexponential fit of the fluorescence lifetime (*right*). The error for n is ±0.5 [125].

possible starting conformation for M(III) complexation (Fig. 5.16, *left*; geometry optimisations: DFT/BP86 level in gas phase; C, N, H and O atoms described by def2-TZVP basis sets provided by Turbomole software package). The proposed ground state conformation is an energy minimum compared to the boat conformation with all acetate arms pointing in the same direction and was confirmed by frequency analysis (no imaginary vibrations) [271].

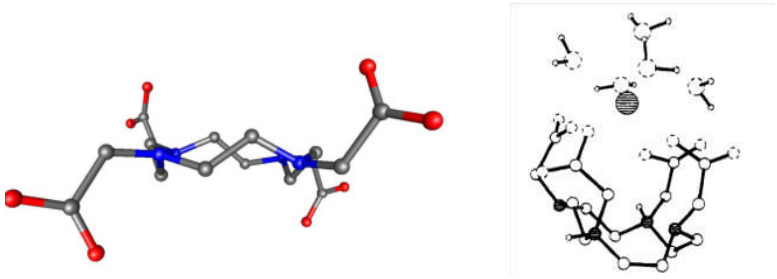

Figure 5.16: *left*: calculated DOTA structure. DFT-calculations show that the ring structure with each two opposed acetate arms pointing up and down is an energy minimum . This is due to the chair conformation of the cyclododecane ring being favourable over the boat conformation which is required to allow all arms to point to the same side of the ring. *right*: Stereoview of the intermediate species $[Eu(H_2DOTA)(H_2O)_5]^+$ proposed by Wu and Horrocks [8].

5.2.1.5 Intermediate species for Eu(III)DOTA

As mentioned before, the fourfold coordinated Cm(III)-DOTA intermediate species at ∼602 nm, complying to the fourfold coordinated Eu(III)-DOTA species reported by Horrocks *et al* [8], could not be concludingly verified. To further investigate this species, the experiments described in the literature were reproduced in order to characterise the Eu(III)-DOTA intermediate and to compare it to the two observed Cm(III)-DOTA intermediate species. The obtained spectra in comparison with the literature spectra by Horrocks *et al* are presented in Figure 5.17.

The obtained spectra for the $^5D_0 \rightarrow {}^7F_0$ transition were found to largely match the reported literature spectra, with the emission band for the Eu(III)DOTA inter-

Table 5.6: Shifts of inorganic ligands and carboxylic acids in Cm(III)-TRLFS.

Species	λ_{max}*[nm]*	τ*[µs]*	*n(H_2O) ±0.5*	*coordinating groups*	*Reference*
$Cm(H_2O)_9$ $Cm(CO_3)_x^{2-2x}$	593.8	64	9		[119]
x = 1	598.5	79	7.3		[119]
x = 2	603.0	89	6.4		[119]
x = 3	605.7	126	4.3		[119]
x = 4	607.5	256	1.6		[119]
$Cm(Prop)^{2+}$	596.5			1 carboxyl	[123]
$Cm(Prop)_2^{+}$	598.9			2 carboxyl	[123]
Cm(III)EDTA	603.8	126	4.4	4 carboxyl, 2 amino	[119]
Cm(III)DTPA	607	271	1.5	5 carboxyl, 3 amino	[119]
Cm(III)DOTA	608.1	278	1.45	4 carboxyl, 4 amino	this work

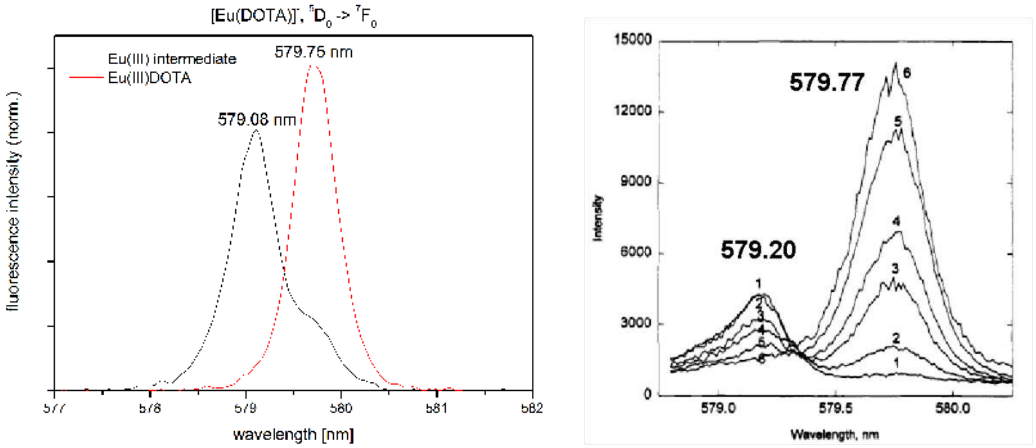

Figure 5.17: Eu(III)DOTA $^5D_0 \rightarrow ^7F_0$ spectra (Eu(III):DOTA = 1:1000, pH 3, *left*) compared to the literature spectra (*right*) [8]. The spectra were recorded during the first 30 min after the reactants were mixed.

mediate species appearing at 579.1 nm instead of 579.2 nm and the final complex at 579.8 nm, respectively.

From the shift ($\Delta\nu$) of the $^7F_0 - ^5D_0$ emission band the coordination number of the ligand (CN_{Lig}) is estimated following the empiric equation established by Choppin *et al* [272]:

$$CN_{Lig} = 0.237 \cdot \Delta\nu + 0.628 \,. \tag{5.1}$$

Although the emission maxima vary only slightly, the discrepance translates into a calculated coordination number of $CN_{Lig} = 2.5$ (p.w.) compared to $CN_{Lig} = 3.2$ calculated for a shift of $\Delta\nu$ =10.81 [cm^{-1}] for the species measured by Horrocks *et al* (see Table 5.7 [8]). This, however, also deviates from the coordination number of four for the observed Eu(III)-DOTA species as it was suggested by the authors. The results are comparable with the values reported for the $[Eu(acetate)_x]^{(3-x)+}$ species with x = 2, 3 and are summarised in Table 5.7.

Table 5.7: Shift ($\Delta\nu$) of relevant Eu(III) $^7F_0 - ^5D_0$ bands.

Species	λ *[nm]*	ν *[cm^{-1}]*	$\Delta\nu$	CN_{Lig}	CN_{calc}	*Reference*
$[Eu(H_2O)]^{3+}$	578.8	17276.00	0	0	0.93	[272]
$[Eu(acetate)]^{2+}$	578.9	17273.24	2.76	1	1.28	[272]
$[Eu(acetate)_2]^{+}$	579.0	17271.15	4.85	2	1.78	[272]
$[Eu(acetate)_3]$	579.2	17265.19	10.81	3	3.19	[272]
$[Eu(DOTA)(H_2O)]^{-}$	579.8	17247.00	29.00	8	7.50	p.w.; [8]
$[Eu(intermediate)]_{CN\ 4}$	579.2	17265.19	10.81	"4"	3.19	[8]
$[Eu(intermediate)]_{CN\ 2}$	579.1	17268.20	7.80	"2 - 4" ?	2.48	p.w.

The findings lead to the conclusion that the intermediate species observed in this work for both the Cm(III)DOTA and Eu(III)DOTA system is likely to be rather coordinated by only two of the acetate arms of DOTA instead of by all four arms. However, a twofold coordinated intermediate species has not been described before. More precise lifetime measurements are required to provide final proof.

5.2.1.6 Intermediate species for M(III)DOTA-NCS

Continuative studies revealed that the complexation reaction with DOTA-NCS proceeds slower than with unfunctionalised DOTA (see paragraph 5.2.2.1 ff for details). The effect was also found for Eu(III)DOTA and Eu(III)DOTA-NCS (Fig. 5.18), where direct comparison of the spectra recorded after 11 minutes clearly shows that the reaction with DOTA-NCS is notably slowed down. This probably results from the steric shielding of one side of the ring by the large, probably axial oriented *p*-SCN-Bn-side chain hampering the approaching of the Cm^{3+} to the two respective acetate arms of the ring. In addition, the energetic cost to rearrange the ring carrying this chain for allowing all acetate arms to point in one direction is increased. The fact that complexation of Cm(III) and formation of one intermediate species occurs readily is hence an argument for twofold coordination of the Cm(III) intermediate.

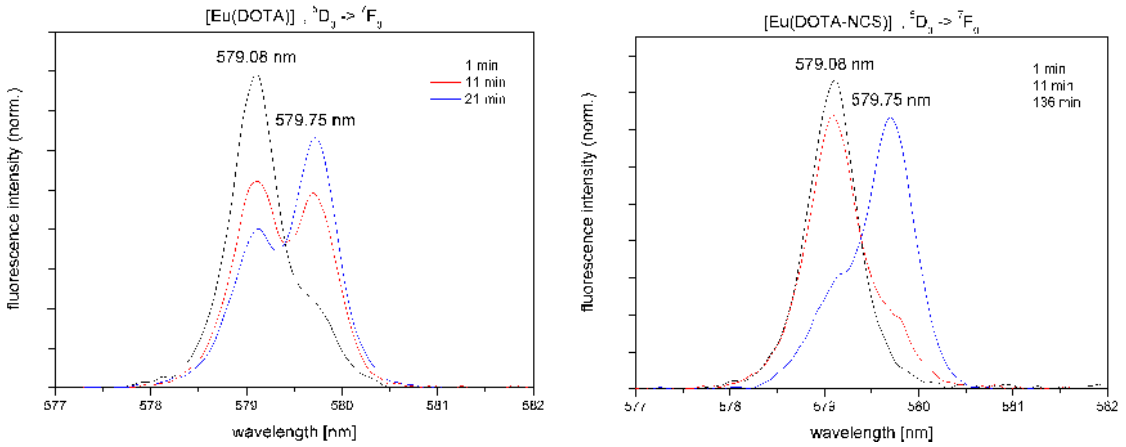

Figure 5.18: Study of the complexation of Eu(III)DOTA *(left)* and Eu(III)DOTA-NCS (*right*) under comparable conditions (Eu:DOTA = 1:1000, pH 3). The emission at 579.1 nm represents the Eu(III) aquo ion, the band at 579.8 nm the final complex.

As the decelerated reaction rates were expected to enable more facile investigation of the rapid transformation of the intermediate species into the final complex, the low-temperature experiment for determination of the fluorescence lifetime of the postulated intermediate Cm(III)-DOTA species (paragraph 5.2.1.4) was repeated with the bifunctionalised ligand (Cm(III) : DOTA-NCS = 1 : 1000). It was possible to slow down the reaction significantly and to obtain emission spectra of only the Cm(III) aquo ion species besides the intermediate species at 598.8 nm straight after mixing of the reactants (Fig. 5.19, *black*), which in the course of the reaction tranformed into the final complex species (608.4 nm, *red*). The minor shoulder at ~602.2 nm is suggestive of the transformation proceeding via the second intermediate species (Fig. 5.14, *right*); however, this spectrum should be considered as an indication rather than a proof for its existence.

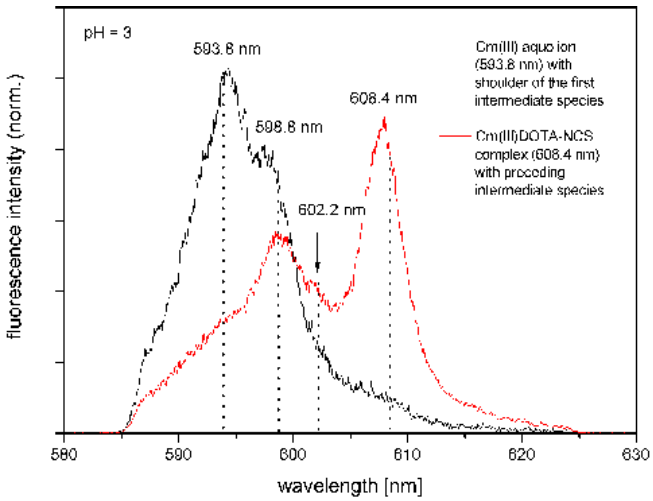

Figure 5.19: Species occuring during the course of the formation of the Cm(III)DOTA-NCS complex, in 0.1 M $NaClO_4$, pH 3.5 - 10 °C.

Complete exclusion of Na^+ from the reaction system by working in $TMAClO_4$ succeeded in a comparatively pure spectrum of the intermediate species of interest at 5 °C (Fig. 5.20), which facilitated a good estimation of the respective fluorescence lifetime. This finding indicates the influence of Na^+ on the M(III)DOTA complexation: in presence of Na^+ the intensity of the emission band of the intermediate complex species (Fig. 5.19) is significantly lower than the intensity of the respective band under sodium-free reaction conditions (Fig. 5.20). It is hence deduced that Na^+ interacts with DOTA, "stealing" free ligand molecules so that not all of DOTA is readily available for the formation of the Cm(III)DOTA-intermediate species. However, since the complex stability of $[Cm(DOTA)]^-$ is expected to be significantly higher than the complex stability of $[Na(DOTA)]^{3-}$ (log K = 4.02 - 4.20 at 25 °C, 0.1 M TMACl [5, 142]), the Cm(III)DOTA complex is still formed quantitatively within reasonable time. In conclusion, the presence of Na^+ in the reaction medium influences the reaction kinetics but not the quantitative formation of the final complex.

Biexponential fitting of the decrease of the fluorescence intensity with the Cm(III) aquo ion being fixed at 65 µs [119] (Fig. 5.20, *right*) revealed a lifetime of τ = 88.2 µs for the first intermediate species at 5 °C. Application of the modified Kimura

equation [125] for low temperatures (reported by Tian et al. [127]) results in almost exactly 7±0.5 H_2O ligands coordinated to Cm^{3+} in this species:

$$Kimura: \quad n(H_2O) = 0.65 \cdot \frac{1}{\tau(ms)} - 0.88 = 6.5 \pm 0.5\ ; \tag{5.2}$$

$$Tian: \quad n(H_2O)_{,(T=10^{\circ}C)} = 0.64 \cdot \frac{1}{\tau(ms)} - 0.3 = 6.9 \pm 0.5\ . \tag{5.3}$$

The biexponential lifetime fit, giving more reliable results than the triexponential fit, substantiates the previous assumption of the Cm(III) being twofold coordinated by DOTA and carrying 7 additional water molecules.

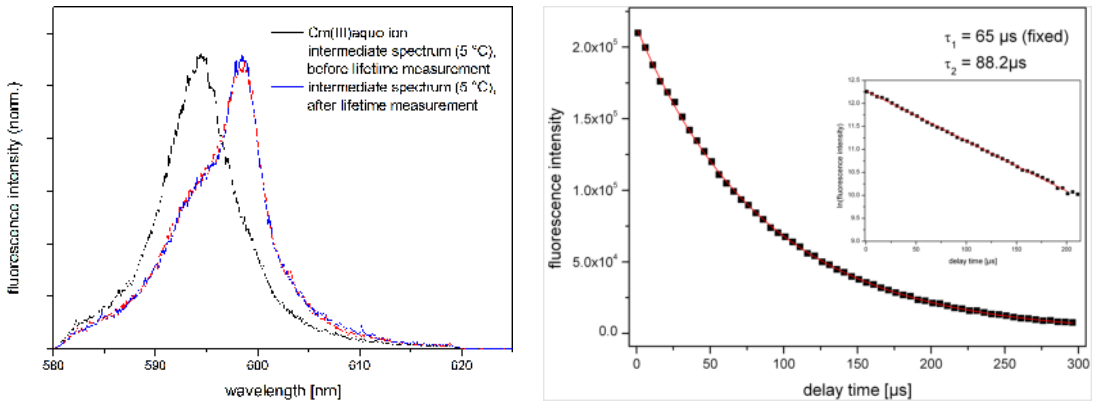

Figure 5.20: *left*: Intermediate species trapped with DOTA-NCS, in $TMAClO_4$, T = 5 °C. The spectra before and after the lifetime measurement are largely identical and hence prove that the reaction was haltet during the experiment. *right*: biexponential fits of the decrease of the flourescence intensity as a function of the delay time.

5.2.1.7 Discussion

The latest result accords with the previous experiments, giving rise to the assumption that the frequently discussed intermediate species occuring during the complexation of trivalent metal cations with DOTA is only coordinated by two of the acetate arms on one side of the DOTA ring. Since it is possible to trap this twofold coordinated intermediate, it is concluded that the rearrangement of the other two arms to the said side of the ring is the rate-determining step of the complexation. Once all four acetate arms are oriented on the same side, the metal cation is fourfold coordinated and very rapidly drawn into the ring to experience full coordination by DOTA. This last step probably happens too fast to be detectable on the TRLFS time-scale.

This sequence is not in exact agreement with the literature on Eu(III)DOTA, where the cation in the first intermediate is described as being already fourfold coordinated [8]. However, with Eu(III) TRLFS no valuable information from characteristic bathochrome shifts of the emission bands is derived, while contrariwise in the case of Cm(III) TRLFS, the position of the emission bands is very sensitive to the coordination state of Cm(III). Thus, the thereof deduced information in combination with τ must be considered as more grave than results gathered solely by analyses

of lifetime measurements, relying on empiric calculations. In direct comparision to the literature for carboxylic acids (Table 5.6), it is apparent that the shift of the emission band of the intermediate complex species to 598.8 nm is a clear argument against fourfold- and in favour of twofold coordination.

In summary, it was possible to successfully characterise all species occuring during the various experiments in terms of fluorescence lifetime and coordination state. The results are summarised in Table 5.8.

Table 5.8: Characteristica of the species occuring in the Cm(III)DOTA/DOTA-NCS system.

Species	λ *[nm]*	τ *[µs]*	$n(H_2O)$ ± 0.5	CN_{DOTA}	*Comment*
$[Cm(H_2O)_9]^{3+}$	593.8	67	8.9	-	
$[Cm(DOTA)(H_2O)]^-$	608.1	278	1.5	8	
$[Cm(DOTA\text{-}NCS)(H_2O)]^-$	608.4	284	1.4	8	
$[Cm(DOTA\text{-}NCS)(H_2O)]_X$-mAb	608.5	312	1.2	8	
Cm(III) intermediate I	598.8	86 - 88	6.7 - 6.9	2	with DOTA, DOTA-NCS
Cm(III) intermediate II	602.3	122	4.5	4	see Eu(III)DOTA [8]

5.2.2 Kinetic Rate of the Complexation at Elevated Temperatures

In general, complex formation rates are influenced not only by the effective ionic radius of the metal ion but also by the rigidity of the binding cavity of the accommodating ligand [273]. Large cations are likely to incorporate more slowely into e.g. DOTA, because the complexation requires reorganisation of the binding cavity.

Working with medical radionuclides requires time-optimised procedures, especially if short-lived radionuclides are employed, since macrocyclic ligands like DOTA are often employed, which warrant high kinetic complex stability. Therefore, protocols for radiolabelling of biomolecules applied in nuclear medicine need to permit facile and rapid synthesis of the therapeutical drug. Hence, optimisation of synthesis protocols in terms of fast reaction process is crucial.

To investigate the pH-dependent formation kinetics of An(III)DOTA, which analogue to Ln(III)DOTA at pH 3 - 5 [164] is expected to be considerably slowed down under acidic conditions, TRLFS measurements were carried out at pH 2.9 in presence of 0.1 M $NaClO_4$. Because the complexation is known to proceeds only very slowly at room temperature, the experiments were conducted at elevated temperatures in the labelling-relevant temperature range up to 90 °C. The results are utilised to define the reaction conditions for the subsequent complexation experiments in the course of this work.

5.2.2.1 The Rate Constants of the Cm(III)DOTA Complex Formation

To investigate the complex formation kinetics, experiments were conducted to determine the rate constants at different temperatures between 25 °C and 93.5 °C (pH 2.9). Samples with various Cm(III):DOTA ratios were prepared as described in paragraph 4.7.2.2. To guarantee even distribution of the reactants in the cuvette, the samples were constantly mixed with a magnetic stir bar. During 1 - 2 hours,

spectra were recorded every minute, immediately starting upon mixing of the reactants. The obtained spectra were subjected to peak-deconvolution and the rate constants k were calculated for each of the respective temperatures.

The complexation of Cm(III) with DOTA is expected to be of first order with respect to both reactants, which results in a total reaction order of two. Since the reaction is known to involve the formation of an intermediate complex species (in the following indicated with asterisk), the equation can be expressed as follows:

$$Cm^{3+} + H_xDOTA^{(4-x)-} \underset{\mathrm{k'_a}}{\overset{\mathrm{k_a}}{\rightleftharpoons}} Cm(H_2DOTA)^{2-*} + (x-2)H^+ \underset{\mathrm{k'_b}}{\overset{\mathrm{k_b}}{\rightleftharpoons}} Cm(DOTA)^- + xH^+ \,. \quad (5.4)$$

This scheme describes a pre-equilibrium between the reactants and the intermediate, for which

$$K = \frac{[Cm(H_2DOTA)^{2-}]^*}{[Cm^{3+}][H_xDOTA^{(4-x)-}]} = \frac{k_a}{k'_a} \quad (5.5)$$

applies.

Assuming that, after an initial period in which the concentration of the intermediate $[Cm(H_2DOTA)^{2-}]^*$ rises from zero, the rates of change of concentration of the intermediate [I] are negligibly small during the major part of the reaction, a quasi-steady-state approximation can be introduced:

$$\frac{d[I]}{dt} = k_a[Cm^{3+}][H_xDOTA^{(4-x)-}] - k'_a[Cm(H_2DOTA)^{2-}]^* - k_b[Cm(H_2DOTA)^{2-}]^* + k'_b\left[Cm(DOTA)^-\right] \approx 0\,. \quad (5.6)$$

Since the complex dissociation step decribed by k'_b is very slow, the last term is insignificant and the equation is rewritten as

$$[Cm(H_2DOTA)^{2-}]^* \approx \frac{k_a[Cm^{3+}][H_xDOTA^{(4-x)-}]}{k'_a + k_b}\,. \quad (5.7)$$

This approximation greatly simplifies the equation for the rate of formation of the product $[CmDOTA]^-$ to

$$\frac{d\,[CmDOTA]^-}{dt} = k_b[Cm(H_2DOTA)^{2-}]^* = \frac{k_b \cdot k_a[Cm^{3+}][H_xDOTA^{(4-x)-}]}{k'_a + k_b}\,, \quad (5.8)$$

$$\nu = k\left[Cm^{3+}\right]\left[H_xDOTA^{(4-x)-}\right], \quad (5.9)$$

with

$$k = \frac{k_b \cdot k_a}{k'_a + k_b}\,. \quad (5.10)$$

To simplify further calculations, the second order rate reaction can be reduced to a pseudo-first order rate equation if the concentration of one of the reactants is so high that it basically remains constant during the course of the reaction. For this simplification to apply, the DOTA ligand is introduced in high excess; hence the concentration of the ligand can be regarded as effectively constant. After inclusion of $\left[H_xDOTA^{(4-x)-}\right]$ in the rate constant, the equation is written as

$$\nu = k'\left[Cm^{3+}\right]\,, \quad (5.11)$$

with

$$k' = k\left[H_xDOTA^{(4-x)-}\right]\,. \quad (5.12)$$

After differentiation the equation can be logarithmised and plotted to obtain the rate constant k' from the slope of the graph:

$$\frac{d\left[Cm^{3+}\right]}{dt} = -k'\left[Cm^{3+}\right] , \tag{5.13}$$

$$ln\left(\frac{\left[Cm^{3+}\right]}{\left[Cm^{3+}\right]_{t=0}}\right) = -k't . \tag{5.14}$$

The pseudo first order fit is, however, only applicable down to an excess of ~100 of one reactant over the other. For the experiments conducted at temperatures higher than 65 °C (ligand excess < 100), a second order rate equation was therefore applied to calculate the k values according to:

$$\frac{d\left[Cm^{3+}\right]}{dt} = -k\left[Cm^{3+}\right]\left[H_xDOTA^{(4-x)-}\right] \tag{5.15}$$

$$ln\left(\frac{\frac{[DOTA]}{[DOTA]_{t=0}}}{\frac{[Cm^{3+}]}{[Cm^{3+}]_{t=0}}}\right) = -\left([DOTA]_{t=0} - \left[Cm^{3+}\right]_{t=0}\right)kt . \tag{5.16}$$

The calculated k values and the respective experimental conditions are displayed in Table 5.9. The coefficient Q_{10} is a measure of the change of rate as a consequence of increasing the temperature by 10 °C and is calculated according to $Q_{10} = \left(\frac{k_2}{k_1}\right)^{10/(T_2-T_1)}$, with $k_2 > k_1$, $T_2 > T_1$. Some of the recorded spectra and corresponding species distributions are exemplarily presented in Figure 5.21. In the spectra recorded at temperatures up to 45 °C, a shoulder at 598.8 nm is observed, corresponding to the emission band of the postulated intermediate species (see paragraph 5.2.1.7). At higher temperatures the intermediate fraction decreases since the conversion into the final complex occurs too rapid for the intermediate species to be detected.

To validate these findings, the experiment was repeated with lower Cm:DOTA ratios in the temperature range of 25 - 55 °C.

Table 5.9: Experimental conditions and respective observed complex formation rates k determined by TRLFS. The pH of all reaction solutions in this experiment was 2.9, I = 0.1 M $NaClO_4$.

Temperature [°C]	*ratio Cm(III) : DOTA*	*Type of fit*	*k [s^{-1}]*	*Q_{10}*
25	1 : 5000	pseudo 1st order	0.9	-
35	1 : 1700	pseudo 1st order	2.8	3.1
45	1 : 600	pseudo 1st order	9.4	3.4
55	1 : 200	pseudo 1st order	29.2	3.1
65	1 : 100	pseudo 1st order	122.2	4.2
75	1 : 50	2nd order	370.2	3.0
85	1 : 10	2nd order	1011.1	2.7
93.5	1 : 5	2nd order	2183.9	2.2
25	1 : 1000	pseudo 1st order	0.8	-
35	1 : 400	pseudo 1st order	2.4	2.7
45	1 : 250	pseudo 1st order	10.0	4.2
55	1 : 100	pseudo 1st order	27.8	2.8

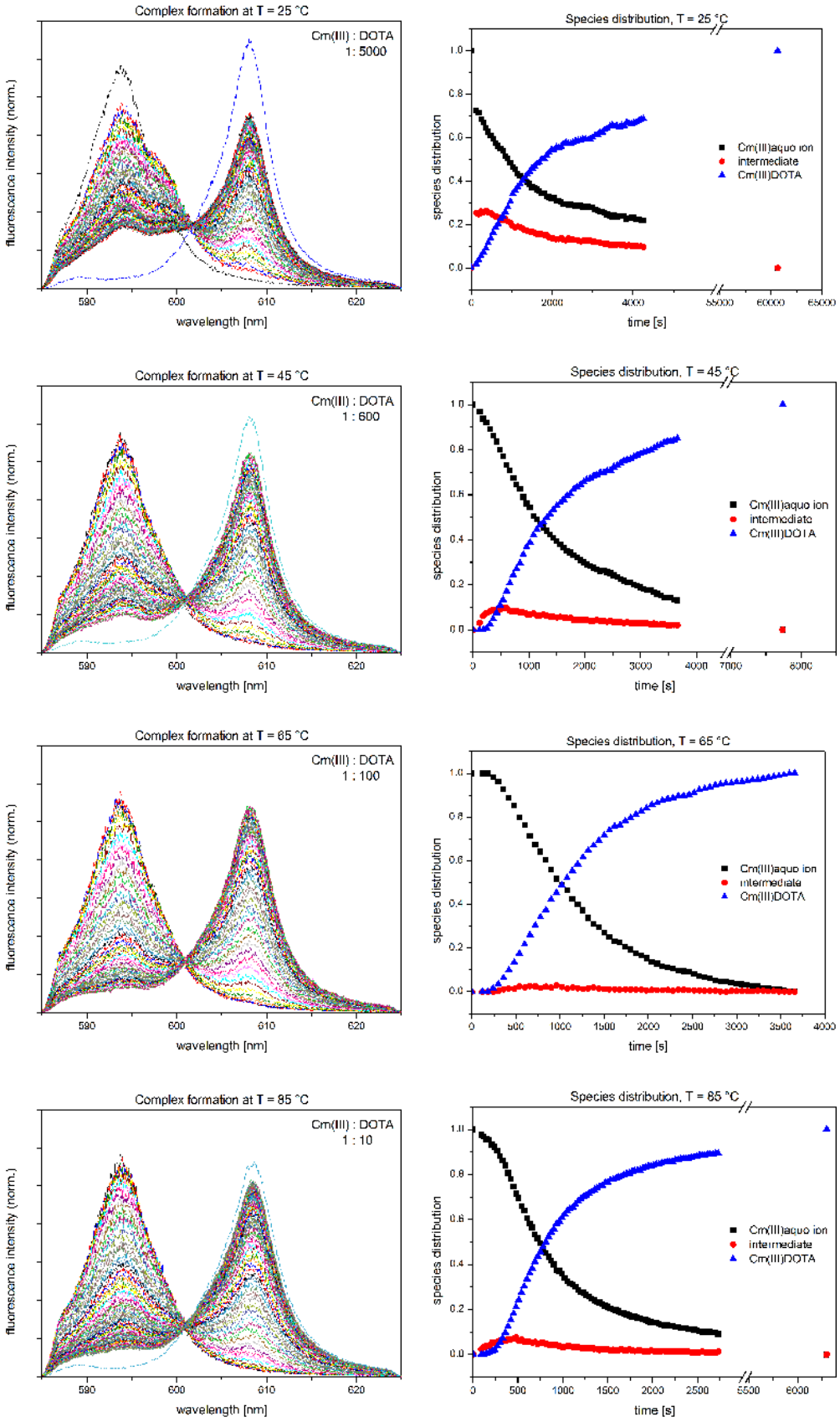

Figure 5.21: *left*: Emission spectra of the transformation of the Cm(III) aquo ion (593.8 nm) via the intermediate species (shoulder at 598.8 nm) into the Cm(III)DOTA complex (608.1 nm) at temperatures of 25, 45, 65 and 85 °C (pH 2.9, 0.1 M $NaClO_4$). *right*: Species distribution of the respective equilibria.

5.2.2.2 Discussion

The obtained rate constants at pH 2.9 (Table 5.9) clearly indicate the accelerating effect of increased temperature on the formation of $[Cm(DOTA)]^-$. In accordance to the empiric RGT rule established by van't Hoff, a temperature increase of 10 °C results in the complexation reaction proceeding approximately 2 - 4 times faster. This is derived from the Q_{10} values, which are associated with the Arrhenius equation (Eq. 5.17). The increased temperatures are expected to induce enhanced flexibility of the DOTA ring. This permits rearrangement of the acetate arms of the ligand in the intermediate species into a position suitable for more rapid incorporation of the metal cation and may be a crucial factor especially with large, discriminating metal cations like Ac^{3+}. This rearrangement is associated with a conformational rearrangement of the cyclododecane ring. For further investigation of the temperature effect on the conformation of the DOTA ring, NMR was chosen as a suitable detection method.

5.2.2.3 Investigation of the Conformational Change of the DOTA Ring at Elevated Temperatures with NMR

It was postulated by McDevitt *et al* that for the formation of highly stable Ac-225-DOTA complexes temperatures of approx. 60 °C are compulsory [6]. This is probably based on the assumption that the ligand flexibility required for rapid and stable complexation is not induced by lower temperatures. However, for radiolabelling of antibodies, temperatures of higher than 42 - 45 °C are not applicable due to denaturation of the biomolecule. It is hence of particular interest to understand if the temperature is the sole driving force for the rearrangement of the ligand. It is expected that the protonation state of the amino groups of the cyclene ring is a regulatory factor hindering (protonated N's) or facilitating (deprotonated N's) conformational changes of the macrocycle. Therefore it is suggested that a combination of both factors, temperature and pH, will allow for enhanced ring flexibility and rapid complexation also at temperatures of $\leq$ 45 °C.

To gain insight into the constitution, conformation and molecular dynamics of a ligand, nuclear magnetic resonance spectroscopy (NMR) in general is an excellent method. Because DOTA is highly symmetric (C4), only two signals with a ratio of 2 : 1 appear in the ^{1}H-NMR spectrum, which are assigned to the 16 chemically equal protons located at the ethylene bridges of the ring (3.1 ppm) and to the 8 chemically equal protons of the acetate arms (3.7 ppm, Fig. 5.22, *left*). Therefore the unsymmetric, bifunctionalised *p*-SCN-Bn-DOTA was chosen for NMR investigations, since it allows for differentiation of the single protons and hence also facilitates determination of the ligand conformation (Fig. 5.22, *right*).

The first spectra of DOTA-NCS were recorded in form of its La(III) complex. The sample with a pH of 9 was subjected to a temperature cycle between 25 and 90 °C. From the recorded spectra it is apparent that at temperatures above 60 °C a change of population of the aromatic signals occurs, eventually resulting in an irreversible extinction of one multiplet at the left end of the spectrum. This was suspected to be either due to chemical transformation of the p-SCN-Bn-chain or attributed to a conformational change of the ligand system. To exclude the former, ESI-TOF-MS spectra were recorded which proved the chemical integrity of the La(III)DOTA-NCS complex; hence, the changes in the spectra are likely to be the effect of an altered ligand conformation.

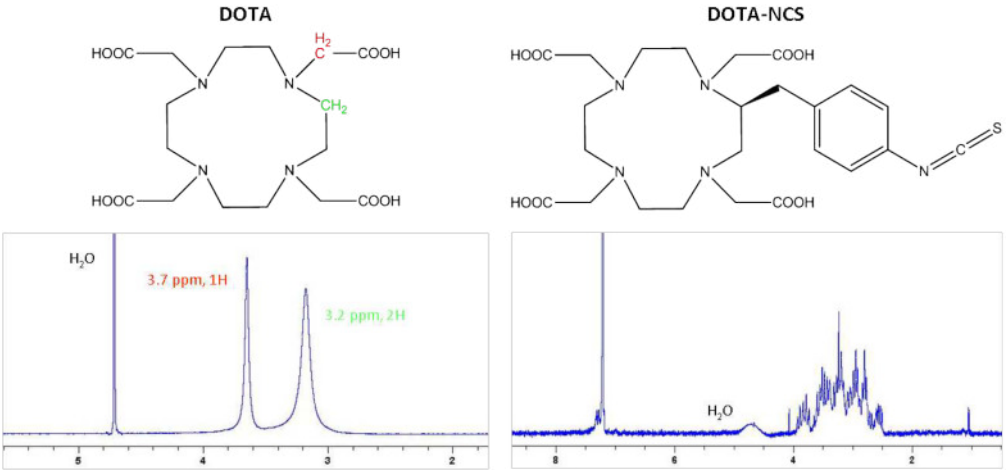

Figure 5.22: ^{1}H-NMR spectra of DOTA (*left*) and *p*-SCN-Bn-DOTA ("DOTA-NCS" , *right*)

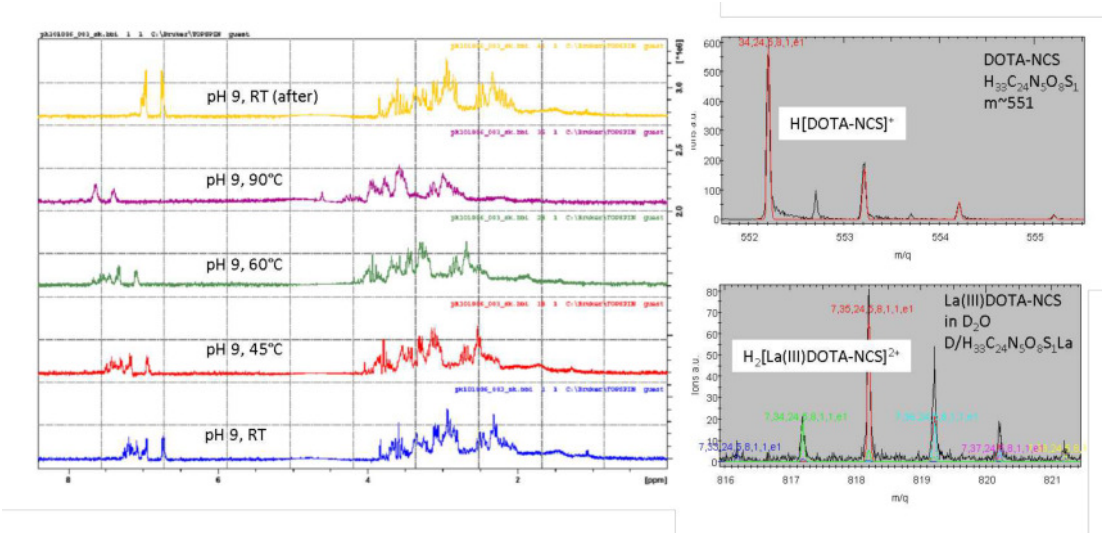

Figure 5.23: ^{1}H-NMR- (*left*) and ESI-TOF-MS- spectrum (*right*) of La(III)DOTA-NCS

Further investigations were made to describe the influence of pH and temperature on these conformational change. Samples of DOTA-NCS were prepared at pH 3, 5.5 and 9 and each of them was processed in a temperature cycle between 25 and 90 °C. The spectra are shown in Figure 5.24.

5.2.2.4 Discussion

Mainly, at all pH values an irreversible change of population of the aromatic signals occured at temperatures above 60 °C, which indicates induction of a change of orientation of the aromatic ring. The effect is particularly pronounced at alcalic pH 9, where all dissociable protons are lost and the ring-nitrogens are more flexibile. The change in the aromatic signals and hence in the orientation of the aromatic ring is a direct effect of the change of ring conformation of the cyclene skeleton. A change of chair- to boat conformation or vice versa will consequently result in a turn of large side chains into energetically more favourable positions, e.g. from axial to equatorial orientation. This is suspected to be the case for the *p*-SCN-Bn side chain of DOTA at elevated temperatures. The reason for the irreversibility for this conformational

change is not only the regained rigidity of the molecule when it is cooled down to room temperature but also the general energetic benefit of orientation of large and bulky ring-substituents into equatorial position.

The *p*-SCN-Bn-chain is expanded but not bulky enough to have this reorientation into equatorial position as a driving force at RT. On the contrary, very bulky and extremely large side chains could function as a lever to force the DOTA ring into a conformation which allows them to adopt equatorial orientation relative to the ring, also at lower temperatures. This would then result in the actetate arms of DOTA being forced to be oriented all on one side of the ring, which concurrently facilitates more rapid complexation of metal cations.

This concept of pre-arrangement of the ring to lower the total energy barrier of complexation, and to thereby potentially increase the formation rate, was proven for the DOTA- derivative CHX-DOTA (2-(p-isothiocyanatobenzyl)-5,6-trans-cyclohexano-DOTA, [257]). In this case, the inclusion of a trans-cyclohexyl ring into the backbone structure of p-NCS-Bn-DOTA adds additional rigidity to the ring and also enhances the pre-organisation geometry of the metal binding orbitals of the tertiary amines. Like this, improved formation kinetics were found due to elimination of energy costs associated with the complexation. This complies with the results of the kinetic investigations of Cm(III) with DOTA, DOTA-NCS and temperature-processed DOTA-NCS accomplished with TRLFS in the present work; this is discussed in more detail in paragraph 5.2.2.5. Here it is proven that processed, and thus probably pre-oriented DOTA-NCS shows faster reaction rates than DOTA, while contrarily the rigid, unprocessed DOTA-NCS shows the slowest reaction rates.

The described effect is a possible explanation for the Ac-225-labelling of the DOTA-chelated antibody also working at temperatures below 60 °C, namely at 37 - 45 °C. The extremely large "*p*-SCN-Bn-antibody" -side chain is most likely always oriented equatorial to the DOTA ring, which allows for the coordinating acetate arms to pre-orientate themselves all into a position suitable for effective complexation of Ac-225. Like that, no thermal energy is required to overcome the energetic barrier for reorientation of the ring system; thus, "low-temperature" labelling of DOTA-antibodies can be readily conducted.

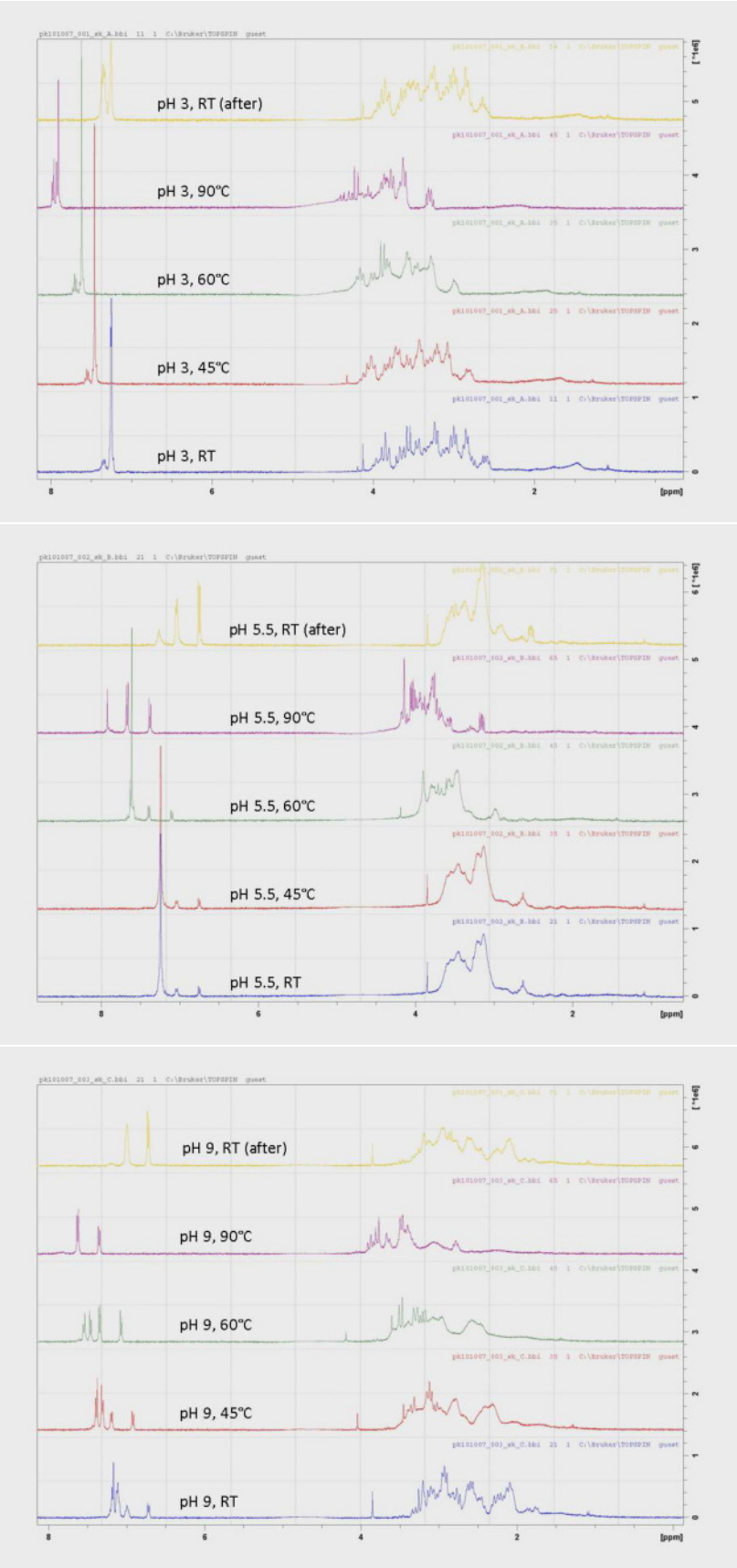

Figure 5.24: ^{1}H-NMR spectra of the temperature cycle with DOTA-NCA at pH 3, 5.5 and 9.

5.2.2.5 Influence of Structural Rearrangement of DOTA-NCS on the Reaction Kinetics

To substantiate the conclusions drawn from the NMR measurements of DOTA-NCS at elevated temperatures, the kinetic experiment previously conducted with DOTA at 25 °C was repeated with the sterically more demanding *p*-SCN-Bn-DOTA under identical reaction conditions. It is expected that, if a persistent structural rearrangent of the ring occurs by temperature, the reaction rate of DOTA-NCS at elevated temperatures will closely match the rate observed with DOTA. At lower temperatures (25 °C) the complexation with DOTA-NCS should proceed significantly slower than with DOTA, resulting from hindered conformational fluctuation. Furthermore, if the "high-temperature" conformation of the DOTA ring is retained upon cooling to room temperature, then the complexation rates with temperature-processed DOTA-NCS should be increased compared to unprocessed DOTA-NCS and hence give strong evidence for the confomational change of DOTA.

The samples containing $1{\cdot}10^{-7}$ M Cm(III) and a 1000-fold excess of DOTA or DOTA-NCS were prepared as described in paragraph 4.7.2.2. The samples with temperature-processed DOTA-NCS were prepared identically, employing DOTA-NCS which has previously been heated to 90 °C for 24 h. The processed ligand was allowed to cool to room temperature for two hours before it was applied to the reaction solution.

To compare the reaction kinetics at 25 °C, spectra were recorded every minute during the first 45 min after mixing of the reactants. The spectra were subjected to peak-deconvolution and the obtained species distribution was employed for calculation of the rate constants. In Figure 5.25, the ratio of coordinated Cm(III) is plotted as a function of the reaction time.

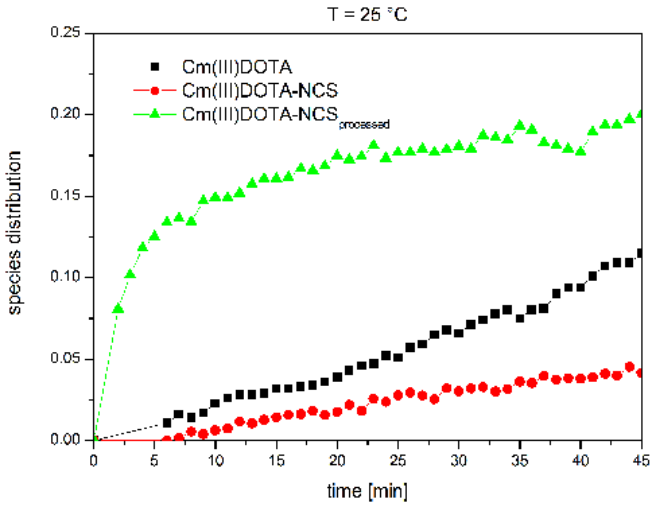

Figure 5.25: Comparison of the reaction kinetics of the complexation of $1{\cdot}10^{-7}$ M Cm(III) with $1{\cdot}10^{-4}$ M DOTA (*black*), DOTA-NCS (*red*) and temperature-processed DOTA-NCS (*green*) at 25 °C, I = 0.1 M $NaClO_4$, pH 2.9.

The obtained species distributions clearly show, that the complexation of Cm(III) with processed DOTA-NCS (*green*) is significantly accelerated compared to unprocessed DOTA-NCS, which suffers from sterical hinderance induced by the probably axial oriented linker (*red*). Despite the linker, at the start the formation rates of processed DOTA-NCS even exceeds the rates observed with DOTA (*black*). This

confirms the initial assumption that by heating to 90 °C a persistent change in the ligand conformation occurs, in which the linker is oriented in equatorial position and all acetate arms are oriented towards one side of the ring. This finding represents an important fact approving the results gained by NMR.

To quantitatively compare the kinetics of the Cm(III) complexation with DOTA, DOTA-NCS and processed DOTA-NCS, further measurements at 30, 45, 60, 75 and 90 °C were conducted. Sample preparation and experimental conditions are described in paragraph 4.7.2.2. The employed metal:ligand ratios as well as the obtained rate contants k are listed in Table 5.10. The spectra were recorded every minute over a period of up to 31 min. The corresponding species distributions and representative spectra are presented in Figure 5.26. The emission band at 593.8 nm represents the Cm(III) aquo ion, the band at 598.8 nm the intermediate species and the band at 608.1 nm the final complex. It is noticeable that with processed DOTA-NCS the formation of the final complex starts immediately, resulting in 15 % complex species after 2 min (*bottom right, red*).

Table 5.10: Experimental conditions and respective rate constants k (pseudo 1st order) for the comparative experiments with DOTA, DOTA-NCS and processed pDOTA-NCS (pH 2.9, I = 0.1 M $NaClO_4$). The factor f is the quotient of the reaction rates of DOTA and DOTA-NCS/processed pDOTA-NCS.

Temp. ***[°C]***	***ratio Cm(III) : ligand***	***DOTA*** ***k [s⁻¹]***	***DOTA-NCS*** ***k [s⁻¹]***	***pDOTA-NCS*** ***k [s⁻¹]***	***f***
30	1 : 2000	2.5	0.15	0.5	5 - 16
45	1 : 1000	19	5	5	3.8
60	1 : 500	122	48	44	2.7
75	1 : 250	572	228	224	2.5
90	1 : 100	1080	810	600	1.5 - 1.8

5.2.2.6 Discussion

From comparision of the species distributions at the various temperatures it is derived that the rate constants of DOTA and DOTA-NCS / processed DOTA-NCS at temperatures above 60 °C become more and more similar. Unlike DOTA or DOTA-NCS, significant amounts of complex are formed with processed DOTA-NCS shortly after mixing of the reactants (*green*), which is a result of the favourable temperature-induced preorganisation of the ligand. At higher temperatures this effect is less pronounced, since the reaction system offers sufficient energy for the unprocessed ligands to also adopt this favourable conformation. This accords to the conformational rearrangement observed in the NMR study with DOTA-NCS and is hence a clear indication for conformational change of the ring occuring at temperatures $\geq$ 60 °C.

In summary, it was shown that, besides the increased concentration of the reactive fully deprotonated ligand species when working at alkaline conditions (paragraph 5.1.4), rapid complexation and hence rapid radiolabelling of DOTA-NCS-mAb is highly dependent on the conformation of the cyclene backbone of DOTA/DOTA-NCS and hence the pre-orientation of the acetate arms. The most suitable conformation has all acetate arms on one side of the ring which is presumably enforced

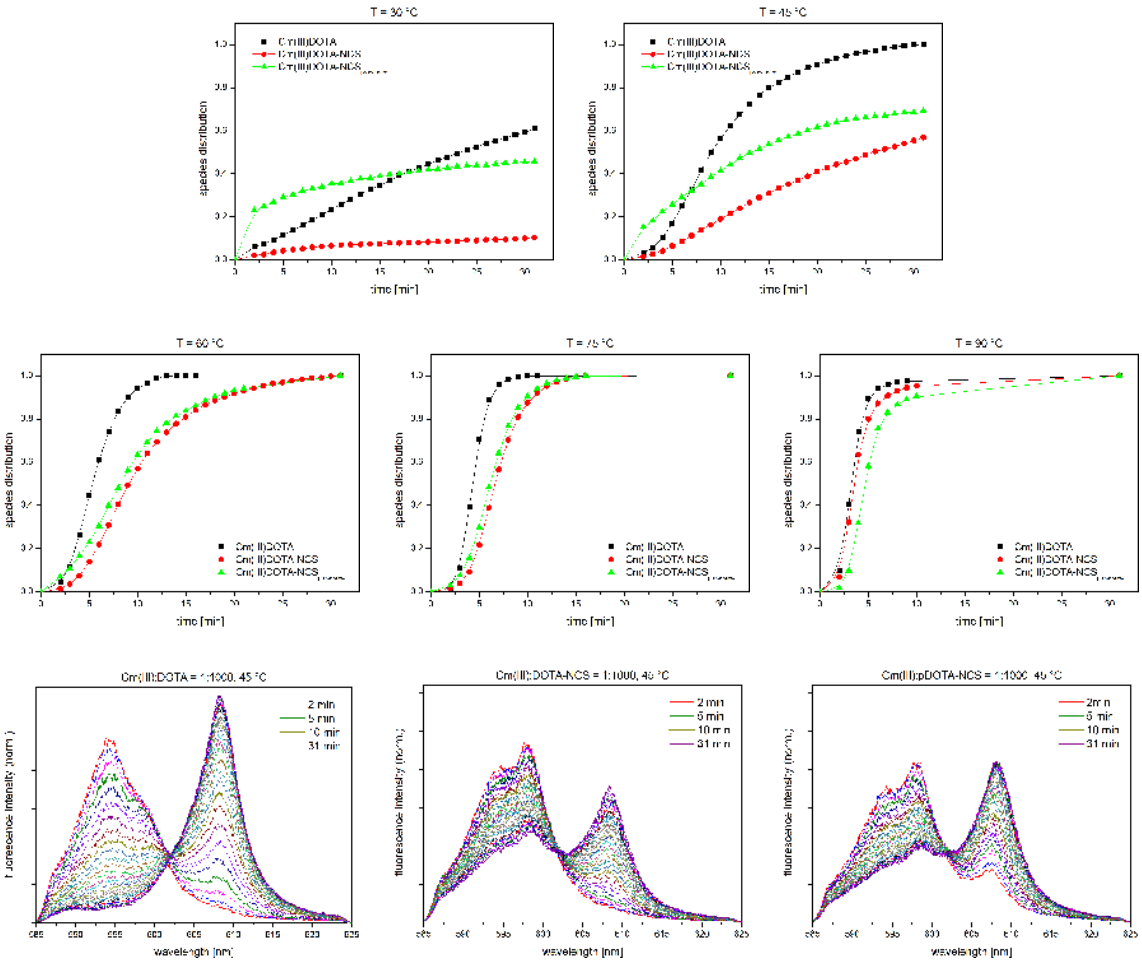

Figure 5.26: *top and middle*: Species distributions of the complexation of $1 \cdot 10^{-7}$ M Cm(III) with DOTA (*black*), DOTA-NCS (*red*) and temperature processed pDOTA-NCS (*green*) at pH 2.9. *bottom*: representative emission spectra for the experiments at 45 °C.

by energetically favourable equatorial orientation of the large p-SCN-Bn side chain induced by temperature or steric factors.

5.2.2.7 The Rate Constants of the Cm(III)DOTA-NCS Complex Formation

To quantify the reaction kinetics of the Cm(III)DOTA-NCS complex formation, the experiments discussed in 5.2.2.1 were repeated with DOTA-NCS in the temperature range of 25 - 55 °C. Samples with various Cm(III):ligand ratios were prepared as described in paragraph 4.7.2.2. During the experiment, the samples were constantly mixed with a magnetic stir bar. Initially spectra were recorded every minute, starting from the moment the reactants were in first contact.

Due to the slow progress of the complexation, measurements were conducted intermittently over a period of up to 8 days. The obtained spectra were subjected to peak-deconvolution and the rate constants k were calculated for each of the respective temperatures. The calculated values and respective experimental conditions are displayed in Table 5.11. The spectra and corresponding species distributions are uniform to those presented in Figure 5.21 and are therefore not shown.

Table 5.11: Experimental conditions and respective calculated rate constants k (pseudo 1st order) for the complexation of $1{\cdot}10^{-7}$M Cm(III) with DOTA-NCS (pH 2.9, I = 0.1 M $NaClO_4$). The value in brackets corresponds to an experiment conducted identically with processed DOTA-NCS.

Temperature [°C]	*ratio Cm(III) : DOTA-NCS*	*Type of fit*	*k [s^{-1}]*
25	1 : 1000	pseudo 1st order	0.1 (0.6)
35	1 : 400	pseudo 1st order	0.9
45	1 : 250	pseudo 1st order	6
55	1 : 100	pseudo 1st order	25.5

5.2.2.8 Discussion

As expected, the rate constants k for the complexation of Cm(III) with DOTANCS are smaller than for the reaction with DOTA, indicating that the complexation and probably the required conformational rearrangement is hindered. This reflects the influence of the sterically demanding *p*-SCN-Bn side chain, which, when oriented in axial position, shields one side of the DOTA ring. At the same time the rotation barrier for rearrangement of the cycldododecane ring may be increased. Once the side chain is oriented into equatorial position, which results in all four acetate arms being oriented towards the same side of the ring, the complexation will proceed readily. To quantitatively express the difference in the rate constants of DOTA and DOTA-NCS/processed DOTA-NCS, the activation energy of the two systems must be compared.

5.2.2.9 The Arrhenius Parameters: Activation Energy, Frequency Factor A

The Arrhenius equation links the kinetic rate constants to the activation energy, which needs to be overcome to allow the reaction to proceed readily. The corresponding Arrhenius diagram displays the natural logarithm of the kinetic rate constants ($\ln(k)$) plotted against the respective inverse temperatures ($1/T$ [1/K]). For a single, thermally activated process, an Arrhenius plot results in a straight line, from which the activation energy E_a of the reaction and the pre-exponential factor A can be determined [274]. The activation energy reflects the energy needed to induce the inversion of the cyclene ring, while A describes the frequency of collisions between the reacting particles.

The Arrhenius equation

$$k = Ae^{-\frac{E_a}{RT}} \tag{5.17}$$

is logarithmised and written as

$$ln(k) = ln(A) - \frac{E_a}{R}\left(\frac{1}{T}\right) \tag{5.18}$$

where k is the rate constant, T the absolute temperature and R the universal gas constant. When plotted as described above, $ln(A)$ is represented by the y-intercept, while the slope of the line equals $-\frac{E_a}{R}$.

The Arrhenius plots based on k (from Tables 5.9, 5.10, 5.11) and a list of the obtained Arrhenius parameters for the respective Cm(III)DOTA and Cm(III)DOTA-NCS systems are shown below (Fig. 5.27).

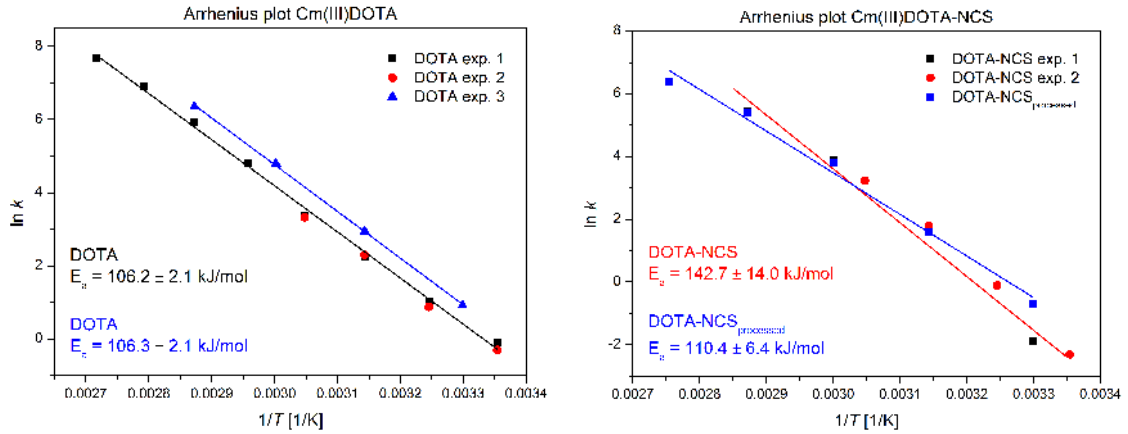

Ligand	*ln (A)*	*A [1/s]*	*E_a[kJ/mol]*
DOTA	42.54	$3{\cdot}10^{18}$	106.2±2.1
	43.14	$5{\cdot}10^{18}$	106.3±2.1
DOTA-NCS	55.09	$8{\cdot}10^{23}$	142.7±14.0
	58.71	$3{\cdot}10^{25}$	150.9±6.7
pDOTA-NCS	43.33	$7{\cdot}10^{18}$	110.4±6.4

Figure 5.27: Arrhenius plots of the determined rate constants k and activation energy E_a. The ln k is plotted as a function of 1/T [K]; the results are summarised in the table above. *left*: plot for Cm(III)DOTA, T = 25 - 93.5 °C; *right*: plot for Cm(III) with DOTA-NCS (*red*) and processed pDOTA-NCS (*blue*), T = 25 - 90 °C.

From comparison of E_a it is apparent that processed DOTA-NCS (E_a =110.4 kJ/mol) has an activation barrier very similar to that of DOTA (E_a =106.3 kJ/mol), while the activation energy of unprocessed DOTA-NCS was determined to be E_a = 143 - 151 kJ/mol. This indicates that by heating of DOTA-NCS a structural rearangement was induced which lowers the activation barrier and allows the otherwise rigidified DOTA-NCS ligand to behave more "DOTA-like" in terms of more rapid complexation.

5.2.2.10 The Eyring-Polanyi Equation: Activation Enthalpy and Entropy

The Eyring-Polanyi equation can be transformed in a way to determine thermodynamic parameters such as the enthalpy and entropy of activation, which are comparable to the Arrhenius parameters [274].

The general form of the equation resembles the Arrhenius equation:

$$k = \frac{k_B T}{h} e^{-\frac{\Delta G^{\ddagger}}{RT}} \quad . \tag{5.19}$$

In this equation, $\Delta_R G^{\ddagger}$ is the Gibbs free enthalpy of activation, k_B is Boltzmann's constant and h is Planck's constant. With $\Delta_R G^{\ddagger}$, the equation is transformed into:

$$k = \left(\frac{k_B T}{h}\right) exp\left(\frac{\Delta S^{\ddagger}}{R}\right) exp\left(\frac{\Delta H^{\ddagger}}{RT}\right) \quad . \tag{5.20}$$

The linear form of the Eyring-Polanyi equation is represented by

$$ln\frac{k}{T} = -\frac{\Delta H^{\ddagger}}{R} \cdot \frac{1}{T} + ln\frac{k_B}{h} + \frac{\Delta S^{\ddagger}}{R} \quad , \tag{5.21}$$

where k is the experimentally determined rate constant and T the respective absolute temperature.$\Delta_R H^{\ddagger}$ and $\Delta_R S^{\ddagger}$ are the enthalpy and entropy of activation to be determined.

A plot of $ln\frac{k}{T}$ versus $\frac{1}{T}$ results in a straight line with the slope $-\frac{\Delta H^{\ddagger}}{R}$ from which the enthalpy of activation is derived, while from the y-intercept $ln\left(\frac{k_B}{h}\right) + \frac{\Delta S^{\ddagger}}{R}$ the entropy of activation is obtained. The enthalpy of activation is directly linked with the activation energy according to Arrhenius' $E_a = \Delta_R H^{\ddagger} + RT$, with RT at room temperature beeing approximately 2.5 kJ/mol. The results of the calculations based on k (from Tables 5.9, 5.10, 5.11) are presented in Figure 5.28.

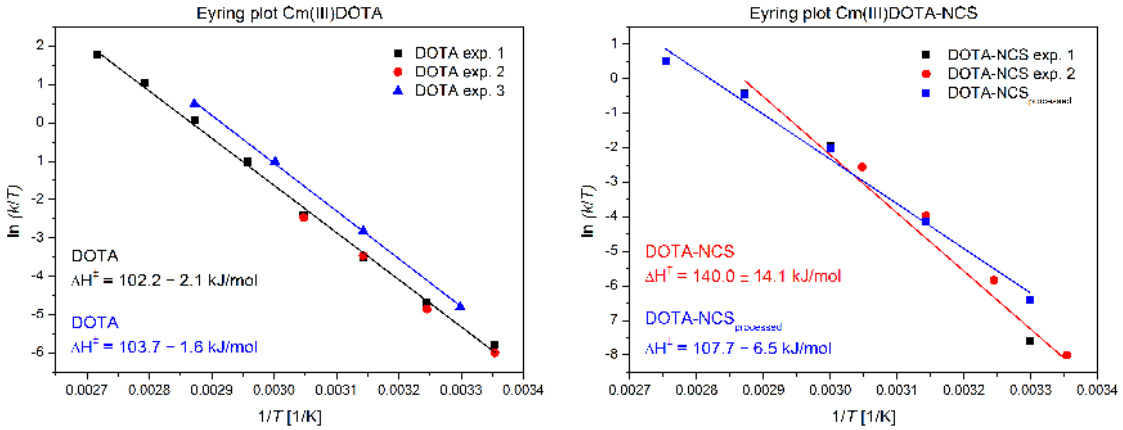

Ligand	$\Delta_R H^{\ddagger}$ ***(from graph)*** ***[kJ/mol]***	$\Delta_R H^{\ddagger}$ ***(calc. from Ea)*** ***[kJ/mol]***	$\Delta_R S^{\ddagger}$ ***[J·mol·K^{-1}]***	$\Delta_R G^{\ddagger}_{25°C}$ ***[kJ/mol]***
DOTA	102.2±2.1	103.7±2.1	95.62	73.69
	103.7±1.6	103.8±2.1	104.68	72.49
DOTA-NCS	140.0±14.1	140.2±14.0	204.11	79.14
	148.4±6.7	148.4±6.7	234.46	78.50
pDOTA-NCS	107.7±6.5	107.9±6.4	106.09	76.07

Figure 5.28: *graphs*: Eyring plot of the determined rate constants k and calculated enthalpy of activation. The ln (k/T) is plotted as a function of 1/T [K]. *left*: plot for Cm(III)DOTA, T = 25 - 93.5 °C; *right*: plot for Cm(III)DOTA-NCS, T = 25 - 90 °C. *table*: calculated activation parameters

5.2.2.11 Discussion

The activation enthalpies determined from the Eyring plot and the Arrhenius' E_a relation are in excellent agreement. From comparison of $\Delta_R H$ for the complexation of Cm(III) by DOTA and DOTA-NCS, a signifcant difference of roughly 40 kJ/mol is observed, with processed DOTA-NCS having an activation enthalpy similar to DOTA. From the lower $\Delta_R H$ it can be concluded that the conformation of DOTA as well as of processed DOTA-NCS must be more favourable than the conformation of the unprocessed DOTA-NCS. This is in agreement with the findings from the previous investigations (paragraph 5.2.2.3-5.2.2.7).

This proves that ligand bifunctionalisation can not only influence the reaction kinetics negatively (e.g. DOTA-NCS), but can result in increased kinetic rates if the

sterically demanding side chains are oriented in energetically favourable positions, forcing the ligand to rearrange beneficially (processed DOTA-NCS). As mentioned previously, this effect is suggested to allow the one-step radiolabelling of DOTA-NCS-antibodies to rapidly take place despite rather low temperatures (45 °C).

5.2.2.12 Consideration for Further Experiments

With respect to the following experiments, the findings from the kinetic studies facilitate estimation of the reaction time which is required to thoroughly establish thermodynamic equilibrium at the respective reaction conditions (temperature, metal ion-to-ligand ratio). It is concluded that heating is required for effective complexation within a reasonable time.

As expected, the highest rate constants were observed at T = 93.5 °C. Here, with a Cm(III):DOTA ratio of 1 : 5, corresponding to $1 \cdot 10^{-7}$ M Cm(III) and $5 \cdot 10^{-7}$ M DOTA, the reaction took 45 min to achieve 90 % conversion. In further experiments it was found that with a ratio of 1 : 4 a heating period of 4 h (T = 90 °C) leads to satisfactory conversion (Fig. 5.29). It is hence deducted that, with a lower ratio of Cm(III):DOTA = $1 \cdot 10^{-7}$: $3 \cdot 10^{-7}$ M, heating to 90 °C for 24 h is sufficient for the reaction to reach full conversion. Heating to 90 °C for longer than 48 h was found to lead to dissociation of the Cm(III)DOTA complex; a reason for this may be degradation of the ligand.

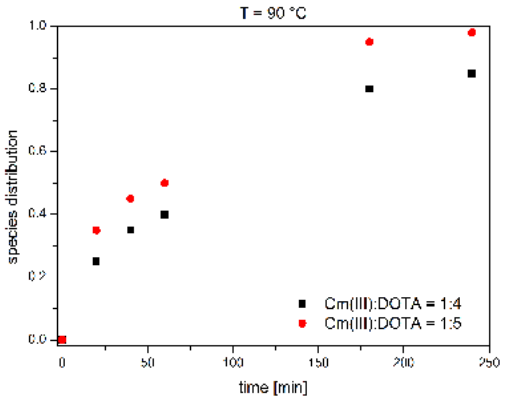

Figure 5.29: Complex formation of $1 \cdot 10^{-7}$ M Cm with DOTA at 90°C, I = 0.1 M $NaClO_4$. The black and red symbols mark the conversion with time for Cm(III):DOTA ratios of 1 : 4 and 1 : 5, respectively.

For experiments at temperatures below 90 °C, the metal ion:ligand ratio as well as the duration of the heating procedure must be reasonably adapted. The selected conditions for the subsequent experiments to determine the thermodynamic properties of the Cm(III)DOTA system are summarised in Table 5.12. All samples were chosen to be heated for 24 h or up to 3 days in case of the experiment at 70 °C, respectively, as it has been reported by Wu and Horrocks [9]. After 40 h of heating, exemplary samples of each temperature batch were remeasured to ensure that equilibrium was attained after 24 h.

5.2.3 Thermodynamic Stability of Cm(III)DOTA at Elevated Temperatures

As shown in the previous chapter, the formation of M(III)DOTA complexes at room temperature exhibits only small rate constants and is known to be very slow

Table 5.12: Experimental conditions selected for the experiments to determine the complex stability constant of Cm(III)DOTA with TRLFS in the temperature range of 45 - 90 °C (c(Cm(III) = $1 \cdot 10^{-7}$ M, I = 0.1 M $NaClO_4$).

Temperature	*Cm(III):DOTA*	*heating period*
45 °C	1 : 50	24 h
60 °C	1 : 5	24 h
70 °C	1 : 3	72 h
80 °C	1 : 3	24 h
90 °C	1 : 3	24 h

when metal ion and ligand are employed in equal concentrations (> 800 days for Eu(III)DOTA, Eu(III):DOTA = 1 : 1 [9]). Thus, the following experiments were accomplished at elevated temperatures and with higher metal ion-to-ligand ratios.

With view to the radiolabellings of antibodies and peptides, temperatures of 45, 60 and 90 °C are of particular interest to understand and compare the thermodynamic stability of the complexes formed when using the established labelling protocols. Therefore the stability constants log K for Cm(III)DOTA, and later also for Ac(III)DOTA, were determined in the range of 45 - 90 °C. From the data obtained at elevated temperatures, the complex stability constant at 25 °C were extrapolated using the van't Hoff equation.

5.2.3.1 Determination of the Thermodynamic Stability Constant: The Relevance of pH for Reactions with DOTA

Since DOTA has four dissociable protons, four possibly reactive ligand species are generated upon stepwise deprotonation. The pH dependence of this speciation can be exploited to adjust the concentration of the most reactive ligand species (see paragraph 3.5.3.1 and Fig. 3.4). For strong chelating ligands like DOTA, which have high stability constants in complexes with M(III) [5], the only way to determine accurate complex stability constants is by introducing the reactive ligand species in very low concentrations (c = 10^{-20} - 10^{-30} M). At the same time, the total concentration of the ligand needs to be sufficiently high for enough free ligand to be present in the reaction solution. However, too high concentrations of the reactive $DOTA^{4-}$ would lead to immediate full conversion of M(III), which would hence prevent determination of $[M(III)_{free}]$ required to calculate K.

Introduction of low concentrations of $DOTA^{4-}$ is feasible by adjustment of the pH to the acid range (2 - 4). With the experimentally obtained species distribution at various pH, the conditional stability constant (valid for I = 0.1 M $NaClO_4$) for the Cm(III)DOTA complexation is calculated using the following equations:

$$Cm^{3+} + \left[DOTA^{4-}\right] \rightleftharpoons [CmDOTA]^{-} \quad with \quad K = \frac{\left[[CmDOTA]^{-}\right]}{[Cm^{3+}]\,[DOTA^{4-}]}\,, \tag{5.22}$$

$$log\,K = log\left(\frac{\left[[CmDOTA]^{-}\right]}{[Cm^{3+}]}\right) - log\left[DOTA^{4-}\right]_{free}\,. \tag{5.23}$$

Since in the present work all studies are conducted in presence of Na^{+} deriving from the background electrolyte $NaClO_4$, the formation of the Na(I)DOTA complex

has to be taken into account. This is done by inclusion of Na(I)DOTA into the DOTA speciation according to:

$$[DOTA^{4-}]_{free} = \left([DOTA]_{tot} - \left[[CmDOTA]^{-}\right]\right) \cdot X_4 \,, \tag{5.24}$$

$$with \quad X_4 = \frac{\beta_4}{[H^+]^4 + \beta_1 [H^+]^3 + \beta_2 [H^+]^2 + \beta_3 [H^+] + \beta_4 + \beta_4 K_{NaDOTA^{3-}} \cdot [Na^+]} \,, \tag{5.25}$$

$$K_{NaDOTA^{3-}} = \frac{\left[[NaDOTA]^{3-}\right]}{[Na^+]\,[DOTA^{4-}]} \,. \tag{5.26}$$

Here, β_n represent the respective relevant (sodium-independent) protonation constants determined in the present work (paragraph 5.1.). For detailed derivation of Eq. 5.24 see Appendix 7.1.

5.2.3.2 Determination of the Stability Constants of [CmDOTA]$^-$ at Elevated Temperatures (45 - 90 °C)

For determination of the log K for Cm(III)DOTA at various temperatures, samples with fixed Cm(III):DOTA ratios were prepared as described in paragraph 4.7.2.3 (see Table 5.12). Because due to the slow kinetics pH titration cannot be performed within reasonable time, the experiments were conducted according to the batch-method. One consistent sample was prepared for each investigated pH value in the range where complex formation is ongoing but not complete [161].

The samples of each batch were prepared as described in paragraph 4.7.2.3 and heated simultaneously at the respective temperature (see Table 5.12). The fluorescence spectra were recorded at the same temperatures without previous cooling of the samples. One representative set of spectra is presented in Figure 5.30; here, the emission band at 593.8 nm respresents the Cm(III) aquo ion and the band at 608.1 nm the Cm(III)DOTA complex. The presence of one isosbestic point at ~602 nm indicates that only these two emitting species are present.

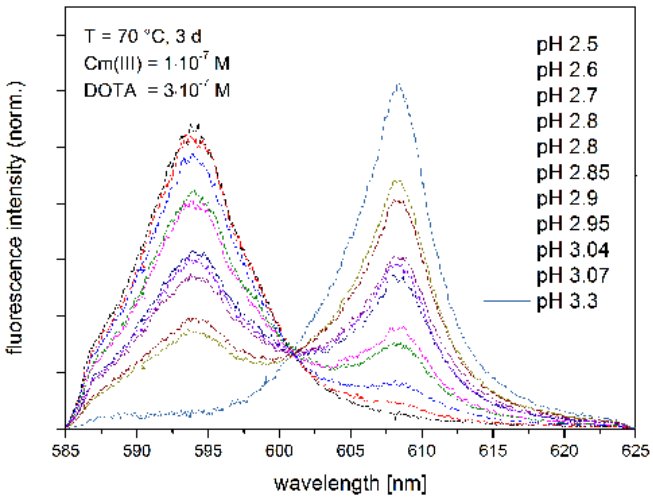

Figure 5.30: Emission spectra for the batch experiment conducted at 70 °C (c(Cm(III) = $1{\cdot}10^{-7}$, c(DOTA) = $3{\cdot}10^{-7}$, I = 0.1 M $NaClO_4$).

The recorded spectra were subjected to peak-deconvolution. The obtained species distributions and corresponding slope analyses for the respective temperatures are

displayed in Figure 5.31. For the latter, a linear curve of log (bound/free Cm(III)) vs log $[DOTA^{4-}]_{free}$ with the slope of 1 indicates the presence of a 1 : 1 complex, while a nonlinear curve would indicate formation of more than one complex [126]. From y = 0 the approximate log K values can be read.

The log K values determined according to Eq. 5.23 are listed in Table 5.13. There is a noticable trend in the determined stability constants, with their values increasing with increasing temperature. The calculated log K are afflicted with an experimental error of ± 0.4 units. This error derives from an assumed uncertainty of ± 0.05 for the pH measurements and has large influence on the calculated concentration of free $DOTA^{4-}$. This error is superior over the inaccuracy of 10 % which is commonly accepted for the peak deconvoloution.

Table 5.13: Experimentally determined log K for Cm(III)DOTA at 45 - 90 °C in NaClO4 and under sodium-free conditions, respectively, in comparison to published stability constants for Eu(III)DOTA.

Conditions (0.1 M)	***slope***	***log K (+/- 0.4)***	***Ref. Eu(III)DOTA***
45 °C, $NaClO_4$	0.92	19.6	
60 °C, $NaClO_4$	0.98	20.0	
70 °C, $NaClO_4$	0.98	20.5	
80 °C, $NaClO_4$	0.83	20.3	
90 °C, $NaClO_4$	0.79	20.9	
45 °C, "Na-free"	0.92	22.6	
60 °C, "Na-free"	0.98	22.9	23.5 [275]
70 °C, "Na-free"	0.98	23.3	26.2 [9]
80 °C, "Na-free"	0.83	23.2	
90 °C, "Na-free"	0.79	23.7	

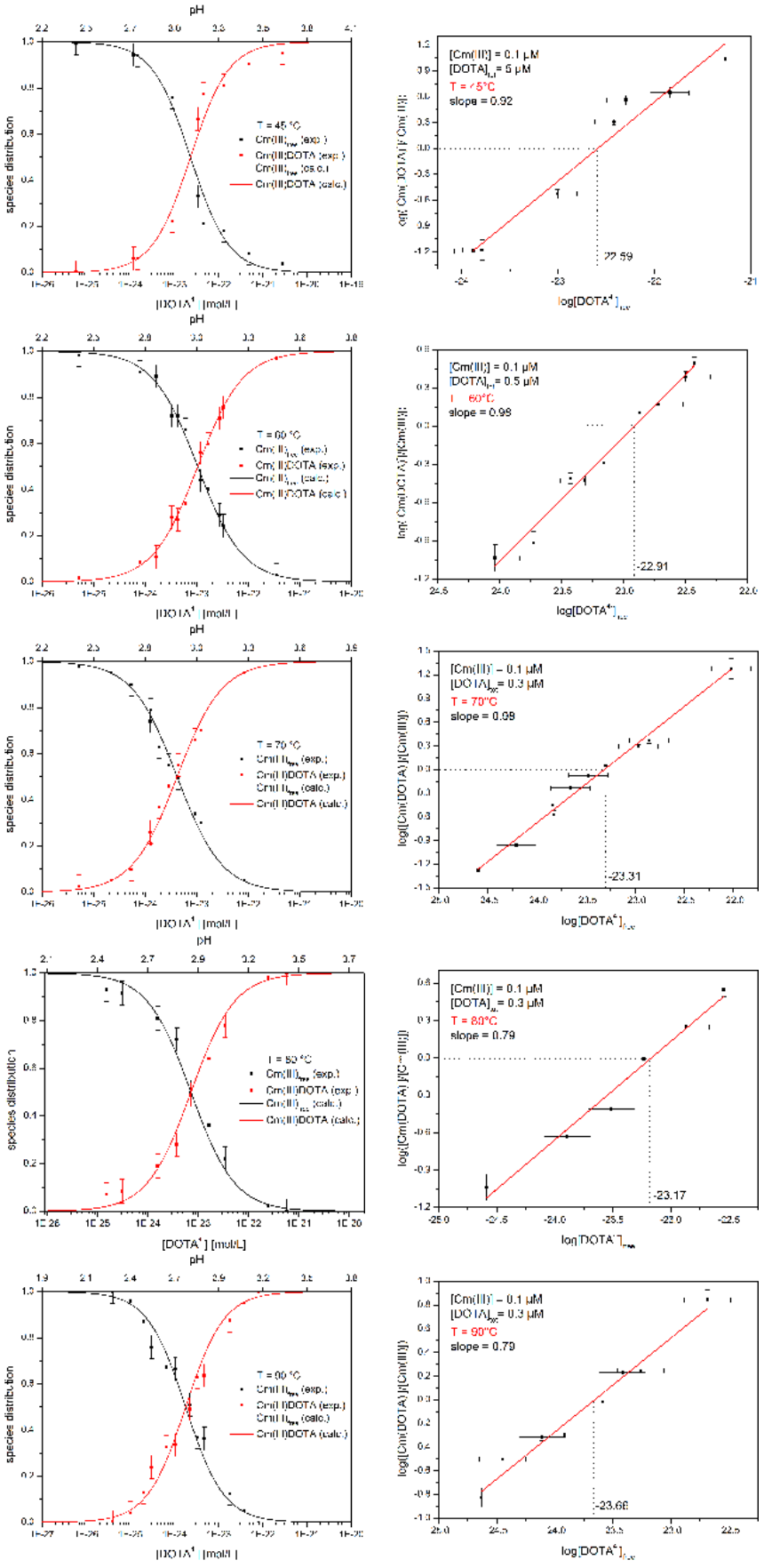

Figure 5.31: *left*: Species distribution of the experiments conducted to determine the stability constants of Cm(III)DOTA at 45 - 90 °C. The black data points represent the Cm(III) aquo ion, while the red data points represent the Cm(III)DOTA complex. *right*: corresponding slope analyses and thereof derived log K values.

5.2.3.3 Discussion

In comparison to the literature values for Eu(III)DOTA, the stability constants obtained for Cm(III)DOTA are reasonable (Table 5.13). The slope analysis for the batch study at 45 - 70 °C resulted in values close to 1 which proves the formation of a Cm(III)DOTA 1:1 complex. The slight deviation of the slopes for the experiments at 80 - 90 °C are tolerable and likely to be caused by minor inaccuracies in concentrations due to solvent evaporation at these temperatures.

The determined constants refer to the temperature during heating and measurement and are reported as average values calculated for each experimental data point. Since Cm(III) ($5f^7$) and Eu(III) ($4f^6$) have similar properties and the difference in the electronic configuration should not be decisive, their stability constants with DOTA are expected to match closely. The determined log K for Cm(III) is a little smaller than the log K reported for Eu(III)DOTA, which is suspected to be due to the smaller ionic radius and hence better encapsulation of Eu(III) compared to Cm(III).

However, the authors of the cited Eu(III)DOTA stability constants declare them to be valid at 25 °C and I = 0.1 M ionic strength, although during the experiment the samples were heated to 70 °C for 3 days [9] or 60 °C, respectively [275], followed by equilibration and measurement of the samples at room temperature. Equilibration of the sample at RT after the heating procedure is believed to be essential to approach the equilibrium properly.

To understand the reason for this approach by Horrocks *et al*, the experiment at 70 °C was reproduced with Cm(III)DOTA. After the three days heating period the samples were measured at this temperature. The obtained spectra were compared with the spectra recorded after these samples were in the following kept at room temperature for 10 days. The obtained species distributions are displayed in Figure 5.32.

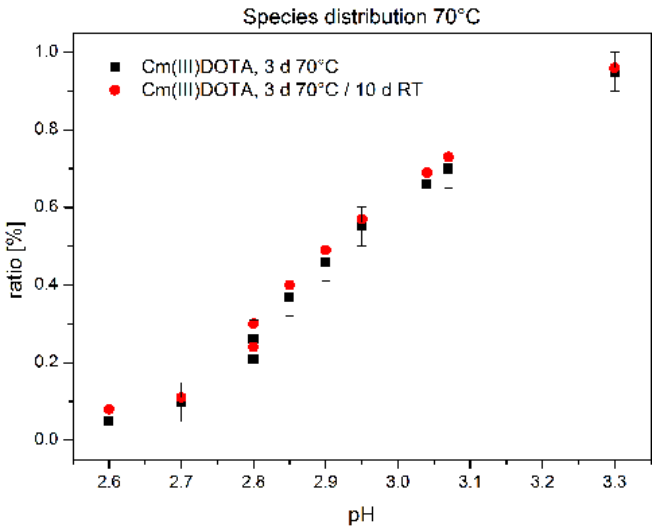

Figure 5.32: Cm(III)DOTA speciation at 70 °C, measured after the 3 d heating period and again after 10 d of room temperature equilibration (c(Cm(III) = $1{\cdot}10^{-7}$ M, c(DOTA) = $3{\cdot}10^{-7}$ M).

In fact, only an insignificant variation within the error range of the 3 d experiment was found between the samples (*black*) and the re-measurement after 10 d of RT

equilibration (*red*), with the ratio of Cm(III)DOTA having only marginally increased after 10 d (log K_{3d}= 23.38±0.4; log $K_{3d/10d}$= 23.43±0.4). Since this finding is in disagreement with the statement of Horrocks *et al*, the constants in the literature should be referred to as valid for the temperatures at which the experiments were carried out. However, this is also erroneous because these log K values were calculated based on the p$K_{a,n}$ values of DOTA at 25 °C instead of the p$K_{a,n}$ values at 70 °C. Until today no other reliable stability constants for Ln(III)DOTA determined at elevated temperatures are available in the literature.

In Table 5.14, some exemplary stability constants for $[Eu(DOTA)]^-$, $[Gd(DOTA)]^-$ and $[An(DOTA)]^-$ are listed; however, they have not been reviewed for reliability by IUPAC [5]. To date, only very few log K for An(III)DOTA complexes were reported. The values given in the respective Ref. [126] have to be questioned though, since the authors neither stated which p$K_{a,n}$ values were used for calculation, nor if the Na(I)DOTA interaction was considered.

Table 5.14: Comparison of some log K values for Ln(III)/An(III)DOTA complexes in the literature.

Metal cation	***log K***	***Conditions***	***Ref.***
Eu^{3+}	23.5	(60 °C), 0.1 M KCl	[275]
Eu^{3+}	23.7	37 °C, 1 M NaCl	[160]
Eu^{3+}	26.2 - 26.7	(70 °C), 0.1 M KCl	[9]
Eu^{3+}	28.2	20 °C, 1 M NaCl	[276]
Eu^{3+}	25.3	25 °C, 1 M NaCl	[164]
Eu^{3+}	23.95	25 °C, 0.1 M $NaClO_4$	[126]
Gd^{3+}	22.1	25 °C, 1 M NaCl	[168]
Gd^{3+}	24.0	25 °C, 0.1 M KCl	[134]
Gd^{3+}	24.7	25 °C, 0.1 M NMe_4Cl	[142]
Cm^{3+}	24.02	25 °C, 0.1 M $NaClO_4$	[126]
Am^{3+}	23.95	25 °C, 0.1 M $NaClO_4$	[126]

In general, proper equilibration has always been a problem for the M(III)DOTA systems and may be one reason for the discrepancies in the log K values reported in the literature. However, the major reason for the spread values is the large range of pKa_1 and pKa_2 values used by different authors, on which the stability constants highly dependent on. Those values are influenced by presence of Na^+/K^+-background salts as discussed in paragraph 5.1; the reported values for pKa_1 range from 9.37 (in 0.1 M NaCl, [162]) to 12.6 (in 0.1 M TMACl, [165]) [11]. Consequently, the authors using Na^+ as supporting electrolyte usually obtian too low log K values. The same occurs in K^+ medium, but since log $K_{K(I)DOTA}$< log $K_{Na(I)DOTA}$ the effect is not as pronounced and other experimental errors are predominant. It is generally best to use ammonium-based background salts to avoid these disturbing interactions [5].

As discussed previously, in the present work it was found that, under the employed reaction conditions, equilibrium is attained after 24 h or 72 hours, respectively (Table 5.12). The slope analyses presented in Figure 5.31 show straight lines with slopes close to the ideal value of one respective $[DOTA^{4-}]$ (Table 5.13) and close to 4 respective $[H^+]$. This approves that a 1 : 1 complex is formed between Cm(III) and

[$DOTA^{4-}$] according to equation 5.22, with four H^+ participating in the reaction resulting from full deprotonation of H_4DOTA. Hence this proves the goodness of the experiment and the obtained log K values can be considered reliable.

5.2.3.4 Temperature Dependence of the Stability Constants

Knowledge of the stability constants at elevated temperatures allows for extrapolation of the log $K_{25\,°C}$ by application of the van't Hoff relation. The van't Hoff relation in chemical thermodynamics relates the change in temperature to the change in the equilibrium constant K:

$$\frac{dlnK}{dT} = \frac{\Delta H}{RT^2} \,, \tag{5.27}$$

$$\Rightarrow\ lnK = -\frac{\Delta H}{RT} + \frac{\Delta S}{R} \,. \tag{5.28}$$

Thus, plotting of the natural logarithm of the determined log K values versus the reciprocal temperature $1/T$[K] gives a straight line if $\Delta_R H$ and $\Delta_R S$ are considered temperature-independent in the respective temperature range. This linear behaviour allows for extrapolation of the ln K values at lower temperatures. The enthalpy $\Delta_R H$ and entropy $\Delta_R S$ are received from the slope m and the y-intercept c of the line:

$$m = -\frac{\Delta H}{R} \,, \tag{5.29}$$

$$c = \frac{\Delta S}{R} \,. \tag{5.30}$$

With these two parameters, the Gibbs free energy $\Delta_R G$ of the complexation reaction at 25 °C is calculated and translated into a ln K and hence log K value following the equations:

$$\Delta G = \Delta H - T\Delta S \,, \tag{5.31}$$

$$\Delta G = RT - lnK \,. \tag{5.32}$$

The results of the van't Hoff plot are presented in Figure 5.33.

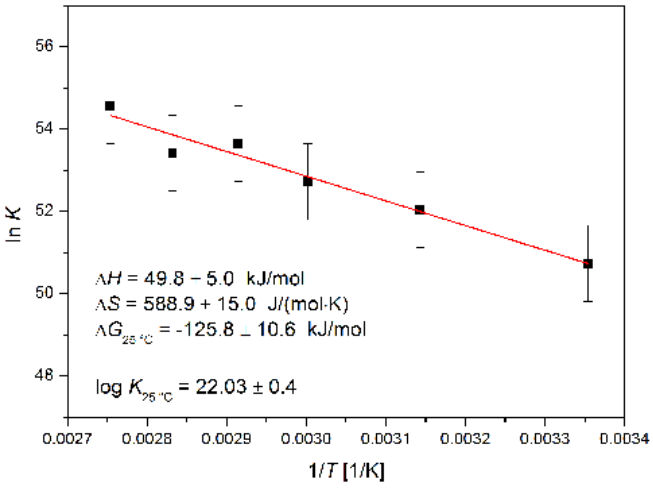

Figure 5.33: Van't Hoff plot and calculated thermodynamic parameters for the Cm(III)DOTA system (sodium-independent).

5.2.3.5 Discussion

The plot of ln K vs. $1/T$ is a straight line, with the stability constant values increasing with temperature (Table 5.13). From this van't Hoff plot, extrapolation to 25 °C yields a sodium-independent log $K_{25\ °C}$ of 22.0±0.4. The parameters $\Delta_R G$ $\Delta_R H$ and $\Delta_R S$ obtained from the Gibbs relation indicate that the complexation is endothermic ($\Delta_R H$) and exergonic ($\Delta_R G$). The complex formation therefore occurs eagerly under the selected conditions, driven by the increase of entropy through release of 9 water molecules ($\Delta_R S$).

Contrary to the experiments on Eu(III)DOTA conducted by Horrocks *et al* [9], in the present study it could not be confirmed that additional RT equilibration of the samples after heating is essential for approaching the thermodynamic equilibrium (see paragraph 5.2.3.3, Fig. 5.32). Also the thermodynamic explanation given by the authors does not comply with the findings from the present study. The authors describe the equilibration procedure as favourable for the complex formation, assuming that $\Delta_R H$ for the reaction is negative, as in the case of Ca(II)DOTA. Thus the stability constants are expected to be smaller at higher temperatures, which means that when cooling to RT occurs, the formation reaction should proceed eagerly while dissociation is negligible [9].

In the present study it was confirmed experimentally, that the Cm(III)DOTA complex dissociation generally occurs much slower than the complex formation and can hence be neglected during cooling of the samples. However, as presented in Figure 5.37, $\Delta_R H$ was found to be positive which complies with the prediction for electrostatic interactions being characterised by $\Delta_R H$ [259, 277]. In an additional experiment it was confirmed that successive heating of an intermittently equilibrated sample to 45 - 55 - 65 °C results in a progressive, stepwise increase of the complex species fraction, proving that the log K increases with temperature. This result also accords to the findings from the kinetic experiments discussed in paragraph 5.2.2 ff, which proved that heating is favourable for the complexation to occur readily as soon as the activation barrier for the conformational rearrangement of DOTA is overcome. This is either achieved by insertion of energy into the system (heating) or by steric factors enforcing pre-orientation into an energetically favoured conformation. The latter effect is suspected to be the reason for efficient radiolabelling of DOTA-chelated antibodies at 45 °C.

5.2.3.6 Modelling of the Experimental Results Using PHREEQC

With the speciation code PHREEQC it is possible to develop a thermodynamic model for the Cm(III)DOTA system under investigation [278]. PHREEQC uses the simple Davies equation -based on the Debye-Hückel theory- to define activity coefficients and hence calculate the stability constants valid at the desired ionic strength (I = 0.1 M):

$$log\gamma_i = -Az_i^2\left(\frac{\sqrt{I}}{1+\sqrt{I}}\right) - 0.3I\,. \tag{5.33}$$

Here, z_i is the ionic charge of the aqueous species i and A is a constant dependent only on temperature (Table 5.15). Taking into account the experimental reaction conditions (pH, background electrolyte), the p$K_{a,n}$ values determined in the respective reaction system, as well as Cm(III)-hydroxide-/carbonate species that possibly form during the reaction, a distribution of all species present in solution is calculated.

From fitting this distribution to the experimentally determined species distribution, the thermodynamic complex stability constant of $[Cm(DOTA)]^-$ is estimated. In the present study, the complexation of DOTA with Na^+ was included into the calculations, since this cation was introduced as $NaClO_4$ to regulate the ionic strength. The stability constants and $pK_{a,n}$ values (Table 5.4) inserted into the fit needed to be recalculated for zero ionic strength (Eq. 5.33) and are listed in Table 5.15.

Table 5.15: Stability constants log K $[Cm(DOTA)]^-$, $[Na(DOTA)]^{3-}$ and $pK_{a,n}$ values determined in the present work (I = 0.1 M), recalculated for I = 0, as well as the A values for the respective temperatures [279].

T[°C]	pKa_1 *I = 0*	pKa_2 *I = 0*	pKa_3 *I = 0*	pKa_4 *I = 0*	*log* K_0 $[Cm(DOTA)]^-$ *I = 0*	*log* K_0 $[Na(DOTA)]^{3-}$ *I = 0*	*A [279]*
25	13.33±0.04	9.88±0.03	4.90±0.03	4.42±0.02	24.9±0.4	5.08±0.03	0.509
45	13.07±0.04	9.69±0.03	5.06±0.03	4.39±0.02	25.6±0.4	5.02±0.03	0.529
60	12.80±0.04	9.51±0.03	4.76±0.03	4.21±0.03	26.0±0.4	5.03±0.04	0.546
70	12.62±0.06	9.24±0.05	5.00±0.04	4.27±0.03	26.5±0.4	4.98±0.05	0.558
80	12.42±0.06	9.22±0.04	4.96±0.05	4.26±0.04	26.5±0.4	4.99±0.04	0.571
90	12.48±0.07	9.27±0.08	4.93±0.06	4.11±0.05	27.1±0.4	5.01±0.07	0.585

Plotting of the experimentally obtained species distribution of the Cm(III) aquo ion and Cm(III)DOTA together with the curves calculated with PHREEQC allows assessment of the experimental results, which ideally should accord with the modelled curves. Some representative results are assessed in Figure 5.34.

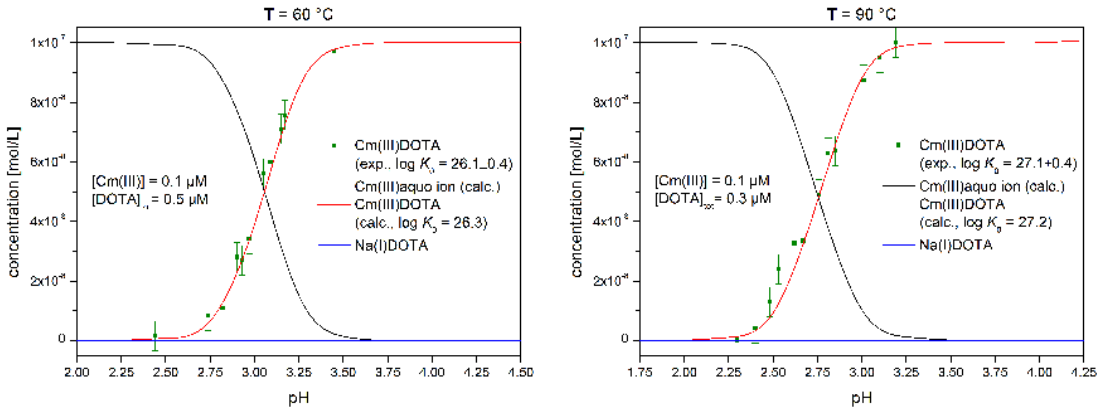

Figure 5.34: Representative speciation curves for the pH dependent formation of $[Cm(III)DOTA]^-$ at 60 °C and 90 °C, I = 0.1 M $NaClO_4$. The experimentally obtained speciation (dots) is plotted onto the speciation curves obtained by calculations with PHREEQC.

5.2.3.7 Discussion

The experimentally obtained speciations (Fig. 5.34, *dots*) are in good agreement with the curves obtained by thermodynamic modelling with PHREEQC. It is hence concluded that under the obtained log K values for Cm(III)DOTA at the respective temperatures and experimental conditions are reliable.

5.3 Thermodynamic Stability of Ac(III)DOTA at Elevated Temperatures

From the findings of the TRLFS study on the complexation of Cm(III) by DOTA, several conclusions are drawn which are fundamental for the understanding of the coordination chemistry of An(III) with DOTA. So far, several studies on the stability of Ln(III)DOTA complexes series were published, but only very few stability constants for An(III)DOTA complexes were reported. Since actinides and lanthanides of same charge and similar ionic radii exhibit similar chemical properties (e.g. Cm(III) and Eu(III), Ac(III) and La(III)), the log K of An(III)DOTA complexes are generally expected to increase with actinide contraction, reflecting the trend observed in the lanthanide series (see paragraph 3.5.2.2. [9]). Hence, the log K for the larger Ac^{3+} with the constrained macrocycle is expected to be lower than for the smaller Cm^{3+}.

For the present work the thermodynamic stability of Ac(III)DOTA is of high importance in order to evaluate DOTA for its suitability in TAT with Ac-225. It is known that radionuclide complexes need to meet certain criteria to remain stable under conditions of the human circulation and metabolism. One of these criteria is the stability of the radioimmunoconjugate towards transchelation to competing ligands in blood serum (HSA, HSTF, carbonate). It has been estimated by Montavon et al. that a log $K > 19$ is required to warrant > 90 % chelate stability under physiological conditions in human blood serum [221].

Various methods are available for speciation, and hence determination of the stability constants of complexes, with non-invasive spectroscopic methods which do not disturb the equilibrium during the measurement being superior to invasive methods such as extraction. Unfortunately, for determination of the log K for Ac(III)DOTA no spectroscopic methods are applicable since neither Ac(III) nor DOTA have suitable spectroscopic properties to enable studies in the low concentration range. However, other radiochemical speciation methods based on solid-liquid-extraction, for example Chelex, are available, allowing for determination of the ratio of uncomplexed Ac-225 to Ac-225-DOTA in the reaction system. This is discussed in the following paragraphs.

5.3.1 Preliminary Speciation Study with Chelex

To obtain a species distribution for Ac(III)DOTA, a complexation study spanning the pH range from 3 - 13 was conducted. From previous experiments with Cm(III)DOTA it is known that these studies must be performed under acidic conditions to have enough free $DOTA^{4-}$ present in the reaction. Nevertheless the investigations were expanded to the alkaline region to simultaneously identify and validate the most suitable pH for future radiolabelling experiments.

A batch experiment setup was developed and an individual sample was prepared for each investigated pH following the protocol described in 4.6.3.1. Since DOTA ($c = 3 \cdot 10^{-6}$ M) is introduced in a 10,000 fold excess over Ac-225 ($c = 3 \cdot 10^{-10}$ M), the reaction is expected to proceed very fast. Heating of the samples is required since it has been demonstrated in pervious works that complexation of Ac-225 with DOTA does not take place at 25 °C even if the pH is alkaline [7].

The pH was adjusted to the desired value by addition of 1 M HNO_3 or 1 M NaOH, respectively. Care was taken to maintain all other reaction parameters such as total volume, ligand concentration and applied activity unchanged, which is challenging due to the decay of Ac-225. It is therefore required to conduct the whole batch study in a very short period of time (1-2 days) to prevent variation in the added volume of Ac-225 stock solution.

In this preliminary experiment the ionic strength of the samples can not be regarded as constant since no background electrolyte is employed. Hence, the results of this pH-dependent speciation will mainly indicate the suitable pH range for conduction of both the future complexation studies and the radiolabellings and will only permit a rough first estimation of the log K.

After heating of the samples (15 min at 60 °C), the solution was passed through the preconditioned Chelex column (pH 7) following the protocol in paragraph 4.6.1. One representative result of this pH-dependent complexation study is plotted in Figure 5.54. From the slope of the curve between pH 3.5 and 5.5, the species distribution and hence the log K for Ac(III)DOTA is derived.

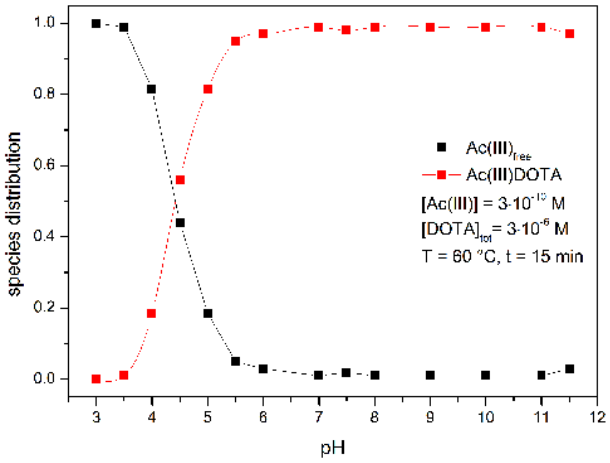

Figure 5.35: Results of the pH dependent speciation study conducted with Chelex. The error bars are omitted. The approximate standard deviation for pH 3 - 5 is $\leq$ 5 %, but particularly high above pH 5 (up to 15 % or higher).

From the obtained species distribution it is apparent that pH $>$ 6 is necessary to ensure full conversion to the Ac(III)DOTA complex. In analogy to Cm(III)DOTA (Eqs. 5.23 - 5.27), from the speciation between pH 3.5 and 5.5 a log $K_{60\,°C}$ = 17.7 for Ac(III)DOTA is estimated based on the equilibrium:

$$Ac^{3+} + \left[DOTA^{4-}\right] \rightleftharpoons \left[AcDOTA\right]^{-} \quad with \quad K = \frac{\left[\left[AcDOTA\right]^{-}\right]}{\left[Ac^{3+}\right]\left[DOTA^{4-}\right]}\,, \tag{5.34}$$

$$log\,K = log\left(\frac{\left[\left[AcDOTA\right]^{-}\right]}{\left[Ac^{3+}\right]}\right) - log\left[DOTA^{4-}\right]_{free}\,. \tag{5.35}$$

For the Chelex experiments, the concentration of the fully deprotonated $DOTA^{4-}$ species at the respective pH was calculated based on the $pK_{a,n}$ values for DOTA at 60 °C determined in the present work (paragraph 5.1.ff).

5.3.1.1 Discussion

The requirement of pH > 6 for efficient complexation of Ac-225 by DOTA (Fig. 5.35) is in agreement with results from the previous work, were pH 8.5 - 9 was found to be ideal for complexation [7] and is higher than the pH 5.5 suggested by McDevitt *et al* [6]. It is therefore recommended to conduct the radiolabelling with Ac-225 at alkaline pH, where DOTA is mainly present as fully deprotonated species (see paragraph 5.1.1).

For speciation studies, the pH range between 3 and 5 appears to be suitable, which is similar to the conditions required for Cm(III)DOTA. The experimentally determined log K of ∼18 for Ac(III)DOTA sufficiently complies with the prevision by computed modelling of the previous results obtained during the Diploma studies (PHREEQC). Since reliable data for Ac(III) was not available, the equilibrium constants of its analogue La(III) (at 25 °C, I = 0) were introduced into the calculation to consider the formation of OH^-, NO_3^-, ascorbate, carbonate and acetate complexes. To account for the interaction of Na^+ with DOTA, also the complex stability constant of log $K_{25°C}$= 4.2 [5] was introduced. Like that, a log $K_{25°C}$ of 19.8 for $[AcDOTA]^-$ (at I = 0) was estimated.

Both log K values determined for Ac(III)DOTA in this study are roughly in the same range. The discrepancy between the model and the experimental results probably arises from the use of constants for La^{3+}, which is smaller than Ac^{3+}. Another source of error is the unadjusted ionic strength of the samples of the experimental batch. Also, since Chelex as invasive method disturbs the equilibrium, the speciation is expected to be afflicted with rather large errors. The standart deviation with this method was found to be ∼5 % below pH 5, but larger than 15 % above pH 5. Therefore efforts were made to implement a speciation method based on ITLC, which is reliable over the whole pH range (see paragraph 5.3.2).

5.3.2 Determination of the Complex Stability Constant of Ac(III)DOTA with Radio-ITLC in the Temperature Range of 45 - 90 °C

Since the Chelex method does not give reliable results particularly in the pH-range above pH 5 (see also paragraph 5.4.2.1), and because separation of the batch samples with Chelex column chromatography is rather time-consuming, an ILTC system was established (Whatmann 3MM/0.9 % NaCl) which facilitates convenient, but still accurate and reliable differentiation while at the same time offering the possibility of high sample through-put (paragraph 4.2.5.2, Fig. 4.12, *right*).

The experimental conditions established for the Cm(III)DOTA TRLFS batch experiment were translated into a setup suitable for ITLC-investiagtion of the Ac-225-DOTA complexation. As described in 4.6.3.2, for each temperature a series of individual samples was prepared for each pH value, followed by heating for 24 h (experiments at 60 - 90 °C) or up to 48 h (45 °C). The metal ion-to-ligand ratio was adjusted for each temperature to allow full conversion in the preset time period. Details are listed in Table 5.16.

After the reaction was halted, aliquots of 10 µl were withdrawn from each batch and separated using ITLC to determine the ratio of complexed to "free" Ac-225. The strips were cut in half and analysed with gamma spectrometry after secular equilibrium was reached. The obtained species distribution and corresponding slope analysis for the various temperatures are plotted in Figure 5.36. Besides Eq. 5.34

and 5.35, for calculation of the complex stability constants the following equations apply:

$$[DOTA^{4-}]_{free} = \left([DOTA] - \left[[AcDOTA]^{-}\right]\right) \cdot X_4 \,, \tag{5.36}$$

$$X_4 = \frac{\beta_4}{[H^+]^4 + \beta_1 [H^+]^3 + \beta_2 [H^+]^2 + \beta_3 [H^+] + \beta_4 + \beta_4 (K_{NaDOTA^{3-}} \cdot [Na^+])} \,, \tag{5.37}$$

$$K_{NaDOTA^{3-}} = \frac{\left[[NaDOTA]^{3-}\right]}{[Na^+]\,[DOTA^{4-}]} \,. \tag{5.38}$$

As in the case of Cm(III)DOTA (paragraph 5.2.3.1), the interaction with Na^+, deriving from the supporting electrolyte $NaClO_4$, has to be accounted for by inclusion of Na(I)DOTA into the DOTA speciation. The calculated mean log K for Ac(III)DOTA of all experiments are listed in Table 5.16. The determined stability constants follow only a weakly distinctive trend, with the log K values increasing with temperature. They are again afflicted with an experimental error of ± 0.4 units deriving from an assumed uncertainty of ± 0.05 for the pH measurements. This error is superior over the error of $[Ac^{3+}]$ originating from the loss of Ac-225 by decay within 24 h or 48 h (< 10 %).

Table 5.16: Experimental conditions and results of the experiments to determine the stability constant log K of Ac(III)DOTA with Radio - ITLC in the temperature range of 45 - 90 °C (c(Ac(III)) = $3 \cdot 10^{-10}$ M, I = 0.1 M).

Conditions (I = 0.1 M)	***Ac(III):DOTA***	***heating period***	***slope***	***log K (± 0.4) $NaClO_4$***	***log K (± 0.4) "Na-free"***	***Chelex study***
45 °C	1 : 1700	48 h	1.00	16.6	19.6	
60 °C	1 : 1500	24 h	0.97	16.7	19.6	17.7
70 °C	1 : 1200	24 h	0.88	17.5	20.3	
80 °C	1 : 1000	24 h	1.01	16.8	19.7	
90 °C	1 : 1000	24 h	0.94	16.9	19.7	

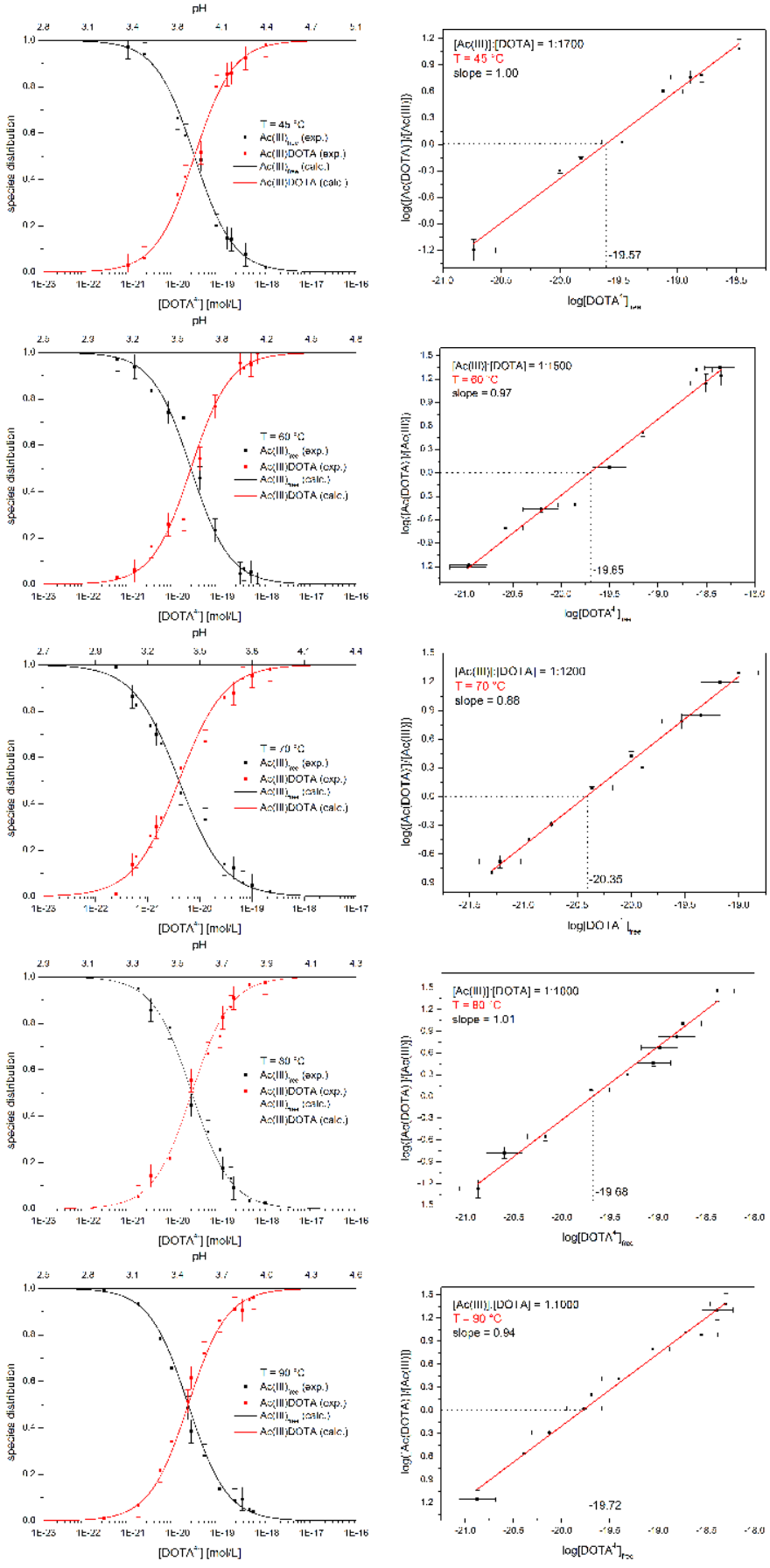

Figure 5.36: pH-dependent species distributions (*left*), slope analyses and thereof derived log K values (*right*) for Ac(III)DOTA in the temperature range of 45 - 90 °C.

5.3.2.1 Discussion

By means of ITLC it was possible to accurately determine the log K values for Ac(III)DOTA at 45 - 90 °C. The slope analyses in Figure 5.36, presenting values close to one, prove the formation of a 1 : 1 complex species. As found for $[CmDOTA]^-$, the stability constants for $[AcDOTA]^-$ increase with higher temperatures. Application of the van't Hoff relation on these results allows extrapolation of the log K at 25 °C to be 19.5±0.4 (Fig. 5.37), which is in good agreement with previous results from the thermodynamic PHREEQC model (log K_0∼19.8 (I = 0, with p$K_{a,n}$ values for 25 °C). The log $K_{25\,°C}$ for Ac(III)DOTA is consequently high enough to meet the criteria for remaining stable complexation in human blood serum (log $K > 19$, [221]). The differences between the log K values at 60 °C, determined with ITLC and estimated previously by using Chelex (log K ∼18), can be traced back to the inaccuracy of the invasive Chelex method (see paragraph 5.3.1.1).

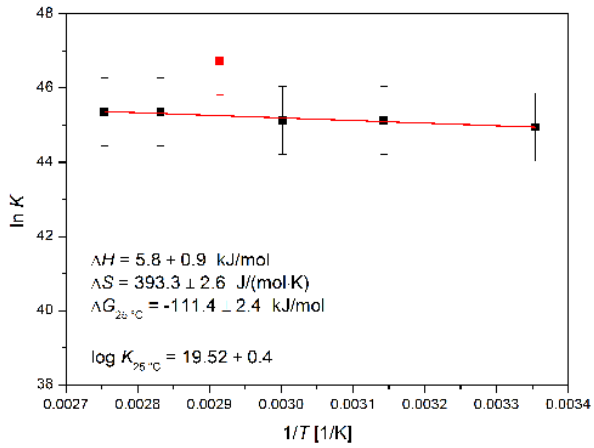

Figure 5.37: Van't Hoff plot for extrapolation of the log K for Ac(III)DOTA to 25 °C (sodium-independent). The log K value determined for 70 °C was found to be too high and was hence excluded from the fit.

In summary, the obtained log K values for Ac(III)DOTA are in the expected range and a bit smaller than the log K values determined for Cm(III)DOTA, which is a consequence of the larger ionic radius of Ac^{3+}. This finding was analogously reported for the log K of the large La^{3+} in comparison to the other Ln(III)DOTA complexes (Table 5.17 [9]). It is commonly agreed upon that there is a linear dependence of the log K upon ionic radius, with Ac^{3+} always having the extreme postition as largest trivalent cation [88, 280].

The difference between the log $K_{25°C}$ for Ac(III)DOTA (19.5±0.4 at I = 0.1 M; 22.4±0.4 at I = 0) and Cm(III)DOTA (22.0±0.4 at I = 0.1 M; 24.9±0.4 at I = 0, Table 5.17) is conform with the result from the extrapolation suggested by Choppin, which allows a rough estimation of 1 : 1 complex formation constants from one actinide complex to others by multiplying the log K values by the ratio of the ionic radii of the respective actinide cations (same valency and coordination number) [97]. According to this, for Ac(III) and Cm(III) it follows that:

$$\frac{r(Ac(III))}{r(Cm(III))} = \frac{112\,pm}{98\,pm} = 1.143\,. \tag{5.39}$$

With e.g. log K Ac(III)DOTA = 19.5±0.4 (I = 0.1 M):

$$log\,K_{(Ac(III)DOTA)} \cdot 1.143 = log\,K_{(Cm(III)DOTA)} = 22.3 \pm 0.4\,(I = 0.1\,M). \tag{5.40}$$

This result is in good agreement with the experimentally determined value for Cm(III)DOTA (22.0±0.4, I = 0.1 M), considering that the ionic radii are valid for CN6 [280, 92]. The approach was also evaluated for the lanthanide-pair La(III)DOTA (i.r. La(III) = 1.032 Å [92], log $K_{25\,^{\circ}C}$= 21.7 [134] or 24.3 [9]) and Eu(III)DOTA (i.r. Eu(III) = 0.95 Å [92], log $K_{25\,^{\circ}C}$= 23.5 [275] or 26.3 [9]).

As in the case of Cm(III)DOTA, the parameters $\Delta_R G$ $\Delta_R S$ and $\Delta_R H$ obtained from the Gibbs relation (Fig. 5.37) indicate that the Ac(III)DOTA complex formation is endothermic, exergonic and occuring eagerly since the reaction is driven by an increase of entropy. The change of Gibbs free energy determined for Cm(III)DOTA ($\Delta_R G^0 \sim$ -142 kJ/mol) is considerably more negative than for Ac(III)DOTA ($\Delta_R G^0 \sim$ -128 kJ/mol), which results from $\Delta_R H$ and $\Delta_R S$ are being smaller for Ac(III)DOTA than for Cm(III)DOTA.

As already discussed in paragraph 5.2.3.5, the enthalpy difference $\Delta_R H$ for the complexation of DOTA with the investigated An(III) is positive. This complies with the (positive) $\Delta_R H$ for the complexation of La^{3+} with the macrocyclic ligands TETA, PEPA and HEHA reported by Kodama *et al*, who found that within the row of macrocycles $\Delta_R H$ becomes more positive with decreasing ring size [259]:

$$\Delta_R H_{(La(III)HEHA^-)} = -17.2\,kJ/mol < \Delta_R H_{(La(III)PEPA^-)} = 2.9\,kJ/mol$$
$$< \Delta_R H_{(La(III)TETA^-)} = 22.6\,kJ/mol\ (I = 0.2\,M\ NaNO_3).$$

Assuming roughly linear behaviour, the predicted value for $\Delta_R H$ would be in the order of ∼40 kJ/mol (I = 0.2 M Na^+), which grants plausibility to the dimensions of the positive values found for Cm(III)DOTA ($\Delta_R H \sim$ 50 kJ/mol (I = 0.1 M Na^+-free), $\Delta_R H \sim$ 58 kJ/mol (I = 0.1 M Na^+) and $\Delta_R H^0 \sim$ 67 kJ/mol).

For both An(III)DOTA complexations investigated in the present study, the driving force is almost exclusively entropic. This is in accordance with the predication that generally, with aminopolycarboxylates and Ln(III)/An(III), the complex formation enthalpies and entropies reflect the dominance of large positive contributions from the dehydration of the cations outweighing a smaller, negative contribution from metal-ligand bond formation ("compensation effect") [259, 281, 282]. The obtained $\Delta_R S$ values for the complexes with DOTA investigated in this work are significantly higher than the values reported for the e.g. Cm(III) and Am(III) complexes with open-chain chelate ligands like EDTA ($\Delta_R S$∼240 J/(mol·K)$^{-1}$) or DTPA ($\Delta_R S$∼270 J/(mol·K)$^{-1}$) [283]. This is traced back to the pre-organisation of the ligand: DOTA profits from a larger entropy increase during complex formation than the unorganised open-chain chelate ligands ("macrocyclic effect"). The latter are forced into an organised structure during complexation and therefore gain less entropy.

In direct comparison with Cm(III)DOTA (Table 5.17) it is found that especially $\Delta_R H^0$ for Ac(III)DOTA significantly differs from the value for Cm(III)DOTA. The difference of $\Delta(\Delta H^0)$∼44 kJ/mol between the Cm(III)DOTA and Ac(III)DOTA complexation accords to the difference reported for the standard formation enthalpies of their aquo ions ($\Delta_f H^0_{(Ac(III)aquo)} = -653 \pm 25\,kJ/mol$, $\Delta_f H^0_{(Cm(III)aquo)} = -615 \pm 6\,kJ/mol$, [88]) and can be regarded as indication for the plausibility of the determined DOTA complex formation enthalpies.

The in comparison to Cm(III)DOTA almost athermic $\Delta_R H_{(I=0.1\,M)} = 5.8 \pm 0.9\ kJ/mol$ or marginal endothermic $\Delta_R H^0 = 22.7 \pm 0.8\ kJ/mol$ found for Ac(III)DOTA result from the less distinct variation of the log K of Ac(III)DOTA

Table 5.17: Summary of the thermodynamic parameters for the complexation of Cm(III) and Ac(III) with DOTA (in sodium-free media, I = 0.1 M). The values in brackets represent the parameters obtained by fitting of the log K values in media containing Na^+ (I = 0.1 M). The values indicates with asterisk are standart data for I = 0.

An(III)	$\Delta_R H$ *[kJ/mol]*	$\Delta_R S$ *[J/(mol·K)]*	$\Delta_R G_{25\ °C}$ *[kJ/mol]*	*log K 25 °C*	*log $K_{25\ °C}$(I = 0.1 M) of Ln(III)DOTA complexes*
Cm(III)	49.8±5.0	588.9±15.0	-125.8±10.6	22.02±0.4	24.02±0.11 for Cm(III) [126],
	(58.2±6.6)	(588.2±20.0)	(-108.3±13.7)	(19.0±0.4)	23.95±0.1 for Eu(III) [126],
	66.9±5.2 *	700.1±15.6 *	-141.8±11.2 *	24.85±0.4 *	26.2±0.1 for Eu(III) [9].
Ac(III)	5.8±0.9	393.3±2.6	-111.4±2.4	19.52±0.4	21.7±0.1 for La(III) [134],
	(14.0±0.7)	(361.6±2.1)	(-93.9±2.1)	(16.4±0.4)	24.2±0.2 for La(III) [9].
	22.7±0.8 *	504.4±2.5 *	-127.7±2.6 *	22.38±0.4 *	

with increasing temperature. This is probably due to the fact that in the case of the larger Ac^{3+} cation, which is less easily fitted into the ligand cage than the smaller Cm^{3+} cation, the increased flexibility of DOTA at elevated temperature still does not allow for proper encapsulation of the metal cation. It is therefore expected that the Ac-N bond length in Ac(III)DOTA complexes is longer and thus weaker than in Cm(III)DOTA complexes because the metal cation is located farther away from the N-plane (Fig. 5.38). Since the log K values at the various elevated temperatures are all very similar, the Ac-N bond length in the complexes formed at slightly elevated temperatures (e.g. 45, 60 °C, log $K_{(I\ =\ 0.1\ M)}$= 19.6±0.4) is hence only marginally shorter than in the complexes formed at higher temperatures (e.g. 80, 90 °C, log $K_{(I\ =\ 0.1\ M)}$= 19.7±0.4). In conclusion, this implies that the complexes formed during Ac-225-labelling of DOTA-chelated antibodies at ∼60 °C (as suggested by McDevitt *et al* [6]), are technically as stable as the complexes formed during radiolabelling at ∼45 °C, which is suggested in the previous and present work. Preferrence is therefore given to the established protocol for radiolabelling at 45 °C, which results in full conversion after 15 min [7], in contrary to the average yields of ∼10 % obtained following the protocoll used by the group of McDevitt.

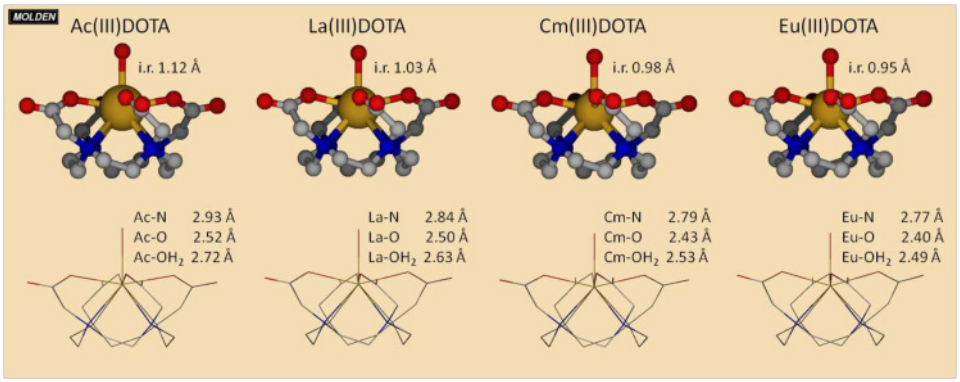

Figure 5.38: Structure of Ln(III)/An(III)DOTA complexes, estimated by applying the ionic radii for CN6 [92]. Structures calculated with Turbomole 6.4 software, graphics drawn with Molden 5.0 software.

5.3.2.2 Modelling of the Experimental Results Using the PHREEQC Code

As described for Cm(III)DOTA (paragraph 5.2.3.6), the experimental results for Ac(III)DOTA are fitted with PHREEQC [278] under consideration of the log K for Na(I)DOTA (paragraph 5.1.2) and the various competing ligands possibly present in the reaction. The log K $[Ac(DOTA)]^-$ were recalculated for zero ionic strength (Table 5.18; for all other constants refer to Table 5.15).

Two representative results for the complexation of Ac(III) with DOTA are assessed in Figure 5.39.

Table 5.18: Stability constants log K $[Ac(DOTA)]^-$ determined in the present work (I = 0.1 M), recalculated for I = 0.

T[°C]	*log K_0 [Ac(DOTA)]⁻*
25	22.4±0.4
45	22.6±0.4
60	23.4±0.4
70	22.9±0.4
80	23.0±0.4
90	23.1±0.4

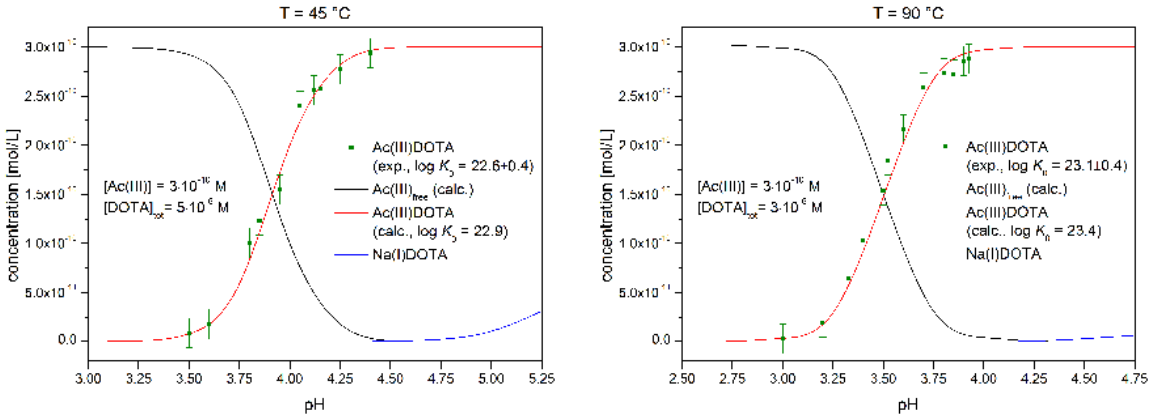

Figure 5.39: Representative speciation curves for the pH dependent formation of $[Ac(III)DOTA]^-$ at 60 °C and 90 °C, I = 0.1 M $NaClO_4$. The experimentally obtained speciation (dots) is plotted onto the speciation curves obtained by calculations with PHREEQC.

5.3.2.3 Discussion

The experimentally obtained species distributions (Fig. 5.39, *dots*) are in good agreement with the curves calculated in the thermodynamic modelling with PHREEQC under the respective experimental conditions and thus indicate the reliability of the log K values of Ac(III)DOTA obtained for the respective temperatures.

5.4 Synthesis and Evaluation of Ac-225-DOTA-Radioimmunoconjugates

The results obtained in the previous paragraphs imply that, under alkaline conditions, Ac-225-radiolabellings of peptides and antibodies in the temperature range of 45 - 90 °C can result in quantitative conversion within reasonably short reaction times. The high log K values indicate sufficient thermodynamic complex stability for application in AIT, provided that the reactants employed in the radiolabelling process are of highest quality and purity. This was already suggested in preceding studies on the developement of a protocol for radiolabelling of antibodies and peptides with low specific activities [7].

Based on the prior work, the scope of the present PhD thesis is the evaluation and optimisation of this antibody labelling protocol (pH 9, 15 min, 45 °C) for higher specific activities like they are required for clinical studies. Interpretation of the results from the previously described kinetic- and thermodynamic investigations with regard to rapid formation of highly stable An(III)DOTA complexes will allow better understanding of the reasons for the somewhat unexpected high efficiency of the radiolabelling at comparably mild conditions.

5.4.1 Optimised Purification of Ac-225

Every once in a while, complexations and radiolabellings with Ac-225 were found to encounter serious difficulties which reflect in low product yields. Several sources for the problem have been considered while attempting to make the procedures fail-safe, with impurities of metallic or organic nature having received the highest attention. Many experiments were therefore performed to assay the quality and chemical purity of the employed reactants.

5.4.1.1 Quality Control of the Ac-225 Stock Solution with ICP-MS

It has been reported by Boll *et al* that metallic impurities are contained in the Ac-225 charges freshly prepared at ORNL [208]. Due to the similar chromatographic production methodolgy (see paragraph 3.7.1) the same is expected to apply for Ac-225 produced at ITU. Even trace metal cation impurities are supposed to be effective competitors for Ac(III) in complexations with the rather unselective DOTA, which is known to discriminate against large cations (early Ln(III)/An(III)) but also to avidly coordinate with a high number of smaller alkaline earth and di-/trivalent transition metal cations [284, 285, 229]. The reported log K values for DOTA with the latter cations are in the same order of magnitude as, or even significantly exceed the log K value determined for Ac(III)DOTA (see Table 3.2). Dependent on their respective concentrations, this can lead to preferred coordination of these metal cations over Ac(III).

In the context of routine quality assessment an attempt was made to monitor the amount of metal cation impurities by comparison of ICP-MS data of various Ac-225 samples (see paragraph 4.1.1.3, [233]). Especially iron and calcium, both forming strong complexes with DOTA due to their small ionic radius and high ionic character [134] (log $K_{(\mathrm{Ca(II)DOTA})}$∼17, log $K_{(\mathrm{Fe(III)DOTA})}$∼29), were found to be present in large amounts. This is in accordance with the results from ORNL, where, besides others, Ca(II) (∼0.1 mg per mCi of Ac-225) and Fe(II)/Fe(III) (5 µg per mCi of Ac-225)

were reported to be the major metal ion impurities [208]. From the anylsis results for Ac, Ca and Fe (t = meas), the relative ratios of Ac:Ca and Ac:Fe were calculated (t = 0, Table 5.19) by substracting the respective blank values (blk) and considering the extraploated concentration of Ac-225 at the day of sample preparation (t = 0). The ratio of Ac-225 vs. Fe(III) and Ac-225 vs. Ca(II) respectively in representative samples were found to be up to (Table 5.19):

$$Ac(III) : Ca(II) = 1 : 2,000 - 1 : 20,000$$

$$Ac(III) : Fe(III) = 1 : 300 - 1 : 5,000$$

Since with progressive decay of Ac-225 the relative ratios will continously increase, either freshly prepared Ac-225 or higher specific activities should be applied in all experiments to generally limit the excess of metal ion impurities.

Table 5.19: Overview of some selected ICP-MS results for various samples taken from three different Ac-225 charges.

sample	***Ac-225 [ng/g]*** ***(t = meas)***	***Ac-225 [ng/g]*** ***(t = 0)***	***Ca [ng/g]*** ***(t = meas)***	***Fe [ng/g]*** ***(t = meas)***	***Ac:Ca*** ***(t=0)***	***Ac:Fe*** ***(t=0)***
blk 1	-	-	11.8±1.4	5.0±0.6	-	-
s 1	0.0025±0.0003	0.005	120±14	1.3±0.2	1:21600	(< blk)
s 2	0.00014±0.00002	0.0003	12±1.4	6.6±0.8	(1:590)	1:5530
blk 2	-	-	13.6±1.6	2.7±0.3	-	-
blk 3	-	-	6.3±0.8	0.9±0.1	-	-
s 3	0.0012±0.0001	0.002	61±7	4.4±0.5	1:21120	1:1060
s 4	0.0009±0.0001	0.002	28.3±3.4	2.7±0.3	1:10430	1:510
blk 4	-	-	8.1±1	1.2±0.1	-	-
s 5	0.025±0.003	0.038	105±13	2.9±0.3	1:2550	(1:45)
s 6	0.025±0.003	0.038	94±11	13.6±1.6	1:2270	1:330

To purify Ac-225 from these metal cation contaminations, DGA extraction chromatography was considered. DGA resins are commonly applied for separation and preconcentration of trivalent lanthanides and actinides in nitric- or hydrochloric acid media, e.g. for separation of Ac-225 from Ra-225 (see paragraph 3.7.1) [213]. Under these conditions, TEHDGA was reported to quantitatively retain Ac(III) and hence efficiently separate it from divalent alkaline earth cations such as Ca(II), which exhibit little or no retention on the resins. This DGA-based purification was tested several times and the obtained Ac-225 stock solutions were measured with ICP-MS to compare them to previously measured samples. However, since concentrations of the metals were very low or even below the background levels (blanks) of the double-destilled nitric acid used for ICP-MS, no clear statement could be made if the purification was sucessful. In further studies it was found, however, that this additional DGA-purification did not improve the labelling yields.

Since it cannot be excluded that the encountered problems with the unsatisfying radiolabelling result from impurities of metallic origin, it is nevertheless recommended to carefully wash all vials with metal free water (MFW) and diluted HCl prior to use. However, this will not improve the metal cation contamination resulting from

the decay of Ac-225. Amongst others, trivalent daughter nuclides are produced by decay, with Bi-213/Bi-209 being known to form particularly stable complexes with DOTA (log $K_{(Bi(III)DOTA)}$∼30) [110].

5.4.1.2 Bismuth as Impurity

For reason of the particularly high complex stability of its DOTA complex, Bi-213 is currently applied in clinical alpha-immunotherapy studies [145]. In form of Bi-213 and Bi-209, Bi(III) is an unavoidable metallic "impurity" accumulating in Ac-225 stock solutions over time. A so-called "aging" effect of the Ac-225 stock solution was observed, giving rise to the assumption that accumulating Bi(III) is severely disturbing the complexation of Ac-225 by DOTA: radiolabellings which have been accomplished succesfully with freshly prepared Ac-225 suddenly failed a couple of days thereafter (approximately 5-6 days; particularly recognisable in the case of the complexation experiments in the low concentration range (paragraph 5.3.2)). A comparable effect was recently reported by Brom *et al* for In-111 and its decay daugther Cd-111 [229].

Direct comparison of the log K values for Ac(III)DOTA (log $K_{25\ °C}$∼20, this work) and Bi(III)DOTA (log K∼30) reveals the immense superior thermodynamic stability of the latter complex by a factor of 10 log units. It is hence expected that Bi(III) will be preferrably coordinated by DOTA even if it is only present in trace amounts. This contributes to the need for insertion of DOTA in large excess over Ac-225 in standard complexation experiments (e.g. Ac-225 : DOTA = 1 : 1700 at 45 °C). It can be questioned though if Bi(III) is the only reason for the poor outcome of some radiolabelling experiments, since in these batches DOTA is usually present in a up to 35,000 fold excess over Ac-225, respectively. Hence, a sufficient amount of DOTA should be available for complexation of both Ac(III) and Bi(III). This is probably true for radiolabellings with freshly prepared Ac-225, but even though Ac(III) is in excess over Bi(III), a nearly 10^{10} times lower concentration of Bi(III) compared to Ac(III) is effectual for competition. From calculation of the number of especially Bi-209 atoms rapidly accumulation in the Ac-225 batch within the first 5 days, reaching a ratio of Ac-225 : Bi-209 of 1 : 1 after the first half life of the mother ($t_{\frac{1}{2}}$ = 10.0 d), it is to be assumed that the concentration of Bi(III) at all time points is too high to be not considered as serious competitor for Ac-225 in terms of complexation by DOTA (Fig. 5.40; see also paragraph 4.1.1.3).

Therefore it was considered to decrease the quantity of accumulated Bi(III) by employing UTEVA and DGA columns to purify Ac-225. It has been reported that in 0.1 M HCl Bi(III) is nearly quantitatively retained on UTEVA as $[H_3O^+][BiCl^{4-}]$ species while Ac(III) does not exhibit any retention under these conditions [213]. This way of purification was tested in the present study but was found inconvenient since it requires various changes of the acid medium.

Preference was given to a more simple purification using a single TEHDGA column. Sufficient separation of Ac(III) from Bi(III) is achieved by extensive washing of the loaded TEHDGA column with several ml of 4 M HNO_3. Like this, Bi(III) is eluted while Ac(III) is retained on the column. The eluent fractions are monitored for the Bi-213 γ-signal which is very intense in the first few eluted fractions and decreases in the following fractions. The washing is stopped when Bi-213 is hardly detectable anymore and before Ac-225 breaks through. Subsequently, after

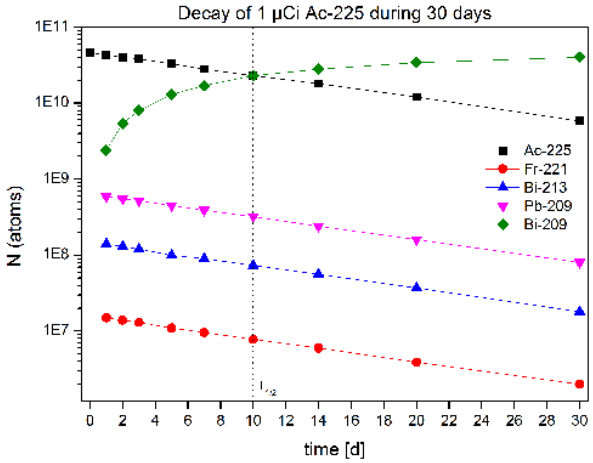

Figure 5.40: Decay of 1 µCi of Ac-225 during 30 days. The number of Bi-209 atoms is rapidly increasing within the first 6 days, reaching a number equal to Ac-225 after 10 days.

incubating the column with one half-bed volume of 0.05 M HNO_3 for 10 min, Ac-225 is then stripped off the column with few milliliters of 0.05 M HNO_3. With this method, a slight improvement of the antibody labelling yields of about 15 % was achieved (e.g. 69 % before and 83 % after TEHDGA purification).

In conclusion, to avoid experiment failure due to ingrowing amounts of Bi(III) ("aging"), radiolabelling experiments with biomolecules in the present study were always carried out with freshly prepared Ac-225 (preferably 1 - 2 d after separation).

5.4.1.3 Organic Impurities

Besides contamination by metal cations, also impurities of organic nature, originating from extraction chromatography resins employed in routine radionuclide production, were considered. These commonly used resins are usually composed of inert matrix material which is impregnated with derivatives of strongly coordinating organic extractants like diglycolamide (DGA), e.g. TODGA/TEHDGA.

Especially resins for retention of metal cations are known to be sensitive to radiolytic damage from high-LET α-particle emitters or γ-radiation [71]. The continous generation of radical species on the resin and in the eluate can eventually lead to poor radiolabelling yields [111]. In the case of DGA resins, for example, the radiolytic degradation induced by γ-rays results in cleavage of the C-N bonds, which leads to increased leaching of organic molecules [286]. Here, TEHDGA (*N,N,N',N'*-tetra-2-ethylhexyl diglycolamide, Fig. 5.41) was found to be more resistant to radiolysis than TODGA. By virtue of its moreover better distribution coefficient, for Ac-225 production at ITU the TODGA resin was exchanged by TEHDGA several years ago [207].

Nevertheless, leaching of DGA is still expected to occur and was made visible by applying ILTC and Cm(III)TRLFS (Fig. 5.42). It was demonstrated that the compound leaching from the column has the property to immediately and quantitatively coordinate An(III) at room temperature. In the TRLFS spectra (*left*), the emission band at 593.8 nm corresponds to the Cm(III) aquo ion, while the emission bands at 598.0 nm and 602.7 nm derive from the eluted and possibly degraded extracting

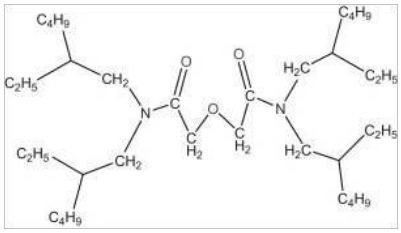

Figure 5.41: The molecule structure of TEHDGA.

agent. Due to hydrolysis of Cm(III), the TRLFS investigations were only possible in the acidic range up to a pH of 5.5; however the compound is assumed to also interfere with the complexation at labelling relevant alkaline pH.

The ITLC study (*right*) was conducted with blank samples from an Ac-225 stock solution which has not been purified before. Usually, clean, unbound Ac(III) is found at $R_f = 0$ while Ac(III) coordinated by (organic) ligands like e.g. DOTA moves with the eluent front ($R_f = 0.9$). From the image it is apparent that a fraction of Ac-225 was ascending ($R_f = 0.15$ - 0.2). This indicates coordination by a compound present in the stock solution which presumably originates from the (fragmented) TEHDGA resin.

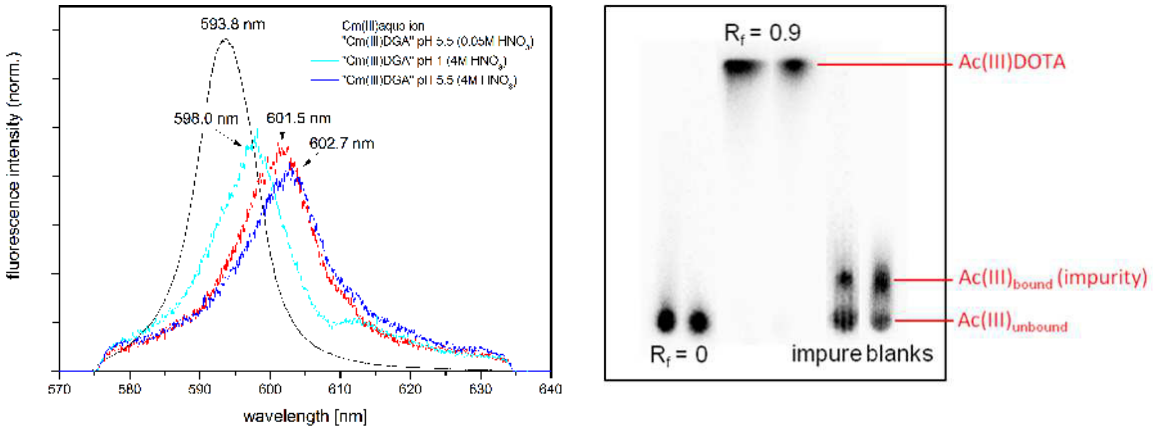

Figure 5.42: *left*: Emission spectrum of Cm(III) species formed with DGA eluate at pH 1 and pH 5.5. Washing of the DGA resin was done with 4 M and 0.05 M HNO_3, respectively. *right*: Radiographic image of the Ac-225 blank ITLC study (3MM / 0.9 % NaCl).

To purify the Ac-225 stock solution from organic contaminations, column chromatography with a so-called pre-filter resin (Eichrom) was tested. The resin is an uncoated inert polymeric support and supposed to act as a non-specific physical filter to eliminate trace amounts of organic compounds from aqueous solutions [287]. At the same time the small metal cations exhibit no retention; in the present study, the recovery for this filtration method was found to be above 95 %. The eluted fraction requires concentration after the process.

Remaining organic impurities contained in the filtered radionuclide solution can be subsequently removed by oxidation. For this, the eluate is first evaporated to dryness, followed by repeated heating and evaporation with concentrated nitric acid at 140 - 150 °C (see praragraph 4.1.2. for details). Afterwards, the residue is redissolved in the desired concentration with 0.05 M HNO_3 and can be applied

for radiolabellings without further treatment. This method presents a facile way for preconcentration of Ac-225. In combination with the pre-filter it was found to give the highest nuclide purities of all methods tested, allowing for reliably high radiolabelling yields of up to 95 % on average.

5.4.1.4 Discussion

In summary, the antibody labelling yields were found to be strongly dependent on the quality of the Ac-225 stock solution. A guideline for successfull purification of Ac-225 was therefore established:

- Avoidance of any contamination of the Ac-225 stock solution with metal cations is mandatory. This also applies for the ligand preparations, where usage of metal spatulas or syringe needles should be avoided whenever possible. Appropriate washing of all reaction vials with MFW and HCl can improve on the metal ion contamination.
- Application of freshly produced Ac-225 minimises the extent of Bi(III) contamination. Aged Ac-225 stock solutions can be purified from accumulated Bi(III) by extraction chromatography with TEHDGA (extensive washing!).
- After each chromatographic separation, the eluted fractions containing Ac-225 require additional filtration (pre-filter) and oxidisation with concentrated HNO_3 to eliminate organic impurities originating from the employed chromatographic resins.

It was demonstrated that, with high-quality Ac-225, radiolabellings with up to 50 µCi (= 1.9 MBq) per 100 µg mAb can be performed without difficulty (Fig. 5.43). Contrarily, with Ac-225 of lower purity a saturation effect is observed, resulting in notably lower yields which correlates with the introduction of higher quantities of disturbing impurities. The labellings were accomplished according to the protocol described in paragraph 4.9.1, which is discussed in detail in the following paragraph.

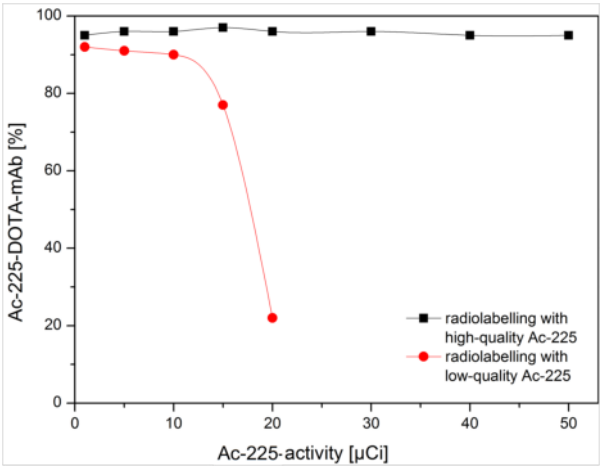

Figure 5.43: Representative antibody radiolabelling yields demonstrating the influence of Ac-225 quality on the activity loaded onto the antibody.

5.4.2 Considerations for Optimisation of the Protocol for Radiolabelling of DOTA-NCS-MabThera® with Ac-225

Based on the previously developed protocol for the synthesis of Ac-225-DOTA-NCS-mAb with lower specific activities (paragraph 3.9.3.2), in the present study investigations with regrads to optimisation of the radiolabelling protocol for application with higher SA were conducted. As discussed before, the purity of the employed $^{225}Ac(NO_3)_3$ solution needs to be as high as possible. It has been validated that alkaline pH is ideal for efficient radiolabelling (paragraph 5.3.1.), as then most of the ligand is present as highly reactive $DOTA^{4-}$ (paragraph 5.1.5); thus, the suggested pH 9 is retained for future radiolabellings.

The temperature of T_{max}~45 °C for mAb-radiolabelling is predetermined by the biomolecule. To ensure conservation of the chemical integrity and biological functionality of the mAb, investigations lead in the direction of lower labelling temperatures of 37 - 42 °C.

Besides these two physical parameters, further optimisations can be made with respect to the contents of the reaction batch. The DOTA-chelated antibody is an invariable parameter specifically selected for the intented therapeutic purpose. It has been reported that, upon conjugation of a ligand to an antibody, the metal-loading kinetics of the ligand can be negatively altered due to steric hindrance caused by the protein conformation (Fig. 5.44) or, in general, also due to competition from other metal ion binding protein sites (unspecific binding) [288, 155]. While the former cannot be directly influenced, the issue of unspecific binding of An(III) was proven to not apply for MabThera® (see paragraph 5.4.4.1).

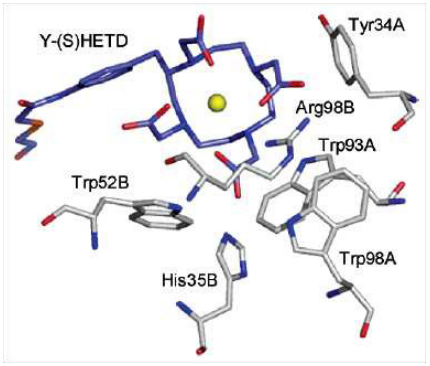

Figure 5.44: Picture of Y-(S)HETD, a modified DOTA compound, in the active site of the 2D12.5 monoclonal antibody [155].

Furthermore, it has been reported before that also the usage of inert buffer medium (e.g. TRIS, HEPES) can improve metal incorporation into DOTA-antibody conjugates [219, 229]. Contrary to that, Toth *et al* reported decreased complexation rates in acetate buffer systems due to competition by acetate for the metal cation [164]. It was also reported by Brom *et al* that lower specific activities are obtained when labelling is conducted in readily coordinating sodium- or NMe_4-acetate buffers [229]. Nonetheless, the protocol for radiolabelling of DOTA-mAb presented by McDevitt *et al* still involves the use of tetramethylammonium acetate in the complexation step at pH 5.5, which probably explains the associated lengthy reaction times of up to 60 min. Contrary to this, the more efficient radiolabellings conducted in the preceding and present studies highlight the necessity to work in inert buffer media such as e.g. 2 M/0.2 M TRIS buffer (pH 9), which is widely used as biochemical buffer [7]. During preliminary TRLFS experiments with Cm(III) under radiolabelling conditions conducted in the context of the present study, no interaction of TRIS (2 M/0.2 M) with the cation (c(Cm(III) = $1 \cdot 10^{-7}$ M) was observed. It is hence concluded that TRIS also does not interfere with the Ac-225-DOTA-NCS-mAb radiolabelling.

The last substance contained in the standard labelling protocol is the scavenger ascorbic acid introduced as radioprotectant. It is commonly agreed on the necessity of protecting the antibody conjugate against radicals formed through radiolysis during labelling and storage of the final radioimmunoconjugate. The influence of ascorbic acid on the radiolabellings is discussed in detail in the following paragraph.

5.4.2.1 The Influence of Ascorbic Acid

Ascorbic acid is a commonly used additive to radiopharmaceuticals and is supposed to not interfere with the metal ion-ligand complexation. However, some findings during the investigation of the pH- dependent formation of Ac(III)DOTA with Chelex (paragraph 5.3.1) gave rise to the assumption that ascorbate possibly competes with DOTA for complexation of Ac(III). A similar competition for metal ion binding by acetate buffer has been reported before [164].

In the studies with Chelex it was found that the blank values for the elution of unbound Ac^{3+} in a solution containing 100 µl 0.2 M NaOAc or TRIS buffer and 50 µl of 20 % ascorbic acid were exceptionally high, in particular at neutral and alkaline pH where TRIS buffer is used (Fig. 5.45); hence, the effect is not correlated to the presence of acetate. This indicates that another ligand is present that is capable of forming complexes with Ac^{3+}.

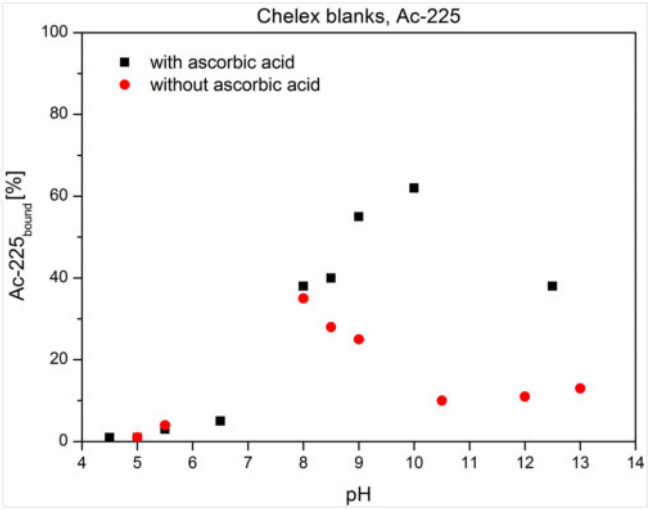

Figure 5.45: Chelex blanks, with (*black*) and without (*red*) ascorbic acid.

Over the whole pH range, the blank values were found to decrease when ascorbic acid was eliminated from the reaction system. The blanks without ascorbic acid are still high, which is assumed to be a problem of the Chelex method (see paragraph 5.3.1).

Since the interference was found to be especially pronounced in the alkaline range, further studies were perfomed to quantify the influence of ascorbic acid on the radiolabelling at pH 9. It was demonstrated that, with otherwise identical reaction conditions (15 min, 45 °C), the labelling yield increases in absence of ascorbic acid (Fig. 5.46).

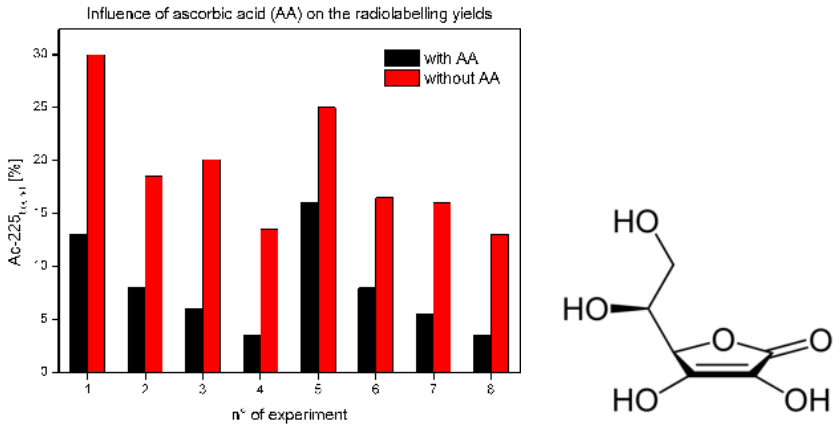

Figure 5.46: Influence of ascorbic acid (AA, *right*) on the labelling yields (15 min, 45 °C).

5.4.2.2 Discussion

The results of the studies (Fig. 5.45 and 5.46) clearly indicated the ability of ascorbate to coordinate Ac-225 especially at alkaline pH. Ascorbate with its hard basic oxygen donor atoms is likely to form strong ionic bonds with the hard Lewis acid Ac^{3+}. The complex formed between the two reactants is expected to have a formation constant of $\log K_{25\,°C} = 2.3$ [289], which is well below the stability constant determined for the Ac(III)DOTA complex ($\log K_{25°C} = 19.5$, this work). However, ascorbic acid is usually inserted in large excess. Due to the rigidity of the DOTA ring, ascorbate probably has more favourable complexation kinetics and hence preferably coordinates to the metal cation. This decreases the rate of Ac(III)DOTA formation and hence the yield if the reaction is halted, e.g. after 15 min (Fig. 5.46). In the course of the reaction, ascorbate will be substituted by the macrocycle to form the substantially more stable Ac(III)DOTA complex.

To account for this issue, the precedingly developed labelling protocol for Ac-225-DOTA-NCS-mAb-conjugates required further modification with respect to exclusion of ascorbic acid from the labelling. To furthermore decide on the necessity of ascorbic acid for the kinetic stability of the RIC during storage and further use, additional studies were conducted.

5.4.2.3 Influence of Ascorbic Acid on the Kinetic Stability of the Radioconjugates in the Reaction Medium

It is well known that during storage the radiolabelled antibody conjugates are likely to be damaged by radicals formed through radiolysis induced by the radionuclide they are labelled with. To prevent this, the samples either require significant dilution or the addition of scavengers such as ascorbic- or gentisic acid [226, 227]. Since it was decided to exclude ascorbate from the labelling, purpose of the following experiments was to estimate the importance of ascorbic acid for the long-term kinetic stability of the radioconjugates.

The Ac(III)DOTA complex and the Ac-225-DOTA-NCS-mAb-conjugate were therefore both synthesised according to the standard protocol (paragraph 4.9.1), with ascorbic acid being replaced by an equal volume of additional TRIS buffer. For the complexation of Ac-225 with DOTA at 60 °C, a quantity of 0.81 µg DOTA

($1.2 \cdot 10^{-5}$ M) was used which corresponds to the number of chelators per 100 µg antibody, assuming that each antibody is conjugated with 4 DOTA-NCS. All complexations and labellings in this experiment were successfully conducted with high SA of 30 or 50 µCi (= 1.1 or 1.9 MBq) per 0.81 µg DOTA or 100 µg mAb, respectively, to induce significant radiolytic effects. The yields were > 96 % with all samples.

For assessment of the kinetic stability during undiluted storage in the reaction medium, each sample was split into two aliqots. To the first aliquot, 13 µl of 20 % ascorbic acid was added while the second aliqot remained untreated. All samples were then incubated at room temperature for a period of 15 days. Intermittently, aliquots of 5 - 10 µl were withdrawn, separated with ILTC (Biodex/0.05 M Na-citrate for mAb, 3MM/0.9 % NaCl for DOTA samples) and analysed with gamma spectrometry. The results of this stability study are presented in Figure 5.47. By comparison of the stability curves with and without ascorbic acid (AA), it can be deduced to which extent ascorbic acid is necessary to prevent or slow down radiolytic degradation of the radioconjugates.

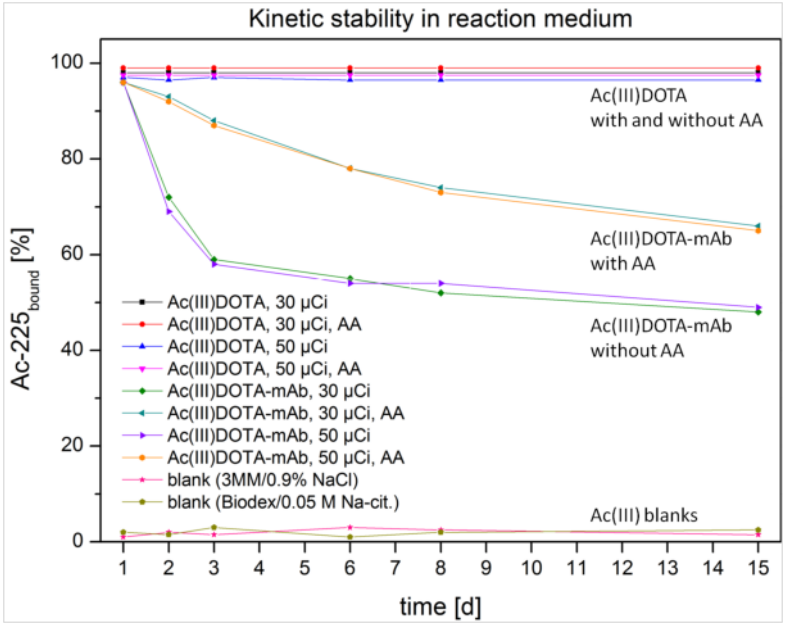

Figure 5.47: Kinetic stability of Ac(III)DOTA and Ac(III)DOTA-NCS-mAb in 2 M TRIS buffer medium. "AA" indicates the aliquots to which ascorbic acid (AA) was added.

5.4.2.4 Discussion

From the curves in Figure 5.47 it is concluded that, unaffected by the presence or absence of ascorbic acid, the Ac(III)DOTA complex remains nearly 100 % stable over the entire observation period. Even though DOTA is available in excess, this proves the integrity of the Ac(III)DOTA complex: if Ac-225 was lost from one DOTA cage, recomplexation by other free DOTA ligands would not occur at room temperature, as complexation of An(III)/Ln(III) by the rigid DOTA was demonstrated to have extremely slow kinetics at 25 °C (e.g. Cm(III), this work; Ac(III) [7]; Eu(III)

[9, 275]). Especially with the reactants present in such low concentrations as in this experiment, the eventuality of a dissociation-association equilibrium being established during 15 days is excluded. Therewith this experiment proves the exceptional stability of M(III)DOTA complexes formed at elevated temperatures (60 °C).

Contrary to this, a drastic decrease in stability within the first three days is visible for all other curves representing the Ac(III)DOTA-NCS-mAb samples (Fig. 5.47). It is apparent though that the effect is less pronounced for the reaction batches with AA. From this finding it is deduced that addition of ascorbic acid slows down the radiolytic degradation of the RIC even at high specific activities. Since instability was anyhow also observed in samples containing ascorbate, it is presumed that more ascorbic acid may be required. Addition of a fair quantity of ascorbic acid to the reaction solution *after* the radiolabelling has terminated, should be considered to stabilise the final product.

Another possibility would be addition of gentisic acid as replacement for ascorbic acid [227]. If, and to what extent gentisic acid could influence the outcome of the radiolabelling was not investigated in the context of this work.

5.4.3 Implementation of a Reliable Protocol for the Synthesis of Ac-225-DOTA-NCS-MabThera®

Considering the conclusions drawn from the previous disscussions, the measures required for refinement of the previously developed protocol for radiolabelling of DOTA-peptides and antibodies are evident. The results of the thermodynamic experiments respective the acid dissociation of DOTA (paragraph 5.1.1) and the complex stability of Ac(III)DOTA (paragraph 5.3.2) are in favour of alkaline pH (pH 9) and T_{max}= 45 °C as reaction conditions for mAb labellings (and 90 °C for peptides, respectively). The only marginally higher thermodynamic stability of the Ac(III)DOTA complex formed at 60 °C over the complex formed at 45 °C has been determined and discussed previously (see paragraph 5.3.2). It was reviewed that TRIS buffer is suitable while ascorbic acid negatively influences the reaction kinetics but is still required for stabilisation of the final product (paragraph 5.4.2.1 ff). Furthermore, the omission of AA allows the reaction to be carried out in weaker buffer medium (0.2 M TRIS).

With or without additional purification, the labelled biomolecules require a high radiochemical purity (RCP $>$ 95 %) because of the large amounts of radioactivity eventually administered, and the toxicity of the radiochemical impurities [242]. High specific activities of labelled peptides and mAb are required as well to allow administration of only a tracer dose of conjugate, preventing target saturation and side effects. Highly pure reactants and sterile vials should be used, in particular when subsequent use of the radioimmunoconjugate for *in vitro* or *in vivo* studies is intended.

With this experimental setup one last variable factor remains, which is the reaction time. The complexation kinetics of DOTA with An(III) were investigated before (paragraph 5.2.2 ff). However, since the ligands' complexation kinetics were reported to be possibly altered by conjugation into the antibody [155], further studies were accomplished to review the mAb labelling kinetics in detail.

5.4.3.1 Reaction Kinetics for the Ac-225 Labelling of DOTA-MabThera®

An extensive kinetic study over the range of pH 4 - 11 was performed with the intention to evaluate the selected reaction conditions (pH 9, 37 - 42 °C). Twelve samples, each containing the identical concentration of DOTA-mAb (50 µg) and Ac-225 (2 µCi (= 74 kBq)) in differnt pH-adjusted buffer media (2 M NaOAc, 2 M TRIS; adjustment of pH with HCl and NH_3) were prepared according to the standard protocol (paragraph 4.2.6.1) and heated to 40±1 °C. After 5, 15, 30 and 60 minutes aliquots of 5 µl were withdrawn from each sample and analysed with ITLC (ITLC-SG/Na-citrate) and γ-spectrometry for the percentage of labelled antibody. The results of the study are summarised in Table 5.20. The poor outcome of the experiments in the acidic pH range using NaOAc buffer (pH 4-7, *red*) is partly attributed to the disturbing influence of Na^+ on the complexation and suggest its omission in the labelling batch.

Table 5.20: Results of the pH-dependent study on the Ac-225-DOTA-mAb labelling kinetics.

	pH 4	***pH 5***	***pH 6***	***pH 6***	***pH 7***	***pH 7***
t [min]	*NaOAc*	*NaOAc*	*NaOAc*	*TRIS*	*NaOAc*	*TRIS*
5	7.9 %	18.8 %	25.3 %	46.9 %	68 %	84.3 %
15	7.3 %	29.4 %	50 %	61.6 %	81.6 %	87.8 %
30	-	-	-	68.1 %	-	88.1 %
60	-	-	-	90.2 %	-	92.1 %

	pH 8	***pH 9***	***pH 9.5***	***pH 10***	***pH 10.5***	***pH 11***
t [min]	*TRIS*	*TRIS*	*TRIS*	*TRIS*	*TRIS*	*TRIS*
5	76.4 %	81.4 %	85 %	82.5 %	91.4 %	92.3 %
15	84.7 %	86.9 %	90.7 %	89.5 %	94.8 %	94.4 %
30	89.2 %	90 %	93.7 %	92.8 %	95.7 %	95.4 %
60	93.3 %	91.9 %	95.7 %	94.6 %	96.3 %	96.7 %

5.4.3.2 Discussion

As already indicated in preceding studies (Diploma thesis, [7]), alkaline pH is essential for rapid high-yield radiolabelling of DOTA-chelated peptides and antibodies. While in the previous work a reaction time of 15 min was suggested to be appropriate, this new study presented in Table 5.20 indicates that with TRIS buffered samples of pH ≥ 7 already after 5 min sufficient radiolabelling (≥ 75 %) is achieved (*blue*; see also Fig. 5.48). In further radiolabelling experiments conducted at 42 - 45 °C it was proven that for specific activities of 5 µCi (= 185 kBq) and 10 µCi (= 370 kBq) per 100 µg of antibody a reaction time of 5 min is sufficient to achieve yields above 96.1 % (Table 5.21). The actual reaction rate is nevertheless dependent on the quality of the used Ac-225.

From Fig. 5.48 it is apparent, that antibody labellings at neutral and alkaline pH (pH ≥7, TRIS, *above the line*) proceed much faster than labellings in the weakly acidic pH range (e.g. pH 6, TRIS; pH ≤6, NaOAc, *below the line*) as suggested by McDevitt *et al* (pH 5.5, TMAA). This is traced back to the significantly higher

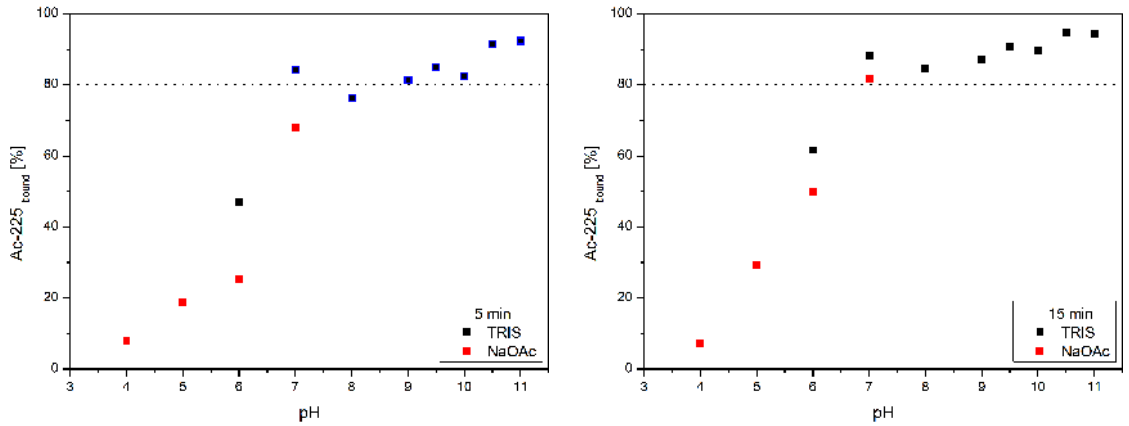

Figure 5.48: Yields of the Ac-225-DOTA-NCS-MabThera® labelling after 5 min (*left*) and 15 min (*right*) with respect to the pH.

concentration of $DOTA^{4-}$ present at pH 8 - 10, where the base-assisted dissociation of the last proton takes place (see paragraph 5.1). Assuming that competition from acetate buffer is not the only reason for the lengthy radiolabelling time reported by this group (30 - 60 min), the supremacy of the optimised protocol developed in the present work mainly constitutes on the more favourable alkaline conditions used for Ac-225-DOTA complexation.

Nonetheless, care has to be taken not to damage the sensitive antibody by applying too harsh conditions, since it will be denatured in too alkaline medium. The M(III)DOTA complex itself is expected to remain stable even after days at alkaline pH, as it has been demonstrated with Bi(III)DOTA at pH 10 [172]. The DOTA complexes are only found to dissociate via a H^+-assisted pathway in (strongly) acidic medium; hence spontaneous dissociation is negligible [164]. The suggested labelling pH of 8.5 - 9 (indicated by the pK_a/buffercapacity of TRIS), offering rapid labelling rates (Fig. 5.48), appears to be safe since it is commonly used for ligand-antibody-chelation and is thus known to be well-tolerated [6].

Besides this pH effect, the assumed pre-orientation of the acetate arms forced by the equatorial orientation of the NCS-mAb-chain (NMR and kinetic TRLFS studies with Cm(III)DOTA-NCS, paragraph 5.2.2), probably also contributes to the accelerated reaction rate of the Ac(III)DOTA complexation. Hence this may present another advantage of the implemented one-step protocol (complexation of Ac-225 by the DOTA-NCS-antibody conjugate) over the two-step protocol, in which the complexation is performed in a seperate step *before* the conjugation to the antibody is carried out subsequently [6].

In summary this all translates into the following refined one-step synthesis protocol:

- 150 µl 0.2 M TRIS buffer, pH 8.5-9
- 100 µg DOTA-NCS-MabThera® in 10 µl 0.15 M NaCl/0.05 M NaOAc buffer
- $\leq$50 µCi $^{225}Ac(NO_3)_3$, purified
- 5 - 15 min at 37 - 42 °C
- addition of AA after the reaction.

No negative effect was found for the stability of the radioconjugates emanating from radiolabellings conducted within 5 min instead of 15 min or at 37 °C instead of 42 °C or 45 °C, respectively. All these conjugates are equally stable, which is discussed in detail in the next paragraph. It is hence concluded that with purified Ac-225 effective, high-yield, high-SA radiolabelling of DOTA-NCS-MabThera® can be performed at moderate conditions of pH 9 and 37 - 42 °C within 5 minutes reaction time (yields > 94 %, RCP > 98 % after purification). A similar success has been reported by Smith-Jones *et al* for the labelling of In-111-DOTA-mAb-conjugates within 5 min at 37 °C, pH 7 [245]. A summary of average radiolabelling yield assessing this refined protocol is given in Table 5.21. Further studies were performed to prove the kinetic stability of the radioimmunoconjugates formed at 37 - 45 °C (see paragraph 5.4.4).

To exclude the possibility of unspecific binding of the Ac-225 to other metal binding sites besides DOTA on the mAb, radiolabelling of an unchelated antibody was tested following the described protocol, resulting in > 99 % of unbound activity.

At labelling temperatures of 90 °C but otherwise identical conditions, radiolabelling of DOTA-SubstanceP can also be accomplished following this protocol which provides improvements compared to the peptide-labelling protocol established in the preceding work [7].

Table 5.21: Average radiolabelling yields achieved for radiolabellings conducted according to the optimised protocol for the synthesis of Ac-225 labelled DOTA-chelated MabThera® with various specific activities. The reactions were conducted at pH 9 and 37, 42 or 45 °C.

Specific activity	*time [min]*	*n° of labellings*	*average yield*
5 µCi Ac-225 / 100 µg mAb	5	2	96.1
	15	8	94.3
10 µCi Ac-225 / 100 µg mAb	5	2	96.3
	15	6	96.0
20 µCi Ac-225 / 100 µg mAb	15	4	96.0
	60	2	95.5
30 µCi Ac-225 / 100 µg mAb	15	4	96.3
40 µCi Ac-225 / 100 µg mAb	15	2	95.1
50 µCi Ac-225 / 100 µg mAb	15	3	94.5

5.4.4 Evaluation of the Kinetic Stability of the Radioimmunoconjugates

Radiolabelled biomolecules must maintain the specified level of radiochemical purity and specific activity over the time period from labelling until administration. Therefore stability studies are conducted, whose results will define the expiry times for kits and radiolabelled mAbs.

To generally assess the kinetic stability of a radionuclide complex towards dissociation, so-called "challenge" experiments are accomplished. These experiments involve either additional ligands, competing for the formation of strong complexes with the radionuclide, or other metal cations, to which the coordinating ligand may preferably bind to. In case of DOTA-derived RIC, challenging experiments with an excess of other multidentate chelate ligands like EDTA and DTPA are of high interest, as well as with blood serum species like proteins, carbonate or metal cations

like Ca^{2+}, Na^{+}. A summary of these human blood components and their respective concentrations is given in Table 3.3, paragraph 3.8.

Before experiments with the active Ac(III)DOTA-NCS-mAb conjugates were started, an exemplary challenge study on the kinetic stability of the Cm(III)DOTA-NCS-mAb conjugate in presence of EDTA was performed. Since in the TRLFS spectra significantly different emission bands are found for Cm(III)EDTA, Cm(III)DOTA/Cm(III)DOTA-NCS-mAb and the Cm(III) aquo species, this method allows for quantification of each of these species in solution. However, the method is not suitable for investigation of dull liquids, which is why the stability of the Cm(III)DOTA-NCS-mAb in human blood serum (HBS) can not be studied with TRLFS.

5.4.4.1 Stability of Cm(III)DOTA-NCS-mAb in Presence of EDTA

Since EDTA is known to coordinate Cm(III) more strongly than serum proteins (e.g HSTF [290]), the TRLFS experiment was accomplished in "competing" buffer media (acetate, carbonate) and presence of EDTA (in excess) to substitute the HBS study.

Two samples were prepaired in 880 µl of 0.05 M NaOAc-buffer (pH 7.4) or 0.05 M Na_2CO_3-buffer (pH 8.5 - 9), respectively, by mixing of $1.2 \cdot 10^{-7}$ M Cm^{3+} with 180 µg of DOTA-NCS-MabThera® (in 20 µl 0.1 M NaCl/0.05 M NaOAc buffer, pH 7.4), which corresponds to a DOTA-NCS concentration of $5 \cdot 10^{-6}$- $7 \cdot 10$ M (4 - 6 Ch/mAb; Cm(III):DOTA-NCS∼1:50). The samples were warmed to 45 °C for 5 min, since under these conditions the complexation of An(III) with DOTA takes place rapidly and quantitatively as it was confirmed by preceding kinetic measurements (paragraph 5.2.2.1). It was also confirmed beforehand by TRLFS that unspecific binding of Cm(III) to other metal binding sites on the antibody conjugate except to DOTA-NCS does not occur (see Fig. 5.12, *bottom left*, paragraph 5.2.1.2), also not at neutral and alkaline conditions.

Afterwards, the solution was cooled to room tempearture and a defined starting quantity of EDTA ($2 \cdot 10^{-5}$ M), which was pre-examined to instantaneously coordinate Cm(III) at 25 °C, was added to prevent any dissociating Cm(III) from precipitating as hydroxide species or its adsorption to the glass cuvette. The total sample volume was 1 ml.

Over a period of 40 days, both samples were kept at 25 °C and were repeatedly measured with TRLFS to monitor potential changes in the emission spectra arising from dissociation of the Cm(III)DOTA-NCS-mAb conjugate, such as

- change of intensity of the Cm(III)DOTA-NCS-mAb emission band,
- the formation of Cm(III)-carbonate and -acetate species, or
- the appearance of a Cm(III)EDTA/Cm(III) aquo ion emission band, for instance.

Intermittently, after 10, 20 and 30 days, 200 µl of 10 mM EDTA were added to the reaction batches until a final excess of 1 : 1,000 of EDTA over DOTA was reached. The pH was readjusted if required. At the end of the observation period, the samples were filtrated using Amicon Millipore centrifugal filter devices (30 kDa pore size) which retain the antibody. It is expected that any Cm(III), which was released from the possibly instable Cm(III)DOTA-NCS-MabThera®, will pass through the filter in form of its carbonate, acetate or EDTA-complex. After filtration, the filtrate is

measured with TRLFS to check for emission bands which can be traced back to these complexes. The results of this kinetic stability study are displayed in Figure 5.51.

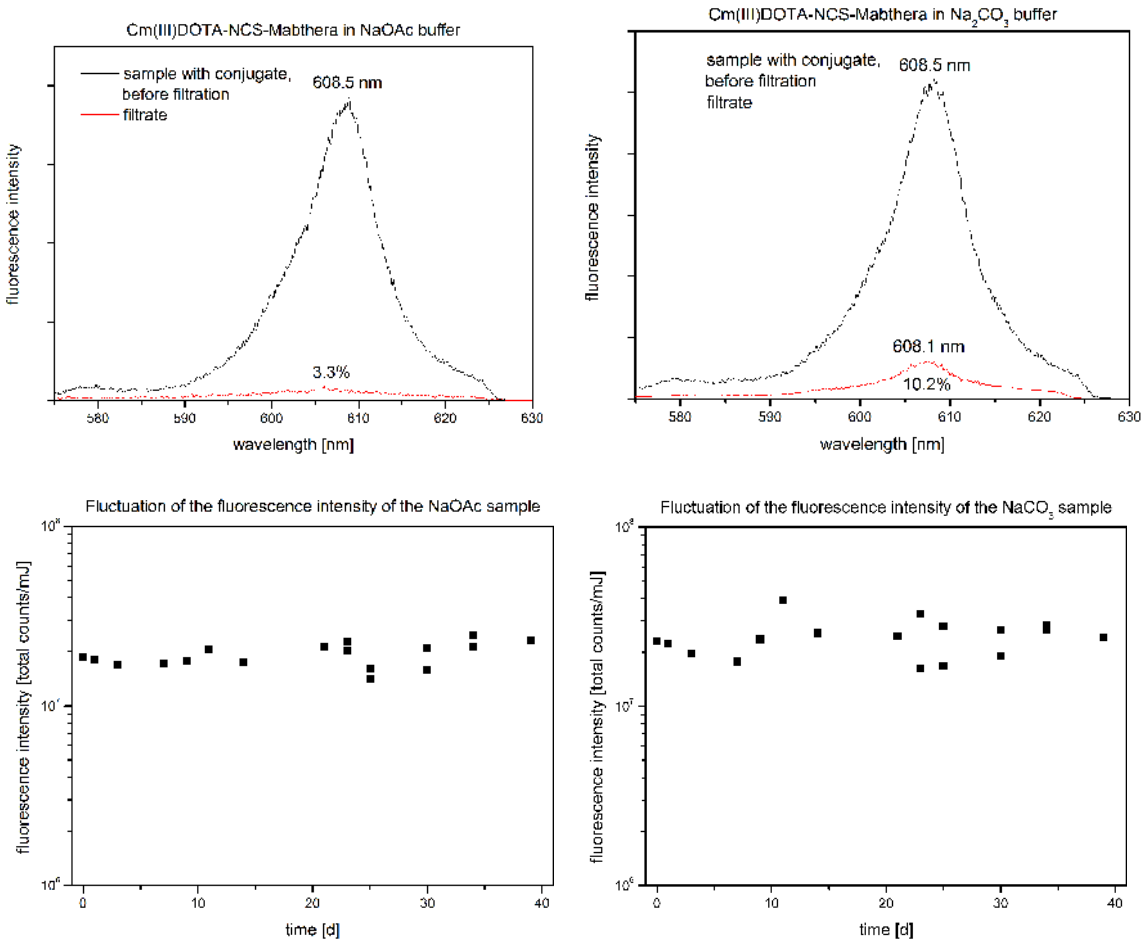

Figure 5.49: Stability study of Cm(III)DOTA-NCS-MabThera® in NaOAc - (*left*) and Na_2CO_3-buffer (*right*). The respective emission spectra (not normalised, *top row*) recorded before and after filtration of the samples only indicate a minimal loss of Cm(III) from the conjugate (*red*). The corresponding fluctuation of the fluorescence intensity of both samples (*bottom row*) remains roughly constant during the 40 days period.

5.4.4.2 Discussion

During 40 days no notable change in the fluorescence spectra of the Cm(III)DOTA-NCS-MabThera® was observed. As it is apparent from Figure 5.49, the average intensity of the emission band at 608.5 nm, representing the conjugate, remains unchanged, which indicates that all Cm(III) is retained. Also, no additional emission bands correlated to other Cm(III) species were detected.

In the fluorescence spectrum of the Na_2CO_3-sample filtrate (Fig. 5.49, *red*), a low-intensity emission band at ~608.1 nm was observed which probably results from the detachment of Cm(III)DOTA or Cm(III)DOTA-NCS from the antibody conjugate; in the filtrate of the NaOAc sample only traces of these species were found. From comparison of the total peak areas, a correlating loss of approx. 3 to 10 % of Cm(III) from the antibody was calculated, which, considering the 40 days period, is regarded as insignificantly small with respect

to the blood residence time of an IgG antibody. Though it appears that the thiourea bonds of the DOTA-NCS-MabThera®-conjugate are slightly more sensitive to cleavage at alkaline pH (carbonate sample), this is expected to have no significant effect on its kinetic stability at physiological pH (acetate sample).

To prove that, if Cm(III) was released from DOTA-NCS-MabThera®, rapid and quantitative complexation by EDTA would have occured, $Cm(ClO_4)_3$ was added to the EDTA containing filtrate of the Na_2CO_3 sample. The filtrate was immediately measured with TRLFS (25 °C, Fig. 5.50) and the obtained spectrum was compared with the emission spectrum of a pure Cm(III)EDTA sample. No emission bands besides the Cm(III)EDTA band were detected in the filtrate, except for the small shoulder at ~608 nm corresponding to the 10 % Cm(III)DOTA(-NCS) released from the antibody.

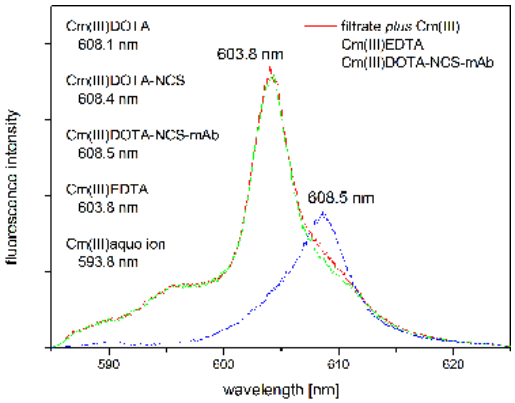

Figure 5.50: Emission spectra of the filtrate with additional Cm(III) (*red*) in comparison to the pure spectra of Cm(III)EDTA (*green*) and Cm(III)DOTA-NCS-MabThera® (*blue*). The maxima of the emission bands of other Cm(III) species which could have possible been formed are indicated on the left.

In summary it is deduced that the Cm(III)DOTA-NCS-MabThera® conjuagte is stable in presence of strong challenging ligands at physiological conditions (pH 7.4) as well as under pH-conditions applied for the Ac-225 radiolabellings (pH 9). This experiment forms the basis for further stability studies with the active Ac(III)DOTA-NCS-MabThera® conjugate.

5.4.4.3 Stability of the Ac(III)DOTA-NCS-mAb Conjugate in Presence of Challengers

To evaluate the kinetic stability of Ac-225-DOTA-NCS-MabThera® in presence of competing ligands, radiolabellings of the DOTA-chelated antibody (10 µCi (= 370 kBq) per 100 µg mAb) were conducted at pH 9 at temperatures of 37, 42 and 45 °C, respectively, as described in 4.9.1.1.

After the labellings (yields > 94 %), the pH was adjusted to physiological pH by addition of 20 % ascorbic acid. Aliquots of the reaction samples were then diluted 1 : 10 with 10 mM EDTA, 0.05 M Na_2CO_3 buffer or phosphate buffered saline (PBS), respectively, and incubated at 25 °C. The aliquots for testing of the stability in EDTA-added serum (DF = 1 : 10) were incubated at 37 °C. Over a period of 15 days, aliquots were withdrawn and analysed for the amount of Ac-225 still stably bound to the antibody (R_f = 0, ITLC-SG/0.05 M Na-citrate; γ-spectrometry). The experiments were paralleled by blank studies of pure Ac-225 in the respective medium (R_f = 0.9). The results of this stability study are summarised in Figure 5.51.

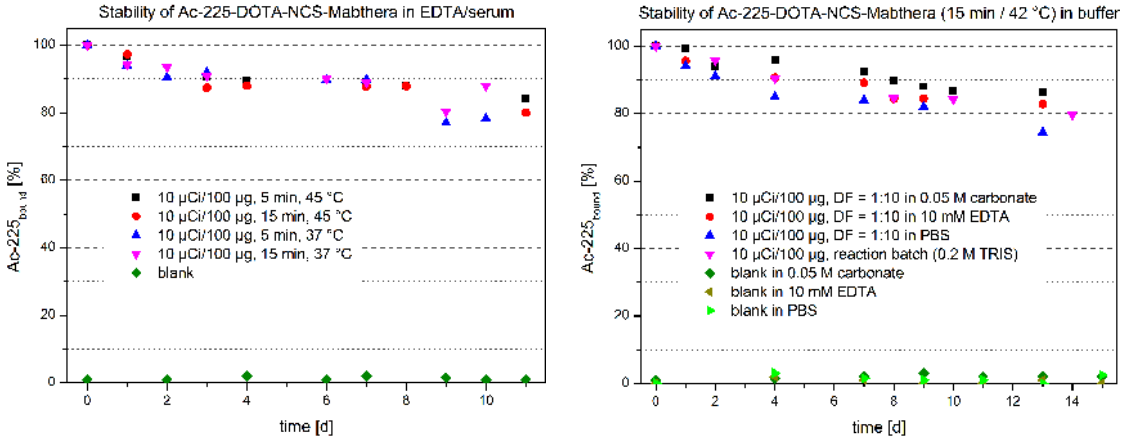

Figure 5.51: Stability study of Ac-DOTA-MabThera® in EDTA/serum (incubation at 37 °C, *left*) and in various buffer media (incubation at 25 °C, *right).*

5.4.4.4 Discussion

The stability curves in Figure 5.51 all show a consistent moderate decrease and appear to be independent from the labelling time and temperature at which the radioimmunoconjugate was formed (*left*: 5 min vs 15 min, 37 °C vs 45 °C; *right*: 42 °C), as well as to be largely unaffected by the medium (*left*: EDTA/serum; *right*: various buffers). The loss of -on average- 20 % of Ac-225 from the conjugate during 15 days is acceptable, since in medical applications the RIC is not expected to reside in the body for much longer time (elimination half-life of rituximab ∼3.2 d following the first infusion [291]); hence, the good results give reason for advanced studies in blood serum under physiological conditions.

5.4.4.5 Stability of the Ac-DOTA-NCS-mAb Conjugate at Physiological Conditions

For application of radioimmunoconjugates in nuclear medicine, it is essential that the radionuclide complex is kinetically stable under physiological conditions in human blood serum (HBS), so that it will not dissociate and lose the cytotoxic nuclide on its way to the target site. Generally, there are several compounds present in HBS that are able to challenge the radioconjugate and potentially form complexes with (dissociated) Ac-225 ("transchelation"), with human serum albumin (HSA) and carbonate being the most abundant competitors for DOTA (see Table 3.3). Stability studies of the Ac-225-DOTA-NCS-mAb conjugates in blood serum are therefore mandatory to estimate their biological serum half-lifes. Various M(III)DOTA complexes, i.a. the Y(III)DOTA/Gd(III)DOTA complex, were reported to undergo negligible dissociation in serum at pH 7 [168], and also the Ac-225-DOTA-HuM195-conjugate was previously reported to be stable in serum [60].

Several radiolabellings at 37, 42 as well as 45 °C were conducted following the optimised protocol (paragraph 4.9.1.1), with reaction times of 5 min or 15 min, respectively. The specific activities were in the range of 10 - 20 µCi (= 370 - 740 kBq) per 100 µg antibody. The reaction was halted after 5 or 15 min and the samples was purified with a PD10 desalting column if labelling yields were lower than 90 %. Ascorbic acid (20 %) was added and the pH of the solutions was adjusted to pH 7.4.

Aliquots of these solutions were then mixed with filtered, heparin-added serum (dilution 1 : 10 or 1 : 20, respectively) and incubated for 15 - 45 d at 37 °C in a humidified incubator with 5 % CO_2 atmosphere. Intermittently, aliquots of 20 µl were withdrawn from the samples, separated with ITLC (ITLC-SG/0.05 M Na-Citrate or 0.05 M EDTA) and measured via gamma spectrometry. For quantification, the ratio of labelled antibody conjugate and unbound radionuclide was calculated by expressing the corresponding activities as a percentage of the total activity on the ITLC plate. Any observed decrease of the stability curves is hence not related to the decay of the Ac-225 but originates from transchelation to serum proteins or from the loss of Ac-225 from the radioconjugate. The experiments were conducted with various radioimmunoconjugate preparations during the last three years and were all paralleled by a blank study of Ac-225 in HBS.

To quantify the influence of transchelation to serum proteins, in the recent stability studies the serum aliquots (20 µl) were incubated with 4 µl of 0.01 M DTPA for 15 min at 37 °C before separation with ITLC was performed [60]. DTPA is supposed to coordinate stronger to Ac-225 than the serum proteins; at the same time it is a weaker chelator than DOTA. Hence, when DTPA is added, transchelation of possibly protein-bound Ac-225 to DTPA will occur while the intact Ac-225-DOTA-NCS-mAb conjugates remain unaffected [257]. This was validated in preceding experiments with PD10 size exclusion chromatography.

A diminished but similar effect is achieved when EDTA is used as mobile phase during ITLC-SG separation. In both cases the Ac-225-EDTA/Ac-225-DTPA complex will travel with the solvent front ($R_f >> 0$) and is hence reliably separated from the Ac-255-DOTA-NCS-mAb-conjugate ($R_f = 0$) [60].

The results of the serum stability studies of the Ac-225-DOTA-NCS-MabThera® conjugates in serum are displayed in Figure 5.52. Some samples in the left diagram have not been incubated under physiolocigal conditions, but are still included for comparison. The samples in the right diagram were incubated in the humidified incubator at 37 °C in 5 % CO_2 atmosphere. A study on the stability of Ac-225-DOTATOC, conducted in our group [292], is included for comparison.

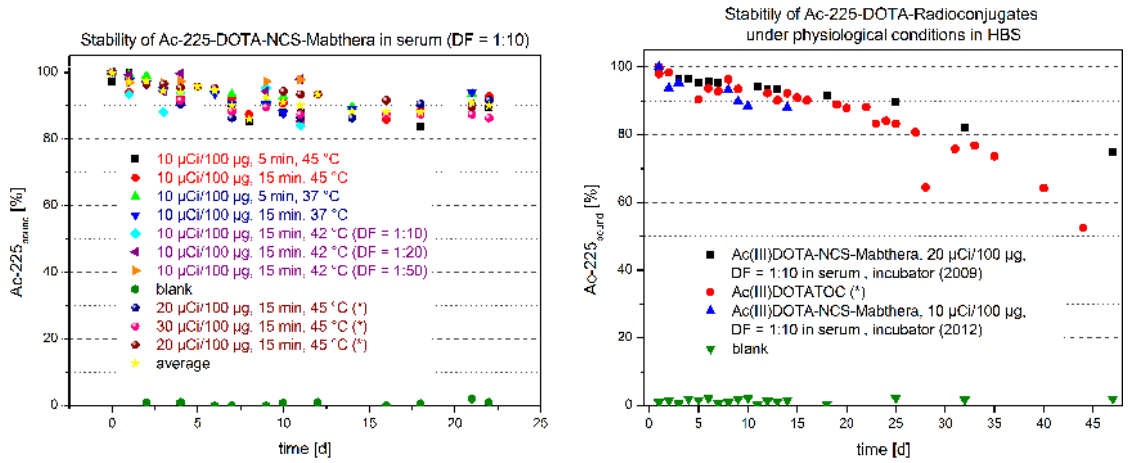

Figure 5.52: Serum stability of the Ac-225-radioconjugates in human blood serum. The samples indicated with (*) (*left diagram*) as well as all samples in the right diagram were incubated under physiological conditions. The stability study on Ac(III)DOTATOC was conducted by coworkers in our group (*right diagram*, *red* [292]).

5.4.4.6 Discussion

The general stability of Ac-225-DOTA-NCS-MabThera® in HBS is satisfying, with the stability curves showing only moderate decrease (Fig. 5.52). The serum stability appears to be largely independent from the selected radiolabelling conditions (37 - 45 °C, 5 - 15 min) and the final dilution factor in serum (1 : 10 - 1 : 50, Fig. 5.52, *left*). The experimental data shows a divergence of roughly ±3 - 6 % from the average value (plotted in *yellow*). For all data sets an average loss of 10 % of the original activity loaded onto the antibody conjugate was observed within the first 15 days, with an overall loss of less than 20 % during 30 days (= 3 half-lifes of Ac-225) under physiological conditions. This loss is comparable with what was reported by coworkers for the peptide conjugate Ac(III)DOTATOC (Fig. 5.52, *right*, *red* [292]). Hence, the investigated Ac-225-RIC is regarded as stable under serum conditions, and with 100 µg of antibody labelled with 10 - 20 µCi (= 370 - 740 kBq) of Ac-225, the specific activity of this conjugate is high enough to be considered for nuclear medicine applications.

From the curves it is evident that the labelling temperature has no influence on the kinetic stability of the final Ac-225-DOTA-NCS-mAb conjugate, since e.g. the graphs for 37 and 45 °C show no significantly different decrease (5.52, *left*, *red* and *blue*). For the same curves, this also applies with regard to the reaction time (5 and 15 min, respectively). It is hence concluded that a labelling temperature of 37 °C is sufficient to form a kinetically stable Ac-225-DOTA-NCS-immunoconjugate within only 5 min. This suggests that the alignment of the carboxylate arms of DOTA must be favourable for rapid complexation at 37 °C. As demonstrated by NMR and TRLFS (paragraph 5.2.2.3 ff), this pre-orientation is not only an effect of temperature but is likely to be also induced by conformational folding of the DOTA ring forced by the preferably equatorial positioning of the large protein chain attached to the ring. It is also apparent that no negative effect is observed when ascorbic acid is not present during the labelling but is only added afterwards. It was already proven in preceding experiments that AA is necessary to prevent middle-term radiolysis of the radioimmunoconjugate (paragraph 5.4.2.3), but since the labelling reaction is completed very rapidly (5 - 15 min), severe radiolytic damage is neither expected nor observed to occur during this short period of time.

Transchelation effects were only found to be of minor significance with the rigid macrocyclic DOTA complex. The experimental data derived from the DTPA-incubated samples fully complies with the data obtained without DTPA-incubation within the error range. Likewise, no difference was found if the ITLCs of the samples were developed with EDTA or Na-citrate. Nevertheless, incubation with DTPA is recommended to improve the reliability of the results, since it was found in prelimi nary experiments that to certain ITLC-papers serum protein-bound Ac-225 exhibits similar adsorption behaviour as the radiolabelled antibody conjugates. This causes false results, as like that the "dissociated-but-now-protein-bound Ac-225" contributes to the "stable Ac-225-antibody conjugate fraction"; thus, these two fractions need to be clearly distinguished.

5.4.4.7 The *in vitro* Serum Half-Life of Ac-225-DOTA-NCS-MabThera®

It is expected that the *in vivo* blood half-life of the Ac-225-DOTA-NCS-mAb conjugates is relatively long (2 - 3 d for e.g. HuM195 [113] up to 8 d for other IgG type

antibodies [182]). Due to the lack of transchelation of Ac-225 from the highly stable Ac(III)DOTA complex, the effective half-life will be mainly dictated by metabolism and the physical half-life of the radionuclide. In the case of Ac-225 the biological half-life of the antibody and the physical half-life ($t_{\frac{1}{2}} = 10.0$ d) are matched well [27], while e.g. for the more commonly used short-lived At-211 the physical $t_{\frac{1}{2}}$ (= 7.2 h) is much shorter than the biological $t_{\frac{1}{2}}$ of the RIC (for definition of the different half-lifes see 7.2 Glossary). The latter consequently demands more injections to maintain therapeutic blood-activity concentrations, which is associated with various side effects.

The curve of the serum stability plot under physiological conditons facilitates easy extrapolation of the biological half-life (*in vitro*) of the RIC in serum (Fig. 5.53) Thus, the effective *in vitro* serum half-life is calculated following the equations:

$$\frac{1}{t_{\frac{1}{2}}(eff)} = \frac{1}{t_{\frac{1}{2}}(phys)} + \frac{1}{t_{\frac{1}{2}}(bio)} , \tag{5.41}$$

with

$$t_{\frac{1}{2}}(bio) = \frac{ln2}{\lambda} . \tag{5.42}$$

For $\lambda = 0.0056$ (Fig. 5.53) and $t_{\frac{1}{2}}$(phys) = 10.0 d it follows that $t_{\frac{1}{2}}$(bio) = 123.8 d and for the effective serum half-life:

$$t_{\frac{1}{2}}(eff) = 9.3\, d . \tag{5.43}$$

As expected, the effective half-life is mainly influenced by the long half-life of the radionuclide and hence is with 9.3 d very similar to the physical half-life of Ac-225.

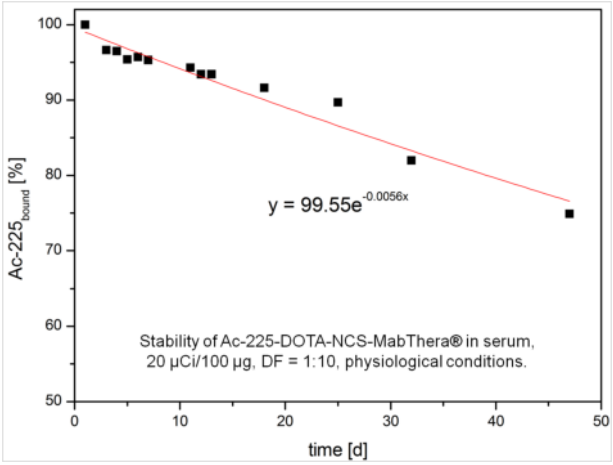

Figure 5.53: Diagram fitted for calculation of the biological half-life in blood serum from the stability curve of Ac-225-DOTA-NCS-MabThera®.

From the results of the *in vitro* serum studies under physiological conditions it is deduced, that DOTA is sufficiently strong to maintain the intergrity of Ac-225-DOTA-NCS-mAb-radioimmunoconjugates *in vitro* over the effective therapeutic lifetime of the conjugate.

The next step is the *in vitro* investigation of the radiobiological behaviour of the antibody towards tumour cells expressing the respective antigen. As MabThera® is specific for CD20, which is expressed with high frequency on most B-cell NHLs (see paragraph 3.6.4.2 for further details), the following cell binding study was carried out with the K422 lymphoma cell line.

5.4.5 First Assessment of the Radiobiological Behaviour of the Ac-225-DOTA-NCS-mAb Conjugate: Saturation Cell Binding Study

For successful binding of an antibody to its antigen, it is mandatory that the chemical integrity of the radiolabelled antibody is guaranteed. Any modification of the molecule structure, which entail altered antigen binding properties, e.g. inactivation of one antigen binding site in case of too high Ch/mAb ratios [293], will impair the affinity and hence effectivity of the antibody-antigen interaction. It is thus crucial to select labelling- and purification conditions which cause no damage to these sensitive biomolecules when developing a radiolabelling protocol for antibodies. In the previous experiments it was demonstrated and evaluated that the synthesis of thermodynamically and kinetically stable Ac-225-labelled DOTA-derived radioimmunoconjugates can be accomplished at mild conditions (T = 37 - 42 °C, 5 - 15 min, pH 9). However, this radiolabelling protocol is not applicable if it turns out to negatively affect the antibodies binding performance. To assess this issue, an *in vitro* cell binding study was conducted according to common standard procedures [294, 193]. With the obtained experimental data, quantification of the cell binding of the RIC by analysis of a saturation binding plot is feasible.

The study was accomplished by incubating the labelled conjugate with excess antigen binding sites as described in paragraph 4.9.4. The RIC was synthesised according to the optimised protocol (15 min at 42 °C, paragraph 4.9.1.1) with a specific activity of 1 µCi (= 37 kBq) per 100 µg antibody. The purification step by PD10-SEC was skipped since the radiolabelling yields were above 92 %, which is sufficient for the intended purpose. The sample was diluted with PBS to obtain a total volume of 2 ml. The pH was tested to be pH 7.4. Overall, the synthesis and preparation of the radioimmunoconjugate in the described way can be completed within 20 min (without purification) to 30 min (with purification).

Defined volumes of the prepared RIC solution were then added to nine cell samples each containing a fixed number of $1 \cdot 10^6$ cells/ml in fresh cell medium, which have been prepared and aliquoted shortly before the radiolabelling. After incubation at 37 °C for ∼60 min (humidified incubator), the samples were centrifuged, the supernatant removed and the cell pellets washed thoroughly with PBS. All washing solutions, the supernatant and the pellets were then measured by gamma spectrometry. The binding affinity is determined from the ratio of activity found in the cell pellet, which corresponds to the bound radioimmunoconjugate fraction, relative to the total activity found in all solutions. In a preceding study, the kinetic stability of the RIC was successfully tested in the applied cell culture media for 18 h to confirm that the radionuclide remains stably attached to the mAb under the conditions of the cell binding study.

The results of the cell binding study are plotted in the following graph (Fig. 5.54). From the nonlinear regression fit of the plot, the binding affinity K_d as well as the maximum number of binding sites B_{max} can be calculated according to:

$$y = \frac{B_{max} \cdot x}{K_d + x} \,. \tag{5.44}$$

The calculations are based on the equilibrium for a simple bimolecular reaction

$$antigen + Ac-225-antibody \rightleftharpoons antigen \cdots Ac-225-antibody \,, \tag{5.45}$$

with K_a for the association constant and K_d for the dissociation constant being

$$K_a = \frac{[antigen \cdots Ac-225-antibody]}{[antigen] \cdot [Ac-225-antibody]} = -\frac{1}{K_d}\,, \tag{5.46}$$

assuming that

- all antigens are equally accessible to the Ac-225-antibody,
- all antigens are either free or bound to the Ac-225-antibody (partial binding is not allowed),
- the binding does not alter the Ac-225-antibody or the antigen and
- the binding is reversible.

The Scatchard plot is a linear transformation of the experimental cell binding data. Here, the ratio of bound over free Ac-225-antibody is plotted on the y-axis and the molar concentration of bound antibody on the x-axis (Fig. 5.54, *inset*). The x-intercept represents the maximum number of binding sites B_{max} (specific binding extrapolated to very high concentrations of RIC), from which the number of binding antigens (ag) per cell is obtained. From the slope of the Scatchard plot, the binding affinity K_a is derived as well as the dissociation constant K_d, which equals the Ac-225-antibody concentration that binds to half of the antigen sites at equilibrium (for further information see 7.2 Glossary) [293]. This dissociation constant indicates the strength of the antigen-antibody binding with respect to how easy it is to separate the antigen-antibody-complex. If high concentrations of antibody and antigen are required to form that complex, this indicates that the binding strength is low and results in K_d being high (mM rather than nM). It follows that the smaller K_d is, the stronger is the binding.

Since the Scatchard transformation distorts the experimental error (x value is used to calculate the y value) and hence violates the assumptions of linear regression, more accurate results are obtained from the nonlinear regression fit (Fig. 5.54) of the experimental data [242].

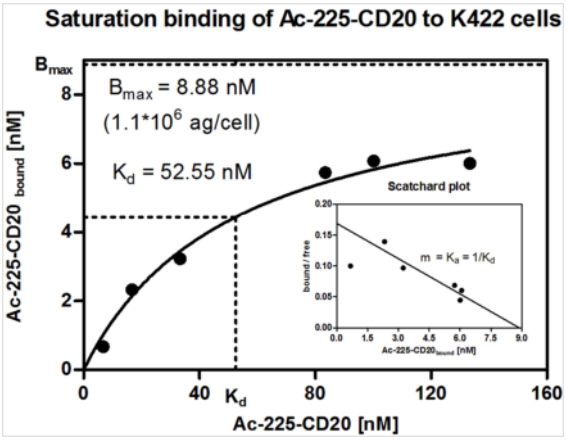

Figure 5.54: Saturation binding curve for Ac-225-DOTA-NCS-MabThera® (SA = 1 µCi/100µg mAb) incubated with K422 lymphoma cells; *graph*: experimentally determined binding curve; *inset*: correlating linear Scatchard plot. The K_d and B_{max} are given in nM and corresponding antigens/cell, respectively. The graph was generated with GraphPad Prism 5 [295].

5.4.5.1 Discussion

The presented binding study of the Ac-225-labelled anti-CD20-antibody MabThera® to the CD20 expressing K422 lymphoma cells was successful. The B_{max} value is 8.88 nM; this denotes that approximately $1.1 \cdot 10^6$ molecules of radiolabelled antibody are bound to $1.1 \cdot 10^6$ antigens per cell at saturation. The determined binding affinity with a K_d of 52.55 nM is small but a factor of 10 lower than the reported binding affinity for naked rituximab to CD20 (approx. 5 nM) [193]. Still, a K_d as derived in the present study incidates rather strong binding, which gives rise to further *in vitro* studies.

Since so far this cell binding experiment was only accomplished once and with low specific activity, the results have to be considered as only preliminary. To ultimately prove the preserved antibody's antigen binding affinity, the cell binding study needs to be repeated several times with clinically relevanct SA of at least up to 10 µCi (= 370 kBq) per 100 µg mAb, paralleled by evaluation of the cytotoxicity of Ac-225-DOTA-NCS-MabThera®.

6 Summary, Conclusion and Outlook

6.1 Summary and Conclusion

For successful application of α-emitters in radioimmunotherapy, profound understanding of the coordination chemistry of the respective system is of peculiar importance to develop protocols for the synthesis of radioimmunoconjugates. The scope of the presented PhD thesis was therefore the experimental characterisation and evaluation of 1,4,7,10-tetraazacyclododecane-1,4,7,10-tetraacetic acid (DOTA) as a suitable chelator for Ac(III) and hence its applicability for the synthesis of thermodynamically and kinetically stable Ac-225-radioimmunoconjugates. For recapitulation, the experimental approach is illustrated by the following graph:

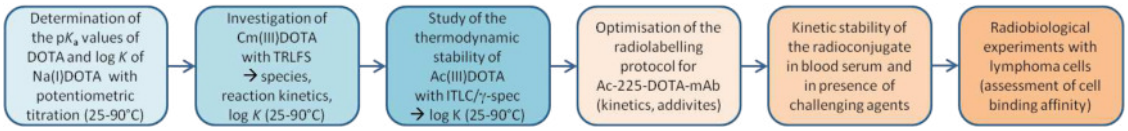

6.1.1 Potentiometry

Basis for the calculation of all thermodynamic parameters is the knowledge of the four acid dissociation constants p$K_{a,n}$ of the H_4DOTA ligand, which have therefore been determined in the temperature range between 25 °C and 90 °C by means of potentiometric titration and subsequent fitting of the experimental data points with Fiteql 4.0 (paragraph 5.1.1 ff). The obtained p$K_{a,n}$ values exhibit a decreasing trend with increasing temperature and are in accordance with the data reported for DTPA and TETA [260, 259]. The thermodynamic parameters $\Delta_R G$, $\Delta_R H$ and $\Delta_R S$ for the stepwise proton dissociation of the macrocyclic DOTA were also calculated and compared with the values reported for its open-chain analogue DTPA. The data are summarised in Table 6.1. As in the case of DTPA, the protonation reactions of DOTA are all exothermic ($\Delta_R H < 0$) and are promoted by favourable entropic factors ($\Delta_R S > 0$).

Since all thermodynamic experiments were carried out in 0.1 M $NaClO_4$ medium, and since it is known that especially the first two protonation constants assigned to the amino groups are sensitive to the influence of the background electrolyte, simultaneously to the p$K_{a,n}$ values in $NaClO_4$ the p$K_{a,n}$ values in $TMAClO_4$ were determined. They were found to be consistent with the literature, with particularly the value for pKa_1 being significantly increased in the latter medium ([165, 162, 266, 11], paragraph 5.1.4). In addition, the corresponding log K values for Na(I)DOTA at 45 - 90 °C were identified and the complexation was characterised as an exothermic reaction ($\Delta_R H < 0$, paragraph 5.1.3).

Both data sets allow for appropriate accounting for the disturbing interaction of Na^+ with DOTA as well as for the accurate calculation of the concentration of reactive $DOTA^{4-}$ species in all subsequent thermodynamic experiments and calculations (Table 6.4).

Table 6.1: Thermodynamic data for the protonation of H_4DOTA in 0.1 M $NaClO_4$and in Na-free medium obtained in this work, in comparison to data for H_5DTPA (1.05 M $NaClO_4$[260]). For DOTA, the $\Delta_R H$, $\Delta_R S$ values in brackets represent the results for the sodium-free conditions, the values indicated with asterisk represent the standard data at I = 0.

equilibrium	*T* [°C]	*pka* $NaClO_4$	*pka* "Na-free"	*pka* $I = 0$	$\Delta_R H$ [kJ/mol]	$\Delta_R S$ [J/(mol·K)]
$H^+ + DOTA^{4-} \rightleftharpoons HDOTA^{3-}$	25	9.31±0.04	12.35±0.04	13.33±0.04		
	45	9.09±0.04	12.05±0.04	13.07±0.04		
	60	8.84±0.04	11.75±0.04	12.80±0.04	-28.1±1.4	85±4
	70	8.70±0.06	11.55±0.06	12.62±0.06	(-34.9±1.5)	(120±5)
	80	8.47±0.06	11.32±0.06	12.42±0.06	-30.4±1.2 *	154±4.3 *
	90	8.52±0.07	11.36±0.07	12.48±0.07		
$H^+ + HDOTA^{3-} \rightleftharpoons H_2DOTA^{2-}$	25	9.14±0.03	9.15±0.03	9.88±0.03		
	45	8.94±0.03	8.93±0.03	9.69±0.03		
	60	8.71±0.03	8.72±0.03	9.51±0.03	-27.8±2.3	82±7
	70	8.44±0.05	8.44±0.05	9.24±0.05	(-26.2±1.7)	(88±5)
	80	8.27±0.04	8.40±0.04	9.22±0.04	-22.8±1.7 *	113±5.2 *
	90	8.43±0.08	8.43±0.08	9.27±0.08		
$H^+ + H_2DOTA^{2-} \rightleftharpoons H_3DOTA^{-}$	25	4.41±0.03	4.41±0.03	4.90±0.03		
	45	4.55±0.03	4.55±0.03	5.06±0.03		
	60	4.24±0.03	4.24±0.03	4.76±0.03	-1.6±2.2	80±7
	70	4.46±0.04	4.46±0.04	5.00±0.04	(-2.0±2.2)	(78±7)
	80	4.41±0.05	4.41±0.05	4.96±0.05	0.3±2.2 *	95±6.7 *
	90	4.39±0.06	4.37±0.06	4.93±0.06		
$H^+ + H_3DOTA^{-} \rightleftharpoons H_4DOTA$	25	4.18±0.02	4.18±0.02	4.42±0.02		
	45	4.14±0.02	4.14±0.02	4.39±0.02		
	60	3.95±0.03	3.95±0.03	4.21±0.03	-3.3±1.2	68±4
	70	4.00±0.03	4.00±0.03	4.27±0.03	(-3.4±1.3)	(68±4)
	80	3.99±0.04	3.99±0.04	4.26±0.04	-6.5±0.6 *	63±1.7 *
	90	3.83±0.05	3.83±0.05	4.11±0.05		

equilibrium	*T* [°C]	*pka*	$\Delta_R H$ [kJ/mol]	$\Delta_R S$ [J/(mol·K)]
$H^+ + DTPA^{5-} \rightleftharpoons HDTPA^{4-}$	10	9.73	-26.2	93
	25	9.43		
	40	9.29		
	70	8.91		
$H^+ + HDTPA^{4-} \rightleftharpoons H_2DTPA^{3-}$	10	8.50	-26.4	69
	25	8.26		
	40	8.05		
	70	7.84		
$H^+ + H_2DTPA^{3-} \rightleftharpoons H_3DTPA^{2-}$	10	4.38	-11.6	42
	25	4.23		
	40	4.20		
	70	4.26		
$H^+ + H_3DTPA^{2-} \rightleftharpoons H_4DTPA^{-}$	10	2.53	-0.8	46
	25	2.56		
	40	2.60		
	70	2.67		
$H^+ + H_4DTPA^{-} \rightleftharpoons H_5DTPA$	10	2.51	1.4	51
	25	2.37		
	40	2.32		
	70	2.48		

Furthermore, the calculation of the temperature-dependent species distribution of the various $H_xDOTA^{(4-x)-}$species (x = 0-4) gives indication for pH- and temperature conditions suitable for rapid radiolabelling of DOTA-chelated peptides / antibodies (paragraph 5.1.5). Since radiolabelling is expected to be more efficient the higher the ratio of the most reactive species ($DOTA^{4-}$) is, alkaline pH conditions (pH 9, [7]) are suggested to be favourable over acidic conditions (pH 5.5, [6]), eventually offering the possibility of using decreased temperature to achieve optimal labelling.

6.1.2 Cm(III)DOTA - TRLFS

For a first assessment of the thermodynamic properties of An(III)DOTA complexes, the complexation mechanism, kinetic rates and particularly the thermodynamic stability and properties of Cm(III)DOTA, as surrogate complex for Ac(III)DOTA, were investigated with TRLFS at elevated temperatures up to 90 °C (paragraph 5.2).

6.1.2.1 Cm(III) Species

Initially, the various solvated Cm(III)- and Cm(III)-DOTA species formed in the course of the complexation were characterised in H_2O and D_2O by fluorescence lifetime measurements, which gave information about the first coordination sphere of the metal cation (paragraph 5.2.1.1 ff, Table 6.2). In low-temperature experiments (5 - 10 °C, paragraph 5.2.1.4 and 5.2.1.6) applying DOTA and DOTA-NCS, an intermediate species, which has not been described before, was observed and characterised. The short lifetime and the shift of the emission band, which is roughly comparable to the shift induced by two carboxylate groups [123], indicate that in this species Cm(III) is presumably coordinated by only two acetate arms of DOTA. The findings were supported by investigation of the corresponding Eu(III) species and compared with correlated literature (paragraph 5.2.1.5). It is concluded that the ensuing rearrangement of the two non-coordinating acetate arms is the rate-determining step of the complexation, with the metal cation subsequently becoming fourfold coordinated and being rapidly drawn into the ring to experience full coordination by DOTA. Investigations of the reaction kinetics at different temperatures also proved the formation of this intermediate Cm(III)DOTA species, which transformed into the final complex during the measurements (paragraph 5.2.2.1).

6.1.2.2 Reaction Kinetics

In nuclear medicine, protocols for radiolabelling of biomolecules need to allow for facile and time-optimised synthesis of the drug, which is why the pH-dependent formation rates of the Cm(III)DOTA and Cm(III)DOTA-NCS comlexes were determined in the labelling-relevant temperature range up to 93.5 °C (paragraph 5.2.2.1 ff and 5.2.2.5 ff). A summary of the kinetic properties of the Cm(III)DOTA and Cm(III)DOTA-NCS complex formation is given in Table 6.3. By applying the Arrhenius and Eyring equations to the experimental data, the activation parameters for the reaction were calculated (paragraph 5.2.2.8 ff).

The obtained rate constants for the complex formation at different reaction temperatures show a clear trend with the reaction proceeding much faster at higher temperatures, reflecting enhanced ligand flexibility which permits more rapid rearrangement of all four acetate arms of the macrocycle (paragraph 5.2.2 ff). By

Table 6.2: Spectroscopic properties of various Cm(III)- and Eu(III) species investigated in the present work in comparison with literature data for Eu(III)DOTA.

Species	λ *[nm]*	*FWHM [nm]*	τ *[µs]*	ν *[cm^{-1}]*	$\Delta\nu$	*n(H_2O)*	*CN_{DOTA}*	*CN_{calc} [272]*
$[Cm(H_2O)_9]^{3+}$	593.8	7.8	68.4	16840.7	0	8.7±0.5	0	n.a.
$[Cm(H_2O)_9]^{3+}$[119]	593.8	7.7	65	16840.7	0	9±0.5	0	n.a.
$[Cm(D_2O)_9]^{3+}$	593.8	-	1158	16840.7	0	-	0	n.a.
$[Cm(DOTA)(H_2O)]^-$	608.1	6.1	278	16445.2	395.5	1.5±0.5	8	n.a.
$[Cm(DOTA)(D_2O)]^-$	608.1	-	787	16444.7	396	-	8	n.a.
$[Cm(DOTA\text{-}NCS)(H_2O)]^-$	608.4	6.3	284	16436.6	404.1	1.4±0.5	8	n.a.
$[Cm(DOTA\text{-}NCS)]_X$-mAb	608.5	6.2	312	16433.9	406.8	1.2±0.5	8	n.a.
Cm(III)intermediate	598.8	n.a.	86.3	16700.1	140.6	6.8±0.5	2	n.a.
$[Eu(H_2O)_9]^{3+}$[272]	578.8	-	-	17276.0	0	-	0	0.93
$[Eu(DOTA)(H_2O)]^-$	579.8	0.54	-	17247.0	29.0	-	8	7.50
$[Eu(DOTA)(H_2O)]^-$[8]	579.8	-	-	17247.0	29.0	-	8	7.50
Eu(III)intermediate	579.1	0.61	-	17268.2	7.8	-	2	2.48
Eu(III)intermediate [8]	579.2	-	210	17265.2	10.8	4.5±0.5	"4"	3.19

means of NMR it was demonstrated that this is associated with a conformational rearrangement of the cyclododecane ring, which is favoured by elevated temperature ($>$ 60 °C) and deprotonation of the amino groups in the alkaline pH region (paragraph 5.2.2.3 ff). Other factors influencing the reaction kinetics were found to be steric hinderance, which in the case of DOTA-NCS slowed down the reaction rates relatively to DOTA, and ligand pre-organisation, as it was proven for Cm(III) with temperature-processed, and thus probably pre-oriented DOTA-NCS. For the latter, accelerated complex formation kinetics were found due to lowering of the total energy barrier for the complex formation, since by equatorial orientation of the *p*-SCN-Bn-chain, acting as a lever, the actetate arms of DOTA are probably forced into suitable pre-arrangement on one side of the ring. This is also reflected in a lowered activation energy and enthalpy which allow the complexation to proceed readily. In conclusion, it was demonstrated that, besides on increased concentration of the reactive $DOTA^{4-}$ species at alkaline conditions (refer to paragraph 6.1.1), rapid complexation is especially dependent on the conformation of the DOTA / DOTA-NCS ring. The described effect is suggested to be the reason for efficient Ac-225-labelling of the DOTA-chelated antibody rapidly taking place also at rather low temperatures (37 - 42 °C).

6.1.2.3 Thermodynamic Stability

For determination of the complex stability constants of Cm(III)DOTA, an experimental batch setup was chosen which allowed for adjusting the concentration of the reactive DOTA species by variation of the pH of the reaction (paragraph 5.2.2.11 and 5.2.3.1). The stability constants log K at elevated temperatures (45 - 90 °C, paragraph 5.2.3.2 ff) were directly determined from the peak-deconvoluted spectra and were, together with the formation of the 1 : 1 complex, evaluated for reliability by slope analysis and thermodynamic modelling (PHREEQC, paragraph 5.2.3.6 ff).

Table 6.3: Kinetic data for the formation of Cm(III)DOTA and Cm(III)DOTA-NCS (pH 2.9, 0.1 M $NaClO_4$). Except for processed pDOTA-NCS, the parameters *k, A,* E_a, $\Delta_R H^{\ddagger}$, $\Delta_R S^{\ddagger}$, $\Delta_R G^{\ddagger}_{25°C}$ are presented as average values from the experiments conducted in the present work. The errors reflect the standard deviation.

Ligand	*T* [°C]	*k* [1/s]	*A* [1/s]	E_a [kJ/mol]	$\Delta_R H^{\ddagger}$ [kJ/mol]	$\Delta_R S^{\ddagger}$ [J·mol^{-1}·K^{-1}]	$\Delta_R G^{\ddagger}_{25°C}$ [kJ/mol]
DOTA	25	0.9±0.1	$4{\cdot}10^{18}$	106.3±0.1	103.0±0.7	100.2±4.6	73.1±0.6
	30	2.5					
	35	2.6±0.2					
	45	12.8±6					
	55	28.5±0.7					
	60	122					
	65	121.3					
	75	471.1±100.1					
	85	1011.1					
	90	1080					
	93.5	2183.9					
DOTA-NCS	25	0.1	$6{\cdot}10^{24}$	146.8±4.1	144.2±4.2	219.3±15.2	78.8±0.3
	30	0.15					
	35	0.9					
	45	5.5±0.5					
	55	25.5					
	60	48					
	75	228					
	90	810					
pDOTA-NCS	25	0.6	$7{\cdot}10^{18}$	110.4±6.4	107.7±6.5	106.09	76.07
	30	0.5					
	45	5					
	60	44					
	75	224					
	90	600					

By application of the van't Hoff law, the temperature dependence of the K values was utilised to extrapolate the log $K_{(I\,=\,0)}$ value at 25 °C to be 22.0±0.4 (paragraph 5.2.3.4 ff). In addition, the thermodynamic parameters $\Delta_R G$, $\Delta_R H$ and $\Delta_R S$ of the complex formation were obtained from the Gibbs Helmholtz relation, indicating an exergonic reaction ($\Delta_R G < 0$) which is driven by entropic factors. The complexation is endothermic as the log K values were found to increase with temperature. This complies with the prediction for electrostatic interactions being charcterised by $\Delta_R H > 0$ [259] and also accords to the findings from the kinetic experiments, which proved that the complex formation reaction is favoured by heating (refer to paragraph 6.1.2.2).

All thermodynamic data derived for the An(III)DOTA complexes investigated in the present work are summarised in Table 6.4. Available literature data for some Ln(III)DOTA and An(III)DOTA complexes are included for comparison. Standard data is summarized in Table 6.5.

Table 6.4: Thermodynamic data for Na(I)DOTA, Cm(III)DOTA and Ac(III)DOTA obtained in this work (p.w.) in comparison with literature data for comparable Ln(III)DOTA and An(III)DOTA complexes. All constants are valid for I = 0.1 M if not stated otherwise.

cation	*ligand*	*conditions (0.1 M)*	*log K*	$\Delta_R H$ *[kJ/mol]*	$\Delta_R S$ *[J·mol^{-1}·K^{-1}]*	$\Delta_R G$ *[kJ/mol]*	*reference*
Na^+	DOTA	25 °C, TMACl	4.2, 4.03	-	-	-	[5, 142]
Na^+	DOTA	25 °C, $NaClO_4$	4.1±0.1	-7.0±0.7	54.8±2.2	-23.4±1.5	p.w.
Na^+	DOTA	45 °C, $NaClO_4$	4.0±0.03				p.w.
Na^+	DOTA	60 °C, $NaClO_4$	3.98±0.04				p.w.
Na^+	DOTA	70 °C, $NaClO_4$	3.91±0.05				p.w.
Na^+	DOTA	80 °C, $NaClO_4$	3.89±0.04				p.w.
Na^+	DOTA	90 °C, $NaClO_4$	3.89±0.07				p.w.
Cm^{3+}	DOTA	25 °C, $NaClO_4$	19.0±0.4	58.2±6.6	588.2±20.0	-108.3±13.7	p.w.
Cm^{3+}	DOTA	45 °C, $NaClO_4$	19.6±0.4				p.w.
Cm^{3+}	DOTA	60 °C, $NaClO_4$	20.0±0.4				p.w.
Cm^{3+}	DOTA	70 °C, $NaClO_4$	20.5±0.4				p.w.
Cm^{3+}	DOTA	80 °C, $NaClO_4$	20.3±0.4				p.w.
Cm^{3+}	DOTA	90 °C, $NaClO_4$	20.9±0.4				p.w.
Cm^{3+}	DOTA	25 °C, "Na-free"	22.0±0.4	49.8±5.0	588.9±15.0	-125.8±10.6	p.w.
Cm^{3+}	DOTA	45 °C, "Na-free"	22.6±0.4				p.w.
Cm^{3+}	DOTA	60 °C, "Na-free"	22.9±0.4				p.w.
Cm^{3+}	DOTA	70 °C, "Na-free"	23.3±0.4				p.w.
Cm^{3+}	DOTA	80 °C, "Na-free"	23.2±0.4				p.w.
Cm^{3+}	DOTA	90 °C, "Na-free"	23.7±0.4				p.w.
Cm^{3+}	DOTA	25 °C, $NaClO_4$	24.02±0.11	-	-	-	[126]
Am^{3+}	DOTA	25 °C, $NaClO_4$	23.95±0.09	-	-	-	[126]
Eu^{3+}	DOTA	20 °C, 1 M NaCl	28.2	-	-	-	[276]
Eu^{3+}	DOTA	25 °C, 1 M KCl	23.5	-	-	-	[161]
Eu^{3+}	DOTA	25 °C, $NaClO_4$	23.95±0.1	-	-	-	[126]
Eu^{3+}	DOTA	37 °C, 1 M NaCl	23.7	-	-	-	[160]
Eu^{3+}	DOTA	(60 °C), KCl	23.50	-	-	-	[275]
Eu^{3+}	DOTA	(70 °C), KCl	26.2±0.1	-	-	-	[9]
Ac^{3+}	DOTA	25 °C, $NaClO_4$	19.4±0.4	14.0±0.7	361.6±2.1	-93.9±2.1	p.w.
Ac^{3+}	DOTA	45 °C, $NaClO_4$	16.6±0.4				p.w.
Ac^{3+}	DOTA	60 °C, $NaClO_4$	16.7±0.4				p.w.
Ac^{3+}	DOTA	70 °C, $NaClO_4$	17.5±0.4				p.w.
Ac^{3+}	DOTA	80 °C, $NaClO_4$	16.8±0.4				p.w.
Ac^{3+}	DOTA	90 °C, $NaClO_4$	16.9±0.4				p.w.
Ac^{3+}	DOTA	25 °C, "Na-free"	19.5±0.4	5.8±0.9	393.3±2.6	-111.4±2.4	p.w.
Ac^{3+}	DOTA	45 °C, "Na-free"	19.6±0.4				p.w.
Ac^{3+}	DOTA	60 °C, "Na-free"	19.6±0.4				p.w.
Ac^{3+}	DOTA	70 °C, "Na-free"	20.3±0.4				p.w.
Ac^{3+}	DOTA	80 °C, "Na-free"	19.7±0.4				p.w.
Ac^{3+}	DOTA	90 °C, "Na-free"	19.7±0.4				p.w.
La^{3+}	DOTA	25 °C, KCl	21.7±0.1	-	-	-	[134]
La^{3+}	DOTA	25 °C, KCl	22.9	-	-	-	[275]
La^{3+}	DOTA	25 °C, KCl	24.2±0.2	-	-	-	[9]
La^{3+}	DOTA	37 °C, 1 M NaCl	20.7	-	-	-	[160]

Table 6.5: Thermodynamic standard data for Na(I)DOTA, Cm(III)DOTA and Ac(III)DOTA obtained in the present work (I = 0)

cation	*ligand*	*T [°C]*	*log K_0*	$\Delta_R H^0$ *[kJ/mol]*	$\Delta_R S^0$ *[J·mol^{-1}·K^{-1}]*	$\Delta_R G^0$ *[kJ/mol]*
Na^+	DOTA	25 °C	5.08±0.03	-2.6±0.9	88.4±2.6	-28.4±1.8
		45 °C	5.02±0.03			
		60 °C	5.03±0.04			
		70 °C	4.98±0.05			
		80 °C	4.99±0.04			
		90 °C	5.01±0.07			
Cm^{3+}	DOTA	25 °C	24.9±0.4	66.9±5.2	700.1±15.6	-141.8±11.2
		45 °C	25.6±0.4			
		60 °C	26.0±0.4			
		70 °C	26.5±0.4			
		80 °C	26.5±0.4			
		90 °C	27.1±0.4			
Ac^{3+}	DOTA	25 °C	22.4±0.4	22.7±0.8	504.4±2.5	-127.7±2.6
		45 °C	22.6±0.4			
		60 °C	23.4±0.4			
		70 °C	22.9±0.4			
		80 °C	23.0±0.4			
		90 °C	23.1±0.4			

6.1.3 Ac(III)DOTA

Based on the results and experiences gathered from the TRLFS experiments on Cm(III)DOTA, the batch experiments to determine the complex stability constants log K were replicated with the Ac(III)DOTA system. Speciation studies in the temperature range of 45 - 90 °C were carried out with radio-ITLC and subsequent data extrapolation according to van't Hoff allowed for determination of the log $K_{(I = 0)}$ at 25 °C to be 19.5±0.4. This value is in good agreement with what has been predicted in previous work (PHREEQC: log K ∼19.8 [7], paragraph 5.3.2 ff) and is expected to be sufficiently high for the Ac-225-DOTA complex to remain stable in HBS (log $K > 19$, [221]). The experimental results were again assessed with slope analysis and computed modelling (paragraph 5.3.2.2 ff). The data is summarised in Table 6.4.

The stability constants for Ac(III)DOTA are smaller than for Cm(III)DOTA, but were also found to increase with temperature. In comparison to the literature values, the stability constants obtained for the An(III)DOTA complexes are reasonable, with the constants being a little smaller than what was reported for Ln(III)DOTA (Fig. 6.1). The trends observed for the log K values for the different M(III)DOTA complexes are traced back to the linear dependence of the log K upon ionic radius[88, 280]. The difference between the log $K_{25°C}$ for Ac(III)DOTA (19.5±0.4, I = 0.1 M) and Cm(III)DOTA (22.0±0.4, I = 0.1 M) is conform with the result from the extrapolation approach according to Choppin [97].

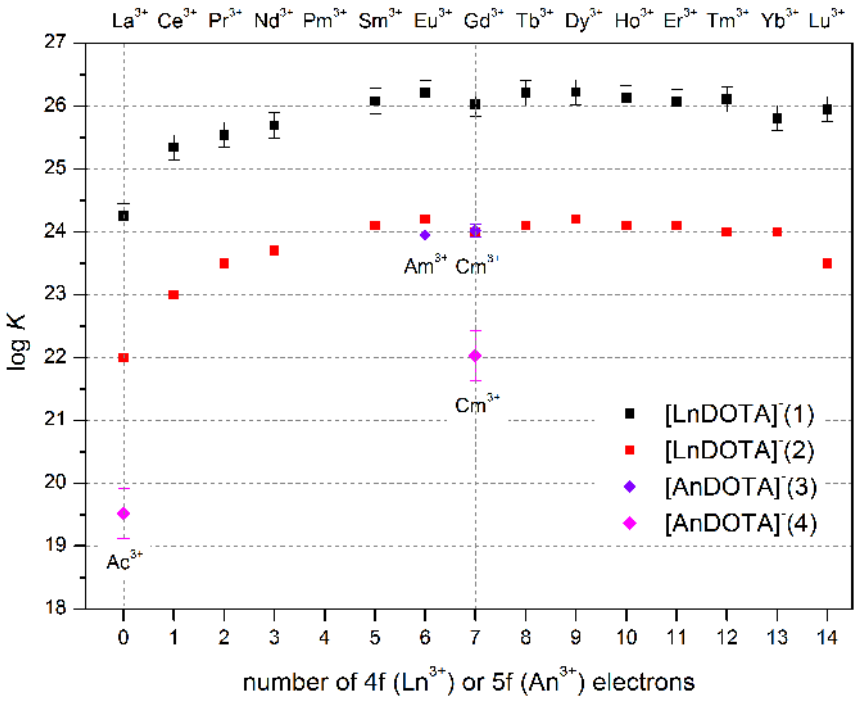

Figure 6.1: Complex formation constants log K [LnDOTA]$^-$ across the lanthanide series, determined by Wu and Horrocks ((1) [9]), in comparison to the log K [LnDOTA]$^-$ from literature databases ((2) [5, 159]), recent publication for [CmDOTA]$^-$, [AmDOTA]$^-$ and [EuDOTA]$^-$ ((3) [126]) and the log K [AcDOTA]$^-$, [CmDOTA]$^-$ determined in the present work (4). All constants are valid for 25 °C, I = 0.1. The reason for the discrepancy between (3) and (4) is discussed in paragraph 5.3.2.1.

Analogous to Cm(III)DOTA, the thermodynamic parameters $\Delta_R G$ obtained from the Gibbs Helmholtz relation indicate that the Ac(III)DOTA complex formation is exergonic, only slightly endothermic and almost exclusively driven by the increase of entropy (paragraph 5.3.2.1). The reason for the almost athermic reaction, resulting in only marginal temperature dependence of the log K for Ac(III)DOTA, is suggested to be the large Ac^{3+}cation not being properly encapsulated by DOTA even at elevated temperatures; it is hence expected to be located far from the N-plane (Fig. 5.38, longest M(III)-N bond length found for Ac(III)-N). This consequently means that Ac-225-DOTA complexes formed during Ac-225-labelling of DOTA-chelated antibodies at ~60 °C [6] are thermodynamically not favoured over complexes formed at lower temperatures of 37 - 42 °C, the optimal labelling temperature suggested in the present work.

6.1.4 Ac-225-DOTA-NCS-radioimmunoconjugate

The results derived from the thermodynamic- ($pK_{a,n}$ (refer to paragraph 6.1.1), log K (refer to paragraph 6.1.2.3 and 6.1.3)) and kinetic investigations (esp. the pre-orientation effect (refer to paragraph 6.1.2.2)) contributed to a better understanding of the coordination chemistry of Ac-225-DOTA. The findings facilitated the optimisation, validation and justification of a robust labelling protocol for effective one-step synthesis of a thermodynamically stable Ac-225-DOTA-NCS-MabThera® conjugate at moderate temperatures (37 - 42 °C) within only 5 - 15 min under al-

kaline conditions (pH 8.5 - 9). By optimisation of the purification procedure for the freshly separated Ac-225 (paragraph 5.4.1 ff) and consideration of the influence of buffer medium and the scavenger ascorbic acid on the reaction (paragraph 5.4.2 ff), a synthesis protocol was implemented which allows for preparation, purification and application of the Ac-225-radioimmunoconjugates within a total time frame of 20 - 30 min (paragraph 5.4.3 ff). The protocol gives average yields of 94 - 96 % of radiochemically pure product (> 98 % after PD10) and was successfully assessed for reliability with high specific activities up to 50 µCi (= 1.9 MBq) per 100 µg antibody. The details of the synthesis protocol, exemplary average radiolabelling yields and pharmacological properties of the radioimmunoconjugate are summarised in Table 6.6.

The *in vitro* studies conducted to evaluate the kinetic stability (particularly under physiological conditions in HBS over a period of 30 days), as well as the preliminary low-SA binding study to assess the affinity of the antibody conjugate to K422 lymphoma cells, proved high stability towards dissociation and suggest functional integrity of the radioimmunoconjugate synthesised according to the newly established protocol (paragraph 5.4.4 ff and 5.4.5 ff, respectively).

Table 6.6: Optimised protocol for the synthesis of thermodynamically and kinetically stable Ac-225-labelled DOTA-NCS-MabThera® conjugates with preserved chemical intergrity and their pharmacological properties determined in the present work.

Radiolabelling conditions	
buffer medium, pH	150 µl 0.2 M TRIS, pH 9
antibody	100 µg, DOTA-NCS-chelated, in 10 µl 0.15 M NaCl/0.05 M NaOAc buffer
activity	≤50 µCi purified Ac-225 in 0.05 M HNO_3, ∼5 µl
total volume	V_{tot} = ∼165 µl
temperature, reaction time	T = 37 °C, 42 °C; t = 5 - 15 min
further preparation	PD10-SEC if required; stabilization of product with 20 % AA after labelling

specific activity	***labelling time***	***average labelling yield***
5 µCi / 100 µg mAb	5 min	96.1 %
10 µCi / 100 µg mAb	5 min	96.3 %
20 µCi / 100 µg mAb	15 min	96.0 %
30 µCi / 100 µg mAb	15 min	96.3 %
40 µCi / 100 µg mAb	15 min	95.1 %
50 µCi / 100 µg mAb	15 min	94.5 %

pharmacological properties of the radioimmunoconjugate (in vitro)	
kinetic stability in HBS, physiological conditions	90 - 95 % Ac-225_{bound} after one $t_{\frac{1}{2}}$(phys)
biological *in vitro* blood half-life	$t_{\frac{1}{2}}$(bio) = 123.8 d
effective *in vitro* blood half-life	$t_{\frac{1}{2}}$(eff) = 9.25 d
binding affinity to CD20	K_d = 52.6 nM; B_{max} = 8.9 nM

6.2 Conclusion

In summary, it was demonstrated in the context of this PhD project that rapid, high-yield radiolabelling of DOTA-chelated mAbs is possible by chosing rather low temperatures and alkaline reaction conditions. The labelling results in thermodynamically and kinetically stable radioimmunoconjugates with high specific activities suitable for application in clinical TAT studies, while the integrity of the antibody seems to be preserved.

6.3 Outlook

In the presented work an optimised radiolabelling protocol for the synthesis of the Ac-225-DOTA-NCS-MabThera® radioimmunoconjugate with high specific activities was implemented based on investigations of the fundamental actinide coordination chemistry. Since this protocol is not applicable if it turns out to negatively affect the antibodies' binding performance, it is required to extensively assess the radiobiology of the RIC. To prove the preserved antibodies' antigen binding affinity and immunoreactivity when labelled with higher SA, additional cell binding studies with conjugates carrying activities of at least up to 10 µCi (= 370 kBq) per 100 µg mAb (clinical relevance) need to be conducted. Parallel to this, further *in vitro* studies are necessary to evaluate the cytotoxicity of the synthesised Ac-225-DOTA-NCS-MabThera®. After successfull completion of the *in vitro* studies, the next evaluation phase would involve the performance of preclinical *in vivo* experiments with small animals, before eventually clinical *in vivo* studies can be considered.

7 Appendix

7.1 Derivation of the Equation for Calculation of the free $DOTA^{4-}$ Concentration for Calulation of the log *K*

For calculation of the conditional thermodynamic stability constants for An(III)DOTA (An(III) = Cm(III), Ac(III)) in presence of sodium salts, the following equilibria have to be considered:

$$HDOTA \rightleftharpoons H_3DOTA^- + H^+, \qquad K_1 = \frac{[H_3DOTA^-][H^+]}{[H_4DOTA]}\ , \tag{7.1}$$

$$HDOTA^- \rightleftharpoons H_2DOTA^{2-} + H^+, \qquad K_2 = \frac{[H_2DOTA^{2-}][H^+]}{[H_3DOTA^-]}\ , \tag{7.2}$$

$$HDOTA^{2-} \rightleftharpoons HDOTA^{3-} + H^+, \qquad K_3 = \frac{[HDOTA^{3-}][H^+]}{[H_2DOTA^{2-}]}\ , \tag{7.3}$$

$$HDOTA^{3-} \rightleftharpoons DOTA^{4-} + H^+, \qquad K_4 = \frac{[DOTA^{4-}][H^+]}{[HDOTA^{3-}]}\ , \tag{7.4}$$

$$Na^+ + DOTA^{4-} \rightleftharpoons NaDOTA^{3-}, \qquad K_{NaDOTA^{3-}} = \frac{[NaDOTA^{3-}]}{[DOTA^{4-}][Na^+]}\ , \tag{7.5}$$

$$An^{3+} + DOTA^{4-} \rightleftharpoons AnDOTA^-, \qquad K_{AnDOTA^-} = \frac{[AnDOTA^-]}{[DOTA^{4-}][An^{3+}]}\ . \tag{7.6}$$

The total ligand concentration [$DOTA_{tot}$] is the sum of all DOTA species in equilibrium and is hence given by:

$$[DOTA_{tot}] = [H_4DOTA] + [H_3DOTA^-] + [H_2DOTA^{2-}] + [HDOTA^{3-}] + [DOTA^{4-}] + [NaDOTA^{3-}] + [AnDOTA^-]\ . \tag{7.7}$$

Applying the above equilibria, this equation is rewritten as:

$$\begin{aligned}[DOTA_{tot}] \quad = \quad & \frac{[DOTA^{4-}][H^+]^4}{K_1K_2K_3K_4} + \frac{[DOTA^{4-}][H^+]^3}{K_2K_3K_4} + \frac{[DOTA^{4-}][H^+]^2}{K_3K_4} + \frac{[DOTA^{4-}][H^+]}{K_4} + [DOTA^{4-}] \\ & + K_{NaDOTA^{3-}}[DOTA^{4-}][Na^+] + [AnDOTA^-]\ .\end{aligned} \tag{7.8}$$

With $K_1K_2K_3K_4$ being set as the common denominator, it follows that:

$$\begin{aligned}[DOTA_{tot}] - [AnDOTA^-] \quad = \quad & \frac{[DOTA^{4-}][H^+]^4 + K_1[DOTA^{4-}][H^+]^3 + K_1K_2[DOTA^{4-}][H^+]^2 + K_1K_2K_3[DOTA^{4-}][H^+]}{K_1K_2K_3K_4} \\ & + \frac{K_1K_2K_3K_4[DOTA^{4-}] + K_1K_2K_3K_4K_{NaDOTA^{3-}}[DOTA^{4-}][Na^+]}{K_1K_2K_3K_4}\ ,\end{aligned} \tag{7.9}$$

$$= \frac{[DOTA^{4-}]([H^+]^4 + K_1[H^+]^3 + K_1K_2[H^+]^2 + K_1K_2K_3[H^+] + K_1K_2K_3K_4 + K_1K_2K_3K_4K_{NaDOTA^{3-}}[Na^+])}{K_1K_2K_3K_4}\ . \tag{7.10}$$

Inversion and further rearragenment gives:

$$\begin{aligned}\frac{[DOTA_{tot}] - [AnDOTA^-]}{[DOTA^{4-}]} \quad = \quad & \frac{[H^+]^4 + K_1[H^+]^3 + K_1K_2[H^+]^2 + K_1K_2K_3[H^+] + K_1K_2K_3K_4}{K_1K_2K_3K_4}\ , \\ & + \frac{K_1K_2K_3K_4K_{NaDOTA^{3-}}[Na^+]}{K_1K_2K_3K_4}\end{aligned} \tag{7.11}$$

$$[DOTA^{4-}] = \frac{K_1K_2K_3K_4([DOTA_{tot}] - [AnDOTA^-])}{[H^+]^4 + K_1[H^+]^3 + K_1K_2[H^+]^2 + K_1K_2K_3[H^+] + K_1K_2K_3K_4 + K_1K_2K_3K_4K_{NaDOTA^{3-}}[Na^+]}\ . \tag{7.12}$$

By expressing K_n as β_n , Eq. 5.24 is obtained (q.e.d.) :

$$[DOTA^{4-}]_{free} = ([DOTA_{tot}] - [AnDOTA^-])\frac{\beta_4}{[H^+]^4 + \beta_1[H^+]^3 + \beta_2[H^+]^2 + \beta_3[H^+] + \beta_4 + \beta_4K_{NaDOTA^{3-}}[Na^+]}\ . \tag{7.13}$$

7.2 Glossary

Radiochemical Terms

α-decay describes the emission of an high-energy α-particle (4 - 9 MeV) which is basically a Helium nucleus ($^4_2He^{2+}$). At the same time a chemical element transformation takes place. The recoil energy is transferred to the remaining nucleus. Alpha-particles have only a short range in human tissue and are exclusively used for therapeutic purposes. The α-decay either occurs into the ground- or excited states of the daughter nuclide; the latter is accompanied by the emission of γ-radiation.

$$^{225}_{89}Ac \rightarrow ^{221}_{87}Fr + \alpha \tag{7.14}$$

Recoil-energy is the energy $\triangle E$ which is released during an α-decay. It is distributed between the α-particle (E_α) and the recoil nucleus (E_N):

$$\triangle E = E_\alpha + E_N \ . \tag{7.15}$$

By applying the principle of conservation of momentum, the recoil-energy for e.g. the α-decay of Ac-225 to Fr-221 can be calculated as follows:

$$m_\alpha \cdot v_\alpha = m_N \cdot v_N \ . \tag{7.16}$$

With $E = \frac{1}{2} m \cdot v^2$ it follows that

$$m_\alpha \cdot E_\alpha \approx m_N \cdot E_N \quad (non - relativistic) \tag{7.17}$$

$$\hookrightarrow E_N \approx \left(\frac{m_\alpha}{m_N} \right) \cdot E_\alpha \ . \tag{7.18}$$

It is $m_\alpha = 4$, $m_N = 221$, $E_\alpha = 5.829\ MeV$:

$$E_N = \left(\frac{4}{221} \right) \cdot 5.829\ MeV = 0.105\ MeV \ . \tag{7.19}$$

This recoil-energy is several orders of magnitude higher than the energy of a chemical bond. Hence, during α-decay, all chemical bonds in close proximity of the decay site are broken. In general, the total energy of an α-decay is higher than the energy of the α-particle by a factor of $(1 + m_\alpha / m_N)$. The approximate range of a recoil nucleus is 80 µm in air and 0.1 µm in tissue.

β-decay describes the emission of an β^- or β^+-particle, respectively. β^--decay typically occurs with neutron-rich nuclei. During the decay, a neutron is transformed into a proton; additionally, an anti-neutrino is formed for conservation of symmetry, mass and momentum. Depending on the radionuclide, the energy of β^--particles is in the range of 20 keV (soft) to 2.5 MeV (hard). β^--emitters are primariliy used for therapy, e.g. I-131:

$$^{131}_{53}I \rightarrow ^{131}_{54}Xe + \beta^- + \nu^- \ . \tag{7.20}$$

During β^+-decay, a proton in the nucleus is transformed into a neutron, which is why this form of decay typically occurs with nuclei having a lack a neutrons. In addition to the positron a neutrino is formed:

$$^A_Z X \rightarrow ^A_{Z-1} Y + \beta^+ + \nu \ . \tag{7.21}$$

β^+-emitters are used for radiodiagnostic, namely for Positron-Emission-Tomography (PET). Here, when a positron collides with an electron, the two annihilation-γ-photons (both 511 keV) can be detected, which are emitted in an angle of 180°.

Auger-electron emission results from the capture of an electron, originating from an inner shell, by the nucleus. The resulting vacancy in the inner shell, which greatly disturbs the energy stability of the atom, is filled by an electron from higher energy levels in order to regain the energy balance. The energy difference of these transitions between the L→K and M→L shells etc. is compensated by emission of characteristic X-rays or emission of Auger-electrons of the respective energy. Electron capture decay or internal transitions are the main sources of Auger-electrons. During the electron capture process, a proton of the nucleus is transformed into a neutron. Additonally, a neutrino is released:

$$p + e^- \rightarrow n + \nu \; . \tag{7.22}$$

Typically 5 to 30 Auger-electrons are released per decay. The energy of Auger-electrons is rather low (∼1 - 15 keV); the range in human tissue is $< 0.5\,\mu m$. It is intended to use Auger-electrons for therapeutic purposes, but this concept is still in an experimental stage.

γ-decay describes the emission of γ-photons. The γ-decay itself does not result in any transformation of the nucleus but is always a consequence of either an α- or β-decay, if the process does not occur to the ground state of the daughter nuclide. Usually, the excited states which are involved in γ-decay have only short lifetimes. However, for application in nuclear medicine, metastable states with remarkably longer life-times are of particular interest for Single Photon Emission Computed Tomography (SPECT-Imaging). A typical SPECT nuclide is Tc-99m with a γ-energy of 0.143 MeV:

$$^{99m}_{43}Tc \rightarrow ^{99}_{43}Tc + \gamma \; . \tag{7.23}$$

Linear energy transfer (LET): The linear energy transfer or LET is the average energy deposited by particles per unit track length which is traversed [units of keV/µm]. L_Δ describes the energy loss dE_Δ in close proximity of the path x of a particle in tissue. Hence, secondary electrons with energies higher than a certain value Δ are not taken into account.

$$L_\Delta = \frac{dE_\Delta}{dx}\left[\frac{keV}{\mu m}\right] \tag{7.24}$$

High LET particles are those with a LET > 10 - 30 keV/µm, e.g. Auger-electrons and especially α-particles, whose LET ranges from 25 to 230 keV/µm, depending on the particle energy. High energy results in lower LET because as the particle moves faster, the interaction probability is reduced and less energy is deposited per unit track length. Radiation with high LET transfers a high energy to a small tissue volume and has a higher biological effectiveness than radiation with low LET.

The different half-lifes: The physical radioactive half-life $t_{\frac{1}{2}}$ defines the period of time it takes for an amount of radionuclides undergoing exponential decay to decrease by half. This half-life is physically determined and unaffected by external physical or chemical conditions. However, if a radionuclide is in a living organism it will be eventually excreted and thus will no longer be a source of radiation exposure to the organism. The rate of this excretion is expressed in form of the biological half-life. The biological half-life cannot be expected to be as precise as the physical half-life. In summary, the rate of decrease of radiation exposure is affected by both the physical and biological half-life, giving an effective half-life for the radionuclide in the body:

$$\frac{1}{t_{\frac{1}{2}}effective} = \frac{1}{t_{\frac{1}{2}}} + \frac{1}{t_{\frac{1}{2}}biological} \; . \tag{7.25}$$

The biological blood half-life of a monoclonal antibody is mainly affected by specific recognition of free circulating mAbs by the immune system which eventually induces mAb clearance. As soon as all antibody binding sites are saturated or cancer cells are cytoreduced, the blood half-life of the mAb increases. Since antibodies are serum proteins, they can exhibit long residence time in blood circulation and at the tumour site; for example, IgGs have serum half-lives of approx. 8 days. For smaller radiolabelled proteins, the blood half-lives are much shorter than that of antibodies and antibody fragments.

Thermodynamic Terms

The chelate-/macrocyclic effect: Complexes formed by mono- and multidentate ligands show significant differences in complex formation and dissociation kinetics, an effect which is referred to as the "chelate effect" . The same applies for formation and dissociation of complexes formed by acylic and macrocyclic ligands ("macrocyclic effect"). The difference between the stability constants of a multidentate- compared to a monodentate ligand is mainly due to a thermodynamic entropy effect. When a multidentate ligand forms a chelate complex, less entropy is lost than when a complex with monodentate ligands is formed. For example, one heaxadentate ligand EDTA will replace 6 monodentate ligands, which results in increased disorder, while 6 monodentate ligands are required to replace 6 other monodentate ligands coordinated to the metal cation; here, the entropy change is practically zero. The chelate effect is also noticable in hindered complex dissociation, since with a chelate complex more than one bond to the metal needs to be broken at once, compared to complexes with monodentate ligands where the ligands can easily dissociate away from the metal. It is also known that the stability of complexes with macrocyclic ligands is much greater than the stability of complexes with the corresponding open-chain ligands. This phenomenon called "the macrocyclic effect" is also interpreted as entropy effect.

Radiopharmaceutical Terms

Specific activity (SA): The activity is defined as decays per second, with 1 decay/second [s^{-1}] = 1 Becquerel [Bq]. Until today, the old unit Curie [Ci] is still applied in nuclear medicine. The conversion factor between old and new unit is 1 Ci = $3.7 \cdot 10^{10}$Bq (1 mCi = 37 MBq). The specific activity is defined as:

$$A = \frac{A}{m} \left[\frac{Bq}{g}\right] , \tag{7.26}$$

with A = activity of the radionuclide and m = summ of the masses of the active and inactive isotopes. However, when talking about radiolabelled compounds, the term "specific activity" is also applied for description of the activity of the radionuclide in relation to the mass of the carrier molecule (e.g. antibody), which corresponds to the unit [Bq / mass biomolecule]. For clinical applications, high SA of labelled peptides and mAb are required to permit administration of only trace doses of conjugate, preventing target saturation and/or side effects.

Cell binding affinity: Cell binding studies are *in vitro* experiments to test the (retained) ability of a radiolabelled mAb conjugate to bind to its antigen on the tumour cell surface:

$$radiolabelled\, mAb + antigen \rightleftharpoons complex\ .$$

Based on the assumption that all antigens are available for reversible binding, with all conjugates/antigens being either bound or free (no partial binding), the binding affinity K_a as well as the total number of binding sites B_{max} can be determined experimentally (Scatchard analysis) following the equations:

$$K_a = \frac{1}{K_d} = \frac{[complex]}{[free\, mAb] \cdot [free\, antigen]} = \frac{[B]}{[L] \cdot ([B_{max}] - [B])} , \tag{7.27}$$

with K_a = association constant, K_d = dissociation constant. It follows that:

$$\frac{[B]}{[L]} = K_a \cdot ([B_{max}] - [B]) , \tag{7.28}$$

$$\hookrightarrow \frac{[B]}{[L]} = K_a \cdot [B_{max}] - K_a \cdot [B] ,$$

with $K_a \cdot [B_{max}]$ being a constant factor. A plot of $\frac{[B]}{[L]}$ versus $[B]$ allows determination of $-K_a$ from the slope of the graph.

7.3 Raw Data

Please find the raw data for the experiments discussed in the present work in chronological order on the following pages. The rest of this page was intentionally left blank.

Raw data for titrations in 0.1 M $NaClO_4$

0.1 M NaOH	25 °C		45 °C		60 °C		70 °C		80 °C		90 °C	
ml	mV	pH	mV	pH	mV	pH	mV	pH	mV	pH	mV	pH
0.00	199	3.02	218	2.80	223	2.80	238	2.72	247	2.72	244	2.97
0.02	197	3.06	215	2.85	221	2.83	235	2.76	245	2.75	242	3.00
0.04	195	3.09	213	2.88	219	2.86	234	2.78	243	2.77	239	3.04
0.06	193	3.12	211	2.91	217	2.89	231	2.82	240	2.82	238	3.06
0.08	190	3.18	208	2.96	214	2.94	228	2.87	237	2.86	235	3.10
0.10	188	3.21	206	2.99	213	2.95	225	2.92	235	2.89	232	3.14
0.12	185	3.26	203	3.04	210	3.00	223	2.95	232	2.94	229	3.19
0.14	182	3.31	200	3.09	207	3.04	219	3.01	229	2.98	226	3.23
0.16	178	3.38	197	3.14	204	3.09	216	3.05	227	3.01	223	3.27
0.18	175	3.43	193	3.20	201	3.14	213	3.10	223	3.07	220	3.31
0.20	171	3.50	190	3.25	198	3.18	211	3.13	220	3.11	219	3.33
0.22	167	3.57	186	3.32	194	3.24	207	3.19	216	3.17	216	3.37
0.24	163	3.63	182	3.38	191	3.29	203	3.25	212	3.23	214	3.40
0.26	160	3.68	179	3.43	188	3.34	200	3.29	209	3.27	210	3.45
0.28	156	3.75	175	3.49	184	3.40	196	3.35	205	3.33	207	3.50
0.30	152	3.82	171	3.56	181	3.44	192	3.41	201	3.39	203	3.55
0.32	148	3.89	168	3.61	177	3.51	188	3.47	197	3.45	199	3.61
0.34	145	3.94	164	3.67	175	3.54	185	3.52	193	3.51	196	3.65
0.36	141	4.01	161	3.72	171	3.60	181	3.58	190	3.55	192	3.71
0.38	138	4.06	158	3.77	168	3.64	178	3.62	186	3.61	189	3.75
0.40	136	4.09	155	3.82	164	3.71	175	3.67	183	3.65	185	3.81
0.42	133	4.14	152	3.86	161	3.75	172	3.72	180	3.70	182	3.85
0.44	130	4.19	149	3.91	159	3.78	169	3.76	177	3.74	179	3.89
0.46	128	4.23	146	3.96	156	3.83	166	3.81	174	3.79	177	3.92
0.48	125	4.28	143	4.01	154	3.86	163	3.85	170	3.84	173	3.98
0.50	123	4.31	140	4.06	151	3.91	160	3.90	167	3.89	170	4.02
0.52	120	4.36	138	4.09	149	3.94	157	3.94	165	3.92	168	4.05
0.54	118	4.40	135	4.14	146	3.98	154	3.99	162	3.96	165	4.09
0.56	116	4.43	133	4.17	143	4.03	151	4.03	159	4.01	162	4.13
0.58	114	4.46	130	4.22	141	4.06	149	4.06	157	4.03	159	4.17
0.60	112	4.50	127	4.27	138	4.11	146	4.11	154	4.08	156	4.21
0.62	109	4.55	125	4.30	135	4.15	143	4.15	151	4.12	153	4.26
0.64	107	4.58	122	4.35	133	4.18	140	4.20	148	4.17	150	4.30
0.66	105	4.62	120	4.38	130	4.23	137	4.24	145	4.21	147	4.34
0.68	102	4.67	117	4.43	127	4.28	134	4.29	142	4.25	144	4.38
0.70	100	4.70	114	4.48	124	4.32	132	4.32	138	4.31	140	4.44
0.72	98	4.73	111	4.53	121	4.37	128	4.38	135	4.36	137	4.48
0.74	95	4.79	108	4.57	118	4.41	125	4.42	132	4.40	133	4.54
0.76	92	4.84	105	4.62	115	4.46	122	4.47	128	4.46	129	4.60
0.78	90	4.87	102	4.67	111	4.52	118	4.53	124	4.52	125	4.65
0.80	89	4.89	98	4.74	107	4.58	115	4.57	124	4.52	121	4.71
0.82	86	4.94	94	4.80	104	4.63	111	4.64	120	4.58	118	4.75
0.84	83	4.99	90	4.86	99	4.71	107	4.70	115	4.65	114	4.81
0.86	79	5.06	85	4.94	94	4.78	102	4.77	110	4.72	107	4.91
0.88	75	5.12	80	5.03	89	4.86	97	4.85	104	4.81	101	4.99
0.90	71	5.19	74	5.12	82	4.97	90	4.95	98	4.90	94	5.09

0.92	66	5.28	66	5.25	75	5.08	83	5.06	91	5.00	85	5.22
0.94	60	5.38	56	5.41	64	5.25	74	5.19	81	5.15	73	5.39
0.96	52	5.51	41	5.65	49	5.48	62	5.37	69	5.32	56	5.63
0.98	41	5.70	12	6.12	21	5.91	42	5.68	50	5.60	24	6.08
1.00	24	5.99	-81	7.62	-61	7.17	-6	6.40	6	6.25	-41	6.99
1.02	-19	6.72	-111	8.11	-96	7.71	-71	7.38	-57	7.17	-72	7.43
1.04	-88	7.89	-124	8.32	-111	7.94	-94	7.73	-82	7.54	-88	7.66
1.06	-123	8.48	-133	8.46	-120	8.08	-106	7.91	-95	7.73	-98	7.80
1.08	-137	8.72	-139	8.56	-126	8.17	-114	8.03	-104	7.86	-106	7.91
1.10	-145	8.85	-143	8.62	-132	8.26	-121	8.14	-110	7.95	-112	7.99
1.12	-151	8.96	-147	8.69	-136	8.32	-126	8.21	-116	8.03	-117	8.06
1.14	-156	9.04	-151	8.75	-140	8.39	-130	8.27	-121	8.11	-122	8.14
1.16	-160	9.11	-154	8.80	-143	8.43	-134	8.33	-125	8.17	-126	8.19
1.18	-163	9.16	-157	8.85	-146	8.48	-137	8.38	-128	8.21	-130	8.25
1.20	-165	9.19	-159	8.88	-149	8.52	-140	8.42	-131	8.25	-133	8.29
1.22	-168	9.24	-162	8.93	-151	8.55	-143	8.47	-135	8.31	-136	8.33
1.24	-170	9.28	-164	8.96	-153	8.59	-146	8.51	-137	8.34	-139	8.38
1.26	-172	9.31	-166	8.99	-156	8.63	-148	8.54	-140	8.39	-141	8.40
1.28	-174	9.35	-168	9.03	-158	8.66	-151	8.59	-143	8.43	-144	8.45
1.30	-176	9.38	-170	9.06	-160	8.69	-153	8.62	-145	8.46	-147	8.49
1.32	-178	9.41	-172	9.09	-162	8.72	-155	8.65	-147	8.49	-149	8.52
1.34	-180	9.45	-173	9.11	-164	8.75	-157	8.68	-149	8.52	-152	8.56
1.36	-181	9.46	-175	9.14	-166	8.79	-160	8.72	-151	8.55	-154	8.59
1.38	-183	9.50	-177	9.17	-168	8.82	-162	8.75	-153	8.58	-156	8.61
1.40	-184	9.51	-179	9.20	-170	8.85	-164	8.78	-155	8.61	-158	8.64
1.42	-186	9.55	-180	9.22	-171	8.86	-166	8.81	-157	8.64	-160	8.67
1.44	-188	9.58	-182	9.25	-173	8.89	-168	8.84	-159	8.66	-162	8.70
1.46	-189	9.60	-184	9.28	-175	8.92	-169	8.86	-161	8.69	-164	8.73
1.48	-191	9.63	-186	9.32	-177	8.95	-171	8.89	-163	8.72	-166	8.76
1.50	-192	9.65	-188	9.35	-179	8.99	-173	8.92	-165	8.75	-167	8.77
1.52	-194	9.68	-190	9.38	-181	9.02	-175	8.95	-167	8.78	-169	8.80
1.54	-196	9.72	-191	9.40	-183	9.05	-177	8.98	-169	8.81	-172	8.84
1.56	-197	9.73	-193	9.43	-185	9.08	-179	9.01	-172	8.85	-174	8.87
1.58	-199	9.77	-195	9.46	-187	9.11	-181	9.04	-174	8.88	-176	8.90
1.60	-201	9.80	-198	9.51	-189	9.14	-184	9.09	-176	8.91	-178	8.93
1.62	-203	9.84	-200	9.54	-192	9.19	-186	9.12	-178	8.94	-180	8.95
1.64	-205	9.87	-202	9.57	-194	9.22	-188	9.15	-180	8.97	-183	9.00
1.66	-207	9.90	-205	9.62	-197	9.26	-190	9.18	-183	9.02	-185	9.02
1.68	-210	9.96	-207	9.65	-199	9.29	-193	9.22	-185	9.05	-188	9.07
1.70	-212	9.99	-210	9.70	-202	9.34	-195	9.25	-187	9.07	-190	9.09
1.72	-215	10.04	-214	9.77	-205	9.39	-198	9.30	-190	9.12	-193	9.14
1.74	-218	10.09	-217	9.82	-208	9.43	-200	9.33	-192	9.15	-195	9.16
1.76	-222	10.16	-221	9.88	-211	9.48	-203	9.37	-195	9.19	-198	9.21
1.78	-226	10.23	-225	9.94	-215	9.54	-206	9.42	-198	9.24	-201	9.25
1.80	-231	10.31	-229	10.01	-218	9.59	-209	9.46	-200	9.27	-203	9.28
1.82	-236	10.40	-234	10.09	-222	9.65	-212	9.51	-203	9.31	-206	9.32
1.84	-242	10.50	-238	10.15	-225	9.69	-215	9.55	-206	9.35	-209	9.36
1.86	-247	10.58	-242	10.22	-228	9.74	-218	9.60	-209	9.40	-211	9.39
1.88	-253	10.68	-246	10.28	-231	9.79	-221	9.64	-212	9.44	-214	9.43
1.90	-258	10.77	-250	10.35	-234	9.83	-224	9.69	-214	9.47	-217	9.48

1.92	-262	10.84	-253	10.40	-237	9.88	-226	9.72	-217	9.51	-219	9.50
1.94	-266	10.90	-256	10.44	-240	9.92	-229	9.76	-219	9.54	-221	9.53
1.96	-270	10.97	-258	10.48	-242	9.96	-231	9.79	-222	9.59	-224	9.57
1.98	-273	11.02	-261	10.53	-245	10.00	-234	9.84	-224	9.62	-226	9.60
2.00	-277	11.09	-260	10.51	-246	10.02	-236	9.87	-226	9.65	-228	9.63
2.05	-283	11.19	-264	10.57	-251	10.09	-240	9.93	-231	9.72	-230	9.66
2.10	-288	11.28	-269	10.65	-255	10.16	-245	10.01	-235	9.78	-235	9.73
2.15	-293	11.36	-272	10.70	-259	10.22	-249	10.07	-240	9.85	-238	9.77
2.20	-296	11.41	-275	10.75	-262	10.26	-253	10.13	-243	9.89	-242	9.83
2.25	-300	11.48	-278	10.80	-265	10.31	-256	10.17	-246	9.94	-245	9.87
2.30			-280	10.83	-268	10.36	-259	10.22	-249	9.98	-247	9.90
2.35			-282	10.86	-270	10.39	-261	10.25	-252	10.03	-249	9.93
2.40			-284	10.90	-272	10.42	-264	10.29	-254	10.06	-252	9.97
2.45			-285	10.91	-274	10.45	-266	10.32	-257	10.10	-254	10.00
2.50			-287	10.94	-276	10.48	-268	10.35	-259	10.13	-255	10.01
2.55			-288	10.96	-278	10.51	-270	10.38	-260	10.14	-257	10.04
2.60			-289	10.98	-279	10.53	-272	10.41	-262	10.17	-259	10.07
2.65			-291	11.01	-281	10.56	-273	10.43	-264	10.20	-260	10.08
2.70			-292	11.03	-282	10.57	-275	10.46	-265	10.22	-262	10.11
2.75			-293	11.04	-283	10.59	-276	10.47	-267	10.25	-263	10.12
2.80			-294	11.06	-285	10.62	-277	10.49	-268	10.26	-264	10.14
2.85			-295	11.07	-286	10.63	-279	10.52	-269	10.28	-265	10.15
2.90			-295	11.07	-287	10.65	-280	10.53	-270	10.29	-266	10.17
2.95			-296	11.09	-288	10.66	-281	10.55	-271	10.31	-267	10.18
3.00			-297	11.11	-288	10.66	-282	10.56	-272	10.32	-268	10.19
3.05			-298	11.12			-283	10.58	-273	10.33	-269	10.21
3.10			-299	11.14			-284	10.59	-274	10.35	-270	10.22
3.15			-300	11.15			-284	10.59	-275	10.36	-271	10.24
3.20			-301	11.17			-285	10.61	-276	10.38	-272	10.25
3.25							-286	10.62	-277	10.39		
3.30							-287	10.64	-278	10.41		
3.35							-288	10.65	-279	10.42		
3.40							-288	10.65	-280	10.44		
3.45							-289	10.67	-280	10.44		
3.50							-290	10.68	-281	10.45		

Raw data for titrations in 0.1 M $TMAClO_4$

0.1 M NaOH	45 °C		60 °C		80 °C		90 °C		0.1 M NaOH	70 °C	
ml	mV	pH	mV	pH	mV	pH	mV	pH	ml	mV	pH
0.00	220	2.76	231	2.72	247	2.82	255	2.87	0.00	234	2.82
0.02	217	2.81	229	2.75	244	2.86	252	2.91	0.02	231	2.86
0.04	215	2.84	226	2.80	242	2.89	250	2.94	0.04	228	2.90
0.06	213	2.87	224	2.83	239	2.93	248	2.96	0.06	225	2.95
0.08	211	2.90	222	2.86	237	2.96	245	3.01	0.08	222	2.99
0.10	209	2.94	220	2.89	234	3.01	242	3.05	0.10	219	3.04
0.12	206	2.98	217	2.94	231	3.05	239	3.09	0.12	216	3.08
0.14	203	3.03	213	3.00	228	3.09	236	3.13	0.14	213	3.13
0.16	200	3.08	210	3.05	225	3.13	232	3.19	0.16	209	3.19
0.18	197	3.13	207	3.09	221	3.19	229	3.23	0.18	205	3.24
0.20	194	3.18	203	3.15	218	3.23	225	3.28	0.20	201	3.30
0.22	190	3.24	200	3.20	214	3.29	222	3.33	0.22	198	3.35
0.24	187	3.29	196	3.26	211	3.33	218	3.38	0.24	194	3.41
0.26	183	3.35	192	3.32	207	3.39	214	3.44	0.26	190	3.47
0.28	179	3.42	188	3.38	203	3.45	210	3.49	0.28	187	3.51
0.30	175	3.48	185	3.43	199	3.51	206	3.55	0.30	183	3.57
0.32	172	3.53	181	3.49	196	3.55	203	3.59	0.32	180	3.62
0.34	168	3.59	178	3.53	192	3.61	199	3.65	0.34	177	3.66
0.36	165	3.64	174	3.60	189	3.65	195	3.70	0.36	174	3.70
0.38	162	3.69	171	3.64	185	3.71	192	3.74	0.38	171	3.75
0.40	159	3.74	168	3.69	182	3.75	189	3.79	0.40	168	3.79
0.42	156	3.78	164	3.75	179	3.79	185	3.84	0.42	165	3.84
0.44	153	3.83	161	3.79	176	3.84	182	3.88	0.44	162	3.88
0.46	150	3.88	159	3.83	173	3.88	179	3.93	0.46	160	3.91
0.48	147	3.93	156	3.87	170	3.92	176	3.97	0.48	157	3.96
0.50	145	3.96	153	3.92	167	3.96	173	4.01	0.50	155	3.99
0.52	142	4.01	150	3.96	164	4.01	170	4.05	0.52	152	4.03
0.54	139	4.06	147	4.01	161	4.05	167	4.09	0.54	149	4.07
0.56	137	4.09	145	4.04	158	4.09	164	4.13	0.56	147	4.10
0.58	134	4.14	142	4.09	156	4.12	161	4.18	0.58	144	4.15
0.60	132	4.17	139	4.13	153	4.16	158	4.22	0.60	142	4.18
0.62	129	4.22	137	4.16	150	4.21	155	4.26	0.62	139	4.22
0.64	127	4.25	134	4.21	148	4.24	153	4.29	0.64	136	4.27
0.66	124	4.30	131	4.25	145	4.28	149	4.34	0.66	134	4.30
0.68	122	4.33	129	4.28	143	4.31	146	4.38	0.68	131	4.34
0.70	119	4.38	126	4.33	140	4.35	142	4.44	0.70	128	4.39
0.72	117	4.41	123	4.38	137	4.39	139	4.48	0.72	125	4.43
0.74	114	4.46	120	4.42	134	4.44	135	4.54	0.74	122	4.47
0.76	111	4.50	117	4.47	132	4.47	132	4.58	0.76	119	4.52
0.78	108	4.55	114	4.51	129	4.51	128	4.64	0.78	115	4.58
0.80	105	4.60	110	4.57	125	4.57	123	4.71	0.80	112	4.62
0.82	102	4.65	107	4.62	122	4.61	121	4.73	0.82	108	4.68
0.84	99	4.70	103	4.68	119	4.65	119	4.76	0.84	103	4.76
0.86	95	4.76	98	4.76	115	4.71	114	4.83	0.86	99	4.82
0.88	91	4.82	94	4.82	111	4.77	109	4.90	0.88	93	4.90
0.90	87	4.89	88	4.91	107	4.82	104	4.97	0.90	87	4.99

0.92	82	4.97	82	5.00	103	4.88	98	5.05	0.92	80	5.10
0.94	76	5.06	75	5.11	98	4.95	91	5.15	0.94	71	5.23
0.96	69	5.18	65	5.26	92	5.04	82	5.28	0.96	58	5.42
0.98	61	5.30	51	5.48	85	5.14	70	5.44	0.98	38	5.72
1.00	49	5.50	26	5.86	76	5.27	53	5.68	1.00	-16	6.52
1.02	31	5.78	-41	6.88	65	5.42	19	6.15	1.02	-77	7.42
1.04	-17	6.55	-93	7.68	47	5.68	-42	7.00	1.04	-100	7.76
1.06	-100	7.88	-113	7.99	11	6.20	-74	7.45	1.06	-113	7.96
1.08	-124	8.26	-126	8.19	-57	7.17	-90	7.67	1.08	-123	8.10
1.10	-137	8.47	-135	8.32	-87	7.60	-102	7.84	1.10	-131	8.22
1.12	-147	8.63	-141	8.41	-102	7.82	-111	7.96	1.12	-138	8.33
1.14	-154	8.74	-148	8.52	-113	7.97	-118	8.06	1.14	-143	8.40
1.16	-160	8.84	-153	8.60	-121	8.09	-124	8.14	1.16	-149	8.49
1.18	-165	8.92	-157	8.66	-128	8.19	-130	8.23	1.18	-153	8.55
1.20	-169	8.98	-161	8.72	-134	8.27	-135	8.30	1.20	-157	8.61
1.22	-173	9.05	-165	8.78	-139	8.35	-140	8.37	1.22	-161	8.67
1.24	-177	9.11	-169	8.84	-144	8.42	-144	8.42	1.24	-165	8.73
1.26	-180	9.16	-172	8.89	-148	8.47	-148	8.48	1.26	-169	8.79
1.28	-183	9.21	-175	8.93	-152	8.53	-152	8.53	1.28	-172	8.83
1.30	-186	9.26	-178	8.98	-156	8.59	-156	8.59	1.30	-175	8.87
1.32	-189	9.30	-181	9.03	-159	8.63	-159	8.63	1.32	-178	8.92
1.34	-192	9.35	-183	9.06	-162	8.67	-162	8.67	1.34	-181	8.96
1.36	-194	9.38	-186	9.10	-166	8.73	-166	8.73	1.36	-184	9.01
1.38	-197	9.43	-188	9.13	-169	8.77	-169	8.77	1.38	-186	9.04
1.40	-199	9.46	-191	9.18	-171	8.80	-172	8.81	1.40	-189	9.08
1.42	-201	9.50	-193	9.21	-174	8.85	-175	8.85	1.42	-191	9.11
1.44	-203	9.53	-195	9.24	-177	8.89	-178	8.90	1.44	-194	9.16
1.46	-206	9.58	-198	9.29	-179	8.92	-181	8.94	1.46	-196	9.19
1.48	-208	9.61	-200	9.32	-182	8.96	-184	8.98	1.48	-198	9.22
1.50	-210	9.64	-202	9.35	-184	8.99	-186	9.01	1.50	-201	9.26
1.52	-212	9.67	-204	9.38	-187	9.03	-189	9.05	1.52	-203	9.29
1.54	-214	9.70	-206	9.41	-189	9.06	-191	9.08	1.54	-205	9.32
1.56	-216	9.74	-208	9.44	-191	9.09	-193	9.10	1.56	-207	9.35
1.58	-218	9.77	-210	9.47	-193	9.12	-195	9.13	1.58	-209	9.38
1.60	-220	9.80	-212	9.50	-196	9.16	-198	9.17	1.60	-212	9.42
1.62	-223	9.85	-214	9.53	-198	9.19	-200	9.20	1.62	-214	9.45
1.64	-225	9.88	-217	9.58	-200	9.22	-202	9.23	1.64	-216	9.48
1.66	-227	9.91	-219	9.61	-202	9.25	-204	9.26	1.66	-218	9.51
1.68	-229	9.94	-221	9.64	-204	9.28	-206	9.29	1.68	-220	9.54
1.70	-231	9.98	-223	9.67	-206	9.30	-208	9.31	1.70	-221	9.56
1.72	-234	10.02	-225	9.70	-208	9.33	-210	9.34	1.72	-224	9.60
1.74	-236	10.06	-227	9.73	-210	9.36	-212	9.37	1.74	-225	9.62
1.76	-238	10.09	-229	9.76	-212	9.39	-213	9.38	1.76	-227	9.64
1.78	-240	10.12	-231	9.79	-214	9.42	-215	9.41	1.78	-229	9.67
1.80	-243	10.17	-233	9.82	-215	9.43	-217	9.44	1.80	-231	9.70
1.82	-245	10.20	-235	9.85	-217	9.46	-219	9.47	1.82	-232	9.72
1.84	-247	10.23	-237	9.88	-218	9.48	-220	9.48	1.84	-234	9.75
1.86	-249	10.26	-239	9.91	-220	9.50	-222	9.51	1.86	-236	9.78
1.88	-252	10.31	-241	9.94	-222	9.53	-224	9.54	1.88	-237	9.79
1.90	-254	10.34	-242	9.96	-223	9.55	-225	9.55	1.90	-239	9.82

1.92	-256	10.38	-244	9.99	-225	9.58	-227	9.58	1.92	-241	9.85
1.94	-258	10.41	-246	10.02	-226	9.59	-228	9.59	1.94	-242	9.87
1.96	-260	10.44	-247	10.04	-228	9.62	-229	9.61	1.96	-244	9.90
1.98	-262	10.47	-249	10.07	-229	9.63	-231	9.63	1.98	-245	9.91
2.00	-264	10.50	-250	10.08	-230	9.65	-232	9.65	2.00	-246	9.93
2.05	-268	10.57	-254	10.14	-234	9.71	-235	9.69	2.02	-248	9.96
2.10	-272	10.63	-258	10.20	-237	9.75	-238	9.73	2.04	-249	9.97
2.15	-276	10.70	-261	10.25	-240	9.79	-242	9.79	2.06	-250	9.99
2.20	-279	10.74	-265	10.31	-244	9.85	-244	9.82	2.08	-252	10.02
2.25	-283	10.81	-267	10.34	-247	9.89	-247	9.86	2.10	-253	10.03
2.30	-286	10.86	-270	10.39	-250	9.93	-249	9.88	2.12	-254	10.04
2.35	-288	10.89	-272	10.42	-252	9.96	-251	9.91	2.14	-255	10.06
2.40	-290	10.92	-274	10.45	-255	10.01	-254	9.95	2.16	-257	10.09
2.45	-293	10.97	-277	10.50	-257	10.03	-255	9.97	2.18	-258	10.10
2.50	-295	11.00	-278	10.51	-259	10.06	-257	10.00	2.20	-259	10.12
2.55	-296	11.02	-280	10.54	-262	10.11	-259	10.02	2.22	-260	10.13
2.60	-298	11.05	-282	10.57	-263	10.12	-260	10.04	2.24	-261	10.15
2.65	-300	11.08	-283	10.59	-265	10.15	-262	10.07	2.26	-262	10.16
2.70			-285	10.62	-267	10.18	-263	10.08	2.28	-263	10.18
2.75			-286	10.63	-268	10.19	-264	10.09	2.30	-264	10.19
2.80			-287	10.65	-270	10.22	-266	10.12	2.32	-264	10.19
2.85			-288	10.66	-271	10.24	-267	10.14	2.34	-265	10.21
2.90			-290	10.69	-273	10.26	-268	10.15	2.36	-266	10.22
2.95			-291	10.71	-274	10.28	-269	10.16	2.38	-267	10.24
3.00			-291	10.71	-275	10.29	-270	10.18	2.40	-268	10.25
3.05			-293	10.74	-276	10.31	-271	10.19	2.42	-268	10.25
3.10			-293	10.74	-277	10.32	-272	10.20	2.44	-269	10.27
3.15			-294	10.76	-278	10.34	-273	10.22	2.46	-270	10.28
3.20			-295	10.77	-280	10.36	-274	10.23	2.48	-270	10.28
3.25			-296	10.79	-281	10.38	-275	10.25	2.50	-271	10.30
3.30			-297	10.80	-282	10.39	-276	10.26	2.55	-272	10.31
3.35			-297	10.80	-283	10.41	-276	10.26	2.60	-274	10.34
3.40			-298	10.82	-284	10.42	-277	10.27	2.65	-275	10.36
3.45			-299	10.83	-285	10.44	-278	10.29	2.70	-277	10.39
3.50			-300	10.85	-286	10.45	-279	10.30	2.75	-278	10.40
3.55					-286	10.45	-280	10.32	2.80	-280	10.43
3.60					-287	10.46	-281	10.33	2.85	-281	10.44
3.65					-288	10.48	-281	10.33	2.90	-282	10.46
3.70					-289	10.49	-282	10.34	2.95	-283	10.47
3.75					-289	10.49	-282	10.34	3.00	-284	10.49
3.80					-290	10.51	-283	10.36	3.05	-285	10.50
3.85					-291	10.52	-284	10.37	3.10	-286	10.52
3.90					-291	10.52	-285	10.39	3.15	-287	10.53
3.95					-292	10.54	-286	10.40	3.20	-288	10.55
4.00					-292	10.54	-288	10.43	3.25	-289	10.56
4.05									3.30	-289	10.56
4.10									3.35	-290	10.58
4.15									3.40	-291	10.59
4.20									3.45	-292	10.61

Raw data for Cm(DOTA) kinetic experiments in 0.1 M $NaClO_4$ (part 1)

	25 °C			35 °C			45 °C			55 °C			65 °C			75 °C		
time	Cm(aquo)	intermed.	Cm(DOTA)	Cm(aquo)	intermed.	Cm(DOTA)	Cm(aquo)	intermed.	Cm(DOTA)	Cm(aquo)	intermed.	Cm(DOTA)	Cm(aquo)	intermed.	Cm(DOTA)	Cm(aquo)	intermed.	Cm(DOTA)
[s]	[%]	[%]	[%]	[%]	[%]	[%]	[%]	[%]	[%]	[%]	[%]	[%]	[%]	[%]	[%]	[%]	[%]	[%]
0	1.00	0.00	0.00	1.00	0.00	0.00	1.00	0.00	0.00	1.00	0.00	0.00	1.00	0.00	0.00	1.00	0.00	0.00
120	0.73	0.25	0.02	0.82	0.16	0.02	0.97	0.03	0.00	1.00	0.00	0.00	1.00	0.00	0.00	0.97	0.03	0.00
180	0.72	0.25	0.04	0.80	0.17	0.03	0.94	0.06	0.00	1.00	0.00	0.00	1.00	0.00	0.00	0.94	0.05	0.01
240	0.68	0.26	0.05	0.78	0.17	0.05	0.92	0.08	0.01	0.97	0.03	0.00	0.98	0.00	0.02	0.90	0.07	0.03
300	0.67	0.26	0.07	0.76	0.17	0.07	0.89	0.08	0.02	0.95	0.04	0.01	0.96	0.00	0.03	0.86	0.07	0.07
360	0.65	0.26	0.09	0.73	0.18	0.09	0.86	0.09	0.05	0.94	0.04	0.03	0.93	0.01	0.06	0.80	0.07	0.13
420	0.63	0.26	0.12	0.71	0.18	0.12	0.84	0.09	0.08	0.90	0.05	0.05	0.89	0.01	0.10	0.73	0.07	0.20
480	0.61	0.25	0.14	0.68	0.17	0.15	0.80	0.09	0.11	0.87	0.05	0.08	0.85	0.01	0.13	0.65	0.07	0.28
540	0.59	0.24	0.16	0.66	0.17	0.18	0.77	0.10	0.13	0.84	0.06	0.11	0.80	0.02	0.18	0.57	0.07	0.36
600	0.57	0.24	0.19	0.63	0.16	0.21	0.73	0.10	0.17	0.81	0.05	0.14	0.76	0.02	0.22	0.50	0.06	0.44
660	0.56	0.23	0.20	0.60	0.17	0.23	0.71	0.09	0.21	0.77	0.06	0.17	0.71	0.03	0.26	0.42	0.06	0.52
720	0.55	0.22	0.23	0.59	0.15	0.25	0.68	0.08	0.24	0.74	0.05	0.21	0.67	0.02	0.30	0.36	0.05	0.59
780	0.54	0.22	0.24	0.57	0.16	0.27	0.64	0.08	0.27	0.69	0.06	0.25	0.64	0.02	0.34	0.31	0.05	0.64
840	0.52	0.23	0.26	0.55	0.15	0.30	0.62	0.08	0.30	0.66	0.05	0.29	0.60	0.02	0.37	0.26	0.04	0.70
900	0.51	0.21	0.28	0.53	0.15	0.32	0.59	0.08	0.33	0.63	0.05	0.32	0.56	0.02	0.42	0.23	0.04	0.74
960	0.49	0.21	0.31	0.52	0.14	0.34	0.56	0.07	0.37	0.59	0.05	0.36	0.52	0.03	0.45	0.20	0.03	0.77
1020	0.46	0.19	0.34	0.49	0.14	0.37	0.54	0.07	0.39	0.57	0.04	0.39	0.49	0.02	0.49	0.17	0.03	0.80
1080	0.45	0.19	0.36	0.48	0.13	0.39	0.51	0.07	0.42	0.54	0.04	0.42	0.46	0.01	0.52	0.15	0.03	0.82
1140	0.44	0.19	0.37	0.47	0.13	0.40	0.49	0.06	0.44	0.51	0.04	0.44	0.43	0.02	0.55	0.14	0.02	0.84
1200	0.43	0.19	0.39	0.45	0.13	0.42	0.47	0.06	0.46	0.50	0.04	0.47	0.40	0.02	0.58	0.12	0.02	0.86
1260	0.41	0.18	0.40	0.44	0.12	0.43	0.45	0.07	0.48	0.47	0.04	0.49	0.37	0.01	0.62	0.11	0.02	0.87
1320	0.41	0.18	0.42	0.42	0.12	0.46	0.44	0.06	0.50	0.45	0.04	0.51	0.34	0.01	0.65	0.10	0.02	0.88
1380	0.40	0.17	0.43	0.41	0.12	0.47	0.42	0.06	0.52	0.44	0.04	0.52	0.31	0.02	0.67	0.09	0.01	0.90
1440	0.39	0.17	0.44	0.40	0.12	0.48	0.41	0.06	0.53	0.41	0.04	0.55	0.29	0.01	0.69	0.08	0.01	0.90
1500	0.37	0.17	0.46	0.39	0.11	0.50	0.39	0.06	0.55	0.40	0.04	0.56	0.27	0.01	0.72	0.07	0.01	0.91
1560	0.37	0.16	0.47	0.38	0.11	0.51	0.38	0.06	0.56	0.39	0.03	0.58	0.25	0.01	0.74	0.07	0.01	0.92
1620	0.36	0.16	0.48	0.37	0.11	0.52	0.37	0.06	0.58	0.38	0.04	0.58	0.23	0.01	0.76	0.06	0.01	0.93
1680	0.35	0.16	0.49	0.36	0.11	0.53	0.35	0.05	0.60	0.36	0.03	0.60	0.23	0.01	0.76	0.06	0.01	0.93

1740	0.34	0.15	0.50	0.35	0.10	0.55	0.34	0.05	0.60	0.35	0.03	0.61	0.21	0.01	0.78	0.05	0.01	0.94
1800	0.34	0.15	0.50	0.34	0.10	0.56	0.33	0.04	0.62	0.34	0.04	0.62	0.19	0.01	0.80	0.05	0.01	0.95
1860	0.33	0.15	0.52	0.34	0.10	0.57	0.32	0.04	0.64	0.33	0.04	0.63	0.18	0.01	0.81	0.04	0.01	0.95
1920	0.33	0.14	0.53	0.32	0.10	0.57	0.31	0.04	0.64	0.33	0.03	0.65	0.17	0.01	0.83	0.04	0.01	0.95
1980	0.32	0.14	0.54	0.32	0.09	0.59	0.30	0.04	0.66	0.31	0.03	0.66	0.15	0.01	0.84	0.04	0.01	0.96
2040	0.32	0.14	0.54	0.31	0.09	0.60	0.29	0.04	0.67	0.31	0.03	0.66	0.14	0.01	0.86	0.03	0.01	0.96
2100	0.31	0.13	0.56	0.30	0.09	0.61	0.28	0.04	0.67	0.30	0.03	0.67	0.13	0.01	0.86	0.03	0.01	0.96
2160	0.31	0.13	0.56	0.29	0.09	0.62	0.28	0.04	0.68	0.29	0.03	0.68	0.12	0.01	0.88	0.03	0.01	0.97
2220	0.30	0.14	0.56	0.28	0.09	0.63	0.27	0.04	0.69	0.28	0.03	0.69	0.11	0.01	0.88	0.03	0.00	0.97
2280	0.30	0.13	0.57	0.28	0.08	0.64	0.26	0.04	0.70	0.27	0.03	0.70	0.11	0.00	0.89	0.02	0.00	0.97
2340	0.30	0.13	0.58	0.27	0.08	0.65	0.26	0.04	0.70	0.27	0.03	0.70	0.10	0.01	0.90	0.02	0.00	0.97
2400	0.29	0.14	0.57	0.26	0.08	0.66	0.26	0.04	0.71	0.27	0.02	0.71	0.09	0.01	0.90	0.02	0.00	0.98
2460	0.29	0.13	0.57	0.25	0.08	0.67	0.25	0.04	0.71	0.26	0.02	0.72	0.09	0.01	0.90			
2520	0.29	0.13	0.58	0.24	0.07	0.69	0.24	0.03	0.72	0.25	0.03	0.72	0.08	0.01	0.91			
2580	0.29	0.13	0.58	0.23	0.07	0.70	0.24	0.03	0.73	0.24	0.02	0.73	0.07	0.01	0.92			
2640	0.29	0.13	0.59	0.22	0.07	0.71	0.23	0.04	0.74	0.24	0.02	0.74	0.07	0.00	0.93			
2700	0.29	0.12	0.59	0.21	0.07	0.72	0.22	0.03	0.75	0.23	0.02	0.74	0.06	0.00	0.94			
2760	0.28	0.13	0.59	0.21	0.06	0.73	0.21	0.03	0.76	0.23	0.02	0.75	0.05	0.00	0.95			
2820	0.28	0.13	0.59	0.20	0.07	0.73	0.21	0.03	0.76	0.22	0.02	0.76	0.05	0.00	0.95			
2880	0.28	0.13	0.59	0.20	0.07	0.73	0.20	0.03	0.77	0.22	0.02	0.76	0.05	0.00	0.95			
2940	0.28	0.13	0.59	0.20	0.06	0.74	0.20	0.03	0.78	0.21	0.02	0.77	0.04	0.00	0.95			
3000	0.28	0.12	0.60	0.19	0.07	0.74	0.19	0.03	0.78	0.20	0.02	0.78	0.04	0.00	0.96			
3060	0.27	0.12	0.61	0.19	0.06	0.75	0.18	0.03	0.79	0.20	0.02	0.78	0.03	0.00	0.96			
3120	0.27	0.12	0.61	0.18	0.06	0.76	0.18	0.03	0.79				0.03	0.00	0.96			
3180	0.26	0.12	0.62	0.19	0.06	0.75	0.18	0.03	0.80				0.03	0.00	0.97			
3240	0.26	0.11	0.63	0.18	0.06	0.76	0.17	0.03	0.81				0.02	0.00	0.97			
3300	0.25	0.11	0.64	0.18	0.06	0.77	0.16	0.02	0.82				0.02	0.00	0.98			
3360	0.25	0.11	0.64	0.17	0.06	0.77	0.15	0.02	0.82				0.02	0.00	0.98			
3420	0.24	0.11	0.65	0.17	0.06	0.77	0.14	0.02	0.83				0.01	0.00	0.98			
3480	0.24	0.11	0.66	0.16	0.05	0.78	0.14	0.02	0.84				0.01	0.00	0.99			
3540	0.24	0.11	0.65	0.16	0.05	0.79	0.14	0.02	0.84				0.01	0.00	0.99			
3600	0.24	0.11	0.65	0.15	0.05	0.80	0.13	0.02	0.84				0.00	0.00	1.00			
3660	0.24	0.11	0.65	0.15	0.05	0.80	0.13	0.02	0.85				0.00	0.00	1.00			

3720	0.24	0.11	0.66	0.15	0.05	0.81										
3780	0.24	0.11	0.65	0.15	0.05	0.81										
3840	0.23	0.10	0.67	0.14	0.05	0.80										
3900	0.23	0.11	0.67	0.14	0.05	0.81										
3960	0.23	0.10	0.66	0.14	0.04	0.82										
4020	0.23	0.10	0.67	0.13	0.04	0.82										
4080	0.22	0.10	0.67	0.13	0.05	0.82										
4140	0.22	0.10	0.68	0.13	0.04	0.83										
4200	0.22	0.10	0.68	0.13	0.04	0.83										
4260	0.22	0.10	0.69	0.12	0.04	0.83										
5700															0.00	0.00	1.00
7620										0.00	0.00	1.00				
7740							0.00	0.00	1.00							
12660				0.00	0.00	1.00										
60660	0.00	0.00	1.00													

Raw data for Cm(DOTA) kinetic experiments in 0.1 M $NaClO_4$ (part 2)

	85 °C			93.5 °C		
time	Cm(aquo)	intermed.	Cm(DOTA)	Cm(aquo)	intermed.	Cm(DOTA)
[s]	[%]	[%]	[%]	[%]	[%]	[%]
0	1.00	0.00	0.00	1.00	0.00	0.00
90	0.98	0.02	0.00	0.99	0.00	0.01
120	0.97	0.03	0.00	0.98	0.02	0.00
150	0.96	0.04	0.00	0.97	0.02	0.00
180	0.95	0.04	0.01	0.95	0.04	0.01
210	0.93	0.05	0.01	0.94	0.05	0.02
240	0.92	0.06	0.02	0.93	0.05	0.02
270	0.91	0.06	0.04	0.89	0.07	0.04
300	0.88	0.06	0.06	0.89	0.06	0.06
330	0.86	0.06	0.07	0.86	0.06	0.08
360	0.84	0.06	0.10	0.83	0.06	0.11
390	0.81	0.07	0.12	0.81	0.07	0.13
420	0.78	0.07	0.15	0.77	0.07	0.16
450	0.75	0.07	0.18	0.73	0.07	0.19
480	0.71	0.07	0.21	0.71	0.06	0.22
510	0.70	0.06	0.24	0.68	0.07	0.26
540	0.66	0.07	0.27	0.65	0.06	0.29
570	0.64	0.06	0.30	0.61	0.07	0.32
600	0.60	0.06	0.34	0.60	0.05	0.35
630	0.58	0.06	0.36	0.56	0.05	0.39
660	0.56	0.05	0.38	0.54	0.06	0.41
690	0.53	0.06	0.41	0.51	0.05	0.43
720	0.52	0.05	0.44	0.49	0.05	0.46
750	0.49	0.05	0.46	0.46	0.05	0.49
780	0.47	0.05	0.48	0.45	0.05	0.50
810	0.45	0.05	0.50	0.42	0.05	0.52
840	0.43	0.04	0.52	0.41	0.04	0.55
870	0.42	0.04	0.54	0.39	0.05	0.56
900	0.40	0.04	0.56	0.38	0.04	0.58
930	0.38	0.04	0.58	0.37	0.04	0.59
960	0.37	0.04	0.59	0.35	0.04	0.61
990	0.36	0.03	0.61	0.33	0.04	0.63
1020	0.34	0.04	0.62	0.33	0.03	0.64
1050	0.33	0.04	0.64	0.31	0.04	0.65
1080	0.32	0.04	0.65	0.31	0.04	0.66
1110	0.31	0.03	0.65	0.30	0.03	0.67
1140	0.30	0.03	0.67	0.29	0.03	0.68
1170	0.29	0.03	0.68	0.27	0.03	0.69
1200	0.28	0.03	0.69	0.26	0.03	0.70
1230	0.27	0.03	0.70	0.26	0.03	0.71
1260	0.27	0.03	0.71	0.25	0.03	0.72
1290	0.26	0.03	0.72	0.24	0.03	0.73
1320	0.25	0.03	0.72	0.24	0.03	0.73
1350	0.24	0.03	0.73	0.23	0.03	0.74
1380	0.23	0.03	0.74	0.22	0.03	0.75
1410	0.23	0.02	0.75	0.22	0.03	0.76
1440	0.22	0.03	0.75	0.21	0.03	0.76
1470	0.22	0.02	0.76	0.21	0.03	0.76
1500	0.21	0.02	0.76	0.20	0.03	0.77
1530	0.21	0.02	0.78	0.20	0.02	0.78
1560	0.20	0.02	0.78	0.19	0.02	0.78
1590	0.20	0.02	0.78	0.19	0.02	0.79
1620	0.19	0.02	0.79	0.18	0.03	0.79
1650	0.18	0.02	0.79	0.18	0.02	0.80
1680	0.18	0.02	0.80	0.17	0.03	0.80
1710	0.18	0.02	0.80	0.17	0.03	0.80
1740	0.17	0.02	0.80	0.16	0.02	0.81
1770	0.17	0.02	0.81	0.17	0.02	0.81
1800	0.17	0.02	0.82	0.16	0.02	0.82
1830	0.16	0.02	0.82	0.16	0.02	0.82
1860	0.16	0.02	0.82	0.15	0.02	0.82
1890	0.16	0.02	0.83	0.15	0.02	0.83
1920	0.15	0.01	0.83	0.15	0.02	0.83
1950	0.15	0.01	0.84	0.14	0.02	0.83
1980	0.14	0.02	0.84	0.14	0.02	0.84
2010	0.14	0.02	0.84	0.14	0.02	0.84
2040	0.14	0.01	0.84	0.14	0.02	0.84
2070	0.14	0.02	0.85	0.14	0.02	0.84
2100	0.13	0.02	0.85	0.13	0.02	0.85
2130	0.13	0.02	0.85	0.13	0.02	0.85
2160	0.13	0.01	0.86	0.13	0.02	0.85
2190	0.13	0.02	0.86	0.13	0.02	0.85
2220	0.13	0.01	0.86	0.13	0.02	0.85
2250	0.12	0.01	0.86	0.13	0.02	0.85
2280	0.12	0.01	0.87	0.12	0.02	0.86
2310	0.12	0.01	0.87	0.12	0.01	0.86
2340	0.12	0.01	0.87	0.12	0.01	0.86
2370	0.12	0.02	0.87	0.12	0.02	0.86
2400	0.11	0.01	0.87	0.12	0.02	0.86
2430	0.11	0.01	0.88	0.12	0.01	0.87
2460	0.11	0.01	0.88	0.12	0.02	0.87
2490	0.11	0.01	0.88	0.12	0.02	0.87
2520	0.10	0.01	0.89	0.12	0.02	0.86
2550	0.10	0.01	0.89	0.12	0.01	0.87
2580	0.10	0.01	0.88	0.11	0.02	0.87
2610	0.10	0.01	0.89			
2640	0.10	0.01	0.89			
2670	0.10	0.01	0.89			
2700	0.10	0.01	0.89			
2730	0.09	0.01	0.90			
3780				0.00	0.00	1.00
6300	0.00	0.00	1.00			

Raw data for Cm(DOTA), Cm(DOTA-NCS), Cm(pDOTA-NCS) kinetic experiments in 0.1 M $NaClO_4$

	30 °C								
time	Cm(aquo)	intermed.	Cm(DOTA)	Cm(aquo)	intermed.	Cm(DOTA-NCS)	Cm(aquo)	intermed.	Cm(pDOTA-NCS)
[s]	[%]	[%]	[%]	[%]	[%]	[%]	[%]	[%]	[%]
0	1.00	0.00	0.00	1.00	0.00	0.00	1.00	0.00	0.00
120	0.59	0.34	0.06	0.28	0.70	0.02	0.21	0.57	0.23
180	0.55	0.37	0.07	0.27	0.70	0.03	0.20	0.57	0.25
240	0.53	0.37	0.09	0.28	0.69	0.04	0.19	0.56	0.27
300	0.51	0.37	0.11	0.27	0.69	0.04	0.19	0.53	0.29
360	0.50	0.36	0.14	0.27	0.69	0.05	0.19	0.53	0.30
420	0.48	0.36	0.16	0.26	0.68	0.05	0.19	0.51	0.32
480	0.46	0.35	0.19	0.26	0.68	0.06	0.19	0.50	0.33
540	0.45	0.34	0.21	0.26	0.68	0.06	0.18	0.50	0.34
600	0.43	0.33	0.24	0.26	0.67	0.07	0.18	0.49	0.35
660	0.42	0.32	0.26	0.27	0.66	0.07	0.17	0.49	0.36
720	0.41	0.31	0.28	0.26	0.67	0.07	0.17	0.48	0.37
780	0.40	0.30	0.31	0.26	0.66	0.07	0.17	0.48	0.38
840	0.38	0.29	0.33	0.26	0.67	0.07	0.17	0.47	0.38
900	0.38	0.28	0.35	0.26	0.66	0.07	0.17	0.47	0.39
960	0.37	0.27	0.37	0.26	0.66	0.08	0.17	0.46	0.40
1020	0.35	0.26	0.39	0.26	0.66	0.08	0.16	0.46	0.40
1080	0.35	0.25	0.41	0.26	0.66	0.08	0.17	0.45	0.41
1140	0.34	0.24	0.43	0.26	0.66	0.08	0.16	0.45	0.41
1200	0.33	0.23	0.44	0.26	0.66	0.08	0.17	0.44	0.42
1260	0.32	0.23	0.46	0.27	0.65	0.09	0.17	0.44	0.42
1320	0.31	0.22	0.48	0.25	0.66	0.09	0.17	0.43	0.43
1380	0.31	0.20	0.50	0.26	0.66	0.09	0.17	0.42	0.43
1440	0.30	0.20	0.51	0.26	0.65	0.09	0.16	0.42	0.44
1500	0.29	0.19	0.52	0.26	0.65	0.09	0.16	0.42	0.44
1560	0.28	0.19	0.54	0.26	0.65	0.09	0.16	0.42	0.44
1620	0.28	0.18	0.55	0.25	0.66	0.09	0.16	0.42	0.45
1680	0.27	0.17	0.56	0.26	0.65	0.10	0.16	0.41	0.45
1740	0.26	0.16	0.58	0.26	0.64	0.10	0.16	0.40	0.45
1800	0.25	0.16	0.59	0.26	0.64	0.10	0.16	0.41	0.46
1860	0.25	0.15	0.61	0.26	0.64	0.10	0.15	0.41	0.46

	45 °C								
time	Cm(aquo)	intermed.	Cm(DOTA)	Cm(aquo)	intermed.	Cm(DOTA-NCS)	Cm(aquo)	intermed.	Cm(pDOTA-NCS)
[s]	[%]	[%]	[%]	[%]	[%]	[%]	[%]	[%]	[%]
0	1.00	0.00	0.00	1.00	0.00	0.00	1.00	0.00	0.00
120	0.73	0.23	0.03	0.43	0.56	0.02	0.37	0.48	0.15
180	0.68	0.26	0.06	0.40	0.57	0.03	0.35	0.48	0.18
240	0.60	0.28	0.10	0.38	0.58	0.04	0.32	0.47	0.22
300	0.54	0.29	0.17	0.37	0.57	0.06	0.31	0.45	0.26
360	0.47	0.27	0.25	0.36	0.55	0.09	0.29	0.43	0.29
420	0.42	0.25	0.33	0.34	0.54	0.11	0.28	0.41	0.32
480	0.36	0.22	0.42	0.33	0.53	0.14	0.27	0.39	0.35
540	0.31	0.19	0.50	0.32	0.51	0.16	0.26	0.37	0.39
600	0.27	0.17	0.56	0.31	0.50	0.19	0.24	0.36	0.41

660	0.24	0.14	0.62	0.31	0.48	0.22	0.23	0.34	0.44
720	0.21	0.12	0.68	0.29	0.46	0.24	0.23	0.31	0.47
780	0.19	0.10	0.72	0.28	0.46	0.27	0.22	0.30	0.50
840	0.17	0.08	0.77	0.28	0.43	0.29	0.21	0.28	0.52
900	0.14	0.07	0.80	0.27	0.42	0.31	0.21	0.27	0.54
960	0.13	0.05	0.82	0.26	0.41	0.33	0.20	0.26	0.56
1020	0.11	0.05	0.85	0.26	0.39	0.35	0.19	0.24	0.57
1080	0.10	0.04	0.87	0.25	0.39	0.37	0.19	0.23	0.59
1140	0.09	0.03	0.89	0.24	0.37	0.39	0.19	0.22	0.60
1200	0.09	0.02	0.91	0.23	0.36	0.41	0.18	0.21	0.62
1260	0.08	0.01	0.92	0.22	0.35	0.43	0.18	0.20	0.63
1320	0.07	0.01	0.93	0.22	0.34	0.44	0.17	0.20	0.64
1380	0.07	0.00	0.95	0.22	0.33	0.45	0.17	0.19	0.65
1440	0.06	-0.01	0.96	0.20	0.33	0.47	0.17	0.18	0.66
1500	0.05	-0.01	0.97	0.20	0.31	0.49	0.17	0.18	0.66
1560	0.05	-0.01	0.97	0.19	0.31	0.50	0.16	0.17	0.67
1620	0.05	-0.02	0.98	0.19	0.30	0.52	0.16	0.17	0.67
1680	0.04	-0.02	0.99	0.19	0.29	0.53	0.16	0.16	0.68
1740	0.04	-0.02	0.99	0.18	0.28	0.54	0.16	0.16	0.68
1800	0.04	-0.02	1.00	0.18	0.27	0.55	0.16	0.16	0.69
1860	0.03	-0.03	1.01	0.17	0.27	0.57	0.15	0.16	0.69

	60 °C								
time [s]	Cm(aquo) [%]	intermed. [%]	Cm(DOTA) [%]	Cm(aquo) [%]	intermed. [%]	Cm(DOTA-NCS) [%]	Cm(aquo) [%]	intermed. [%]	Cm(pDOTA-NCS) [%]
0	1.00	0.00	0.00	1.00	0.00	0.00	1.00	0.00	0.00
120	0.78	0.18	0.04	0.59	0.40	0.01	0.58	0.35	0.07
180	0.67	0.21	0.12	0.54	0.43	0.04	0.52	0.37	0.11
240	0.52	0.21	0.27	0.50	0.43	0.07	0.48	0.36	0.17
300	0.38	0.17	0.45	0.44	0.41	0.14	0.43	0.35	0.23
360	0.27	0.12	0.61	0.39	0.39	0.22	0.38	0.32	0.31
420	0.18	0.08	0.74	0.34	0.35	0.31	0.33	0.28	0.40
480	0.12	0.05	0.84	0.30	0.30	0.41	0.28	0.24	0.48
540	0.08	0.03	0.90	0.26	0.25	0.49	0.24	0.20	0.56
600	0.06	0.01	0.94	0.21	0.22	0.57	0.20	0.17	0.63
660	0.04	0.00	0.97	0.18	0.18	0.64	0.18	0.14	0.69
720	0.02	0.00	0.99	0.15	0.16	0.69	0.15	0.11	0.74
780	0.02	-0.01	1.00	0.13	0.13	0.74	0.13	0.09	0.78
840	0.01	-0.01	1.01	0.11	0.11	0.78	0.12	0.07	0.81
900	0.01	-0.02	1.01	0.10	0.10	0.81	0.10	0.06	0.84
960	0.01	-0.02	1.02	0.09	0.08	0.84	0.09	0.04	0.86
1020				0.08	0.06	0.87	0.08	0.03	0.89
1080				0.06	0.06	0.88	0.08	0.02	0.90
1140				0.06	0.05	0.90	0.07	0.01	0.92
1200				0.05	0.04	0.92	0.06	0.01	0.93
1260				0.04	0.03	0.93	0.05	0.00	0.94
1320				0.03	0.03	0.94			
1380				0.03	0.02	0.95			
1440				0.03	0.02	0.96			
1500				0.03	0.01	0.97			

1560				0.02	0.01	0.98			
1620				0.02	0.00	0.98			
1680				0.02	0.00	0.99			
1740				0.01	0.00	0.99			
1800				0.01	0.00	1.00			
1860				0.01	0.00	1.00			

	75 °C								
time [s]	Cm(aquo) [%]	intermed. [%]	Cm(DOTA) [%]	Cm(aquo) [%]	intermed. [%]	Cm(DOTA-NCS) [%]	Cm(aquo) [%]	intermed. [%]	Cm(pDOTA-NCS) [%]
0	1.00	0.00	0.00	1	0	0	1	0	0
120	0.91	0.08	0.01	0.7642	0.2254	0.016	0.7801	0.2005	0.0289
180	0.75	0.14	0.11	0.6842	0.2777	0.0384	0.6933	0.2385	0.0751
240	0.46	0.14	0.39	0.6013	0.3037	0.0927	0.5888	0.258	0.1563
300	0.21	0.08	0.71	0.4987	0.2804	0.2174	0.477	0.2271	0.2986
360	0.08	0.04	0.89	0.3797	0.2276	0.3885	0.3493	0.1708	0.4836
420	0.03	0.02	0.96	0.2655	0.1649	0.5659	0.2415	0.119	0.6409
480	0.01	0.01	0.99	0.1858	0.1063	0.7047	0.1574	0.0739	0.7682
540	0.00	0.01	0.99	0.1212	0.0681	0.8088	0.1059	0.0396	0.8528
600	0.00	0.00	1.00	0.0837	0.0387	0.875	0.0716	0.0196	0.9051
660	0.00	0.00	1.00	0.0559	0.0215	0.9202	0.0488	0.0074	0.9401
720				0.0359	0.0088	0.9513	0.035	-0.005	0.9652
780				0.0259	-8.00E-04	0.9709	0.0263	-0.0113	0.9786
840				0.0161	-0.0054	0.9849	0.0196	-0.015	0.9899
900				0.0127	-0.0111	0.9942	0.0138	-0.0159	0.995
960				0.0073	-0.0138	1.0019	0.0099	-0.0188	1.0023

	90 °C								
time [s]	Cm(aquo) [%]	intermed. [%]	Cm(DOTA) [%]	Cm(aquo) [%]	intermed. [%]	Cm(DOTA-NCS) [%]	Cm(aquo) [%]	intermed. [%]	Cm(pDOTA-NCS) [%]
0	1.00	0.00	0.00	1	0	0	1	0	0
120	0.85	0.06	0.10	0.7578	0.1712	0.0699	0.9	0.0918	0.0165
180	0.52	0.07	0.40	0.5163	0.1583	0.3219	0.7673	0.1393	0.0983
240	0.22	0.04	0.74	0.2743	0.0862	0.6347	0.55	0.1331	0.3191
300	0.09	0.02	0.89	0.1471	0.0457	0.802	0.3322	0.0856	0.5818
360	0.05	0.01	0.94	0.0952	0.0241	0.8727	0.1946	0.0477	0.7554
420	0.02	0.01	0.96	0.0643	0.0174	0.909	0.1344	0.0309	0.8302
480	0.02	0.01	0.97	0.0466	0.0134	0.9296	0.0997	0.0269	0.8671
540	0.01	0.00	0.98	0.0346	0.0084	0.9454	0.0805	0.0199	0.8903
600				0.028	0.005	0.9543	0.0679	0.0169	0.9061

Raw data thermodynamic experiments Cm(DOTA), Ac(DOTA) in 0.1 M $NaClO_4$

45 °C				60 °C				70 °C				80 °C				90 °C			
pH	$DOTA^{4-}$ mol/L	Cm(aquo) [%]	Cm(DOTA) [%]	pH	$DOTA^{4-}$ mol/L	Cm(aquo) [%]	Cm(DOTA) [%]	pH	$DOTA^{4-}$ mol/L	Cm(aquo) [%]	Cm(DOTA) [%]	pH	$DOTA^{4-}$ mol/L	Cm(aquo) [%]	Cm(DOTA) [%]	pH	$DOTA^{4-}$ mol/L	Cm(aquo) [%]	Cm(DOTA) [%]
2.45	5.9E-26	0.99	0.00	2.44	5.3E-26	0.98	0.02	2.44	5.1E-26	0.98	0.02	2.22	2.1E-26	1.00	0.00	2.30	4.0E-26	1.00	0.00
2.55	1.2E-24	0.94	0.06	2.74	8.0E-25	0.91	0.08	2.60	2.2E-25	0.95	0.05	2.44	1.5E-25	0.93	0.07	2.40	9.9E-26	0.96	0.04
2.80	1.4E-24	0.94	0.06	2.82	1.6E-24	0.89	0.11	2.70	5.4E-25	0.90	0.10	2.52	3.2E-25	0.92	0.08	2.48	2.0E-25	0.87	0.13
2.95	8.8E-24	0.76	0.22	2.90	3.3E-24	0.72	0.28	2.80	1.3E-24	0.79	0.21	2.70	1.6E-24	0.81	0.19	2.53	3.0E-25	0.76	0.24
3.00	3.4E-23	0.33	0.67	2.93	4.3E-24	0.72	0.27	2.80	1.3E-24	0.74	0.26	2.80	3.8E-24	0.72	0.28	2.62	6.6E-25	0.67	0.33
3.15	4.5E-23	0.21	0.77	2.97	6.1E-24	0.66	0.34	2.85	1.9E-24	0.63	0.37	2.88	7.2E-24	0.50	0.49	2.67	1.0E-24	0.66	0.34
3.30	1.3E-22	0.18	0.81	3.05	1.2E-23	0.44	0.56	2.90	2.9E-24	0.55	0.46	2.98	1.7E-23	0.36	0.64	2.76	2.2E-24	0.51	0.49
3.45	4.8E-22	0.08	0.90	3.09	1.7E-23	0.40	0.60	2.95	4.4E-24	0.50	0.55	3.07	3.5E-23	0.22	0.78	2.81	3.3E-24	0.37	0.63
3.65	2.7E-21	0.04	0.95	3.15	2.8E-23	0.29	0.71	3.04	9.4E-24	0.34	0.66	3.30	2.4E-22	0.02	0.98	2.85	4.7E-24	0.36	0.64
				3.17	3.3E-23	0.24	0.76	3.07	1.2E-23	0.30	0.70	3.40	5.8E-22	0.00	1.00	3.01	1.8E-23	0.13	0.87
				3.45	3.5E-22	0.03	0.97	3.30	8.3E-23	0.05	0.95					3.10	3.7E-23	0.05	0.95
																3.19	8.1E-23	0.00	1.00

45 °C				60 °C				70 °C				80 °C				90 °C			
pH	$DOTA^{4-}$ mol/L	Ac(aquo) [%]	Ac(DOTA) [%]	pH	$DOTA^{4-}$ mol/L	Ac(aquo) [%]	Ac(DOTA) [%]	pH	$DOTA^{4-}$ mol/L	Ac(aquo) [%]	Ac(DOTA) [%]	pH	$DOTA^{4-}$ mol/L	Ac(aquo) [%]	Ac(DOTA) [%]	pH	$DOTA^{4-}$ mol/L	Ac(aquo) [%]	Ac(DOTA) [%]
3.50	7.8E-22	0.97	0.03	3.20	4.5E-22	0.97	0.03	3.10	2.5E-22	0.99	0.01	3.10	7.5E-27	1.00	0.00	3.00	2.3E-22	0.99	0.01
3.60	1.8E-21	0.94	0.06	3.30	1.1E-21	0.94	0.06	3.18	5.1E-22	0.86	0.14	3.20	1.3E-21	0.95	0.05	3.20	1.3E-21	0.93	0.07
3.80	1.0E-20	0.67	0.34	3.30	1.1E-21	0.94	0.06	3.20	6.0E-22	0.83	0.17	3.28	2.5E-21	0.86	0.14	3.33	4.1E-21	0.78	0.22
3.85	1.5E-20	0.59	0.41	3.40	2.6E-21	0.84	0.16	3.27	1.1E-21	0.74	0.26	3.37	6.8E-21	0.78	0.22	3.40	7.4E-21	0.66	0.34
3.95	3.4E-20	0.48	0.52	3.50	6.2E-21	0.74	0.26	3.30	1.5E-21	0.70	0.30	3.50	2.0E-20	0.45	0.55	3.50	1.7E-20	0.49	0.51
4.05	7.5E-20	0.20	0.80	3.60	1.4E-20	0.72	0.28	3.33	1.8E-21	0.66	0.34	3.60	4.8E-20	0.33	0.67	3.52	2.0E-20	0.38	0.62
4.12	1.3E-19	0.15	0.85	3.70	3.2E-20	0.46	0.54	3.43	4.3E-21	0.45	0.55	3.70	9.0E-20	0.26	0.74	3.60	3.9E-20	0.28	0.72
4.15	1.6E-19	0.14	0.86	3.80	7.0E-20	0.23	0.77	3.55	1.3E-20	0.33	0.67	3.73	1.0E-19	0.18	0.83	3.70	8.8E-20	0.14	0.86
4.25	3.4E-19	0.08	0.92	3.97	2.5E-19	0.05	0.95	3.65	2.9E-20	0.14	0.86	3.78	1.6E-19	0.13	0.87	3.80	1.9E-19	0.09	0.91
4.40	9.6E-19	0.02	0.98	4.00	3.1E-19	0.07	0.93	3.70	4.5E-20	0.12	0.88	3.80	1.8E-19	0.09	0.91	3.85	2.8E-19	0.09	0.91
				4.05	4.3E-19	0.04	0.96	3.75	6.7E-20	0.06	0.94	3.90	4.1E-19	0.03	0.97	3.90	4.1E-19	0.05	0.95
				4.05	4.5E-19	0.05	0.95	3.80	1.0E-19	0.05	0.95	3.90	9.1E-19	0.03	0.97	3.93	5.0E-19	0.04	0.96
				4.10	6.2E-19	0.00	1.00	3.90	2.2E-19	0.02	0.98								

Raw data ICP-MS of various Ac-225 charges

Element	Date Prep.	Date Meas.	blank 1 ng/g	Sample 1 ng/g	Sample 2 ng/g	Ratio	Sample 1	Sample 2
Ac225+Ra225	27.2.	9.3.	n.d.	0.0025 ± 0.0003	0.00014 ± 0.00002			
Ca	27.2.	9.3.	11.80 ± 1.40	120.05 ± 14.41	11.95 ± 1.43	Ac: Ca	43194.80	1170.13
Fe	27.2.	9.3.	5.00 ± 0.60	1.30 ± 0.16	6.56 ± 0.79	Ac: Fe	-1470.66	11057.97

Element	Date Prep.	Date Meas.	blank 2 ng/g	blank 3 ng/g	Sample 3 ng/g	Sample 4 ng/g	Ratio	Sample 3	Sample 4
Ac225+Ra225	20.3.	1.4.	n.d.	n.d.	0.0012 ± 0.0001	0.00088 ± 0.00011			
Ca	20.3.	1.4.	13.60 ± 1.60	6.30 ± 0.80	61.46 ± 7.37	28.33 ± 3.40	Ac:Ca	42242.505	20863.346
Fe	20.3.	1.4.	2.70 ± 0.13	0.90 ± 0.10	4.37 ± 0.52	2.68 ± 0.32	Ac:Fe	2121.20	1022.78

Element	Date Prep.	Date Meas.	blank 4 ng/g	Sample 5 ng/g	Sample 6 ng/g	Ratio	Sample 5	Sample 6
Ac225+Ra225	8.10.	14.10.	n.d.	0.025 ± 0.003	0.025 ± 0.003			
Ca	8.10.	14.10.	8.10 ± 1.00	104.52 ± 12.54	94.14 ± 11.30	Ac:Ca	3817.898	3390.872
Fe	8.10.	14.10.	1.20 ± 0.10	2.87 ± 0.34	13.64 ± 1.64	Ac:Fe	66.978	490.683

Raw data labelling of DOTA-NCS-MabThera with Ac-225

specific activity	time [min]	yield [%]	average [%]
5 µCi/100 µg	5	98.3	96.1
		93.8	
5 µCi/100 µg	15	94.0	94.3
		93.5	
		94.0	
		95.0	
		92.7	
		93.0	
		96.0	
		96.5	
10 µCi/100 µg	5	96.6	96.3
		96.0	
10 µCi/100 µg	15	95.0	96.0
		94.5	
		95.4	
		95.5	
		98.3	
		97.0	

specific activity	time [min]	yield [%]	average [%]
20 µCi/100 µg	15	96.2	96.0
		97.1	
		95.6	
		94.9	
20 µCi/100 µg	60	96.3	95.5
		94.6	
30 µCi/100 µg	15	96.1	96.3
		96.3	
		95.9	
		96.8	
40 µCi/100 µg	15	94.0	95.1
		96.1	
50 µCi/100 µg	15	93.0	94.5
		96.4	
		94.0	

Raw data kinetic stability Ac-DOTA-NCS-mAb conjugate in various media, SA = 10 µCi/100 µg

	in EDTA/serum					in 0.05 M carbonate		in 10 mM EDTA		in PBS		in 0.2 M TRIS
	37 °C		45 °C			15 min/42 °C		15 min/42 °C		15 min/42 °C		15 min/42 °C
time	5 min	15 min	5 min	15 min	blank	DF = 1:10	blank	DF = 1:10	blank	DF = 1:10	blank	reaction batch
[d]	[%]	[%]	[%]	[%]	[%]	[%]	[%]	[%]	[%]	[%]	[%]	[%]
0	100.0	100.0	100.0	100.0	1.0	100.0	1.0	100.0	0.0	100.0	0.0	100.0
1	93.9	94.1	96.7	97.3		99.4		95.5		94.0		
2	90.4	93.4			1.0	94.0				91.0		95.7
3	91.8	90.8	90.6	87.3								
4			89.5	87.9	2.0	95.7	1.5	90.6	2.0	84.9	3.0	90.3
5												
6	89.6	90.0			1.0							
7	89.8	88.9	88.9	87.7	2.0	92.5	2.0	89.1	1.0	83.9	1.5	
8			88.1	87.8		89.9		84.3				84.6
9	77.0	80.3			1.5	88.0	3.0	84.4	0.0	81.9	1.0	
10	78.2	87.9			0.9	86.8						84.2
11			84.3	80.0	1.0		2.0		0.0		1.0	
12												
13						86.3	2.0	82.8	1.0	74.4	0.0	
14												79.7
15							2.0		0.0		2.5	

Raw data kinetic stability Ac-DOTA-NCS-mAb conjugate in serum

	10 µCi/100 µg, DF = 1:10					10 µCi/100 µg,			DF = 1:10			
	37 °C		45 °C			15 min/42 °C			15 min/45 °C			
time	5 min	15 min	5 min	15 min	blank	DF = 1:10	DF = 1:20	DF = 1:50	20 µCi/100 µg		30 µCi/100 µg	average
[d]	[%]	[%]	[%]	[%]	[%]	[%]	[%]	[%]	[%]	[%]	[%]	[%]
0	100.0	100.0	97.2	100.0		100.0	100.0	100.0	100.0	100.0	100.0	99.7
1	99.4	97.4	100.0	93.9		93.4	99.3	97.0				97.2
2	98.9	96.6			1.0					96.6		97.4
3	95.5	94.8	95.0	94.9		88.1	94.4	96.8		96.5		94.5
4			91.8	92.5	1.0	93.8	99.7	97.3	90.5	95.4	91.6	94.1
5										95.7		95.7
6	94.7	93.6			0.0					95.3		94.5
7	93.4	90.4	90.7	92.6	0.0				86.3		88.4	90.0
8			85.4	87.4								86.0
9	91.4	90.4			0.0	95.4	94.3	97.3	89.5		89.5	92.5
10	92.8	87.8	88.1	90.8	0.9					94.3		91.0
11			87.9	85.2		84.1	97.9	97.8	86.3	93.4	87.4	90.0
12					1.0					93.4		93.4
13												
14	89.7	89.1							86.3			88.4
16			87.5	85.9	0.0				87.4	91.6	87.4	88.0
18			83.7	88.5	0.5				90.5		87.4	88.0
21	93.6	94.1			2.0				90.5	89.7	87.4	91.0
22			89.6	92.8	1.0				91.6		86.3	90.0

Raw data kinetic stability Ac-DOTA-conjugates in serum, physiological conditions

	Ac(III)DOTA-NCS-Mabthera			Ac(III)DOTATOC
time	20 µCi/100 µg, DF = 1:10	10 µCi/100 µg, DF = 1:10	blank	Ref. [283]
[d]	[%]	[%]	[%]	[%]
0				100
1	100	100	1	97.9
2		93.8	1.5	98.4
3	96.6	95.3	0.6	
4	96.5		2	
5	95.4		1.7	90.4
6	95.7		2.1	93.7
7	95.3		0.6	92.8
8		93.2	1	96.3
9		89.8	1.9	93.5
10		88.4	2.1	
11	94.3		0.3	
12	93.4		1.4	92.3
13	93.4		1.2	90.1
14		88	1.6	92.3
15				90.9
16				90.1
18	91.6		0.4	
19				88.9
20				87.8
22				88.1
23				83.2
24				84
25	89.7		2.2	83.2
27				80.7
28				64.5
31				75.7
32	82		1.8	
33				76.8
35				73.6
40				64.2
44				52.5
47	74.9		2	

7.4 Lists of Abbreviations

α alpha

(L-)AA (L-)ascorbic acid

A *spectroscopy*: absorbance; *kinetics*: frequence factor

Å Angstrom; 1Å = 10^{-10} m

AIT alpha immunotherapy

An, An(III) (trivalent) actinide elements

β^- beta decay, emission of electrons e^-

β^+ beta decay, emission of positrons e^+

BFCA bifuntional(ised) chelating agent

Bn benzyl

Bq Becquerel; 1 Bq = 1 s^{-1}

bzw. beziehungsweise; respectively

c concentration

CD20 cluster of differentiation (on B-lymphocytes

CDR complementarity determining region

Ch/mAb chelators per antibody molecule

CHX-DOTA 2-(*p*-isothiocyanatobenzyl)-5,6-cyclohexano-1,4,7,10-tetraazacyclododecane-1,4,7,10-tetraacetic acid

CHX-DTPA 2-(*p*-isothiocyanatobenzyl)-cyclohexyl-diethylenetriaminepentaacetic acid

Ci Curie; 1 Ci = 3.7 x 10^{10} Bq

cm centimetre, 10^{-2}m

CN coordination number

cpm counts per minute

d day

Da dalton, unified atomic mass unit (also: u)

DGA diglycolamide

DNA desoxyribonucleic acid

DOTA 1,4,7,10-tetraazacyclodecane-1,4,7,10-tetraacetic acid

DOTA-NCS 2-(*p*-isothiocyanatobenzyl)-1,4,7,10-tetraazacyclodecane-1,4,7,10-tetraacetic acid

(pDOTA-NCS temperature-processed DOTA-NCS)

DOTATOC (DOTA(0)-Phe(1)-Tyr(3))octreotid

DSB double-strand break

DTPA diethylenetriaminepentaacetic acid

ε extinction coefficient

E_a activation energy

EBRT external beam radiotherapy

e.g. exempli gratia, for example

E_{kin} kinetic energy

EDTA ethylenediaminetetraacetic acid

et al and others

F fluorescence

FDA Food and Drug Administration (US)

Fig. figure

fs femtosecond, 10^{-15} s

FWHM full width at half maximum

γ gamma

g gram

GBq giga becquerel, 10^{9} Bq

Gy gray, J/kg

h hour

HAMA human anti-mouse antibody

HBS human blood serum

HEHA 1,4,7,10,13,16-hexaazacyclooctadecane-1,4,7,10,13,16-hexaacetic acid

HPLC high performance liquid chromatography

HSA human serum albumin

HSAB Pearson "hard and soft (Lewis) acids and bases" concept

HSTF human serum transferrin

I *spectroscopy*: intensity; *thermodynamics*: ionic strength

i.a. inter alia, amongst others

IC internal conversion

ICP-MS inductively-coupled-plasma mass-spectrometry

IgG immunoglobulin G

IPPE Institute of Physics and Power Engineering (RU)

i.r. ionic radius

ISC inter system crossing

ITLC instant thin layer chromatography

ITU Institute for Transuranium Elements

IUPAC International Union of Pure and Applied Chemistry

kBq kilo becquerel

kDa kilo dalton, 10^{3} Da

keV kilo electron volt, 10^{3} eV

λ wavelength

L ligand

LET linear energy transfer

Ln, Ln(III) (trivalent) lanthanide elements

µCi micro Curie, 10^{-6}Ci

µg microgram, 10^{-6}g

µl microlitre, 10^{-6}l

µm micrometre, 10^{-6}m

µs mircosecond, 10^{-6}s

M molar / molarity

mAb monoclonal antibody

MBq mega becquerel, 10^{6}Bq

mCi milli Curie, 10^{-3}Ci

MeV mega electron volt, 10^{6}eV

MFW metal free water (MilliQ)

mg milligram, 10^{-3}g

min minute

ml millilitre, 10^{-3}l

mm millimetre, 10^{-3}m

MRI magnetic resonance imaging

ms millisecond, 10^{-3}s

Mw molecular weight

n(H_2O) number of (water) molecules

NaOAc sodium acetate

NHL non-Hodgkin lymphoma

NIST National Institute of Standards and Technology

nm nanometer, 10^{-9}m

NMR nuclear magnetic resonance

OAc acetate

ORNL Oak Ridge National Laboratories

P phosphorescence

PBS phosphate buffered saline

PET positron emission tomography

PEPA 1,4,7,10,13-pentaazacyclopentadecane-1,4,7,10,13-pentaacetic acid

pH potentia hydrogenii, power of hydrogen

ps picosecond, 10^{-12} s

p-SCN para-isothiocyanato

p.w. present work

RCP radiochemical purity

RIC radioimmunoconjugate

RIT radioimmunotherapy

Rf retention factor

SA specific activity

SAP square antiprismatic

scFv single-chain variable fragment

SEC size exclusion chromatography

SE-HPLC size-exclusion HPLC

SG silica gel

SPECT single-photon emission computed tomography

SSB single-strand break

t time

$\mathbf{t_{\frac{1}{2}}}$ half-life

τ fluorescence lifetime

T temperature

TAT targeted alpha therapy

TEHDGA N,N,N',N' tetrakis-2-ethylhexyldiglycolamide

TETA 1,4,8,11-tetraazacyclotetradecane-1,4,8,11-tetraacetic acid

TF transferrin

$\mathbf{TMA^+}$ tetramethylammonium

TMAA tetramethylammonium acetate

TMACl tetramethylammonium chloride

$\mathbf{TMAClO_4}$ tetramethylammonium perchlorate

TODGA N,N,N',N' tetraoctyldiglycolamide

TRIS tris(hydroxymethyl)aminomethane

TRLFS time resolved laser fluorescence spectroscopy

TSAP twisted-square antiprismatic

US United States of America

UTEVA resin for retention of uranium and tetravalent actinides

UV ultraviolet

Vis visible light

VR vibronic relaxation

List of Figures

List of Tables

Bibliography

[1] Scheinberg, D.A. and McDevitt, M.R., *Actinium-225 in Targeted Alpha-Particle Therapeutic Applications*, Current Radiopharmaceuticals, **4**, 306–320, **2011**.

[2] Deal, K.A.; Davis, I.A.; Mirzadeh, S.; Kennel, S.J.; and Brechbiel, M.W., *Improved in vivo stability of actinium-225 macrocyclic complexes*, Journal of Medicinal Chemistry, **42**(15), 2988–2992, **1999**.

[3] Miederer, M.; Henriksen, G.; Alke, A.; Mossbrugger, I.; Quintanilla-Martinez, L.; Senekowitsch-Schmidtke, R.; and Essler, M., *Preclinical evaluation of the alpha-particle generator nuclide Ac-225 for somatostatin receptor radiotherapy of neuroendocrine tumors*, Clinical Cancer Research, **14**(11), 3555–3561, **2008**.

[4] Miederer, M.; Scheinberg, D.A.; and McDevitt, M.R., *Realizing the potential of the Actinium-225 radionuclide generator in targeted alpha particle therapy applications*, Advanced Drug Delivery Reviews, **60**(12), 1371–1382, **2008**.

[5] Anderegg, G.; Arnaud-Neu, F.; Delgado, R.; Felcman, J.; and Popov, K., *Critical evaluation of stability constants of metal complexes of complexones for biomedical and environmental applications (IUPAC Technical Report)*, Pure and Applied Chemistry, **77**(8), 1445–1495, **2005**.

[6] McDevitt, M.R.; Ma, D.S.; Simon, J.; Frank, R.K.; and Scheinberg, D.A., *Design and synthesis of Ac-225 radioimmunopharmaceuticals*, Applied Radiation and Isotopes, **57**(6), 841–847, **2002**.

[7] Kannengiesser, S., *Radiolabelling of antibodies and peptides with Ac-225*, Diplomarbeit, University of Heidelberg, **2009**.

[8] Wu, S.L. and Horrocks, W.D., *Kinetics of complex-formation by macrocyclic polyaza polycarboxylate ligands - Detection and characterization of an intermediate in the Eu3+-Dota system by Laser-excited luminescence*, Inorganic Chemistry, **34**(14), 3724–3732, **1995**.

[9] Wu, S.L. and Horrocks, W.D., *Direct determination of stability constants of lanthanide ion chelates by Laser-excited europium(III) luminescence spectroscopy: Application to cyclic and acyclic aminocarboxylate complexes*, Journal of the Chemical Society - Dalton Transactions, (9), 1497–1502, **1997**.

[10] Wu, S.L. and Horrocks, W.D., *General method for the determination of stability constants of lanthanide ion chelates by ligand - ligand competition: a Laser-excited Eu3+ luminescence excitation spectroscopy*, Analytical Chemistry, **68**(2), 394–401, **1996**.

[11] Moreau, J.; Guillon, E.; Pierrard, J.C.; Rimbault, J.; Port, M.; and Aplincourt, M., *Complexing mechanism of the lanthanide cations Eu3+, Gd3+, and Tb3+ with 1,4,7,10-tetrakis(carboxymethyl)-1,4,7,10-tetraazacyclododecane (dota) - Characterization of three successive complexing phases: Study of the thermodynamic and structural properties of the complexes by potentiometry, luminescence spectroscopy, and EXAFS*, Chemistry - a European Journal, **10**(20), 5218–5232, **2004**.

[12] Huber, R.; Seidl, C.; Schmid, E.; Seidenschwang, S.; Becker, K.F.; Schuhmacher, C.; Apostolidis, C.; Nikula, T.; Kremmer, E.; Schwaiger, M.; and Senekowitsch-Schmidtke, R., *Locoregional alpha-radioimmunotherapy of intraperitoneal tumor cell dissemination using a tumor-specific monoclonal antibody*, Clinical Cancer Research, **9**(10), 3922s–3928s, **2003**.

[13] Friesen, C.; Glatting, G.; Koop, B.; Schwarz, K.; Morgenstern, A.; Apostolidis, C.; Debatin, K.M.; and Reske, S.N., *Breaking chemoresistance and radioresistance with [Bi-213]anti-CD45 antibodies in leukemia cells*, Cancer Research, **67**(5), 1950–1958, **2007**.

[14] Kassis, A.I. and Adelstein, S.J., *Radiobiologic principles in radionuclide therapy*, Journal of Nuclear Medicine, **46**, 4S–12S, **2005**.

[15] von Mehren, M.; Adams, G.P.; and Weiner, L.M., *Monoclonal antibody therapy for cancer*, Annual Review of Medicine-selected Topics In the Clinical Sciences, **54**, 343–369, **2003**.

[16] Davis, T.A.; Kaminski, M.S.; Leonard, J.P.; Hsu, F.J.; Wilkinson, M.; Zelenetz, A.; Wahl, R.L.; Kroll, S.; Coleman, M.; Goris, M.; Levy, R.; and Knox, S.J., *The radioisotope contributes significantly to the activity of radioimmunotherapy*, Clinical Cancer Research, **10**(23), 7792–7798, **2004**.

[17] Kwekkeboom, D.J.; Mueller-Brand, J.; Paganelli, G.; Anthony, L.B.; Pauwels, S.; Kvols, L.K.; O'Dorisio, T.M.; Valkema, R.; Bodei, L.; Chinol, M.; Maecke, H.R.; and Krenning, E.P., *Overview of results of peptide receptor radionuclide therapy with 3 radiolabeled somatostatin analogs*, Journal of Nuclear Medicine, **46**, 62S–66S, **2005**.

[18] Grubbé, E.H., *Priority in the therapeutic use of X-rays*, Radiology, **21**, 156–162, **1933**.

[19] Bernier, J., *Principles and practice of re-irradiation (external and brachytherapy)*, Radiotherapy and Oncology, **73**, S184, **2004**.

[20] Gaunt, W.; Griffith, H.; and Irving, J., *The assimilation of radioactive phosphorus following phosphorus deficiency in rats*, Journal of Physiology, **100**, 372–384, **1942**.

[21] Brans, B.; Linden, O.; Giammarile, F.; Tennvall, J.; and Punt, C., *Clinical applications of newer radionuclide therapies*, European Journal of Cancer, **42**(8), 994–1003, **2006**.

[22] Milenic, D.E. and Brechbiel, M.W., *Targeting of radio-isotopes for cancer therapy*, Cancer Biology & Therapy, **3**(4), 361–370, **2004**.

[23] Witzig, T.E., *Radioimmunotherapy for B-cell non-Hodgkin lymphoma*, Best Practice & Research Clinical Haematology, **19**(4), 655–668, **2006**.

[24] Press, O.W., *Radioimmunotherapy for non-Hodgkin's lymphomas: A historical perspective*, Seminars in Oncology, **30**(2), 10–21, **2003**.

[25] *ZEVALIN® (ibritumomab tiuxetan) injection for intravenous use - A resource guide for patients and their caregivers, 2012 Spectrum Pharmaceuticals, Inc.*

[26] Gordon, L.I., *Getting the facts: Zevalin*, Lymphoma Research Foundation, **2008**.

[27] McDevitt, M.R.; Sgouros, G.; Finn, R.D.; Humm, J.L.; Jurcic, J.G.; Larson, S.M.; and Scheinberg, D.A., *Radioimmunotherapy with alpha-emitting nuclides*, European Journal of Nuclear Medicine, **25**(9), 1341–1351, **1998**.

[28] Zalutsky, M.R.; Reardon, D.A.; Pozzi, O.R.; Vaidyanathan, G.; and Bigner, D.D., *Targeted alpha-particle radiotherapy with At-211-labeled monoclonal antibodies*, Nuclear Medicine and Biology, **34**(7), 779–785, **2007**.

[29] Hall, E., *Radiobiology for the Radiobiologist*, Lippincott, **2006**.

[30] Kassis, A.I., *Therapeutic radionuclides: Biophysical and radiobiologic principles*, Seminars in Nuclear Medicine, **38**(5), 358–366, **2008**.

[31] Qu, C.F.; Song, E.Y.; Li, Y.; Rizvi, S.M.A.; Raja, C.; Smith, R.; Morgenstern, A.; Apostolidis, C.; and Allen, B.J., *Pre-clinical study of Bi-213 labeled PAI2 for the control of micrometastatic pancreatic cancer*, Clinical & Experimental Metastasis, **22**(7), 575–586, **2005**.

[32] Ritter, M.A.; Cleaver, J.E.; and Tobias, C.A., *High-LET radiations induce a large proportion of non-rejoining DNA breaks*, Nature, **266**(5603), 653–655, **1977**.

[33] Vispe, S. and Satoh, M.S., *DNA repair patch-mediated double strand DNA break formation in human cells*, Journal of Biological Chemistry, **275**(35), 27.386–27.392, **2000**.

[34] Allen, B.J.; Raja, C.; Rizvi, S.; Li, Y.; Tsui, W.; Graham, P.; Thompson, J.F.; Reisfeld, R.A.; Kearsley, J.; Morgenstern, A.; and Apostolidis, C., *Intralesional targeted alpha therapy for metastatic melanoma*, Cancer Biology & Therapy, **4**(12), 1318–1324, **2005**.

[35] Macklis, R.M., *How and why does radioimmunotherapy work?*, International Journal of Radiation Oncology Biology Physics, **59**(5), 1269–1271, **2004**.

[36] Geerlings, M.W.; Kaspersen, F.M.; Apostolidis, C.; and Vanderhout, R., *The feasibility of Ac-225 as a source of alpha-particles in radioimmunotherapy*, Nuclear Medicine Communications, **14**(2), 121–125, **1993**.

[37] Boswell, C.A. and Brechbiel, M.W., *Development of radioimmunotherapeutic and diagnostic antibodies: an inside-out view*, Nuclear Medicine and Biology, **34**(7), 757–778, **2007**.

[38] Volkert, W.A. and Hoffman, T.J., *Therapeutic radiopharmaceuticals*, Chemical Reviews, **99**(9), 2269–2292, **1999**.

[39] Giese, A.; Bjerkvig, R.; Berens, M.E.; and Westphal, M., *Cost of migration: Invasion of malignant gliomas and implications for treatment*, Journal of Clinical Oncology, **21**(8), 1624–1636, **2003**.

[40] Srivastava, S. and Dadachova, E., *Recent advances in radionuclide therapy*, Seminars in Nuclear Medicine, **31**(4), 330–341, **2001**.

[41] Howell, R.W.; Goddu, S.M.; and Rao, D.V., *Proliferation and the advantage of longer-lived radionuclides in radioimmunotherapy*, Medical Physics, **25**(1), 37–42, **1998**.

[42] Schultz, M.K.; Borgman, M.P.; Coleman, T.; Bakhlanov, S.; Marchenkov, N.; and Line, B.R., *An assessment of radionuclidic impurities of Po-210 produced via neutron irradiation of Bi-209 for use in targeted alpha-particle radiotherapy*, Applied Radiation and Isotopes, **65**(7), 784–792, **2007**.

[43] Brechbiel, M.W., *Targeted alpha-therapy: past, present, future?*, Journal of the Chemical Society - Dalton Transactions, (43), 4918–4928, **2007**.

[44] Liu, S., *Bifunctional coupling agents for radiolabeling of biomolecules and target-specific delivery of metallic radionuclides*, Advanced Drug Delivery Reviews, **60**(12), 1347–1370, **2008**.

[45] Dearling, J.L.J. and Pedley, R.B., *Technological advances in radioimmunotherapy*, Clinical Oncology, **19**(6), 457–469, **2007**.

[46] Wheldon, T.E.; ODonoghue, J.A.; Barrett, A.; and Michalowski, A.S., *The curability of tumors of differing size by targeted radiotherapy using I-131 or Y-90*, Radiotherapy and Oncology, **21**(2), 91–99, **1991**.

[47] Couturier, O.; Supiot, S.; Degraef-Mougin, M.; Faivre-Chauvet, A.; Carlier, T.; Chatal, J.F.; Davodeau, F.; and Cherel, M., *Cancer radioimmunotherapy with alpha-emitting nuclides*, European Journal of Nuclear Medicine and Molecular Imaging, **32**(5), 601–614, **2005**.

[48] Jurcic, J.G.; Larson, S.M.; Sgouros, G.; McDevitt, M.R.; Finn, R.D.; Divgi, C.R.; Ballangrud, A.M.; Hamacher, K.A.; Ma, D.S.; Humm, J.L.; Brechbiel, M.W.; Molinet, R.; and Scheinberg, D.A., *Targeted at particle immunotherapy for myeloid leukemia*, Blood, **100**(4), 1233–1239, **2002**.

[49] ODonoghue, J.A.; Bardies, M.; and Wheldon, T.E., *Relationships between tumor size and curability for uniformly targeted therapy with beta-emitting radionuclides*, Journal of Nuclear Medicine, **36**(10), 1902–1909, **1995**.

[50] Chong, H.S.; Ma, X.; Le, T.; Kwamena, B.; Milenic, D.E.; Brady, E.D.; Song, H.A.; and Brechbiel, M.W., *Rational design and generation of a bimodal bifunctional ligand for antibody - Targeted radiation cancer therapy*, Journal of Medicinal Chemistry, **51**(1), 118–125, **2008**.

[51] Stewart, J.S., *Intraperitoneal yttrium-90-labeled monoclonal antibody in ovarian cancer.*, Journal of Clinical Oncology, **8**, 1941–1950, **1990**.

[52] Bernhardt, P.; Forssell-Aronsson, E.; Jacobsson, L.; and Skarnemark, G., *Low-energy electron emitters for targeted radiotherapy of small tumours*, Acta Oncologica, **40**(5), 602–608, **2001**.

[53] Feinendegen, L.E. and McClure, J.J., *Meeting report - Alpha-emitters for medical therapy - Workshop of the United States Department of Energy - Denver, Colorado, May 30-31, 1996*, Radiation Research, **148**(2), 195–201, **1997**.

[54] Milenic, D.E.; Brady, E.D.; and Brechbiel, M.W., *Antibody-targeted radiation cancer therapy*, Nature Reviews Drug Discovery, **3**(6), 488–498, **2004**.

[55] Imam, S.K., *Advancements in cancer therapy with alpha-emitters: A review*, International Journal of Radiation Oncology Biology Physics, **51**(1), 271–278, **2001**.

[56] Beyer, G.J.; Miederer, M.; Vranjesduric, S.; Comor, J.J.; Kunzi, G.; Hartley, O.; Senekowitsch-Schmidtke, R.; Soloviev, D.; and Buchegger, F., *Targeted alpha therapy in vivo: direct evidence for single cancer cell kill using Tb-149-rituximab*, European Journal of Nuclear Medicine and Molecular Imaging, **31**(4), 547–554, **2004**.

[57] Allen, B.J., *Targeted alpha therapy: Evidence for potential efficacy of alpha-immunoconjugates in the management of micrometastatic cancer*, Australasian Radiology, **43**(4), 480–486, **1999**.

[58] Sgouros, G., *Alpha-particles for targeted therapy*, Advanced Drug Delivery Reviews, **60**(12), 1402–1406, **2008**.

[59] McDevitt, M.R.; Finn, R.D.; Ma, D.; Larson, S.M.; and Scheinberg, D.A., *Preparation of alpha-emitting Bi-213-labeled antibody constructs for clinical use*, Journal of Nuclear Medicine, **40**(10), 1722–1727, **1999**.

[60] McDevitt, M.R.; Ma, D.S.; Lai, L.T.; Simon, J.; Borchardt, P.; Frank, R.K.; Wu, K.; Pellegrini, V.; Curcio, M.J.; Miederer, M.; Bander, N.H.; and Scheinberg, D.A., *Tumor therapy with targeted atomic nanogenerators*, Science, S. 1537–1540, **2001**.

[61] Borchardt, P.E.; Yuan, R.R.; Miederer, M.; McDevitt, M.R.; and Scheinberg, D.A., *Targeted actinium-225 in vivo generators for therapy of ovarian cancer*, Cancer Research, **63**(16), 5084–5090, **2003**.

[62] ODonoghue, J.A., *Strategies for selective targeting of Auger electron emitters to tumor cells*, Journal of Nuclear Medicine, **37**(4), S3–S6, **1996**.

[63] ODonoghue, J.A. and Wheldon, T.E., *Targeted radiotherapy using Auger electron emitters*, Physics In Medicine and Biology, **41**(10), 1973–1992, **1996**.

[64] Buchegger, F.; Perillo-Adamer, F.; Dupertuis, Y.M.; and Delaloye, A.B., *Auger radiation targeted into DNA: a therapy perspective*, European Journal of Nuclear Medicine and Molecular Imaging, **33**(11), 1352–1363, **2006**.

[65] Areberg, J.; Norrgren, K.; and Mattsson, S., *Absorbed doses to patients from Pt-191-;Pt-193m- and Pt-195m-cisplatin*, Applied Radiation and Isotopes, **51**(5), 581–586, **1999**.

[66] Huguenin, P.; Beer, K.T.; Allal, A.; Rufibach, K.; Friedli, C.; Davis, J.B.; Pestalozzi, B.; Schmid, S.; Thoni, A.; Ozsahin, M.; Bernier, J.; Topfer, M.; Kann, R.; Meier, U.R.; Thum, P.; Bieri, S.; Notter, M.; Lombriser, N.; and Glanzmann, C., *Concomitant cisplatin significantly improves locoregional control in advanced head and neck cancers treated with hyperfractionated radiotherapy*, Journal of Clinical Oncology, **22**(23), 4665–4673, **2004**.

[67] Nikula, T.K.; McDevitt, M.R.; Finn, R.D.; Wu, C.C.; Kozak, R.W.; Garmestani, K.; Brechbiel, M.W.; Curcio, M.J.; Pippin, C.G.; Tiffany-Jones, L.; Geerlings, M.W.; Apostolidis, C.; Molinet, R.; Geerlings, M.W.; Gansow, O.A.; and Scheinberg, D.A., *Alpha-emitting bismuth cyclohexylbenzyl DTPA constructs of recombinant humanized anti-CD33 antibodies: Pharmacokinetics, bioactivity, toxicity and chemistry*, Journal of Nuclear Medicine, **40**(1), 166–176, **1999**.

[68] Khalkin, V.A.; Tsupko-Sitnikov, V.V.; and Zaitseva, N.G., *Radionuclides for radiotherapy. Properties, preparation, and application of actinium-225*, Radiochemistry, **39**(6), 483–492, **1997**.

[69] Henriksen, G.; Hoff, P.; and Larsen, R.H., *Evaluation of potential chelating agents for radium*, Applied Radiation and Isotopes, **56**(5), 667–671, **2002**.

[70] Henriksen, G.; Schoultz, B.W.; Michaelsen, T.E.; Bruland, O.S.; and Larsen, R.H., *Sterically stabilized liposomes as a carrier for alpha-emitting radium and actinium radionuclides*, Nuclear Medicine and Biology, **31**(4), 441–449, **2004**.

[71] Kaspersen, F.M.; Bos, E.; Doornmalen, A.V.; Geerlings, M.W.; Apostolidis, C.; and Molinet, R., *Cytotoxicity of Bi-213-immunoconjugates and Ac-225-immunoconjugates*, Nuclear Medicine Communications, **16**(6), 468–476, **1995**.

[72] Hoppe, B.S.; Flampouri, S.; Lynch, J.; Slayton, W.; Zaiden, R.; Li, Z.; and Mendenhall, N.P., *Improving the therapeutic ratio in Hodgkins Lymphoma through the use of proton therapy*, Oncology, **26 (5)**, **2012**.

[73] Wiseman, G.A.; White, C.A.; Sparks, R.B.; Erwin, W.D.; Podoloff, D.A.; Lamonica, D.; Bartlett, N.L.; Parker, J.A.; Dunn, W.L.; Spies, S.M.; Belanger, R.; Witzig, T.E.; and Leigh, B.R., *Biodistribution and dosimetry results from a phase III prospectively randomized controlled trial of Zevalin (TM) radioimmunotherapy for low-grade, follicular, or transformed B-cell non-Hodgkin's lymphoma*, Critical Reviews In Oncology Hematology, **39**(1-2), **2001**.

[74] Jain, R.K., *Physiological barriers to delivery of monoclonal antibodies and other macromolecules in tumors*, Cancer Research, **50**(3), S814–S819, **1990**.

[75] Jain, R.K., *Vascular and interstitial barriers to delivery of therapeutic agents in tumors*, Cancer and Metastasis Reviews, **9**(3), 253–266, **1990**.

[76] Jain, R.K., *Barriers to drug-delivery in solid tumors*, Scientific American, **271**(1), 58–65, **1994**.

[77] Arista, A.; Sturiale, C.; Riva, P.; Tison, V.; Frattarelli, M.; Moscatelli, G.; Franceschi, G.; and Spinelli, A., *Intralesional administration of I-131-labeled monoclonal antibodies in the treatment of malignant gliomas*, Acta Neurochirurgica, **135**(3-4), 159–162, **1995**.

[78] Carlsson, J.; Ren, Z.P.; Wester, K.; Sundberg, A.L.; Heldin, N.E.; Hesselager, G.; Persson, M.; Gedda, L.; Tolmachev, V.; Lundqvist, H.; Blomquist, E.; and Nister, M., *Planning for intracavitary anti-EGFR radionuclide therapy of gliomas. Literature review and data on EGFR expression*, Journal of Neuro-Oncology, **77**(1), 33–45, **2006**.

[79] Riva, P.; Arista, A.; Franceschi, G.; Frattarelli, M.; Sturiale, C.; Riva, N.; Casi, M.; and Rossitti, R., *Local treatment of malignant gliomas by direct infusion of specific monoclonal antibodies labeled with I-131 - Comparison of the results obtained in recurrent and newly-diagnosed tumors*, Cancer Research, **55**(23), **1995**.

[80] Bloechl, S.; Beck, R.; Seidl, C.; Morgenstern, A.; Schwaiger, M.; and Senekowitsch-Schmidtke, R., *Fractionated locoregional low-dose radioimmunotherapy improves survival in a mouse model of diffuse-type gastric cancer using a Bi-213-conjugated monoclonal antibody*, Clinical Cancer Research, **11**(19), 7070s–7074s, **2005**.

[81] Zalutsky, M.R., *Targeted radiotherapy of brain tumours*, British Journal of Cancer, **90**(8), 1469–1473, **2004**.

[82] Shahar, T.; Ram, Z.; and Kanner, A.A., *Convection-enhanced delivery catheter placements for high-grade gliomas: complications and pitfalls*, Journal of Neuro-Oncology, **107**(2), 373–378, **2012**.

[83] Milenic, D.E.; Garmestani, K.; Chappell, L.L.; Dadachova, E.; Yordanov, A.; Ma, D.S.; Schlom, J.; and Brechbiel, M.W., *In vivo comparison of macrocyclic and acyclic ligands for radiolabeling of monoclonal antibodies with Lu-177 for radioimmunotherapeutic applications*, Nuclear Medicine and Biology, **29**(4), 431–442, **2002**.

[84] Biggin, C., *Radiation protection and alpha emitters in clinical trials. The Alpharadin (TM) experience.*, European Journal of Nuclear Medicine and Molecular Imaging, **34**, **2007**.

[85] Nilsson, S.; Strang, P.; Aksnes, A.K.; Franzen, L.; Olivier, P.; Pecking, A.; Staffurth, J.; Vasanthan, S.; Andersson, C.; and Bruland, O.S., *A randomized, dose-response, multicenter phase II study of radium-223 chloride for the palliation of painful bone metastases in patients with castration-resistant prostate cancer*, European Journal of Cancer, **48**(5), 678–686, **2012**.

[86] Sartor, O.; Heinrich, D.; Helle, S.I.; O'Sullivan, J.M.; Chodacki, A.; Demkow, T.; Logue, J.; Seke, M.; Widmark, A.; Johannessen, D.C.; Nilsson, S.; Hoskin, P.; Solberg, A.; James, N.D.; Syndikus, I.; Vogelzang, N.; O'Bryan-Tear, C.G.; Garcia-Vargas, J.; Shan, M.; and Parker, C., *Radium-223 chloride (alpharadin) impact on overall survival and skeletal-related events in patients with castration-resistant prostate cancer with bone metastases: A Phase III randomized trial (alsympca)*, Journal of Urology, **187**(4), **2012**.

[87] McDevitt, M., *personal communication*, email, **2012**.

[88] various Authors, *The chemistry of the actinide and transactinide elements, Third edition, Volume 1*, Springer, **2008**.

[89] Ansoborlo, E.; Prat, O.; Moisy, P.; Den Auwer, C.; Guilbaud, P.; Carriere, M.; Gouget, B.; Duffield, J.; Doizi, D.; Vercouter, T.; Moulin, C.; and Moulin, V., *Actinide speciation in relation to biological processes*, Biochimie, **88**(11), 1605–1618, **2006**.

[90] Fanghaenel, T., *Actinide Chemistry*, Lecture Skript, **2012**.

[91] Choppin, G.R. and Bond, A.H., *Actinide oxidation state speciation*, Journal of Analytical Chemistry, **51**(12), 1129–1138, **1996**.

[92] Shannon, R.D., *Revised effective ionic radii and systematic studies of interatomic distances in halides and chaleogenides*, Acta Crystallographica, **A32**, 751, **1976**.

[93] Panak, P.J. and Geist, A., *Complexation and extraction of trivalent actinides und lanthanides by triazinylpyridine N-donor ligands*, Chemical Reviews, **(submitted)**.

[94] Trumm, S., *Untersuchungen zur Komplexierung von Cm(III) und Eu(III) mit partitioning-relevanten Liganden*, Diss, University of Heidelberg, **2009**.

[95] Choppin, G.R., *Covalency in f-element bonds*, Journal of Alloys and Compounds, **344**, 55–59, **2002**.

[96] Schmidt, M., *Untersuchungen zum Einbaumechanismus von Actiniden und Lanthaniden in Calcium-haltige Sekundaerphasen*, Dissertation, University of Heidelberg, **2009**.

[97] Choppin, G.R., *Actinide speciation in aquatic systems*, Marine Chemistry, **99**(1-4), 83–92, **2006**.

[98] Choppin, G.R., *Factors in Ln(III) complexation*, Journal of Alloys and Compounds, **249**(1-2), 1–8, **1997**.

[99] Kim, J.I.; Neck, V.; and Fanghaenel, T., *Aquatic chemistry and thermodynamic modeling of trivalent actinides*, Abstracts of Papers of the American Chemical Society, **216**, U344–U344, **1998**.

[100] Adloff, J.P., *The centenary of a controversial discovery: actinium*, Radiochimica Acta, **88**(3-4), 123–127, **2000**.

[101] Kugler, H.K. and Keller, C., *Gmelin Handbook of inorganic and organometallic chemistry*, Springer, **1981**.

[102] Kulikov, E.V.; Novgorodov, A.F.; and Schumann, D., *Hydrolysis of actinium-225 trace quantities*, Journal of Radioanalytical and Nuclear Chemistry-Letters, **164**(2), 103–108, **1992**.

[103] Zielinska, B. and Bilewicz, A., *The hydrolysis of actinium*, Journal of Radioanalytical and Nuclear Chemistry, **261**(1), 195–198, **2004**.

[104] McDevitt, M.R. and Scheinberg, D.A., *Ac-225 and her daughters: the many faces of Shiva*, Cell Death and Differentiation, **9**(6), 593–594, **2002**.

[105] Kennel, S.J.; Chappell, L.L.; Dadachova, K.; Brechbiel, M.W.; Lankford, T.K.; Davis, I.A.; Stabin, M.; and Mirzadeh, S., *Evaluation of Ac-225 for vascular targeted radioimmunotherapy of lung tumors*, Cancer Biotherapy and Radiopharmaceuticals, **15**(3), 235–244, **2000**.

[106] Martinez, L.R.; Bryan, R.A.; Apostolidis, C.; Morgenstern, A.; Casadevall, A.; and Dadachova, E., *Antibody-guided alpha radiation effectively damages fungal biofilms*, Antimicrobial Agents and Chemotherapy, **50**(6), 2132–2136, **2006**.

[107] Apostolidis, C.; Molinet, R.; McGinley, J.; Abbas, K.; Mollenbeck, J.; and Morgenstern, A., *Cyclotron production of Ac-225 for targeted alpha therapy*, Applied Radiation and Isotopes, **62**(3), 383–387, **2005**.

[108] Kennel, S.J.; Lankford, T.; Garland, M.; Sundberg, J.P.; and Mirzadeh, S., *Biodistribution of Ra-225 citrate in mice: retention of daughter radioisotopes in bone*, Nuclear Medicine and Biology, **32**(8), 859–867, **2005**.

[109] Hassfjell, S. and Brechbiel, M.W., *The development of the alpha-particle emitting radionuclides Bi-212 and Bi-213, and their decay chain related radionuclides, for therapeutic applications*, Chemical Reviews, **101**(7), 2019–2036, **2001**.

[110] Stavila, V.; Davidovich, R.L.; Gulea, A.; and Whitmire, K.H., *Bismuth(III) complexes with aminopolycarboxylate and polyaminopolycarboxylate ligands: Chemistry and structure*, Coordination Chemistry Reviews, **250**(21-22), 2782–2810, **2006**.

[111] McDevitt, M.R.; Finn, R.D.; Sgouros, G.; Ma, D.S.; and Scheinberg, D.A., *An Ac-225/Bi-213 generator system for therapeutic clinical applications: construction and operation*, Applied Radiation and Isotopes, **50**(5), 895–904, **1999**.

[112] Apostolidis, C.; Molinet, R.; Rasmussen, G.; and Morgenstern, A., *Production of Ac-225 from Th-229 for targeted alpha therapy*, Analytical Chemistry, **77**(19), 6288–6291, **2005**.

[113] Miederer, M.; McDevitt, M.R.; Sgouros, G.; Kramer, K.; Cheung, N.K.V.; and Scheinberg, D.A., *Pharmacokinetics, dosimetry, and toxicity of the targetable atomic generator, Ac-225-HuM195, in nonhuman primates*, Journal of Nuclear Medicine, **45**(1), 129–137, **2004**.

[114] Ma, D.H.; McDevitt, M.R.; Finn, R.D.; and Scheinberg, D.A., *Breakthrough of Ac-225 and its radionuclide daughters from an Ac-225/Bi-213 generator: development of new methods, quantitative characterization, and implications for clinical use*, Applied Radiation and Isotopes, **55**(5), 667–678, **2001**.

[115] Cole, W.C.; Denardo, S.J.; Meares, C.F.; Mccall, M.J.; Denardo, G.L.; Epstein, A.L.; Obrien, H.A.; and Moi, M.K., *Comparative serum stability of radiochelates for antibody radiopharmaceuticals*, Journal of Nuclear Medicine, **28**(1), 83–90, **1987**.

[116] Meares, C.F.; Moi, M.K.; Diril, H.; Kukis, D.L.; Mccall, M.J.; Deshpande, S.V.; Denardo, S.J.; Snook, D.; and Epenetos, A.A., *Macrocyclic chelates of radiometals for diagnosis and therapy*, British Journal of Cancer, **62**, 21–26, **1990**.

[117] Voss, D.A.; Farquhar, E.R.; Horrocks, W.D.; and Morrow, J.R., *Lanthanide(III) complexes of amide derivatives of DOTA exhibit an unusual variation in stability across the lanthanide series*, Inorganica Chimica Acta, **357**(3), 859–863, **2004**.

[118] Scapolan, S.; Ansoborlo, E.; Moulin, C.; and Madic, C., *Uranium(VI)-transferrin system studied by time-resolved laser-induced fluorescence*, Radiation Protection Dosimetry, **79**(1-4), 505–508, **1998**.

[119] Edelstein, N.M.; Klenze, R.; Fanghanel, T.; and Hubert, S., *Optical properties of Cm(III) in crystals and solutions and their application to Cm(III) speciation*, Coordination Chemistry Reviews, **250**(7-8), 948–973, **2006**.

[120] Fanghaenel, T. and Kim, J.I., *Spectroscopic evaluation of thermodynamics of trivalent actinides in brines*, Journal of Alloys and Compounds, **271**, 728–737, **1998**.

[121] Horrocks, W.D. and Sudnick, D.R., *Lanthanide ion probes of structure in biology - Laser-induced luminescence decay constants provide a direct measure of the number of metal-coordinated water-molecules*, Journal of the American Chemical Society, **101**(2), 334–340, **1979**.

[122] Horrocks, W.D. and Sudnick, D.R., *Time-resolved europium(III) excitation spectroscopy - luminescence probe of metal-ion binding-sites*, Science, **206**(4423), 1194–1196, **1979**.

[123] Skerencak, A., *Spectroscopic studies on the thermodynamics of the complexation of trivalent curium with propionate in the temperature range from 20 to 90°C*, Journal of Solution Chemistry, **accepted**, **2012**.

[124] Skerencak, A.; Panak, P.J.; Hauser, W.; Neck, V.; Klenze, R.; Lindqvist-Reis, P.; and Fanghaenel, T., *TRLFS study on the complexation of Cm(III) with nitrate in the temperature range from 5 to 200 degrees C*, Radiochimica Acta, **97**(8), 385–393, **2009**.

[125] Kimura, T. and Choppin, G.R., *Luminescence study on determination of the hydration number of Cm(III)*, Journal of Alloys and Compounds, **213**, **1994**.

[126] Thakur, P.; Conca, J.L.; and Choppin, G.R., *Complexation studies of Cm(III), Am(III) and Eu(III) with linear and cyclic carboxylates and polyaminocarboxylates*, Journal of Coordination Chemistry, **64**, 3214–3236, **2011**.

[127] Tian, G.; Edelstein, N.M.; and Rao, L., *Spectroscopic properties and hydration of the Cm(III) aqua Ion from 10 to 85 degrees C*, Journal of Physical Chemistry A, **115**(10), 1933–1938, **2011**.

[128] Davis, I.A.; Glowienka, K.A.; Boll, R.A.; Deal, K.A.; Brechbiel, M.W.; Stabin, M.; Bochsler, P.N.; Mirzadeh, S.; and Kennel, S.J., *Comparison of (225)actinium chelates: Tissue distribution and radiotoxicity*, Nuclear Medicine and Biology, **26**(5), 581–589, **1999**.

[129] Moi, M.K.; Denardo, S.J.; and Meares, C.F., *Stable Bifunctional Chelates of Metals Used in Radiotherapy*, Cancer Research, **50**(3), S789–S793, **1990**.

[130] Hancock, R.D. and Martell, A.E., *Ligand design for selective complexation of metal-ions in aqueous-solution*, Chemical Reviews, **89**(8), 1875–1914, **1989**.

[131] Thunus, L. and Lejeune, R., *Overview of transition metal and lanthanide complexes as diagnostic tools*, Coordination Chemistry Reviews, **184**, 125–155, **1999**.

[132] Brechbiel, M.W. and Gansow, O.A., *Backbone-substituted DTPA ligands for Y-90 radioimmunotherapy*, Bioconjugate Chemistry, **2**(3), 187–194, **1991**.

[133] Mewis, R.E. and Archibald, S.J., *Biomedical applications of macrocyclic ligand complexes*, Coordination Chemistry Reviews, **254**(15-16), 1686–1712, **2010**.

[134] Clarke, E.T. and Martell, A.E., *Stabilities of trivalent metal-ion complexes of the tetraacetate derivatives of 12-membered, 13-membered and 14-membered tetraazamacrocycles*, Inorganica Chimica Acta, **190**(1), 37–46, **1991**.

[135] Clarke, E.T. and Martell, A.E., *Stabilities of the alkaline-earth and divalent transition-metal complexes of the tetraazamacrocyclic tetraacetic acid ligands*, Inorganica Chimica Acta, **190**(1), 27–36, **1991**.

[136] Jones-Wilson, T.M.; Deal, K.A.; Anderson, C.J.; McCarthy, D.W.; Kovacs, Z.; Motekaitis, R.J.; Sherry, A.D.; Martell, A.E.; and Welch, M.J., *The in vivo behavior of copper-64-labeled azamacrocyclic complexes*, Nuclear Medicine and Biology, **25**(6), 523–530, **1998**.

[137] Ma, D.S.; Lu, F.; Overstreet, T.; Milenic, D.E.; and Brechbiel, M.W., *Novel chelating agents for potential clinical applications of copper*, Nuclear Medicine and Biology, **29**(1), 91–105, **2002**.

[138] Chappell, L.L.; Deal, K.A.; Dadachova, E.; and Brechbiel, M.W., *Synthesis, conjugation, and radiolabeling of a novel bifunctional chelating agent for Ac-225 radioimmunotherapy applications*, Bioconjugate Chemistry, **11**(4), 510–519, **2000**.

[139] Jang, Y.H.; Blanco, M.; Dasgupta, S.; Keire, D.A.; Shively, J.E.; and Goddard, W.A., *Mechanism and energetics for complexation of Y-90 with 1,4,7,10-tetraazacyclododecane-1,4,7,10-tetraacetic acid (DOTA), a model for cancer radioimmunotherapy*, Journal of the American Chemical Society, **121**(26), 6142–6151, **1999**.

[140] Viola-Villegas, N. and Doyle, R.P., *The coordination chemistry of 1,4,7,10-tetraazacyclododecane-N,N,N,N-tetra acetic acid (H4DOTA): Structural overview and analyses on structure-stability relationships*, Coordination Chemistry Reviews, **253**(13-14), 1906–1925, **2009**.

[141] Bianchi, A.; Calabi, L.; Corana, F.; Fontana, S.; Losi, P.; Maiocchi, A.; Paleari, L.; and Valtancoli, B., *Thermodynamic and structural properties of Gd(III) complexes with polyamino-polycarboxylic ligands: basic compounds for the development of MRI contrast agents*, Coordination Chemistry Reviews, **204**, 309–393, **2000**.

[142] Bianchi, A.; Calabi, L.; Giorgi, C.; Losi, P.; Mariani, P.; Paoli, P.; Rossi, P.; Valtancoli, B.; and Virtuani, M., *Thermodynamic and structural properties of Gd3+ complexes with functionalized macrocyclic ligands based upon 1,4,7,10-tetraazacyclododecane*, Journal of the Chemical Society - Dalton Transactions, (5), 697–705, **2000**.

[143] Chong, H.S.; Milenic, D.E.; Garmestani, K.; Brady, E.D.; Arora, H.; Pfiester, C.; and Brechbiel, M.W., *In vitro and in vivo evaluation of novel ligands for radioimmunotherapy*, Nuclear Medicine and Biology, **33**(4), 459–467, **2006**.

[144] Cordier, D.; Forrer, F.; Bruchertseifer, F.; Morgenstern, A.; Apostolidis, C.; Good, S.; Muller-Brand, J.; Macke, H.; Reubi, J.C.; and Merlo, A., *Targeted alpha-radionuclide therapy of functionally critically located gliomas with Bi-213-DOTA-[Thi(8),Met(O-2)(11)]-substance P: a pilot trial*, European Journal of Nuclear Medicine and Molecular Imaging, **37**(7), 1335–1344, **2010**.

[145] Bruchertseifer, F.; Cordier, D.; Forrer, F.; Kneifel, S.; Apostolidis, C.; Morgenstern, A.; Merlo, A.; and Maecke, H.R., *Synthesis of Bi-213-DOTA-Substance P for targeted alpha-radionuclide therapy in patients with malignant glioma*, Cancer Biotherapy and Radiopharmaceuticals, **23**(4), 513–513, **2008**.

[146] Cooper, M.S.; Ma, M.T.; Sunassee, K.; Shaw, K.P.; Williams, J.D.; Paul, R.L.; Donnelly, P.S.; and Blower, P.J., *Comparison of (64)Cu-complexing bifunctional chelators for radioimmunoconjugation: Labeling efficiency, specific activity, and in vitro/in vivo stability.*, Bioconjugate Chemistry, **23**, 1029–1039, **2012**.

[147] Kodama, M. and Kimura, E., *Thermodynamic and kinetic interpretation of macrocyclic effect -Polarographic studies on copper(II) 1,4,7,10-tetraazacyclododecane complexation*, Journal of the Chemical Society - Chemical Communications, (9), 326–327, **1975**.

[148] Aime, S.; Barge, A.; Benetollo, F.; Bombieri, G.; Botta, M.; and Uggeri, F., *A novel compound in the lanthanide(III) DOTA series. X-ray crystal and molecular structure of the complex Na[La(DOTA)La(HDOTA)]*10H2O*, Inorganic Chemistry, **36**(19), 4287–4289, **1997**.

[149] Muller, G.; Kean, S.D.; Parker, D.; and Riehl, J.P., *Temperature and pressure dependence of excitation spectra as a probe of the solution structure and equilibrium thermodynamics of a Eu(III) complex containing a modified dota ligand*, Journal of Physical Chemistry A, **106**(51), 12.349–12.355, **2002**.

[150] Marques, M.P.M.; Geraldes, C.F.G.C.; Sherry, A.D.; Merbach, A.E.; Powell, H.; Pubanz, D.; Aime, S.; and Botta, M., *NMR conformational study of the lanthanide(III) complexes of Dota in aqueous solution*, Journal of Alloys and Compounds, **225**(1-2), 303–307, **1995**.

[151] Viswanathan, S.; Kovacs, Z.; Green, K.N.; Ratnakar, S.J.; and Sherry, A.D., *Alternatives to gadolinium-based metal chelates for magnetic resonance imaging*, Chemical Reviews, **110**(5), 2960–3018, **2010**.

[152] Benetollo, F.; Bombieri, G.; Aime, S.; and Botta, M., *A holmium complex of a macrocyclic ligand (DOTA) and its isostructural europium analogue*, Acta Crystallographica Section C-Crystal Structure Communications, **55**, 353–356, **1999**.

[153] Aime, S.; Botta, M.; Fasano, M.; Marques, M.P.M.; Geraldes, C.F.G.C.; Pubanz, D.; and Merbach, A.E., *Conformational and coordination equilibria on DOTA complexes of lanthanide metal ions in aqueous solution studied by H-1-NMR spectroscopy*, Inorganic Chemistry, **36**(10), 2059–2068, **1997**.

[154] Micskei, K.; Helm, L.; Brucher, E.; and Merbach, A.E., *O-17 NMR-study of water exchange on [Gd(Dtpa)(H2o)]2- and [Gd(Dota)(H2o)]- related to NMR imaging*, Inorganic Chemistry, **32**(18), 3844–3850, **1993**.

[155] Lau, E.Y.; Lightstone, F.C.; and Colvin, M.E., *Environmental effects on the structure of metal ion-DOTA complexes: An ab initio study of radiopharmaceutical metals*, Inorganic Chemistry, **45**(23), 9225–9232, **2006**.

[156] Asti, M.; Tegoni, M.; Farioli, D.; Iori, M.; Guidotti, C.; Cutler, C.S.; Mayer, P.; Versari, A.; and Salvo, D., *Influence of cations on the complexation yield of DOTATATE with yttrium and lutetium: a perspective study for enhancing the Y-90 and Lu-177 labeling conditions*, Nuclear Medicine and Biology, **39**(4), 509–517, **2012**.

[157] Desreux, J.F., *Nuclear magnetic resonance and potentiometric studies of the protonation scheme of two tetraaza tetraacetic macrocycles*, Inorganic Chemistry, **20 (4)**, 987–991, **1981**.

[158] Chaves, S.; Delgado, R.; and J., D.S.J., *The stability of the metal complexes of cyclic tetraazatetraacetic acids*, Talanta, **39**, 249–254, **1992**.

[159] www.nist.gov, *Thermodynamic database*.

[160] Toth, E. and Brucher, E., *Stability constants of the lanthanide(III)-1,4,7,10-tetraazacyclododecane-N,N',N",N"'-tetraacetate complexes*, Inorganica Chimica Acta, **221**(1-2), 165–167, **1994**.

[161] Pasha, A.; Tircso, G.; Benyo, E.T.; Brucher, E.; and Sherry, A.D., *Synthesis and characterization of DOTA-(amide)4 derivatives: Equilibrium and kinetic behavior of their lanthanide(III) complexes*, European Journal of Inorganic Chemistry, (27), 4340–4349, **2007**.

[162] Kumar, K.; Chang, C.A.; Francesconi, L.C.; Dischino, D.D.; Malley, M.F.; Gougoutas, J.Z.; and Tweedle, M.F., *Synthesis, stability and structure of gadolinium(III) and yttrium(III) macrocyclic polyamino carboxylates*, Inorganic Chemistry, **33**(16), 3567–3575, **1994**.

[163] Brucher, E.; Laurenczy, G.; and Makra, Z., *Studies on the Kinetics of Formation and Dissociation of the Cerium(III)-Dota Complex*, Inorganica Chimica Acta, **139**(1-2), 141–142, **1987**.

[164] Toth, E.; Brucher, E.; Lazar, I.; and Toth, I., *Kinetics of formation and dissociation of lanthanide(III)-Dota complexes*, Inorganic Chemistry, **33**(18), 4070–4076, **1994**.

[165] Burai, L.; Fabian, I.; Kiraly, R.; Szilagyi, E.; and Brucher, E., *Equilibrium and kinetic studies on the formation of the lanthanide(III) complexes, [Ce(dota)](-) and [Yb(dota)](-) (H(4)dota=1,4,7,10-tetraazacyclododecane-1,4,7,10-tetraacetic acid)*, Journal of the Chemical Society - Dalton Transactions, (2), 243–248, **1998**.

[166] Chang, C.A.; Liu, Y.L.; Chen, C.Y.; and Chou, X.M., *Ligand preorganization in metal ion complexation: Molecular mechanics/dynamics, kinetics, and laser-excited luminescence studies of trivalent lanthanide complex formation with macrocyclic ligands TETA and DOTA*, Inorganic Chemistry, **40**(14), 3448–3455, **2001**.

[167] Kumar, K. and Tweedle, M.F., *Ligand basicity and rigidity control formation of macrocyclic polyamino carboxylate complexes of gadolinium(III)*, Inorganic Chemistry, **32**(20), 4193–4199, **1993**.

[168] Wang, X.Y.; Jin, T.Z.; Comblin, V.; Lopezmut, A.; Merciny, E.; and Desreux, J.F., *A kinetic investigation of the lanthanide Dota chelates - stability and rates of formation and of dissociation of a macrocyclic gadolinium(III) polyaza polycarboxylic MRI contrast agent*, Inorganic Chemistry, **31**(6), 1095–1099, **1992**.

[169] Desreux, J.F., *Nuclear magnetic resonance spectroscopy of lanthanide complexes with a tetraacetic tetraaza macrocycle - unusual conformation properties*, Inorganic Chemistry, **19**(5), 1319–1324, **1980**.

[170] Sosabowski, J.K. and Mather, S.J., *Conjugation of DOTA-like chelating agents to peptides and radiolabeling with trivalent metallic isotopes*, Nature Protocols, **1**(2), 972–976, **2006**.

[171] Brechbiel, M.W.; Pippin, C.G.; McMurry, T.J.; Milenic, D.; Roselli, M.; Colcher, D.; and Gansow, O.A., *An effective chelating agent for labeling of a monoclonal antibody with Bi-212 for alpha-particle mediated radioimmunotherapy*, Journal of the Chemical Society - Chemical Communications, (17), 1169–1170, **1991**.

[172] Gansow, O.A., *Newer approaches to the radiolabeling of monoclonal-antibodies by use of metal-chelates*, Nuclear Medicine and Biology, **18**(4), 369–381, **1991**.

[173] Chappell, L.L.; Dadachova, E.; Milenic, D.E.; Garmestani, K.; Wu, C.C.; and Brechbiel, M.W., *Synthesis, characterization, and evaluation of a novel bifunctional chelating agent for the lead isotopes Pb-203 and Pb-212*, Nuclear Medicine and Biology, **27**(1), 93–100, **2000**.

[174] Smith-Jones, P.M.; Vallabahajosula, S.; Goldsmith, S.J.; Navarro, V.; Hunter, C.J.; Bastidas, D.; and Bander, N.H., *In vitro characterization of radiolabeled monoclonal antibodies specific for the extracellular domain of prostate-specific membrane antigen*, Cancer Research, **60**(18), 5237–5243, **2000**.

[175] Antczak, C.; Jaggi, J.S.; LeFave, C.V.; Curcio, M.J.; McDevitt, M.R.; and Scheinberg, D.A., *Influence of the linker on the biodistribution and catabolism of actinium-225 self-immolative tumor-targeted isotope generators*, Bioconjugate Chemistry, **17**(6), 1551–1560, **2006**.

[176] Behr, T.M.; Gotthardt, M.; Barth, A.; and Behe, M., *Imaging tumors with peptide-based radioligands*, Quarterly Journal of Nuclear Medicine, **45**(2), 189–200, **2001**.

[177] Sheikholvaezin, A.; Eriksson, D.; Ahlstrom, K.R.; Johansson, L.; and Stigbrand, T., *Tumor radioimmunolocalization in nude mice by mono- and divalent-single-chain Fv antiplacental alkaline phosphatase antibodies*, Cancer Biotherapy and Radiopharmaceuticals, **22**(1), 64–72, **2007**.

[178] Batra, S.K.; Jain, M.; Wittel, U.A.; Chauhan, S.C.; and Colcher, D., *Pharmacokinetics and biodistribution of genetically engineered antibodies*, Current Opinion In Biotechnology, **13**(6), 603–608, **2002**.

[179] Tolmachev, V.; Orlova, A.; Pehrson, R.; Galli, J.; Baastrup, B.; Andersson, K.; Sandstrom, M.; Rosik, D.; Carlsson, J.; Lundqvist, H.; Wennborg, A.; and Nilsson, F.Y., *Radionuclide therapy of HER2-positive microxenografts using a Lu-177-labeled HER2-specific affibody molecule*, Cancer Research, **67**(6), 2773–2782, **2007**.

[180] Davies, C.D.; Berk, D.A.; Pluen, A.; and Jain, R.K., *Comparison of IgG diffusion and extracellular matrix composition in rhabdomyosarcomas grown in mice versus in vitro as spheroids reveals the role of host stromal cells*, British Journal of Cancer, **86**(10), 1639–1644, **2002**.

[181] Heldin, C.H.; Rubin, K.; Pietras, K.; and Ostman, A., *High interstitial fluid pressure - An obstacle in cancer therapy*, Nature Reviews Cancer, **4**(10), 806–813, **2004**.

[182] Dadachova, E. and Casadevall, A., *Antibodies as delivery vehicles for radioimmunotherapy of infectious diseases*, Expert Opinion on Drug Delivery, **2**(6), 1075–1084, **2005**.

[183] Sharkey, R.M. and Goldenberg, D.M., *Use of antibodies and immunoconjugates for the therapy of more accessible cancers*, Advanced Drug Delivery Reviews, **60**(12), 1407–1420, **2008**.

[184] Olafsen, T.; Tan, G.J.; Cheung, C.W.; Yazaki, P.J.; Park, J.M.; Shively, J.E.; Williams, L.E.; Raubitschek, A.A.; Press, M.F.; and Wu, A.M., *Characterization of engineered anti-pI85(HER-2) (scFv-C(H)3)(2) antibody fragments (minibodies) for tumor targeting*, Protein Engineering Design & Selection, **17**(4), 315–323, **2004**.

[185] Drecoll, E.; Gaertner, F.C.; Miederer, M.; Blechert, B.; Vallon, M.; Müller, J.M.; Alke, A.; Seidl, C.; Bruchertseifer, F.; Morgenstern, A.; Senekowitsch-Schmidtke, R.; and Essler, M., *Treatment of peritoneal carcinomatosis by targeted delivery of the radio-labeled tumor homing peptide 213Bi-DTPA-[F3]2 into the nucleus of tumor cells*, **2008**.

[186] Otte, A.; Herrmann, R.; Heppeler, A.; Behe, M.; Jermann, E.; Powell, P.; Maecke, H.R.; and Muller, J., *Yttrium-90 DOTATOC: first clinical results*, European Journal of Nuclear Medicine, **26**(11), 1439–1447, **1999**.

[187] Norenberg, J.P.; Krenning, B.J.; Konings, I.R.H.M.; Kusewitt, D.F.; Nayak, T.K.; Anderson, T.L.; de Jong, M.; Garmestani, K.; Brechbiel, M.W.; and Kvols, L.K., *Bi-213-[DOTA(0),Tyr(3)]octreotide peptide receptor radionuclide therapy of pancreatic tumors in a preclinical animal model*, Clinical Cancer Research, **12**(3), 897–903, **2006**.

[188] Kneifel, S.; Cordier, D.; Good, S.; Ionescu, M.C.S.; Ghaffari, A.; Hofer, S.; Kretzschmar, M.; Tolnay, M.; Apostolidis, C.; Waser, B.; Arnold, M.; Mueller-Brand, J.; Maecke, H.R.; Reubi, J.C.; and Merlo, A., *Local targeting of malignant gliomas by the diffusible peptidic vector 1,4,7,10-tetraazacyclododecane-1-glutaric acid-4,7,10-triacetic acid-substance P*, Clinical Cancer Research, **12**(12), 3843–3850, **2006**.

[189] Good, S., *Entwicklung neuer rezeptorgesteuerter Radiopharmazeutika fuer die Therapie von malignen Hirntumoren und medullaeren Schilddruesenkarzinomen*, Diss, **2006**.

[190] Kohler, G. and Milstein, C., *Continuous cultures of fused cells secreting antibody of predefined specificity*, Nature, **256**(5517), 495–497, **1975**.

[191] Dadachova, E. and Casadevall, A., *Treatment of infection with radiolabeled antibodies*, Quarterly Journal of Nuclear Medicine and Molecular Imaging, **50**(3), 193–204, **2006**.

[192] Azinovic, I.; DeNardo, G.L.; Lamborn, K.R.; Mirick, G.; Goldstein, D.; Bradt, B.M.; and DeNardo, S.J., *Survival benefit associated with human anti-mouse antibody (HAMA) in patients with B-cell malignancies*, Cancer Immunology Immunotherapy, **55**(12), 1451–1458, **2006**.

[193] Dias, C.R.; Jeger, S.; Osso, J.A.; Mueller, C.; De Pasquale, C.; Hohn, A.; Waibel, R.; and Schibli, R., *Radiolabelling of rituximab with Re-188 and Tc-99m using the tricarbonyl technology*, Nuclear Medicine and Biology, **38**, 19–28, **2011**.

[194] Sofou, S. and Yu, Y.B., *Delivery systems for the targeted radiotherapy of cancer - Preface*, Advanced Drug Delivery Reviews, **60**(12), 1317–1318, **2008**.

[195] Hernandez, M.C. and Knox, S.J., *Radiobiology of radioimmunotherapy: Targeting CD20 B-cell antigen in non-Hodgkin's lymphoma*, International Journal of Radiation Oncology Biology Physics, **59**(5), 1274–1287, **2004**.

[196] www.DrugBank.ca, *Drug card for rituximab (DB00073).*

[197] Allen, B.J., *Clinical trials of targeted alpha therapy for cancer*, Reviews on Recent Clinical Trials, **3**(3), 185–191, **2008**.

[198] Maloney, D.G., *Concepts in radiotherapy and immunotherapy: Anti-CD20 mechanisms of action and targets*, Seminars in Oncology, **32**(1), S19–S26, **2005**.

[199] Vandenbulcke, K.; Thierens, H.; Offner, F.; Janssens, A.; de Gelder, V.; Bacher, K.; Philippe, J.; De vos, F.; Dierckx, R.; Apostolidis, C.; Morgenstern, A.; and Slegers, G., *Importance of receptor density in alpha radioimmunotherapy in B-cell malignancies: an in-vitro study*, Nuclear Medicine Communications, **25**(11), 1131–1136, **2004**.

[200] Maloney, D.G., *Immunotherapy for non-Hodgkin's lymphoma: Monoclonal antibodies and vaccines*, Journal of Clinical Oncology, **23**(26), 6421–6428, **2005**.

[201] Jurcic, J.G.; McDevitt, M.R.; Pandit-Taskar, N.; Divgi, C.R.; Finn, R.D.; Sgouros, G.; Apostolidis, C.; Chanel, S.; Larson, S.M.; and Scheinberg, D.A., *Alpha-particle immunotherapy for acute myeloid leukemia (AML) with bismuth-213 and actinium-225*, Cancer Biotherapy and Radiopharmaceuticals, **21**(4), 396–396, **2006**.

[202] Nadler, L.M.; Ritz, J.; Hardy, R.; Pesando, J.M.; Schlossman, S.F.; and Stashenko, P., *A unique cell-surface antigen identifying lymphoid malignancies of B-cell origin*, Journal of Clinical Investigation, **67**(1), 134–140, **1981**.

[203] Melville, G. and Allen, B.J., *Cyclotron and linac production of Ac-225*, Applied Radiation and Isotopes, **67**(4), 549–555, **2009**.

[204] Mirzadeh, S., *Generator-produced alpha-emitters*, Applied Radiation and Isotopes, **49**(4), 345–349, **1998**.

[205] Morgenstern, A.; Abbas, K.; Bruchertseifer, F.; and Apostolidis, C., *Production of alpha emitters for targeted alpha therapy*, Current Radiopharmaceuticals, **1**, 135–143, **2008**.

[206] Morgenstern, A.; Bruchertseifer, F.; and Apostolidis, C., *Bismuth-213 and Actinium-225 - Generator Performance and Evolving Therapeutic Applications of Two Generator-Derived Alpha-Emitting Radioisotopes*, Current Radiopharmaceuticals, **5**, 221–227, **2012**.

[207] Zielinska, B.; Apostolidis, C.; Bruchertseifer, F.; and Morgenstern, A., *An improved method for the production of Ac-225/Bi-213 from Th-229 for targeted alpha therapy*, Solvent Extraction and Ion Exchange, **25**(3), 339–349, **2007**.

[208] Boll, R.A.; Malkemus, D.; and Mirzadeh, S., *Production of actinium-225 for alpha particle mediated radioimmunotherapy*, Applied Radiation and Isotopes, **62**(5), 667–679, **2005**.

[209] Melville, G.; Meriarty, H.; Metcalfe, P.; Knittel, T.; and Allen, B.J., *Production of Ac-225 for cancer therapy by photon-induced transmutation of Ra-226*, Applied Radiation and Isotopes, **65**(9), 1014–1022, **2007**.

[210] Melville, G.; Liu, S.F.; and Allen, B.J., *A theoretical model for the production of Ac-225 for cancer therapy by photon-induced transmutation of Ra-226*, Applied Radiation and Isotopes, **64**(9), 979–988, **2006**.

[211] Lambrecht, R.M.; Tomiyoshi, K.; and Sekine, T., *Radionuclide generators*, Radiochimica Acta, **77**(1-2), 103–123, **1997**.

[212] Knapp, F.F. and Mirzadeh, S., *The continuing important role of radionuclide generator systems for nuclear medicine*, European Journal of Nuclear Medicine, **21**(10), 1151–1165, **1994**.

[213] McAlister, D.R. and Horwitz, E.P., *Automated two column generator systems for medical radionuclides*, Applied Radiation and Isotopes, **67**(11), 1985–1991, **2009**.

[214] Morgenstern, A., *Radionuklide in der Medizin*, Lecture Script, **2011**.

[215] Dahle, J.; Borrebaek, J.; Jonasdottir, T.J.; Hjelmerud, A.K.; Melhus, K.B.; Bruland, O.S.; Press, O.W.; and Larsen, R.H., *Targeted cancer therapy with a novel low-dose rate alpha-emitting radioimmunoconjugate*, Blood, **110**(6), 2049–2056, **2007**.

[216] Larsen, R.H.; Borrebaek, J.; Dahle, J.; Melhus, K.B.; Krogh, C.; Valan, M.H.; and Bruland, O.S., *Preparation of Th227-labeled radioimmunoconjugates, assessment of serum stability and antigen binding ability*, Cancer Biotherapy and Radiopharmaceuticals, **22**(3), 431–437, **2007**.

[217] Melhus, K.B.; Larsen, R.H.; Stokke, T.; Kaalhus, O.; Selbo, P.K.; and Dahle, J., *Evaluation of the binding of radiolabeled rituximab to CD20-Positive lymphoma cells: An in vitro feasibility study concerning low-dose-rate Radioimmunotherapy with the alpha-emitter Th-227*, Cancer Biotherapy and Radiopharmaceuticals, **22**(4), 469–479, **2007**.

[218] Vidaud, C.; Dedieu, A.; Basset, C.; Plantevin, S.; Dany, I.; Pible, O.; and Quemeneur, E., *Screening of human serum proteins for uranium binding*, Chemical Research in Toxicology, **18**(6), 946–953, **2005**.

[219] Lewis, M.R.; Raubitschek, A.; and Shively, J.E., *A Facile, water-soluble method for modification of proteins with Dota - Use of elevated temperature and optimized pH to achieve high specific activity and high chelate stability in radiolabeled Žimmunoconjugates*, Bioconjugate Chemistry, **5**(6), 565–576, **1994**.

[220] Fatemi, S.J.A.; Kadir, F.H.A.; and Moore, G.R., *Aluminum transport in blood-serum - binding of aluminum by human transferrin in the presence of human albumin and citrate*, Biochemical Journal, **280**, 527–532, **1991**.

[221] Montavon, G.; Apostolidis, C.; Bruchertseifer, F.; Repinc, U.; and Morgenstern, A., *Spectroscopic study of the interaction of U(VI) with transferrin and albumin for speciation of U(VI) under blood serum conditions*, Journal of Inorganic Biochemistry, **103**(12), 1609–1616, **2009**.

[222] Abbas Rizvi, S.M.; Li, Y.; Song, E.Y.J.; Qu, C.F.; Raja, C.; Morgenstern, A.; Apostolidis, C.; and Allen, B.J., *Preclinical studies of bismuth-213 labeled plasminogen activator inhibitor type 2 (PAI2) in a prostate cancer nude mouse xenograft model.*, Cancer Biology & Therapy, **5**(4), 386–393, **2006**.

[223] Song, H.; Hobbs, R.F.; Vajravelu, R.; Huso, D.L.; Esaias, C.; Apostolidis, C.; Morgenstern, A.; and Sgouros, G., *Radioimmunotherapy of breast cancer metastases with alpha-particle emitter Ac-225: Comparing efficacy with Bi-213 and Y-90*, Cancer Research, **69**(23), 8941–8948, **2009**.

[224] Wilbur, D.S., *Chemical and radiochemical considerations in radiolabeling with alpha-emitting radionuclides.*, Current radiopharmaceuticals, **4**(3), 214–47, **2011**.

[225] Kishore, R.; Eary, J.F.; Krohn, K.A.; Nelp, W.B.; Menard, T.W.; Beaumier, P.L.; Hellstorm, K.E.; and Hellstorm, I., *Autoradiolysis of iodinated monoclonal antibody preparations*, Nuclear Medicine and Biology, **13**(4), 457–459, **1986**.

[226] Liu, S.; Ellars, C.E.; and Edwards, D.S., *Ascorbic acid: Useful as a buffer agent and radiolytic stabilizer for metalloradiopharmaceuticals*, Bioconjugate Chemistry, **14**(5), 1052–1056, **2003**.

[227] Chakrabarti, M.C.; Le, N.; Paik, C.H.; DeGraff, W.G.; and Carrasquillo, J.A., *Prevention of radiolysis of monoclonal antibody during labeling*, Journal of Nuclear Medicine, **37**(8), 1384–1388, **1996**.

[228] Larsen, R.H. and Bruland, O.S., *Radiolysis of radioimmunoconjugates - Reduction in antigen-binding ability by alpha-particle radiation*, Journal of Labelled Compounds & Radiopharmaceuticals, **36**(10), 1009–1018, **1995**.

[229] Brom, M.; Joosten, L.; Oyen, W.J.; Gotthardt, M.; and Boerman, O.C., *Improved labelling of DTPA- and DOTA-conjugated peptides and antibodies with In-111 in HEPES and MES buffer*, EJNMMI Research, **2:4**, **2012**.

[230] Weadock, K.S.; Sharkey, R.M.; Varga, D.C.; and Goldenberg, D.M., *Evaluation of a remote radioiodination system for radioimmunotherapy*, Journal of Nuclear Medicine, **31**(4), 508–511, **1990**.

[231] Lindegren, S., *Direct Procedure for the Production of 211-At-Labeled Antibodies with an e-Lysyl-3-(Trimethylstannyl)Benzamide Immunoconjugate*, The Journal of Nuclear Medicine, **49**, 1537–1545, **2008**.

[232] Sofou, S.; Kappel, B.J.; Jaggi, J.S.; McDevitt, M.R.; Scheinberg, D.A.; and Sgouros, G., *Enhanced retention of the alpha-particle-emitting daughters of actinium-225 by liposome carriers*, Bioconjugate Chemistry, **18**(6), 2061–2067, **2007**.

[233] Houk, R.S.; Fassel, V.A.; Flesch, G.D.; Svec, H.J.; Gray, A.L.; and Taylor, C.E., *Inductively coupled argon plasma as an ion-source for mass-spectrometric determination of trace-elements*, Analytical Chemistry, **52**(14), 2283–2289, **1980**.

[234] www.nucleonica.net, *Decay engine*.

[235] www.nucleonica.net, *Gamma library*.

[236] Malmbeck, R.; Apostolidis, C.; Carlos, R.; Glatz, J.P.; Molinet, R.; Morgenstern, A.; Nicholl, A.; Pagliosa, G.; Roemer, K.; Schaedel, M.; Saetmark, B.; and Trautmann, N., *Separation of 248Cm from a 252Cf Neutron Source for Production of Cm Targets*, Radiochimica Acta, **89**, 543–549, **2001**.

[237] *Chelatierung der Antikörper, Protocol Mirjam Weis (AIT-ITU)*.

[238] Brady, E.D.; Chong, H.S.; Milenic, D.E.; and Brechbiel, M.W., *Development of a spectroscopic assay for bifunctional ligand-protein conjugates based on copper*, Nuclear Medicine and Biology, **31**(6), 795–802, **2004**.

[239] *DC Protein assay instruction manual, Bio-Rad Laboratories*.

[240] Grimsley, G. and Pace, C.N., *Spectrophotometric determination of protein concentration*, Current Protocols in Protein Science, **Supplement 33**, 311–319, **2003**.

[241] Repinc, U., *Radiolabelling of biomolecules (Final Report)*, Techn. Ber., Institute for Transuranium Elements, **2010**.

[242] various Authors, *Monoclonal antibody and peptide-targeted radiotherapy of cancer*, Wiley, **2010**.

[243] Dadachova, E.; Chappell, L.L.; and Brechbiel, M.W., *Spectrophotometric assay for determination of polyazacarboxylate-macrocyclic ligands in ligand-protein conjugates.*, Abstracts of Papers of the American Chemical Society, **218**, U139–U139, **1999**.

[244] Dadachova, E.; Chappell, L.L.; and Brechbiel, M.W., *Spectrophotometric method for determination of bifunctional macrocyclic ligands in macrocyclic ligand-protein conjugates*, Nuclear Medicine and Biology, **26**(8), 977–982, **1999**.

[245] Smith-Jones, P.M.; Pandit-Taskar, N.; Cao, W.; O'Donoghue, J.; Philips, M.D.; Carrasquillo, J.; Konner, J.A.; Old, L.J.; and Larson, S.M., *Preclinical radioimmunotargeting of folate receptor alpha using the monoclonal antibody conjugate DOTA-MORAb-003*, Nuclear Medicine and Biology, **35**(3), 343–351, **2008**.

[246] Herbelin and Westall, *Fiteql 4.0, a non-linear least-squares optimisation program*, available from John C. Westall of the Oregon State University, **1999**.

[247] Montavon, G.; Repinc, U.; Apostolidis, C.; Bruchertseifer, F.; Abbas, K.; and Morgenstern, A., *Investigation of para-sulfonatocalix[n]arenes [n=6, 8] as potential chelates for U-230*, Journal of the Chemical Society - Dalton Transactions, **39**(5), 1366–1374, **2010**.

[248] *Chelex 100 and Chelex 20 chelating ion exchange resin instruction manual, Bio-Rad Laboratories.*

[249] Millar, A.M.; Beattie, L.A.; Craig, F.; and O'Brien, L.M., *An evaluation of GMCP-SA as a replacement for ITLC-SG when measuring the levels of radiochemical impurities in Tc-99m radiopharmaceuticals by thin-layer chromatography*, Journal of Labelled Compounds & Radiopharmaceuticals, **52**(13-14), 538–542, **2009**.

[250] Wunderlich, G.; Herrling, P.; Zurn, A.; Anders, P.; and Kotzerke, J., *Chromatographic determination of radiochemical purity Replacement of ITLC-SG*, Nuklearmedizin - Nuclear Medicine, **49**(2), 73–77, **2010**.

[251] Cole, W.C.; Denardo, S.J.; Meares, C.F.; Mccall, M.J.; Denardo, G.L.; Epstein, A.L.; Obrien, H.A.; and Moi, M.K., *Serum stability of Cu-67 chelates - comparison with In-111 and Co-57*, Nuclear Medicine and Biology, **13**(4), 363–368, **1986**.

[252] *PD-10 Desalting columns, Instructions 52-1308-00 BB, GE Healthcare.*

[253] Camera, L.; Kinuya, S.; Garmestani, K.; Wu, C.C.; Brechbiel, M.W.; Pai, L.H.; Mcmurry, T.J.; Gansow, O.A.; Pastan, I.; Paik, C.H.; and Carrasquillo, J.A., *Evaluation of the serum stability and in-vivo biodistribution of CHX-DTPA and other ligands for yttrium labeling of monoclonal antibodies*, Journal of Nuclear Medicine, **35**(5), 882–889, **1994**.

[254] Chen, J.Q.; Cheng, Z.; Owen, N.K.; Hoffman, T.J.; Miao, Y.B.; Jurisson, S.S.; and Quinn, T.P., *Evaluation of an In-111-DOTA-rhenium cyclized alpha-MSH analog: A novel cyclic-peptide analog with improved tumor-targeting properties*, Journal of Nuclear Medicine, **42**(12), 1847–1855, **2001**.

[255] Iznaga-Escobar, N., *Direct radiolabeling of monoclonal antibodies with rhenium-188 for radioimmunotherapy of solid tumors - a review of radiolabeling characteristics, quality control and in vitro stability studies*, Applied Radiation and Isotopes, **54**(3), 399–406, **2001**.

[256] Chong, H.S.; Mhaske, S.; Lin, M.; Bhuniya, S.; Song, H.A.; Brechbiel, M.W.; and Sun, X., *Novel synthetic ligands for targeted PET imaging and radiotherapy of copper*, Bioorganic and Medicinal Chemistry Letters, **17**(22), 6107–6110, **2007**.

[257] Chappell, L.L.; Ma, D.; Milenic, D.E.; Garmestani, K.; Venditto, V.; Beitzel, M.P.; and Brechbiel, M.W., *Synthesis and evaluation of novel bifunctional chelating agents based on 1,4,7,10-Tetraazacyclododecane-N,N,N,N-Tetraacetic acid for radiolabeling proteins*, Nuclear Medicine and Biology, **30**(6), 581–595, **2003**.

[258] Bonavia, A.S.; McDevitt, M.R.; Curcio, M.J.; and Scheinberg, D.A., *Immunoreactivity assay for alpha-particle emitting monoclonal antibody constructs*, Applied Radiation and Isotopes, **64**(4), 470–474, **2006**.

[259] Kodama, M.; Koike, T.; Mahatma, A.B.; and Kimura, E., *Thermodynamic and kinetic studies of lanthanide complexes of 1,4,7,10,13-pentaazacyclopentadecane-N,N',N",N"',N""-pentaacetic acid and 1,4,7,10,13,16-hexaazacyclooctadecane-N,N',N",N"',N"",N""'-hexaacetic acid*, Inorganic Chemistry, **30**(6), 1270–1273, **1991**.

[260] Tian, G. and Rao, L., *Effect of temperature on the protonation of the TALSPEAK ligands: Lactic and diethylenetrinitropentaacetic acids*, Separation Science and Technology, **45**(12-13), **2010**.

[261] Nilsson, N., *Competitive surface complexation of o-phthalate and phosphate on goethite particles*, Geochimica et Cosmochimica Acta, **60**, 4385–4395, **1996**.

[262] Luetzenkirchen, J., *Comparison of various models to describe the charge-pH dependence of poly(acrylic acid)*, J. Chem. Eng. Data, **56 (4)**, 1602–1612, **2011**.

[263] Thakur, P.; Mathur, J.N.; Moore, R.C.; and Choppin, G.R., *Thermodynamics and dissociation constants of carboxylic acids at high ionic strength and temperature*, Inorganica Chimica Acta, **360**, 3671–3680, **2007**.

[264] Kasprzyk, S.P. and Wilkins, R.G., *Kinetics of interaction of metal ions with two tetraazatetraacetate macrocycles*, Inorganic Chemistry, **21 (9)**, 3349–3352, **1982**.

[265] Hummel; Anderegg; and Rao, *Chemical thermodynamics of compounds and complexes of U, Np, Pu, Am, Tc, Se, Ni and Zr with selected organic ligands*, Elsevier Science Publisher, **2005**.

[266] Pippin, C.G.; McMurry, T.J.; Brechbiel, M.W.; McDonald, M.; Lambrecht, R.; Milenic, D.; Roselli, M.; Colcher, D.; and Gansow, O.A., *Lead(II) complexes of 1,4,7,10-tetraazacyclododecane-N,N,N,N-tetraacetate: solution chemistry and application to tumour localization with Pb-203 labelled monoclonal antibodies*, Inorganic Chimica Acta, **239**, 43–51, **1995**.

[267] Wang, Z., *A fluorescence spectroscopic study on the speciation of Cm(III) and Eu(III) in the presence of organic chaletes in highly basic solutions*, Radiochimica Acta, **91**, 329–337, **2003**.

[268] Lindqvist-Reis, P.; Klenze, R.; Schuber, G.; and Fanghaenel, T., *Hydration of Cm3+ in Aqueous Solution from 20 to 200 °C. A Time-Resolved Laser Fluorescence Spectroscopy Study*, Jorurnal of Physical Chemistry B, **109**, 3077–3083, **2005**.

[269] Schmitt, O., *Spektroskopische Untersuchung der Komplexierung von Cm(III) mit DTPA*, Techn. Ber., FH Aachen, Campus Jülich, **2011**.

[270] Brunet, E.; Juanes, O.; and Rodriguez-Ubis, J.C., *Supramolecularly organized lanthanide complexes for efficient metal excitation and luminescence as sensors in organic and biological applications*, Current Chemcial Biology, **1**, 11–39, **2007**.

[271] Robert Polly, K.I., *DFT-calculations*.

[272] Choppin, G.R. and Wang, Z.M., *Correlation between ligand coordination number and the shift of the 7F0-5D0 transition frequency in europium(III) complexes*, Inorg. Chem., **36 (2)**, 249–252, **1997**.

[273] Alimarin, I.P., *Kinetics of complex formation of metals with organic ligands in analytical chemistry*, Pure and Applied Chemistry, **34**, 1 – 12, **1973**.

[274] Atkins, P. and DePaula, J., *Atkins' Physical Chemistry*, Oxford University Press, **2006**.

[275] Cacheris, W.P.; Nickle, S.K.; and Sherry, A.D., *Thermodynamic study of lanthanide complexes of 1,4,7-triazacyclononane-N,N,N-triacetic acid and 1,4,7,10-tetraazacyclododecane-N,N,N,N-tetraacetic acid*, Inorganic Chemistry, **26**(6), 958–960, **1987**.

[276] Loncin, M.F., *Coordination of lanthanides by two polyamino polycarboxylic macrocycles: formation of highly stable lanthanide complexes*, Inorganic Chemistry, **25 (15)**, 2646–2648, **1986**.

[277] Anderegg, G., *Zur Deutung der thermodynamischen Daten von Komplexbildungsreaktionen I*, Helvetica Chimica Acta, **51**, 1856, **1968**.

[278] Parkhurst, D. and Appelo, T., *PHREEQC, aqueous geochemical modelling code*, **1999**.

[279] Guillaumont, R.; Fanghänel, T.; Neck, V.; Fuger, J.; Palmer, D.; Grenthe, I.; and Rand, M., *Update on the chemical thermodynamics of Uranium, Neptunium, Plutonium, Americium and Technetium, Chemical Thermodynamics 5*, Elsevier Science Publisher, **2003**.

[280] various Authors, *Handbook of elemental speciation II*, Wiley, **2003**.

[281] Choppin, G.R. and Schneide, J.K., *Acetate Complexing by Trivalent Actinide Ions*, Journal of Inorganic and Nuclear Chemistry, **32**, 3283, **1970**.

[282] Cernochova, K.; Mathur, J.N.; and Choppin, G.R., *Chemical speciation of Am, Cm and Eu with EDTA at high ionic strength: thermodynamics and laser fluorescence spectroscopy studies.*, Radiochimica Acta, **93**, 733–739, **2005**.

[283] Rizkalla, E.N.; Sullivan, J.C.; and Choppin, G.R., *Calorimetric studies of americium(III) complexation by amino carboxylates.*, Inorganic Chemistry, **28**, 909–911, **1989**.

[284] Pippin, C.G.; Parker, T.A.; Mcmurry, T.J.; and Brechbiel, M.W., *Spectrophotometric method for the determination of a bifunctional Dtpa ligand in Dtpa monoclonal antibody conjugates*, Bioconjugate Chemistry, **3**(4), 342–345, **1992**.

[285] Velikyan, I.; Beyer, G.J.; and Langstrom, B., *Microwave-supported preparation of Ga-68 bioconjugates with high specific radioactivity*, Bioconjugate Chemistry, **15**(3), 554–560, **2004**.

[286] Deepika, P.; Sabharwal, K.N.; Srinivasan, T.G.; and Rao, P.R.V., *Studies on the use of N,N,N,N-tetra(2-ethylhexyl) diglycolamide (TEHDGA) for actinide partitioning II: Investigation on radiolytic stability*, Solvent Extraction and Ion Exchange, **29**, 230–246, **2011**.

[287] http://www.eichrom.com/products/info/prefilter.aspx, *Technical information on Pre-filter Material.*

[288] Keire, D.A. and Kobayashi, M., *NMR studies of the metal-loading kinetics and acid-base chemistry of DOTA and butylamide-DOTA*, Bioconjugate Chemistry, **10**(3), 454–463, **1999**.

[289] *NIST Database*, www.nist.gov.

[290] C. M. Ruff, N.B., *personal communication.*

[291] Levi, M.; Li, J.; Frey, N.; Kheoh, T.; and Ren, S., *Characterization of the time-varying clearance of rituximab in Non-Hodgkins Lymphoma patients using a population pharmacokinetic analysis*, http://tucson2008.go-acop.org/pdfs/Levi.pdf.

[292] Sander, A.; Bruchertseifer, F.; and Morgenstern, A., *Serum stability of Ac-225-DOTATOC*, presented at WPA, **2012**.

[293] Badger, C.C.; Krohn, K.A.; and Bernstein, I.D., *In vitro measurement of avidity of radioionated antibodies*, Nuclear Medicine and Biology, **14**, 605–610, **1987**.

[294] Song, H.; Esaias, C.; Vajravelu, R.; Hobbs, R.F.; Apostolidis, C.; Morgenstern, A.; and Sgouros, G., *Improved efficacy of alpha-emitters (Ac-225, Bi-213) over beta-emitter (Y-90) labeled anti-HER-2/neu monoclonal antibody against early stage pulmonary metastasis*, Cancer Biotherapy and Radiopharmaceuticals, **23**(4), 519–519, **2008**.

[295] *GraphPad Prism 5 is available from http://www.graphpad.com/scientific-software/prism/.*

Eidesstattliche Versicherung gemäß § 8 der Promotionsordnung der Naturwissenschaftlich-Mathematischen Gesamtfakultät der Universität Heidelberg

1. Bei der eingereichten Dissertation zu dem Thema

_____

_____

_____

handelt es sich um meine eigenständig erbrachte Leistung.

2. Ich habe nur die angegebenen Quellen und Hilfsmittel benutzt und mich keiner unzulässigen Hilfe Dritter bedient. Insbesondere habe ich wörtlich oder sinngemäß aus anderen Werken übernommene Inhalte als solche kenntlich gemacht.

3. Die Arbeit oder Teile davon habe ich wie folgt/bislang nicht[1)] an einer Hochschule des In- oder Auslands als Bestandteil einer Prüfungs- oder Qualifikationsleistung vorgelegt.

Titel der Arbeit:_____

_____

Hochschule und Jahr:_____

Art der Prüfungs- oder Qualifikationsleistung:_____

4. Die Richtigkeit der vorstehenden Erklärungen bestätige ich.

5. Die Bedeutung der eidesstattlichen Versicherung und die strafrechtlichen Folgen einer unrichtigen oder unvollständigen eidesstattlichen Versicherung sind mir bekannt.

Ich versichere an Eides statt, dass ich nach bestem Wissen die reine Wahrheit erklärt und nichts verschwiegen habe.

_____ _____

Ort und Datum Unterschrift

[1)] Nicht Zutreffendes streichen. Bei Bejahung sind anzugeben: der Titel der andernorts vorgelegten Arbeit, die Hochschule, das Jahr der Vorlage und die Art der Prüfungs- oder Qualifikationsleistung.